The spectra and variability of accreting black holes

Andrea Merloni

Institute of Astronomy
&
Queens' College

October 3, 2001

A dissertation submitted to the University of Cambridge
for the degree of Doctor of Philosophy

Declaration

This thesis, entitled *The spectra and variability of accreting black holes*, is submitted for the degree of Doctor of Philosophy at the University of Cambridge. The research described was performed in the Institute of Astronomy between October 1998 and September 2001. The work contained in this dissertation is original, except where explicit reference to the results of others is given. Parts of this work, which are indicated in the text, were performed in collaboration and some of the results have appeared or will appear in published form:

- **A. Merloni**, A. C. Fabian & R. R. Ross: *On the interpretation of the multicolour disc model for black hole candidates.* Mon. Not. R. Astron. Soc. , **313**, 193-197 (2000).
- **A. Merloni**, T. Di Matteo & A. C. Fabian: *Magnetic flares and the optical variability of the X-ray transient XTE J1118+480.* Mon. Not. R. Astron. Soc. , **318**, L15 (2000).
- E. Ramirez-Ruiz & **A. Merloni**: *Quiescent times in gamma-ray bursts: I. An observed correlation between the durations of subsequent emission episodes.* Mon. Not. R. Astronom. Soc., **320**, L25 (2001).
- **A. Merloni** & A. C. Fabian: *Accretion disc coronae as magnetic reservoirs.* Mon. Not. R. Astronom. Soc., **321**, 549 (2001).
- P.-O. Petrucci, **A. Merloni**, A. C. Fabian, F. Haardt, E. Gallo: *The effects of a comptonizing corona on the appearance of the reflection components in accreting black hole spectra.* Accepted for publication in MNRAS.
- **A. Merloni** & A. C. Fabian: *Thunderclouds and accretion discs: a model for the spectral and temporal variability of Seyfert 1 galaxies.* Accepted for publication in MNRAS.
- **A. Merloni** & A. C. Fabian: *Coronal outflow dominated accretion discs: a new possibility for low luminosity black holes?.* Submitted to MNRAS.

The length of this work does not exceed 60,000 words.

Andrea Merloni
Cambridge
October 3, 2001

Acknowledgments

There are many people I have to thank for their guidance, help, support and encouragement during these Cambridge years.

First and foremost, my supervisor Andy Fabian, for the many things I have learnt from him, for his trust, his inspiration and his way of being a teacher.

Secondly, PPARC and the TMR Network 'Accretion onto black holes, neutron stars and protostars', for the financial support. Also, all the people at the IoA, from Paul to Pamela, Eileen, Margaret, John, Judith, Elsie and all the others, students, postdocs and staff, for they make this place such a great working environment. Finally, Max Pettini, for the effort he put in helping me, and all of us students, through these PhD years.

All the members of the X-ray group, present and past: Carolin, Stefano (the Fantacalcio-man), Steve, Roderick (for his precious help and efficiency), Kazushi (who knows so many things!), Robert, Simon, Julia, Andy Y., Richard, Mateusz, David B., Poshak (because he is the kindest of us all), Glenn (who liked being with 'los latinos', but not as much as we liked being with him), David S. (who took my work so seriously...), Jeremy, and in particular Raquel (with whom I shared much more than the discussions about science). From all of them together I have learnt the importance of team work.

The people I had the chance to work with: Randy Ross (who was the first), Martin Rees (who has always had time for discussion), Tiziana Di Matteo (for her enthusiasm), Enrico (for so many things...) and Pierre-Olivier Petrucci (the nicest of the collaborators, and a good friend). Also I am indebted to Juri Poutanen and Annalisa Celotti, for the many fruitful discussions, to Mario Vietri and Luigi Stella, for their help and encouragement to come to Cambridge in the first place.

The many friends at the IoA: Manuela (for being herself), Pigi, Giulia and Silvia, Claudia and Felipe (for all the dinners that we had together), Jarle, Kristin and Enrico (who have always been so generous), Elena and Davide, Cristiano, Glenda, Francine (for all the old movies).

Anna and Stefano (for they were an example), Sara and Carlo: with them we have always been so happy.

Celine (so many lunch breaks...), because we went through all these years together: I've always known I could count on you.

The many friends in Cambridge: Daniele (not for the car, for all the rest), Salvatore (so roman, so english), Sukhy (who always put the others first), Rob and Sam, Ranjiit, Francesca, Elena, Kate, Alessandro, Enrico (Cambridgiano onorario), and all the others who made my days here more interesting and joyful.

My father, my mother and my sister (who maybe think I am doing something important), and all my friends in Italy.

Irene, per la felicitá degli ultimi dieci mesi.

Alessandra, perche' ti ho seguito, e mi hai mostrato le orbite giuste.

Summary

The spectral energy distribution (SED) of the gravitational power released as electromagnetic radiation when matter accretes onto a compact object and its temporal variability is the subject of my dissertation. Such SED is far from universal. Different accretion modes are possible, with different radiative properties. The main goal of accretion flows theory is to distinguish and understand all the possible different modes of accretion, and classify the observed sources in terms of of such modes. The state of the art of both accretion theory and observations is briefly reviewed in the first chapter. The spectra of accreting black holes clearly show different components, that are produced by different physical processes and originate from different regions of the accretion flow. One of those components is a quasi-thermal hump, produced by a geometrically thin, optically thick accretion disc, and its spectrum is discussed in the fourth chapter, where I also present a critical analysis of the usual interpretation of the most common model used to fit observed disc spectra (the so-called multicolour disc model). I show that such a model not only underestimates systematically the value of the inner disc radius, but that, when the accretion rate through the disc is allowed to change, the inner edge of the disc, as inferred from the multicolour model, appears to move even when it is in fact fixed at the innermost stable orbit. Most accreting black holes, either of stellar mass or supermassive, when observed with hard X-rays show also signs of a hot Comptonizing component in the flow, the so-called *corona*. This is the main subject of the work presented in the second and third chapters of the dissertation. Firstly, I argue that the observed properties of hard X-ray emission from accreting black holes constitute strong supporting evidence for a magnetically-dominated corona. I demonstrate how the inferred thermal energy content of the corona is far too low to explain the observed X-ray luminosities, unless the corona itself is in fact a reservoir, where the energy is mainly stored in the form of a magnetic field. Then I consider the emission of galactic black holes in the low/hard state and of low-luminosity AGN, that all are thought to be sources accreting at low rates. Advection (or convection) dominated accretion flows are usually considered the best candidates to explain their SED. I present an alternative possibility, involving strong, unbound, magnetic coronae. I discuss reasons why energetically dominant coronae are ideal sites for launching powerful jets/outflows, both MHD and thermally driven. In analysing the spectral properties of such coronal outflow dominated accretion discs, I reach the important conclusion that if the jet/outflow is, as it is likely, radiatively inefficient, then so is the source overall, even without advection of energy into the black hole being relevant for the dynamics of the accretion flow. To conclude the part of the thesis dedicated to the spectral properties, in the third chapter I will describe the effects of the presence of a hot corona on the observational properties of the reflection components. In the fifth chapter I consider the rapid aperiodic time variability observed in accreting black holes, focusing in particular on the simultaneous spectral variations associated with such noise. X-ray observations of Seyfert 1 galaxies offer the unique

possibility of observing spectral variability on timescales comparable to the dynamical time of the inner accretion flow. I show how a model of the heating of the corona in terms of correlated reconnecting magnetic structures (the 'thundercloud model') can be used to explain the observed short-term spectral and temporal variability. Finally, in the sixth chapter I apply the magnetic corona models previously discussed to the X-ray transient XTE J1118+480, which displays spectral properties typical of GBHC in the low/hard state, and unusually strong quasi-periodic oscillations both in the optical and in the X-ray bands. I make the case for a magnetically dominated outflowing corona as a plausible explanation for all the above mentioned phenomena in this source.

Contents

Contents **x**

List of Figures **xiii**

List of Tables **xv**

1 Introduction **1**
1.1 Overview 1
1.1.1 A second golden age? 3
1.2 Accretion discs around black holes 5
1.2.1 Standard accretion disc theory 6
1.2.2 The SLE solution 11
1.2.3 Radiatively inefficient accretion flows: I. optically thin solutions . 12
1.2.4 Radiatively inefficient accretion flows: II. optically thick solutions 13
1.2.5 Summary 13
1.3 Observations 14
1.3.1 Galactic Black Hole Candidates(GBHC) 14
1.3.2 Active Galactic Nuclei (AGN) and Quasars 18
1.4 Outline of the thesis 23

2 The physics of magnetic accretion disc coronae **25**
2.1 Introduction: magnetized accretion flows and coronae 25
2.2 The structure equations of a disc–corona system 27
2.2.1 The standard viscosity law case 28
2.2.2 The modified viscosity law case 29
2.3 Energetics of the observed accretion disc coronae 29
2.4 The spectrum of a structured magnetic corona 33
2.4.1 Structured coronae and thermal Comptonization 33
2.4.2 The X-ray spectrum 34
2.5 Coronal outflow dominated discs 39
2.5.1 Coronal strength at low accretion rates 40
2.5.2 The fate of the coronal energy: coronal heating and Jet launching mechanisms 43
2.5.3 Predicted spectra 49
2.5.4 ADAFs or Jets? 50
2.6 Summary and conclusions 54

3 The effects of a Comptonizing corona on the observed reflection component in black hole spectra 56
3.1 Introduction . . . 56
3.2 The model . . . 58
3.3 Comptonization effects on the reflection hump shape . . . 59
3.3.1 Dependence on the physical parameters of the corona . . . 59
3.3.2 Dependence on the inclination angle . . . 63
3.4 Comptonization effects on the iron line . . . 64
3.5 Application to fitting procedures . . . 66
3.6 Observational consequences . . . 69
3.6.1 The case of NGC 4258 . . . 69
3.6.2 Correlations between reflection features and X-ray spectral slope . 71
3.6.3 Consequences for the X-ray background . . . 72
3.7 Summary and conclusions . . . 73

4 The spectrum of an accretion disc 76
4.1 Introduction: theoretical models . . . 76
4.2 The observational perspective . . . 77
4.2.1 The multicolour disc model . . . 78
4.3 A critical assessment of the multicolour disc model . . . 79
4.3.1 Results from simulations . . . 82
4.4 Summary and conclusions . . . 85

5 Aperiodic time variability in black hole accretion flows 89
5.1 Introduction . . . 89
5.1.1 Variability in AGN . . . 89
5.1.2 Variability in GBHC . . . 91
5.2 The thundercloud model . . . 91
5.2.1 Active regions distribution and luminosity . . . 93
5.2.2 Time variability and Power Density Spectra . . . 96
5.2.3 The full picture: results from simulated lightcurves . . . 96
5.2.4 Discussion . . . 110
5.2.5 Conclusions . . . 115
5.3 Quiescent times in gamma-ray bursts . . . 117
5.3.1 Introduction . . . 117
5.3.2 Observational results: a new correlation . . . 118
5.3.3 Discussion . . . 121
5.4 Summary and conclusions . . . 125

6 The case of the X-ray transient XTE J1118+480 127
6.1 Introduction . . . 127
6.2 Observations . . . 127
6.3 Cyclo-synchrotron emission from a magnetic corona . . . 130
6.4 Models for the broad-band spectrum . . . 132
6.4.1 The ADAF model . . . 132
6.4.2 The coronal outflow model . . . 134
6.4.3 Jet power and magnetic field intensity . . . 138
6.4.4 The warm absorber . . . 138
6.5 The evolution of the ~ 0.1 Hz QPO and the inner disc . . . 141
6.6 Discussion . . . 142

7 Conclusions and future work **144**
7.1 Future work . . . 148
7.1.1 Coronal outflows . . . 148
7.1.2 Magnetic flare models and X-ray spectral variability . . . 148
7.1.3 Models for the accretion disc spectra . . . 148
7.1.4 Time variability in galactic black hole candidates . . . 149
7.1.5 Internal shock and temporal structures in gamma-ray bursts . . . 149

Bibliography **150**

List of Figures

1.1 Branches of radiatively efficient of inefficient accretion flows for two values of the viscosity parameter 15

2.1 Relative energy densities of the cooling terms for coronal active regions of different sizes 36
2.2 Equilibrium temperature and spectral index of a coronal active region as a function of its size 38
2.3 The integral fraction of accretion power dissipated into the corona as a function of the accretion rate for $\alpha_{\mathrm{v}} = 0.3$ and for two different values of central black hole 42
2.4 Variation of the optical depth and electron temperature in the corona, and of the X-ray spectral index as functions of the accretion rate 47
2.5 Relative strength of thermally driven coronal outflow as a function of the accretion rate 48
2.6 Accretion rate at which most of the energy is dissipated outside the disc ($f > 0.5$) or into the jet/outflow ($f\eta > 0.5$) as a function of the central source mass 49
2.7 SED of coronal dominated outflow solutions at different accretion rates for $m = 10$. 51
2.8 SED of coronal dominated outflow solutions at different accretion rates for $m = 10^8$. 52

3.1 (a)The comptonized and uncomptonized reflection humps, R_{comp} and R_{dir}, for different values of the coronal optical depth, the temperature being fixed to kT_{e}=50 keV and (b) Differences (in %) between the outgoing spectra in the two cases 58
3.2 As in Figures 3.1a and 3.1b, but for a constant Compton parameter y equal to 0.6 60
3.3 R_{comp} (solid line), R_{dir} (dashed line) and R_{pexrav} (dot-dashed line) at two different viewing angles: (a) μ=0.9 and (b) μ=0.3. 61
3.4 (a) Comptonized (solid lines) and uncomptonized (dashed lines) reflection humps, R_{comp} and R_{dir}, for different viewing angles and (b) Deviations (in %) between the outgoing spectra 62
3.5 Reduced equivalent width $EW_{\mathrm{comp}}(\mu)/EW_{\mathrm{dir}}(\mu = 1)$ of the comptonized iron line as a function of the optical depth of the corona for different inclination angles 65
3.6 Ratio R_1/R_2 as a function of the coronal optical depth for different viewing angles at constant $y = 0.6$ 67
3.7 Ratio $E_{c,2}/E_{c,1}$ versus the coronal optical depth, for different values of μ . 68

3.8 Intrinsic (before Comptonization) iron line equivalent widths for the three Seyfert 1 spectral classes as defined in LZ01 in the case of slab and spherical geometry for the corona 70
3.9 Angle-averaged reflection humps, direct and comptonized, that may be relevant for models of the X-ray background 74

4.1 Emergent spectra at $r = 7$ in the cases of lowest energy dissipated in the disc 83
4.2 Comparison between realistic accretion disc spectra and multicolour models 84
4.3 (a) Estimated inner disc radius $R_{\rm col}$ as a function of the gravitational power dissipated in the disc. (b) The spectral hardening factor needed to rescale the computed $R_{\rm col}$ to the real $R_{\rm in}$. 86

5.1 Two maps of the accretion disc corona generated by two random realization of the thundercloud model 95
5.2 An AGN lightcurve with the thundercloud model 97
5.3 Power density spectrum of a simulated lightcurve 98
5.4 The photon index – luminosity correlation as obtained from thundercloud model simulations 100
5.5 The photon index – luminosity correlation as observed in the Seyfert 1 galaxy MCG–6-30-15 by *RXTE* in 1997 102
5.6 The photon index – luminosity correlation as observed in the Seyfert 1 galaxy MCG–6-30-15 in 1999 by *ASCA* 103
5.7 Variation of the power density spectrum with the covering fraction 106
5.8 Variance–luminosity correlation. Different durations, at fixed resolution . 108
5.9 Variance–luminosity correlation. Different time resolutions, at fixed duration 109
5.10 The estimated iron line luminosity as a function of the observed flux in the 3-10 keV band as obtained from thundercloud model simulations . . . 114
5.11 Time profile of two long GRBs exhibiting quiescent times 119
5.12 Distribution of GRB durations 120
5.13 Correlations between the temporal properties of the different emission periods 122

6.1 Time evolution of the low frequency QPO in XTE J1118+480 129
6.2 The geometrical factor $g(H_a/R_a)$ 131
6.3 SED for XTE J1118+480 and ADAF spectral models. From Esin *et al.* (2001) 133
6.4 Magnetic flare model SED for XTE J1118+480 137
6.5 Cloudy model for the high energy SED of XTE J1118+480 observed by *BeppoSAX* on April 14-15, 2000. 139
6.6 Cloudy model for the high energy SED of XTE J1118+480 observed by *Chandra-RXTE* on April 18, 2000. 140

List of Tables

1.1 AGN taxonomy 20

4.1 Physical parameters for our accretion disc models 82
4.2 Multicolour disc fit parameters. 85

5.1 Results from simulations and best fit parameters for the Γ-luminosity relation, fitted with a function of the form $\Gamma = \Gamma_0 - KL^{\delta}$ 104
5.2 Fractional rms from thundercloud simulations with fixed $\tau = 1.5$ as a function of C and D 107
5.3 Results from simulations and best fit parameters for the σ-luminosity relation at fixed time resolution. 109
5.4 Results from simulations and best fit parameters for the σ-luminosity relation, at fixed segment length and different time resolutions 110

6.1 Model parameters for the two predicted SED of XTE J1118+480 136

Chapter 1

Introduction

1.1 Overview: Theory and observations of black holes in the universe. A second golden age ?

The scientific concept of a black hole is a perfect example of the vital interplay between experimental scientists (or observers) and theorists. Indeed, black hole astrophysics began and developed into a mature science in the same decade during which the mathematical theory of black holes made its greatest progress. Although the many different scientific communities involved in those years (radio, optical and X-ray astronomers on the observational side, mathematicians and theoretical physicists on the theoretical one) did not interact very closely, such a temporal coincidence cannot be accidental. The history of the development of black hole physics (both theoretical and observational) in the years between the early '60s and the early '70s (the so-called *golden age*[1]) has been beautifully written about by Kip Thorne in his book "Black Holes and time warps: Einstein's outrageous legacy" (Thorne, 1994), where the reader can find a more complete set of references and biographical notes. Here I briefly summarize some of the most important and influential discoveries of the epoch.

From the theoretical point of view, those were the years when the "beauty" of black holes as mathematical entities was fully acknowledged. Of course, mathematical beauty appeals to a quite different aesthetic than the one we refer to in our everyday life judgments. Indeed, we say that black holes are beautiful because they are very simple mathematical objects (in the sense that they are relatively easy to define rigorously), but they are sources of immense complexity (in the sense that their physical interactions with the external universe are very difficult to predict). Both these aspects of simplicity and far reaching complexity were explored during the golden age as never before or after. The Kerr solution for the Einstein equations was discovered in 1962 (Kerr, 1963), and in the early '70s it was clear that such a solution described every uncharged black hole that could possibly exist. In those years, thanks in particular to the work of B.

[1] This name was given to those years by the Caltech graduate Bill Press (Thorne, 1994)

Carter (see e.g. Carter, 1968), the physical properties of this solution were investigated. Geodesic orbits of free particles around spinning black holes were calculated exactly from the Kerr metric, and the foundations were laid for the rigorous development of relativistic accretion theory. Furthermore, the idea that "black holes have no hair", i.e. that all their physical properties are completely described by just three parameters (mass, charge and angular momentum) was first conjectured in 1964, and decisive steps towards its proof were made in the same years. A great effort was also devoted to the study of the conditions under which collapsing stars leave a black hole remnant behind. Finally, it is worth mentioning the discovery, made by Penrose in 1969, that a spinning black hole stores rotational energy in the region of the space-time just outside the horizon (therefore called *ergosphere*) and that this energy can actually be extracted. Such a fundamental discovery paved the way for a number of astrophysical new ideas about how powerful jets can be launched by a black hole, the first and foremost of which was the Blandford-Znajek effect (Blandford and Znajek, 1977).

Along with the above mentioned progress achieved mainly by general relativists during the golden age in the basic understanding of the mathematical structure of black hole space-time, a number of more strictly astrophysical problems were tackled in the same years, concerning the interaction between black holes and their environment. The very concept of an accretion disc as a source of radiation powerful enough to be the origin of quasar light and of the high energy emission from X-ray binaries (see below) was proposed by Lynden-Bell (1969) and formalized into what is still considered the standard picture by Shakura and Sunyaev (1973) (see Section 1.2 for more details). By studying the effects of space-time dragging around rotating holes on the accretion discs around them (the general relativistic analogous of the Lense-Thirring effect), Bardeen and Petterson (1975) realized that rapidly spinning black holes behave like gyroscopes. Not only do they keep their axis of rotation fixed, but they also force the accreting gas swirling around them to remain oriented in the same direction. Such powerful gyroscopes are indeed what is needed to explain the perfect alignment of many observed extra-galactic jets.

The observational perspective was also revolutionized in the same years. X-ray astronomy was born in 1962, when the first Geiger-counter was launched and the first galactic X-ray source was discovered (the neutron star Sco X-1). A few years later, what subsequently became the first black hole candidate, Cyg X-1, was discovered (1964), while the first X-ray telescope, *UHURU*, launched in 1970, by providing accurate positions made possible multiwavelength studies of X-ray binaries. Those led, in the following three decades, to the identification of a dozen more black hole candidates in the galaxy (see Section 1.3.1).

The sixties were also the years during which quasars and active galactic nuclei were discovered. In 1960, Allan Sandage discovered an odd-looking star-like object (a quasi-star, or *Quasar*) while observing the error box of the radio galaxy 3C48 with a five meters optical telescope. Other similar objects were discovered immediately afterwards, but it was only three years later that a revolutionary explanation was found for their spectra, when Maarten Schmidt realized that one of them, 3C273, was in fact a very distant object, whose light (and spectral lines) were red-shifted as a result of the universe's expansion. In a few years, with the evidence accumulating for many other very luminous, extremely variable quasars, it became clear that gravity, in the form of accreting supermassive black holes ($\sim$100 million times heavier than the sun), was the only reasonable source of power for those extraordinary objects (as originally proposed by Salpeter, 1964 and Zeldovich and Novikov, 1964). The radio emission from quasars, their spectra and morphologies were also the subjects of intense study during the golden age. Indeed, it was in the early seventies (Rees, 1971; Longair *et al.*, 1973) that the explanation of the observed radio lobes as gas jets powered by the very same central sources ('active galactic nuclei') powering the radio and optical cores was put forward.

To summarize, in approximately fifteen years between 1960 and 1975, black hole astrophysics was transformed from an exotic subject into a well established science, with a solid theoretical background and an active observational side. At the end of the golden age, many physicists could assert that black holes existed and could be studied as dynamical celestial bodies.

1.1.1 A second golden age?

Approximately twenty years after the end of the golden age, black hole astrophysics has apparently burst into a new period of great prosperity, that still lasts today. Is it a second golden age?

Once again, both theoretical and observational astrophysicists are responsible for such a flourishing. Theorists have renewed their interest in accretion theory since the ADAF solution was rediscovered by Narayan and Yi (1994). The systematic study and classification of the different accretion modes carried out in the last few years, has brought us to a better understanding of the interactions between a black hole and its environment (see Section 1.2). Also, in the last ten years, great progresses have been made in theory of accretion disc turbulent viscosity (Balbus and Hawley, 1998), to the extent that we believe we now understand the basic micro-physical nature of accretion. At the same time, the rapid improvement of numerical simulations will make it possible, in the near future, to study the complexities of accretion flows with computer experiments.

On the observational side, black holes are being used to test general relativity in the strong field regime for the first time. This has been possible thanks to X-ray spectroscopy (studies of the broad fluorescent iron line profiles from AGN accretion discs; see Fabian *et al.*, 2000, and references therein) and timing analysis (studies of rapid quasi-periodic oscillations in X-ray binaries; see van der Klis, 2000, and references therein). But probably the most important observational evidence that has accumulated in recent years, is the existence of massive black holes in the nuclei of many, perhaps *all* galaxies (Magorrian *et al.*, 1998; Kormendy and Richstone, 1995). Even more crucially, the tight correlation found between nuclear black hole masses and host galaxies velocity dispersions (Ferrarese and Merritt, 2000; Gebhardt *et al.*, 2000) has made clear that the formation and evolution of galaxies and black holes are intertwined subjects. Thus, to understand galaxy formation we have to take into account the black holes in their center. Ideally, a complete 'black hole demography' at all redshift, i.e. the census of all accreting black holes and of their most important parameters (mass, spin, accretion rate, radiative efficiency, outflowing rate) would be the final goal, and would probably give a decisive contribution to our understanding of galaxy formation. This is a daunting task. Even measuring the masses of the more distant supermassive black holes would be of the greatest importance today. But to do so, we can rely only on the observed properties of the nuclear spectral energy distribution and variability. Therefore, we need to know better how black hole accretion works.

It is also becoming clear that black hole *formation* plays a fundamental role in the early stages of the life of a galaxy, and is therefore regarded now as an interesting problem for cosmology, not only for stellar evolution. Gamma-ray bursts (GRBs) may be of crucial importance regarding this latter point. As a matter of fact, since the discovery of X-ray and optical counterparts of GRBs in 1997, the idea that such extraordinary events are the manifestation of the collapse of a massive star forming a black hole has become widely accepted. If we are able to deduce from the observed properties of bursts and afterglows the properties of the inner engines powering them, and unveil some of the physics of black hole formation, another giant step will be made towards the understanding of the formation of the first structures in the universe.

To summarize, three are the main rationales for the study of black holes today. Firstly, as the existence of black holes is the most far-reaching implication of the theory of general relativity (together with the Big Bang cosmological theory), we can use them to *test GR*, and we can do this better than with cosmology, as there is no dark matter problem to complicate the interpretation of our observations.

Secondly, we would like to better understand how black hole accretion and jet production work *per se*, because they are extremely interesting (and complex) astrophysical problems. Their study requires a great amount of knowledge of different fields of physics and astronomy, from magneto-hydrodynamics to radiative transfer, from general relativity to atomic physics.

Thirdly, as we have just illustrated, we would like to understand black hole formation and evolution in order to understand the formation and the evolution of the first structures of the universe.

During the first golden age of black holes astrophysics, the main goals were finding proofs of their mere existence and defining their basic interactions with the environment. Such goals only touched on the first two of the rationales listed above. In the last few years, instead, black hole astrophysics has acknowledged the relevance of its subject for a broader cosmological context, and for this reason it seems appropriate to talk of a second golden age.

The work presented in this thesis is aimed at a better understanding of the phenomenon of accretion onto black holes, with the final goal of determining its physical properties from the observable ones. From such a point of view, it will be natural to discuss, at times, stellar mass and supermassive black holes, and even γ-ray bursts, to the extent that studying any of these, admittedly very different, classes of objects can be useful to understand another class, and, in the end, to unveil the physics of black holes and their role in the universe.

1.2 Accretion discs around black holes

Accretion is the physical process by which celestial bodies aggregate matter from their surroundings. The gravitational binding energy that such matter must release for accretion to occur is a powerful source of luminosity. If the accreting material possesses angular momentum, though, gravitational contraction is severely impeded by a centrifugal barrier, as specific angular momentum is hard to dispose of, and not easily separated from infalling fluid elements. The formation of a disc in this case is unavoidable. It is this disc that mediates the process of accretion: neighboring annuli of differentially rotating matter experience a viscous shear (of some kind) that transports angular momentum outwards and allows matter to slowly spiral in towards the center of the gravitational potential.

The efficiency of the process, defined as the ratio of the output luminosity divided by the rest mass energy accretion rate,

$$\epsilon \equiv L/\dot{M}c^2, \tag{1.1}$$

depends crucially on the inner boundary condition, therefore on the nature of the central accreting body. Gas falling from infinity on a gravitating body of mass M must dissipate an amount of energy equal to GM/R_* to be brought to rest at the distance R_* from the center of the potential (for example on the surface of a star). Alternatively, if the infalling matter settles into a Keplerian orbit at the distance R, the amount of energy that must be dissipated is equal to $GM/2R$. In both cases, for a given central body mass M and external accretion rate $\dot{M}$, the more compact the central gravitational body is, the closer to it the matter can get, and the larger is the amount of potential energy that must be radiated. Thus, the higher radiative efficiency is associated to the most compact of all celestial bodies: black holes[2].

The bolometric luminosity of an accretion disc is usually characterized (and in general limited) by the so-called *Eddington luminosity* $L_{\rm E}$. This quantity is the luminosity at which the radiative momentum flux from a spherically symmetric source is balanced by the gravitational force of the central object. Because both the radiation flux and the Newtonian force diminish as the inverse square of the distance, the Eddington luminosity depends only on the central mass and on fundamental constants:

$$L_{\rm E} = \frac{4\pi G m_{\rm p} M c}{\sigma_{\rm T}} \simeq 1.3 \times 10^{38} \frac{M}{M_\odot} \text{ erg s}^{-1}, \tag{1.2}$$

[2]It is worth stressing here that, in the case of black holes and neutron stars, general relativistic modifications of the metric outside the compact sources play an important role in determining the accretion efficiency (Novikov and Thorne, 1973).

where $m_{\rm p}$ is the proton mass, c the speed of light and $\sigma_{\rm T}$ the Thompson scattering cross section.

When in the 1960s the first compact X-ray sources were discovered, with luminosity comparable to the Eddington one for a stellar mass object, it was soon realized that accretion discs were a natural candidate to explain them (Prendergast and Burbidge, 1968)[3]. The accretion disc/black hole paradigm for the central power source of quasars soon followed (Lynden-Bell, 1969), and the so-called "standard model" of accretion discs was in place already in 1973 thanks to the seminal works of Pringle and Rees (1972), Shakura and Sunyaev (1973), and to their general relativistic generalization by Novikov and Thorne (1973).

Since then, as the observational evidences of accreting black holes steadily grew with the evolution of X-ray astronomy, it became clear that the spectral energy distribution (SED) of the gravitational power released as electromagnetic radiation when matter accretes onto a compact object is far from universal. Different accretion modes are possible, and often the same initial conditions at the outer boundaries admit more than one solution for the accretion flow configuration at the inner boundary, with different radiative properties. Therefore, the main goal of accretion flows theory has become to distinguish and understand all the possible different modes of accretion, and classify the observed sources in terms of such modes.

In the following sections I will briefly outline the theoretical properties of the different accretion modes. I will first describe the standard, radiatively efficient disc solution originally discovered by Shakura and Sunyaev (1973) and present a slightly different derivation of the structure equations (Section 1.2.1); then I will briefly introduce alternative accretion flow solutions (Sections 1.2.2, 1.2.3 and 1.2.4), before summarizing our understanding of the relationships between them.

1.2.1 Standard accretion disc theory

In the following section the main equations for a standard, geometrically thin and optically thick accretion disc, that will be used throughout this thesis, will be derived in a simple way. A full discussion of the many issues of the standard accretion disc theory that will not be covered here can be found in Pringle (1981); Frank *et al.* (1992); Papaloizou and Lin (1995).

Our fiducial disc system consists of a point mass potential situated at the center of the disc (and of our coordinate system, in which we will denote by z the vertical axis) and a gaseous flow around it. In a steady state, the disc structure is determined by solving simultaneously four conservation equations (conservation of vertical momentum, mass, angular momentum and energy). If the equations of state for the pressure P and opacity κ as functions of density and temperature of the infalling matter are also given

$$P = P(\rho, T)$$

[3] In fact, the importance of accretion processes onto collapsed objects was first pointed out by Salpeter (1964) and Zeldovich and Novikov (1964) to explain the extremely large luminosity of Quasars.

$$\kappa = \kappa(\rho, T)$$

together with a viscosity law, the full disc structure can be calculated exactly.

The flow is assumed to be geometrically thin, in the sense that its pressure vertical scaleheight, $H \equiv \frac{1}{2P}\frac{\partial P}{\partial z}$, at a distance R, is much smaller than the radial coordinate $H \ll R$. In fact, since there is no *net* motion of the gas in the vertical direction, conservation of vertical momentum reduces to the equation of hydrostatic equilibrium

$$\frac{\partial P}{\partial z} = -\frac{\rho G M}{R^3} z, \tag{1.3}$$

that determines the disc vertical structure. From this equation it is easy to show that

$$\frac{H}{R} \simeq \frac{c_{\rm s}}{v_{\rm K}}, \tag{1.4}$$

namely the ratio of the vertical pressure disc scaleheight to the disc radius is approximately equal to the ratio of the local isothermal sound speed $c_{\rm s} = (P/\rho)^{1/2}$ to the local Keplerian velocity $v_{\rm K} = (GM/R)^{1/2}$. It will be demonstrated below that *assuming* discs are geometrically thin, the structure equations will indeed lead to the conclusion that such discs are "cool" enough in that $kT \ll GMm_{\rm p}/R$, and therefore $H/R \simeq c_{\rm s}/v_{\rm K} \ll 1$.

The mass conservation equation for steady state accretion reads

$$\dot{M} = -2\pi R \Sigma v_r, \tag{1.5}$$

where $\Sigma = \int_{-\infty}^{+\infty} \rho dz \simeq 2H\rho$ is the surface density and v_r is the radial velocity of the spiraling matter.

Angular momentum conservation can be expressed by equaling the torque exerted by viscous stresses to the net rate of change of angular momentum. This yields

$$W_{R\phi} = \frac{\dot{M}\Omega}{2\pi\Sigma}\left[1 - \left(\frac{R_{\rm in}}{R}\right)^{1/2}\right], \tag{1.6}$$

where $W_{R\phi}$ is the dominant $R - \phi$ component of the stress tensor, $\Omega = (GM/R^3)^{1/2}$ is the angular velocity and the last term in square bracket comes from the no-torque at the inner boundary condition, and simply measures the rate at which the angular momentum is deposited onto the compact object.

From the energy conservation equation we obtain that the radial flux of energy $\mathcal{F}_{\rm E}$ is given by the sum of two terms: the first is due to the local release of gravitational energy, the second comes from the energy flow induced by the forces that transport angular momentum outwards,

$$\mathcal{F}_{\rm E} = \frac{\dot{M} R \Omega^2}{4\pi} + \Sigma R \Omega W_{R\phi} = \frac{3GM\dot{M}}{4\pi R^2}\left[1 - \frac{2}{3}\left(\frac{R_{\rm in}}{R}\right)^{1/2}\right]. \tag{1.7}$$

The surface emissivity can then be calculated by taking the opposite of the divergence of the flux. Dividing by a factor of two for each side of the disc yields a final value for the emissivity (heat production rate) of

$$Q_+ = \frac{3GM\dot{M}}{8\pi R^3}\left[1 - \left(\frac{R_{\rm in}}{R}\right)^{1/2}\right], \tag{1.8}$$

which is completely independent on the yet unspecified viscosity law.

Understanding the nature of the disc viscosity, and therefore understanding *how* can the disc accrete, has been (and partially still is) the central problem of accretion disc theory (see e.g. Papaloizou and Lin, 1995; Brandenburg, 1998 and Balbus and Hawley, 1998 for recent reviews on the subject of viscosity and turbulence in accretion discs). From the observational point of view, the accretion rates needed to explain the luminosities we see are many orders of magnitude larger than standard microscopic viscosities (see e.g. Spitzer, 1962) could provide. If, on the other hand, the disc is turbulent, the effective viscosity due to interacting eddies could easily be large enough to provide the needed accretion rates. Shakura and Sunyaev (1973), recognizing the central importance of the nature of the stress tensor $W_{R\phi}$, in face of the theoretical uncertainties, proposed the dimensional scaling

$$W_{R\phi} = \alpha_{\rm v} c_{\rm s}^2, \tag{1.9}$$

that allows the closure of the system of equation for the accretion disc structure. They also recognized that the viscosity parameter should be limited by $\alpha_{\rm v} \lesssim 1$, because the turbulent velocities, whose correlation determines $W_{R\phi}$, would be limited by the local sound speed, otherwise shocks would develop in the flow, reducing the turbulent velocities below $c_{\rm s}$.

Finally, let us examine the equation of state and the equation of radiative transport. In the conditions typical of accretion flows around compact objects the main contribution to the opacity of the matter come from Thompson scattering on free electrons, for which

$$\bar{\kappa}_{\rm es} \simeq 0.4 \text{ cm}^2 \text{ g}^{-1}, \tag{1.10}$$

and from free-free absorption, for which

$$\bar{\kappa}_{\rm ff} \simeq 0.64 \times 10^{23} \rho T^{-7/2} \text{ cm}^2 \text{ g}^{-1}. \tag{1.11}$$

Roughly, the total Rosseland mean opacity satisfies

$$\frac{1}{\bar{\kappa}(\rho, T)} \approx \frac{1}{\bar{\kappa}_{\rm ff}} + \frac{1}{\bar{\kappa}_{\rm es}} \tag{1.12}$$

For what concerns the equation of state, the total pressure in the disc is given by the sum of thermal gas and radiation pressure. For ionized hydrogen this yields

$$P(\rho, T) = P_{\rm gas} + P_{\rm rad} = \frac{2\rho k T}{m_{\rm p}} + \frac{aT^4}{3}. \tag{1.13}$$

In geometrically thin accretion disc the internally generated heat Q_+ is transported vertically by radiation before being radiated at the surface. For optically thick discs, photons are transported to the surface via diffusion, then the vertical photon flux is given by

$$F(z) = \frac{c}{\rho \bar{\kappa}} \frac{dP_{\rm rad}}{dz}. \tag{1.14}$$

Therefore the energy dissipation is locally balanced by radiation from the two disc surfaces, and we have

$$Q_- = \int_{-H}^{+H} F(z)dz \equiv F_0 = Q_+, \tag{1.15}$$

so that we can say thin discs are radiatively efficient.

Disc structure equations

The final expressions for the physical quantities that determines the disc structure as functions of central source mass (in units of a solar mass $m \equiv M/M_\odot$), accretion rate (in units of Eddington accretion rate $\dot{m} \equiv \epsilon \dot{M} c^2/L_{\rm Edd}$), viscosity parameter and distance from the center (in units of Schwarzschild radii $r \equiv R/R_{\rm S} = Rc^2/2GM$) have simple algebraic expression when both total pressure and opacity are dominated by one of the two terms that contribute to their determination. For what concerns opacity, as the free-free absorption is strongly suppressed at high temperatures, electron scattering dominates as the main source of opacity in the inner, hotter parts of the disc, while free-free absorption dominates in the outermost, colder parts. Analogously, gas pressure dominates in the outer regions of the disc, while radiation pressure becomes predominant in the inner regions. Overall, three regions can be distinguished in a standard geometrically thin, optically thick accretion disc (Shakura and Sunyaev, 1973):

(a) An inner part where electron scattering determines the opacity and radiation pressure is larger than gas pressure.

(b) A middle region where electron scattering is still more important than free-free absorption, but gas pressure dominates over radiation pressure;

(c) An outer region, where thermal gas pressure dominates and free-free absorption is the main source of opacity.

We summarize below the main equation for the structure of the two inner parts (a) and (b), using for simplicity the Newtonian approximation, as in Shakura and Sunyaev (1973), and an efficiency $\epsilon = 0.082$ appropriate for non-rotating (Newtonian) black holes. For simplicity, we introduce also the function $J(r) = 1 - \sqrt{r_{\rm in}/r}$, with $r_{\rm in} = 3$ corresponding to the innermost stable circular orbit of a free particle around a non-rotating black hole.

(a) If gas pressure can be neglected and electron scattering is the main source of opacity, Eq. (1.14) for the flux radiated at the disc surface becomes

$$F_0 = Q = \frac{2acT^4}{3\rho H \bar{\kappa}_{\rm es}}. \tag{1.16}$$

Therefore we obtain, for the disc scaleheight, pressure, density (both calculated at the disc mid-plane), temperature, and ratio of the radiation to gas pressure, respectively:

$$
\begin{aligned}
h &\equiv \frac{H}{R_{\rm S}} \simeq 10.6\dot{m}J(r) &(1.17)\\
P &\simeq 3.58\times 10^{15}(\alpha_{\rm v}m)^{-1}r^{-3/2}\ \text{dyne} &(1.18)\\
\rho &\simeq 1.42\times 10^{-7}(\alpha_{\rm v}m)^{-1}r^{3/2}[\dot{m}J(r)]^{-2}\ \text{g cm}^{-3} &(1.19)\\
T &\simeq 3.45\times 10^{7}(\alpha_{\rm v}m)^{-1/4}r^{-3/8}\ \text{K} &(1.20)\\
\frac{P_{\rm rad}}{P_{\rm gas}} &\simeq 4.36\times 10^{6}(\alpha_{\rm v}m)^{1/4}r^{-21/8}[\dot{m}J(r)]^{2}. &(1.21)
\end{aligned}
$$

However, it is worth stressing that such radiation pressure dominated solution is viscously (Lightman and Eardley, 1974) and thermally (Shakura and Suniaev, 1976; Pringle, 1976) unstable, that makes its physical interpretation somewhat problematic. For a review of disc instability see Krolik (1999).

(b) If, instead, gas pressure dominates, and electron scattering is still the main source of opacity, Eq. (1.14) becomes

$$
F_0 = Q = \frac{8\xi acT^4}{3\rho H\bar{\kappa}_{\rm es}}, \tag{1.22}
$$

where we have introduced the numerical factor ξ to take into account the difference in the vertical density profile that should enter in the definition of the disc scaleheight H. The value of ξ can be fixed by imposing continuity of all physical quantities at the boundary between regions (a) and (b) and turns out to be $\xi \simeq 1/3$. The disc structure can be summarized as follows:

$$
\begin{aligned}
h &\simeq 2.02\times 10^{-2}\xi^{-3/32}(\alpha_{\rm v}m)^{-1/10}r^{21/20}[\dot{m}J(r)]^{1/5} &(1.23)\\
P &\simeq 1.88\times 10^{18}\xi^{3/32}(\alpha_{\rm v}m)^{-9/10}r^{-51/20}[\dot{m}J(r)]^{4/5}\ \text{dyne} &(1.24)\\
\rho &\simeq 20.3\xi^{11/32}(\alpha_{\rm v}m)^{-7/10}r^{-33/20}[\dot{m}J(r)]^{2/5}\ \text{g cm}^{-3} &(1.25)\\
T &\simeq 5.6\times 10^{8}\xi^{-1/4}(\alpha_{\rm v}m)^{-1/5}r^{-9/10}[\dot{m}J(r)]^{2/5}\ \text{K} &(1.26)\\
\frac{P_{\rm rad}}{P_{\rm gas}} &\simeq 1.31\times 10^{2}\xi^{-35/32}(\alpha_{\rm v}m)^{1/10}r^{-21/20}[\dot{m}J(r)]^{4/5}. &(1.27)
\end{aligned}
$$

The boundary between the two regions can be found by solving for r in the equation

$$
\frac{r}{J(r)^{16/21}} \simeq 350\alpha_{\rm v}^{2/21}m^{2/21}\dot{m}^{16/21}. \tag{1.28}
$$

For the left hand side in Eq. (1.28) has a minimum (for $r = 5.72$), there exist a critical value for the accretion rate below which there is no radiation pressure dominated zone in the disc, $\dot{m}_{\rm c} \simeq 1.42\times 10^{-2}\alpha_{\rm v}^{1/8}m^{1/8}$.

Equations (1.17) and (1.23) demonstrate what we had anticipated at the beginning of the section, namely that the disc is thin ($h \ll 1$), and therefore cool ($c_{\rm s} \ll v_{\rm K}$, see Eq. 1.4). This can be understood in terms of the relevant timescales in the disc. In fact, the time available for the accreting gas to radiate the energy released by the viscous stresses is given by the *viscous* (or accreting) timescale, which is

$$
t_{\rm v} = \frac{R}{-v_{\rm r}} = \frac{J(r)}{\alpha_{\rm v}\Omega}\left(\frac{R}{H}\right)^2, \tag{1.29}
$$

where we have made use of Eqs. (1.5), (1.6), (1.9) and (1.4). This is much larger than the typical *thermal* timescale, which gives the typical time over which the thermal equilibrium is reached in the disc by virtue of heating–cooling balance $Q_- = Q_+$ and is given by:

$$t_{\rm th} \simeq \frac{1}{\alpha_{\rm v}\Omega} \tag{1.30}$$

if the disc is thin.

The argument, though, is somewhat circular: if the disc is thin and $h \ll 1$, we can safely assume that the viscous heating is balanced locally by the radiative cooling from the disc surface, so that $Q_+ = Q_-$. In turn, the structure equations we can derive from this latter assumption ensure that $h \ll 1$. In the following sections we will discuss different possible solutions for an accretion flow with angular momentum, that are geometrically thick and/or radiatively inefficient.

1.2.2 The SLE solution

The first self consistent alternative solution for rotating accretion flows around black holes was discovered by Shapiro *et al.* (1976) as a way to explain the hard spectrum of the classical black hole candidate Cygnus X-1. Their solution is a *two temperature* one, with the protons much hotter than the electrons $T_{\rm p} \gg T_{\rm e}$. This would be the case if the energy released by viscous dissipation was distributed equally among the carriers of mass, i. e. mostly to the protons (which radiate very inefficiently) and only a fraction $m_{\rm e}/m_{\rm p} = 1/1833$ to the electrons. The hot proton component then dominates the pressure and keeps the disc geometrically thick. This in turn leads to low density (which scales as H^{-3} for given $\alpha_{\rm v}$ and $\dot{m}$) and low Coulomb energy exchange between protons and electrons, that self-consistently implies $T_{\rm p} \gg T_{\rm e}$. The four main equation of the disc structure are the same as in the standard model (see Section 1.2.1), but the heating–cooling balance is now described by two separate equations for the two species, where the electrons mainly cool by up-scattering soft radiation coming from an outer cold disc or from dense cloudlets embedded in the hot flow. The complete set of structure equations are described in Shapiro *et al.* (1976). The model was further developed to include effects of pair production (Liang, 1979; Björnsson and Svensson, 1992), a non-thermal particle distribution (Kusunose and Mineshige, 1995), and cyclo-synchrotron radiation (Kusunose and Zdziarski, 1994).

Although the model is able to reproduce reasonably well observed spectra of accreting black holes, it is thermally unstable (Piran, 1978): an increase in $T_{\rm p}$ would lead to disc expansion in the vertical direction, further reduction of Coulomb cooling and increase of proton temperature, leading to an instability.

This instability is cured if the effect of advection is taken into account in the energy equation, as will be briefly outlined in the following section.

1.2.3 Radiatively inefficient accretion flows: I. optically thin solutions

It was first noted by Ichimaru (1977) that, in an optically thin, geometrically thick accretion disc such as the one proposed by Shapiro *et al.* (1976), the density may be so low that the ions are unable to transfer energy to the electrons at an high enough rate for the radiative electronic cooling to balance the viscous heating. In this case, part of the energy is advected with the proton flow and swallowed by the central black hole. The energy equation then can be rewritten in a vertically integrated form:

$$q_+ - q_- = q_{\rm adv} \equiv \Sigma v_{\rm r} T \frac{\partial S}{\partial R}, \tag{1.31}$$

where S is the specific entropy of the gas, and $q_+ = \int Q_+ dz$, $q_- = \int {\rm div} F_r dz$.

This kind of solution was named the 'ion supported torus' by Rees *et al.* (1982), who also demonstrated that such a solution can be established only for accretion rates lower than a critical value

$$\dot{m} \lesssim \dot{m}_{\rm crit} \sim \alpha_{\rm v}^2, \tag{1.32}$$

ensuring that the density is low enough, either because the accretion rate is low, or the viscosity high. The flow is optically thin and radiatively inefficient. In recent years, much work has been devoted to the detailed study of such flows, renamed Advection Dominated Accretion Flows (ADAF) after Narayan and Yi (1994) presented a full analytical self-similar 1D solution to the problem (Narayan and Yi, 1995a,b; Abramowicz *et al.*, 1995; Narayan *et al.*, 1999). This self-similar solution reveals the basic properties of an ADAF:

(i) The radial accretion time-scale is much shorter that that of a thin disc;

(ii) Sub-Keplerian rotation occurs, due to large internal pressure support;

(iii) The flow is geometrically thick, in that the vertical scaleheight $H \sim R$.

More uncertain, but crucial, issues for two temperature advective flows are the assumptions that ions and electrons interact only through Coulomb collisions (see e.g. Begelman and Chiueh, 1988, for an alternative possibility involving collective plasma instabilities); that only a tiny fraction of the turbulent energy is dissipated into the electrons (Bisnovatyi-Kogan and Lovelace, 1997; Quataert and Gruzinov, 1999) and that the (tangled) magnetic field pressure is in equipartition with the gas pressure. These issues are important for determining not only physical, but also observable properties of an ADAF.

Furthermore, it is obvious that 1D, self-similar solutions are only approximate, and that the full solution is inherently two dimensional (Igumenshchev and Abramowicz, 2000). In fact, when the full 2D nature of the problem is analysed, both from the theoretical point of view (Abramowicz *et al.*, 2000; Narayan *et al.*, 2000) and from numerical simulations (Igumenshchev *et al.*, 2000), it is clear that radiatively inefficient flows are subject to to strong convective instabilities (and therefore should be better called Convection Dominated Accretion Flow, CDAF; Stone *et al.*, 1999; Quataert and Gruzinov, 2000). Depending on the values of the viscosity parameter $\alpha_{\rm v}$ and of the adiabatic index γ, four types of flow may exist: convective flows, large-scale circulations, pure inflows and bipolar outflows (Blandford and Begelman, 1999; Igumenshchev and Abramowicz, 2000). The energy is redistributed in the flow in different ways, and therefore the observed spectral energy distributions may be significantly different.

1.2.4 Radiatively inefficient accretion flows: II. optically thick solutions

The last class of accretion modes comprises the solutions for accretion rates close to (or above) the Eddington one. In these cases, the inflow timescale in the inner part of the disc becomes smaller than the time it takes for a photon to escape from the disc, and the radiation produced is trapped by the flow and advected with it (Katz, 1977; Begelman and Meier, 1982; Beloborodov, 1998). The radius inside which radiation is trapped (the so-called *trapping radius* Rees, 1978) moves outwards as the accretion rate increases.

When the accretion rate is of the order of the Eddington one, the disc thickness stays moderate and a vertically integrated approximation may be retained (*slim discs*, Abramowicz et al. 1988). In the limit $\dot{m} \gg 1$, though, the behaviour of the disc and the possible relevance of strong outflows (Meier, 1982; Lipunova, 1999) still remain open issues. Once again, the problem is inherently 2D, and the simultaneous roles of convection, advection and outflows have to be assessed in order to model properly the expected SED.

Unlike for the the optically thin ADAF/CDAF cases, the observable features of these optically thick solutions have been poorly investigated so far, thus reducing the general appreciation of their importance for the interpretation of observations. Szuszkiewicz *et al.* (1996) were the first to start investigating along this line. Watarai *et al.* (2000) studied the super-critical accretion flow in the context of galactic black hole candidates, while Mineshige *et al.* (2000) used the slim disc solution to model the spectra of Narrow-Lines Seyfert 1 galaxies (NLS1, see §1.3.2).

1.2.5 Summary

In this Section we have described the main theoretical properties of the different solutions for an accretion flow around a black hole. We have discussed in more detail, and outlined the derivation of, the structure equations for the standard geometrically thin and optically thick discs, that will be used extensively throughout the thesis.

Some of the main properties of the different solutions can be summarized by the diagram that places them in the optical depth (τ)–accretion rate ($\dot{m}$) plane (at fixed distance from the central source), as shown in Fig. 1.1. For low values of the viscosity parameter $\alpha_{\rm v}$, which is the most interesting and realistic case, the solutions split into two separate branches: the optically thin and the optically thick one. Optically thin solutions exist only at low accretion rates: they are the ADAF (thermally stable) and SLE (Shapiro-Lightman-Eardley, thermally unstable). On the other hand, at the same low accretion rates, also the Shakura and Sunyaev solution (1973, 'standard disk' in Fig. 1.1) is acceptable; it changes from being stable to unstable at the value of the accretion rate for which radiation pressure becomes larger than gas pressure at the given distance from the black hole. At even higher accretion rates only the radiatively inefficient, optically thick solution exists ('slim disk'), which is thermally stable. The topology of the diagram changes for high viscosity parameter: the advective, radiatively inefficient solutions (ADAF, slim disk) become a single joined branch, while the radiatively efficient solutions form a second branch, that exists only up to a critical accretion rate. The critical value of the viscosity parameter for which the change in topology occurs depends strongly on the radius and weakly on the black hole mass and has been found to be $\alpha_{\rm cr} \sim 1$ (Björnsson *et al.*, 1996). For a more detailed discussion of such unification schemes for the different branches of the accretion flow solutions see Abramowicz (1998).

We have therefore seen how theory predicts a rich variety of different accretion modes, with different observable properties, that have to be tested against the observations. In particular, one of the most interesting open questions regards the nature of the flow at sub-Eddington rates. In fact, both ADAF (or CDAF) and standard Shakura-Sunyaev models provide stable solutions for the flow equations. In the next section we will briefly describe the main observational properties both of galactic black hole candidates (GBHC) and active galactic nuclei (AGN), that can help us to better understand the nature of the inner accretion flow around black holes.

1.3 Observations

1.3.1 Galactic Black Hole Candidates (GBHC): X-ray binaries and microquasars

The theories of general relativity and stellar evolution unavoidably predict that the most massive stars, at the end of their nuclear-burning life cycle, will collapse and form a compact object. Furthermore, the laws of quantum physics and of the fundamental forces as we know them today, also predict that neutron stars more massive than about 3 solar masses (Rhoades and Ruffini, 1974) are unstable and must therefore collapse to form black holes, too. Then, according to our present knowledge, our own galaxy must be populated by a large number of black holes, remnants of the massive stars that first evolved off the main sequence. But how do we detect them?

In this section the main observational facts about GBHC are briefly summarized. For a more thoroughly discussion we refer the reader to the reviews by Tanaka and Lewin (1995) and Charles (1998).

Isolated black holes

Isolated stellar mass black holes, may accrete matter from the diffuse intergalactic medium, more likely in a spherical manner (Ipser and Price, 1982, 1983) or in the form of an optically thin ADAF (Fujita *et al.*, 1998). However, the expected

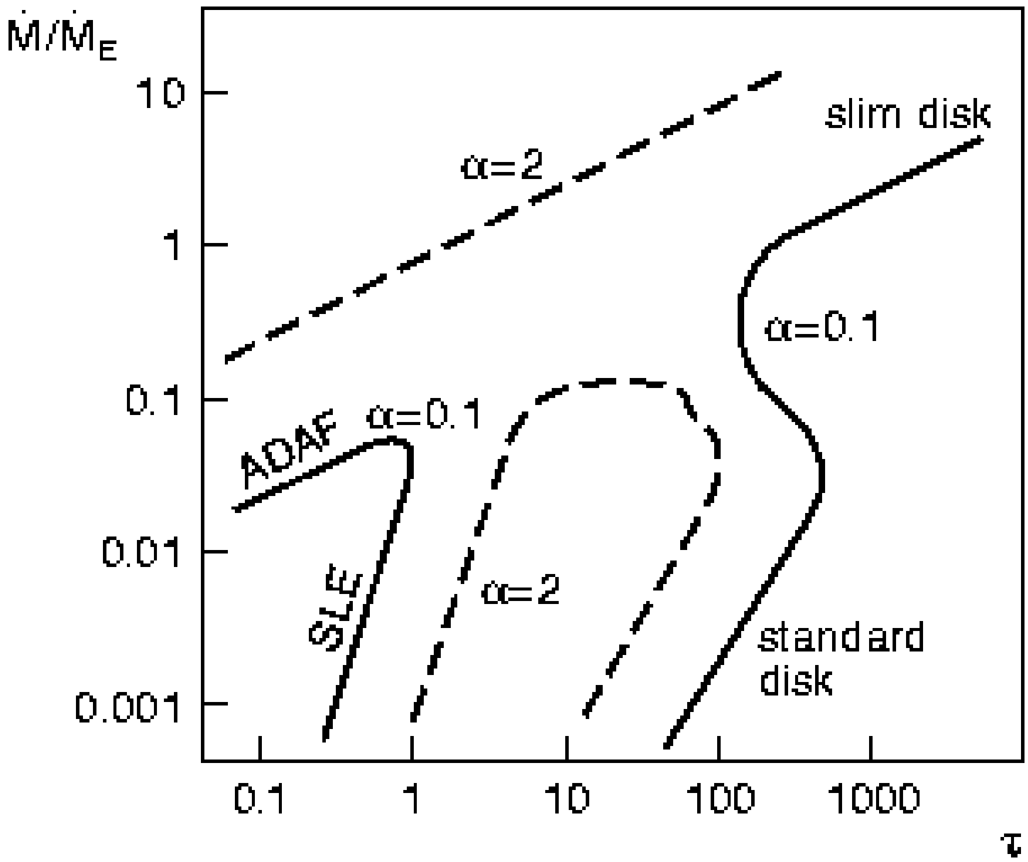

Figure 1.1: Schematic representation of the different branches of both radiatively efficient and inefficient accretion flows, for two values or the viscosity parameter $\alpha_{\rm v}$, as functions of accretion rate ($\dot{M}/\dot{M}_{\rm E}$, vertical axis) and (vertical) optical depth (τ, horizontal axis) of the flow (after Chen *et al.*, 1995 and Zdziarski, 1998). Optically thin branches are the ADAF and SLE (Shapiro-Lightman-Eardley) solutions, optically thick ones the radiation dominated ('slim disk') and Shakura-Sunyaev (or standard thin disk). Advection dominated are the ADAF and slim disk. The SLE solution is a thermally unstable branch, while the Shakura-Sunyaev solution has two branches: the gas pressure dominated one (positive slope, low accretion rate) is thermally stable, the radiation pressure dominated one (negative slope, high accretion rate) is thermally unstable. From Spruit (2000).

accretion rates and efficiencies and far too low to allow a direct observation with current or future X-ray telescopes, apart from the case of isolated black holes embedded in dense molecular clouds (Campana and Pardi, 1993; Fujita *et al.*, 1998). Alternatively, in the presence of a magnetic field, rotational energy could be extracted from black holes via the Blandford-Znajek (Blandford and Znajek, 1977) mechanism (BZ). If the black hole is rapidly rotating, the power from electromagnetic energy extraction exceeds the accretion luminosity for ADAFs at sufficiently low accretion rates (Armitage and Natarajan, 1999). Indeed, Armitage and Natarajan (1999) argue that their estimates of the BZ power are energetically consistent with associating isolated black holes with some unidentified EGRET gamma-ray sources (Dermer, 1997).

Black hole binaries and the state classification

Clearly, black holes in binary system are much more likely to interact strongly with their surroundings, and to accrete from the companion star at a high enough rate to be detected. In fact, the couple of dozen of candidates that has been added to the list of black holes in the Galaxy in the last thirty years are all members of a binary system.

When a compact object (neutron star or black hole) in a binary system accretes matter from its companion, either via a wind or via Roche lobe overflow, the inner part of the accretion flow becomes a bright X-ray emitter, resulting in what is usually called a X-ray Binary (XRB). X-ray binaries may be persistent or transient (X-ray novae).

The ideal way to firmly establish the nature of a compact source is to dynamically measure its mass. This has to be done when the compact object is in quiescence (i.e. its accretion rate is strongly reduced), and is therefore a more suitable method for X-ray novae. When the compact source is in its quiescent state, the absorption-line velocities of the companion star can be determined precisely, and the mass function, an absolute lower limit on the mass of the compact object, measured. Reliable values of the mass function have been obtained for 13 X-ray novae, and for 11 of them the value of the mass function is greater than $3M_\odot$ (Narayan *et al.*, 2001). These are the strongest black hole candidates we know of. X-ray binaries may also be included in the GBHC list according to X-ray spectral characteristics, if they remind those of dynamically established black hole binaries.

As we can expect, given our theoretical knowledge of the different possible accretion modes onto a black hole (see §1.2), the high energy spectra of GBHC are not unique. Very broadly speaking, the spectral properties of black hole candidates are usually characterized in terms of their broadband luminosity and of the relative contribution to this luminosity of two main primary continuum component (see e.g. the recent review by Done, 2001, and references therein). The first one is a quasi-thermal hump, that, when present, contributes mostly to the flux below 10 keV, and is commonly interpreted as emission from an optically thick accretion disc (see the detailed discussion of Chapter 4). The second component is much harder and extends above 10 keV. As a first order approximation, it can be modeled as a power-law, although more sophisticated models are often required (see e.g. Frontera *et al.*, 2001, and the discussion therein; see also Chapters 2 and 6). In addition, secondary spectral components, as those produced by reflection of the X-rays on colder matter are often observed, and can be used to further disentangle geometrical properties of the inner accretion flow (see Chapter 3).

In the recent years, a unified classification scheme for the X-ray emission of GBHC has emerged. From timing and spectral properties, four separate states (plus the quiescent state for transient system) have been identified:

(i) The *low/hard* state (Tananbaum *et al.*, 1972; Oda, 1977) with a very weak (or absent) quasi-thermal component and a flat (photon index $\Gamma = 1.5 - 2$) power-law spectrum, rolling over at ~ 100 keV.

(ii) The *intermediate* state (Mendez and van der Klis, 1997), in which the 2-10 keV flux is a factor ~ 4 higher that in the *low/hard* state, a soft component is present in the energy spectrum, while the power-law component is softer than in the *low/hard* state ($\Gamma = 2 - 3$).

(iii) The *high/soft* state (Tananbaum *et al.*, 1972; Oda, 1977), in which the 2-10 keV flux is usually an order of magnitude higher than in the *low/hard* state and the spectra are dominated by a soft quasi-thermal component at $kT \sim 1$ keV, which is weakly Comptonized by low temperature thermal electrons with $kT \sim 5 - 20$ keV (see e. g. Gierliński *et al.*, 1999). The power-law tail is very weak and steep ($\Gamma = 2 - 3$) and extends out beyond 511 keV in the few objects with good high energy data (Grove *et al.*, 1998).

(iv) The *very high* state (Miyamoto *et al.*, 1991) characterized by a high 2-20 keV X-ray luminosity (higher than in the *high/soft* state), a strongly Comptonized ultra-soft quasi-thermal component and a relatively strong power-law tail, with $\Gamma \simeq 2.5$. Apart from its higher 2-20 keV flux, such a state is spectrally similar to the *intermediate* one; the distinction coming from the fact that they are separated in time by intervals in which a source is in the *high/soft* state, that has markedly different properties.

The order in which black hole transients have been observed to move through these states during the decays from their outbursts suggests that the accretion rate is the highest in the *very high* state and decreases through the *high/soft* and *intermediate* states giving rise to the *low/hard* state at a level of few per cent of Eddington. However, often a second driving parameter, different from the accretion rate, is required to explain, for example, transitions between the same spectral states occurring at different bolometric luminosities in the same source (Homan *et al.*, 2001).

Furthermore, not only do transient sources in outburst evolve through a sequence of the four main spectral states, but also persistent sources may undergo state transitions. Unfortunately, such transitions are very rare, making the accumulation of extensive datasets on different states difficult. Transient systems are more promising, but their very transient nature limits the number of states and of state transitions that can be observed from one system to a few, and the comparison between systems is always problematic.

Microquasars and compact jet sources

Since 1994, radio astronomers have discovered a handful of GBHC that produce transient radio jets traveling at velocities $\sim 0.9c$ (Mirabel and Rodríguez, 1999). These sources are referred to as *microquasars*, since they appear to be scaled-down versions of the jets in AGN. Interest in microquasars is heightened by the opportunity to observe the formation and evolution of mass ejections and their relationships with the evolution of the inner accretion flow on timescales of seconds to days, while such processes take years to millennia to unfold in quasars.

The best studied example, though still the most puzzling and intriguing, is that of the superluminal source GRS 1915+105 (Mirabel and Rodriguez, 1994). Associated with an extremely variable and complex X-ray lightcurve (Belloni *et al.*, 2000a), it shows different types of jets: explosive bipolar outflows at relativistic speeds, weaker oscillatory ejections at regular intervals and steady compact jets which may persist from days to months.

This latter feature is not unique of microquasars. There is in fact growing evidence (Fender, 2001; Stirling *et al.*, 2001) that almost *all* black hole candidates in their *low/hard* state, either transient or persistent sources, show a steady flat or inverted (in that $S_\nu \sim \nu^\alpha$ with $\alpha \gtrsim 0$) radio spectrum. Furthermore, in none of those systems has a high frequency cut-off to this spectral component been clearly detected, suggesting that it may extend up to the near infrared or even optical regime (see the discussion about the X-ray transient XTE J1118+480 in Chapter 6). This spectral component is considered to arise in synchrotron emission from a conical, partly self-absorbed jet, with the higher frequency emission originating from the base of the jet.

1.3.2 Active Galactic Nuclei (AGN) and Quasars

Some galaxies are known to emit radiation with extremely high luminosities in the γ-ray, X-ray and UV continuum from a very concentrated volume in the nuclear region. Such active cores are the so-called Active Galactic Nuclei (AGN) and their radiation is believed to be produced by physical processes other than the nuclear fusion that powers stars, most likely accretion onto a supermassive ($M \gtrsim 10^6 M_\odot$) black hole.

Although, at present, such a basic structure of an AGN is generally agreed on (Antonucci, 1993; Urry and Padovani, 1995), still the detailed physics behind the enormous variety of observed sources is to be fully understood. Furthermore, the intrinsically complex nature of such systems and the differences in the terminology among different scientific communities (radio, optical, X-ray astronomers) has led in the years to an extremely complicated nomenclature for the AGN zoo. As the wealth of observations piled up, and with them the number of different AGN types, the opposite enterprise of finding unification schemes has progressively gained support. The basic idea behind any unification scheme is that AGN are *asymmetric* and *anisotropic* systems. This is natural, as all rotating systems necessarily single out a preferential axis in space and break the full spherical symmetry of non-rotating bodies. Therefore, the orientation of the AGN rotation axis with respect to our line of sight becomes another important parameter that can make observationally different two sources that are intrinsically identical.

According to the current widely accepted paradigm, there are two principal causes of anisotropic radiation: *obscuration* and *relativistic beaming*. The former is usually associated with a torus[4] of gas and dust obscuring the optical, UV and (sometimes) soft X-ray radiation along some line of sights, the latter with outflows of energetic particles (jets) along the symmetry axis: the high velocity plasma in the jet beams radiation relativistically in the forward direction.

The powerful source of radiation and the launching site of the collimated jet lies in the center of the system. The very nature of the accretion/ejection flow ultimately responsible for the observed broadband radiation is therefore sometimes masked by these anisotropic sources of obscuration and beaming. Goal of any unification scheme is to unveil the intrinsic properties of the inner (sometimes hidden) engine common to all the observed AGN.

A fundamental unification scheme for luminous AGN

Active galactic nuclei emit over a very broad range of the electromagnetic spectrum, with roughly equal energy output extending from the far-infrared (FIR) to the X-rays in all of them, with extensions to γ-rays in few cases. This makes multiwavelength campaign necessary in order to understand and classify their spectral energy distributions.

Following the approach of Urry and Padovani (1995), we present a classification of the principal luminous AGN types in Table 1.1 (adapted from Lawrence, 1987), organized according to their radio loudness (vertical axis) and their optical spectra, i.e. to whether they have broad line emission lines (Type 1), only narrow lines (Type 2), or weak or unusual line emission (Type 0). Within each group, different types of AGN are listed by increasing luminosity. Nearby, low-luminosity AGN (Ho, 1999) will be discussed in a separate subsection.

Radio loudness is thought to be related to the presence of the collimated relativistic outflows/jets in the system, and is usually defined in terms of the ratio of radio (5 GHz) to optical (B-band) flux: $F_5/F_B \gtrsim 10$. About 15%–20% of all AGN satisfy this condition, but such fraction increases with increasing optical or X-ray luminosities (La Franca *et al.*, 1994; della Ceca *et al.*, 1994; but see also Ho and Peng, 2001, for an alternative view). In general, optical and ultraviolet emission-line spectra and the FIR to soft X-ray continuum of most radio-loud and radio-quiet AGN are very similar (Sanders

[4]The toroidal geometry for the obscuring medium is generally adopted as a matter of convenience. In fact, there is little evidence to date to indicate whether it is actually a torus, a warped disk, or some other distribution (Urry and Padovani, 1995).

Table 1.1: AGN taxonomy, from Urry and Padovani (1995). See text for details.

<table>
<tr><th></th><th>Type 1
(Broad Lines)</th><th>Type 2
(Narrow Lines)</th><th>Type 0
(Unusual)</th></tr>
<tr><td rowspan="3">Radio Quiet</td><td>Sy 1</td><td>Sy 2</td><td rowspan="3">BAL QSO ?</td></tr>
<tr><td rowspan="2">Radio Quiet
Quasars (QSO)</td><td>NELG</td></tr>
<tr><td>Type 2 QSO ?</td></tr>
<tr><td rowspan="3">Radio Loud</td><td>BLRG</td><td rowspan="3">NLRG $\left\{ \begin{array}{l} \text{FRI} \\ \text{FRII} \end{array} \right.$</td><td rowspan="3">Blazars $\left\{ \begin{array}{l} \text{BL Lac} \\ \text{(FSRQ)} \end{array} \right.$</td></tr>
<tr><td>SSRQ</td></tr>
<tr><td>FSRQ</td></tr>
<tr><td></td><td colspan="3">– Decreasing angle to line of sight $\longrightarrow$</td></tr>
</table>

et al., 1989; Elvis *et al.*, 1994), suggesting similar mechanisms for their production; at present, the origin of the characteristic of radio loudness itself is not well understood, and is still one of the major open issues in AGN astrophysics.

Based on the characteristics of their optical and ultraviolet spectra, AGN can be separated into three broad types, shown in Table 1.1.

(1) Those with bright continua and broad emission lines from hot, high-velocity gas, presumably located deep in the gravitational well of the central black hole, are known as Type 1 AGN. In the radio-quiet group, these include the Seyfert 1 galaxies (Sy 1), which have relatively low-luminosities and therefore are seen only nearby, where the host galaxy can be resolved, and the higher-luminosity radio-quiet quasars (QSO), which are typically seen at greater distances because of their relative rarity locally and thus are usually unresolved and rarely show an obvious galaxy surrounding the bright central source. The radio-loud Type 1 AGN are called Broad-Line Radio Galaxies (BLRG) at low luminosities and Radio-Loud Quasars at high luminosities, either Steep Spectrum Radio Quasars (SSRQ) or Flat Spectrum Radio Quasars (FSRQ) depending on radio continuum shape, with the dividing line set at radio spectral slope $\alpha_r = 0.5$ (where the radio spectrum is measured at a few GHz). Other than luminosity, little distinguishes Seyfert 1s from radio-quiet quasars, or BLRG from radio quasars.

(2) Type 2 AGN have weak continua and only narrow emission lines, meaning either that they have no high velocity gas or, as we now believe, the line of sight to such gas is obscured by a thick wall of absorbing material. Radio-quiet Type 2 AGN include Seyfert 2 galaxies at low luminosities, as well as the narrow-emission-line X-ray galaxies (NELG). The high-luminosity counterparts are not clearly identified,

but likely candidates are the heavily obscured quasars recently detected in the X-rays by *Chandra* (Norman *et al.*, 2001; Crawford *et al.*, 2001). Radio-loud Type 2 AGN, often called Narrow-Line Radio Galaxies (NLRG), include two distinct morphological types: the low-luminosity Fanaroff-Riley type I (FR I) radio galaxies (Fanaroff and Riley, 1974), which have symmetric radio jets whose intensity falls away from the nucleus, and the high-luminosity Fanaroff-Riley type II (FR II) radio galaxies, which have more highly collimated jets leading to well-defined lobes with prominent hot spots.

(3) A small number of AGN have very unusual spectral characteristics. Following Urry and Padovani (1995), we call these objects 'Type 0' AGN and speculate that they are characterized by a small angle to the line of sight. These include the BL Lacertae (BL Lac) objects, which are radio-loud AGN that lack strong emission or absorption features. In addition, roughly 10% of radio-quiet AGN have unusually broad P-Cygni-like absorption features in their optical and ultraviolet spectra, and so are known as BAL (Broad Absorption Line) quasars. If BAL spectral features are caused by polar outflows at small angles to the line of sight, they too are Type 0 AGN as indicated in Table 1.1. A subset of Type 1 quasars, including those defined variously as Optically Violently Variable (OVV) quasars, Highly Polarized Quasars (HPQ), Core-Dominated Quasars (CDQ) or Flat-Spectrum Radio Quasars (FSRQ), are probably also found at a small angle to the line of sight. Their continuum emission strongly resembles that of BL Lac objects (apart from the presence of a blue "bump" in a few cases) and, like BL Lac objects, they are characterized by very rapid variability, unusually high and variable polarization, high brightness temperatures, and superluminal velocities of compact radio cores. Although the names OVV, HPQ, CDQ, and FSRQ reflect different empirical definitions, evidence is accumulating that they are all more or less the same thing; that is, the majority of flat-spectrum radio quasars tend to show rapid variability, high polarization, and radio structures dominated by compact radio cores, and vice-versa. Collectively, BL Lacs and FSRQ are called *blazars.*

X-ray spectra of radio quiet AGN

As the work presented in this thesis deals mainly with the study of X-ray emission from black hole powered sources, we give here a brief overview of the main X-ray spectral properties of AGN. To concentrate on the high energy emission from the accretion flow, we will limit our discussion to radio-quiet AGN, and to Seyfert galaxies in particular, both because they are the best studied cases and in order to avoid contamination to the X-ray emission from the jet phenomenon. More detailed discussions and references can be found in the review articles by Mushotzky *et al.* (1993), Madejski (1998), Zdziarski (1999).

To first order, X-ray spectra of Seyfert 1 are remarkably similar to those of black hole binaries in the *hard/low* state. They can be characterized by a simple power-law and typical indices of $\Gamma \sim 1.5 - 3$. The strongest broad spectral feature in the 0.1-100 keV energy range is low energy photoelectric absorption of cold (neutral) or warm (partly ionized) material in the line of sight of the nucleus. According to the unification scheme presented above, Seyfert 2 galaxies belong to the same class as Seyfert 1, and therefore possess the same intrinsic spectrum. However, their orientation close to edge-on results in larger photoelectric absorption and strong obscuration in the optical/UV and X-ray bands. The intrinsic hard X-ray power-law spectra of Seyfert galaxies often break at $\sim 100 - 200$ keV, but the shape of such high energy cut-off is known much less accurately in the case of AGN than in the case of GBHC. However, the average spectra of radio-quiet Seyfert 1 and 2, detected in the 50-1000 keV band by the Oriented Scintillation Spectrometer Experiment (*OSSE*) on the Compton Gamma Ray Observatory (*CGRO*) satellite, show the significant presence of high energy cut-off (Zdziarski, 1999).

This primary continuum component is accompanied, in most cases, by signatures of reprocessing by a cold medium. Iron is the most abundant heavy element and its large absorption cross section at high energy, combined with a high fluorescent yield, indicates that the strongest spectral features at $E > 6$ keV should be due to Fe (Fe fluorescent emission at 6.4 keV from near-neutral material, He-like and H-like lines at 6.67 and 6.97 keV from ionized material and K absorption edges between 7.1 and 9.3 keV, depending on the ionization state of the material). The analysis of a number of Seyfert spectra observed by the *ASCA* satellite by Nandra *et al.* (1997a) suggest that many Seyfert indeed show the Fe Kα, broadened by Doppler and gravitational redshift, requiring an emission close to the black hole. The region beyond the Fe K line in the spectra of Seyfert shows a general hardening, accompanied by the edge due to Fe K; this is a signature of Compton reflection (Lightman and White, 1988) from cold matter. The intensity of this component is consistent with the reflector being a semi-infinite plane; it peaks at ~ 30 keV, and beyond this, it steepens gradually, most likely due to Compton recoil and Klein-Nishina effects.

A distinct class appears to be formed by Narrow-Line Seyfert 1 (NLS1, Vaughan *et al.*, 1999), whose X-ray spectra are often dominated by a strong, quasi-thermal, soft excess, which can be modeled as blackbody emission (with temperature $T_{\rm bb} \sim 100 - 300$ eV) superimposed on the underlying power-law continuum, thus bearing some similarities with black hole binaries in their *high/soft* or *very/high* state.

Spectral studies of more distant, high luminosity QSOs are obviously more difficult due to the lack of enough X-ray photons. However, results from Laor *et al.* (1997), Nandra *et al.* (1997b) and Reeves and Turner (2000) indicate that the continuum X-ray spectra of luminous QSOs are similar to those of Seyfert galaxies, but with much less Compton reflection and almost no strong Fe Kα lines, possibly an effect of nearly-complete ionization of the accreting material.

Low-luminosity AGN

At the low-luminosity ends of the broadly defined classes we have introduced in the previous subsection, things seem to be rather different.

Beside the best studied case of the black hole at the centre of our Galaxy (Melia and Falcke, 2001, and references therein), recent multi-wavelength campaigns on nearby low-luminosity AGNs (LLAGN) (Ho, 1999; Nagar *et al.*, 2000; Falcke *et al.*, 2000; Ho *et al.*, 2001) have revealed nuclear SEDs markedly different from the canonical broadband continua of high luminosity AGN (as compiled, e.g., by Elvis *et al.*, 1994). The most striking difference is the lack of UV excess, the so-called 'big blue bump' associated with the emission from an optically thick, geometrically thin accretion disc (Ho, 1999). In addition, VLA (Nagar *et al.*, 2000) and VLBA (Falcke *et al.*, 2000) radio observations of LLAGN have revealed flat or inverted compact radio cores, similar to those found in bright radio-loud blazars, and, for the sources observed at higher spatial resolution with VLBA, very high brightness temperatures ($T_b \gtrsim 10^8$K). Also, in low-luminosity nearby radio galaxies observed with HST (Capetti *et al.*, 2000) compact optical cores seem very common. Furthermore, Chiaberge *et al.* (1999), analysing HST images of a complete sample of 33 FR I radio galaxies, demonstrated that the luminosity of compact optical cores in these sources correlate linearly with that of the radio cores, suggesting a common non-thermal synchrotron emission origin for both, although not in the form of well-collimated large-scale jets.

These findings not only validate the unification scheme between FR I and BL Lac at the lowest luminosities, but also call for a different accretion scenario for those low-luminosity sources, reminiscent of the galactic black hole candidates in their low/hard state (see Section 1.3.1). As a matter of fact, the recent work of Ho and Peng (2001) challenges the popular wisdom concerning Seyfert 1 galaxies that they are essentially radio quiet: high resolution, multiwavelength observations of nearby Sy 1 also reveal compact radio cores, and ratios of radio to optical flux $F_5/F_B \sim 1-100$, on both sides of the dividing line between radio quiet and radio loud objects.

1.4 Outline of the thesis

The remainder of this dissertation is divided into five chapters. Chapter 2 will deal with the physical properties of the part of the accretion flow which is responsible for the hard X-ray power-law emission, ubiquitous in the spectra of black hole powered sources: the so-called *corona*. It will be demonstrated how the corona must be magnetically dominated and therefore its physics related to the fundamental issue of the nature of the magnetic viscosity inside the accretion disc itself. Also in Chapter 2, a structured magnetic corona model for the primary high energy continuum of black hole spectra will be presented. Finally, I will discuss the relationships between coronal power and accretion rate and the role of the coronal medium in launching powerful outflows/jets from the inner regions of the accretion flow and propose an alternative scenario for the accretion mode in low-luminosity AGN and GBHC in their low/hard state. In Chapter 3, the effects of a Comptonizing corona on the appearance of the secondary spectral components (reflection features, fluorescent iron lines, etc.) will be discussed. To conclude the part of this dissertation that is focused on black hole spectral properties, the spectrum produced by an optically thick and geometrically thin accretion disc will be discussed in Chapter 4. It will be shown that careful modeling of the disc vertical structure is necessary, for any meaningful conclusion about the inner disc geometry to be drawn from accretion disc spectroscopy alone. Chapter 5 deals with the complementary problem of aperiodic time variability in the emission from accretion flows around black holes. A model (the 'thundercloud model') will be presented aimed at bridging X-ray spectral and temporal studies, in order to put tighter constraints on the nature of the inner part of the accretion disc–corona system. As an aside, we will also show how the study of accretion flows in the time domain could shed some light on one of the biggest mysteries of high energy astrophysics: γ-ray bursts (GRB) and black hole formation. We found a new correlation between the durations of subsequent emission episodes in the lightcurves of long, variable bursts. Such a correlation, analogous to that found in accreting black hole sources, may provide us with vital information, not only on the nature of the central engines of GRBs, but also on the very nature of the accretion flow in such extreme conditions as those found during the collapsing stages of a massive star. Finally, in Chapter 6, the model of a structured magnetic corona and of coronal outflow dominated accretion discs is applied to the X-ray transient source XTE J1118+480. This is a key object for black hole astronomy, as its position high on the galactic plane during its last recent outburst has allowed us to determine its broadband spectrum with unprecedented accuracy. Once again, in the study of this source we have tried to take full advantage of simultaneous temporal and spectral analysis to constrain the emission properties and the elusive geometry of the inner accretion flow in GBHC in their *low/hard* state. Concluding remarks and ideas for future work are presented in the final Chapter.

Chapter 2

The physics of magnetic accretion disc coronae

2.1 Introduction: magnetized accretion flows and coronae

As we have discussed in section 1.3, a hard X-ray power-law is a common feature of most astrophysical systems powered by an accreting black hole (Zdziarski, 1999, and references therein). In the case of GBHC, for example, it is the relative strength of the power-law component with respect to the quasi-blackbody one, due to thermal emission from an accretion disc, that is used to classify the different observed spectra from different sources into the four states.

The vast majority of spectral studies of galactic black hole candidates (GBHC) and radio-quiet Seyfert 1 galaxies clearly suggest that the primary hard X-ray continua of these sources are produced by thermal Comptonization (Shapiro *et al.*, 1976; Sunyaev and Titarchuk, 1980; see Zdziarski, 1999, and reference therein) in a hot, rarefied plasma (hereafter, the *corona*) that probably resides where most of the accretion energy is released, namely in the inner part of the flow. Furthermore, there is clear evidence that this hot, Comptonizing medium strongly interacts with the colder thermal component: such an interaction is not only required to explain the ubiquitous reflection features in the X-ray spectra (Lightman and White, 1988; George and Fabian, 1991; Matt *et al.*, 1991; Fabian *et al.*, 2000), but could also provide the feedback mechanism that forces the observed values of coronal temperature and optical depth to lie in a very narrow range for all the different observed sources (Haardt and Maraschi, 1991). Nonetheless, because the observed power-law X-ray spectra represent a universal signature of a specific physical process (inverse Compton scattering) rather than of a specific accretion dynamics, the geometry of the hot and cold phases is still matter of debate. Such a geometry could in principle be deduced with good enough spectral information: for example, the reflection features produced by a cold, optically thick medium illuminated by the hard X-ray power-law continuum are sensitive to the detail of the relative geometry of the two components (George and Fabian, 1991; Matt *et al.*, 1991; Magdziarz and

Zdziarski, 1995). Simultaneous studies of UV (likely produced by thermal emission from the optically thick medium) and X-ray radiation can probe the region of the flow where the hot and the cold phases are interfaced. In fact, the observed broad distribution of the ratio $F_{\rm UV}/F_{\rm X}$ of the UV to X-rays fluxes has already been used in many cases to rule out a slab geometry for the corona in favour of a patchy one, made of a number of separate active regions (Haardt *et al.*, 1994; Stern *et al.*, 1995; Di Matteo *et al.*, 1999). Also, the observed correlation between the X-ray photon index and the reflection strength (Zdziarski *et al.*, 1999; Gilfanov *et al.*, 2000) has demonstrated the need for a geometrical/dynamical parameter to describe the long-term evolution of a system, such as relativistic bulk motion velocity of the coronal material (Beloborodov, 1999; Malzac *et al.*, 2001) and/or truncation radius of the inner accretion disc (Zdziarski *et al.*, 1999).

The theoretical uncertainties about the physical nature and geometrical properties of the hot coronal flow are paralleled by the ones about the nature of the angular momentum transport mechanism in the cold disc. In the following sections we will argue that the magnetic field is the necessary ingredient needed to improve our basic understanding of both issues.

As we have discussed in the previous chapter, the theoretical idea that a disc configuration could explain the nature of the power source in black hole systems was recognized as early as in 1969 (Lynden-Bell, 1969), and the basic elements of what is still today considered the standard accretion disc theory were already in place in 1973 (Shakura and Sunyaev, 1973; Novikov and Thorne, 1973; Pringle, 1981). Although successful in explaining many observed features of black hole candidates (both stellar and supermassive), standard accretion disc theory left unspecified the nature of both the angular momentum transport mechanism needed to sustain the disc in the first place, and of the hot Comptonizing medium giving rise to the hard spectral component.

In fact, it is well known that micro-physical viscosity are in general too inefficient to drive accretion at rates comparable to the observed ones, and enhanced/turbulent viscosity is therefore a theoretical necessity. As astrophysical discs are bound to be seeded with magnetic fields, magneto-rotational instability (MRI; Velikhov, 1959; Chandrasekhar, 1960; Balbus and Hawley, 1991) is the best candidate to date to produce the self-sustained turbulence that is able to transport angular momentum in rotationally supported discs. Any weak, sub-thermal magnetic field, coupled with outwardly decreasing differential rotation (two conditions easily met by any accretion flow endowed with angular momentum), generates the turbulence that in turn is able to regenerate the field. This instability results in a greatly enhanced effective viscosity that is able to transport angular momentum outward (Balbus and Hawley, 1998).

What is the fate of the magnetic field which is amplified inside an accretion disc? Two competing mechanisms should operate there: dissipation and buoyancy. On one hand, part of the field *must* be dissipated, if the turbulence has to be sustained and MRI relied upon to transport angular momentum. It has been shown (Balbus and Hawley, 1998) that, in a steady state disc, if angular momentum transport is due solely to magneto rotational instability, magnetic fields must be sub-thermal. This in turn implies that buoyancy cannot be a very efficient mechanism to get rid of the disc field: to cross one disc scaleheight in less than a dynamical time, $t_{\rm dyn} = 1/\Omega$, a velocity of the order of the sound speed is required, which would correspond to an equipartition magnetic field. Such strong field would suppress the MRI (Balbus and Hawley, 1998).

On the other hand, we can expect the magnetic field configuration in the disc to be highly intermittent (Politano and Poquet, 1995), with the field concentrated in small regions (flux tubes and ropes) with relatively low filling factor (see e.g. Blackman, 1996, or the simulation presented in Machida *et al.*, 2000). These structures can more easily rise buoyantly and emerge in the low density part of the flow above the accretion disc to form a magnetic atmosphere, the corona, where the field is finally dissipated.

It is not clear what is the relative importance of the two mechanisms of field saturation, if they coexist in a typical disc, or instead alternate in a cyclic fashion (for example, low disc field $\rightarrow$ MRI $\rightarrow$ stronger field $\rightarrow$ buoyancy $\rightarrow$ field expulsion $\rightarrow$ suppression of the MRI $\rightarrow$ low disc field $\rightarrow$ MRI).

Numerical simulations of vertically stratified discs (Brandenburg *et al.*, 1995; Stone *et al.*, 1996) seem to suggest that, although dissipation is the main saturation mechanism for the instability, buoyancy is indeed capable of transporting vertically a substantial fraction of magnetic energy to power a strong corona (see in particular Miller and Stone, 2000, where the largest vertical extent has been explored), without quenching the MRI in the underlying disc.

In the next section, we investigate how changes in the internal disc structure, associated with variations in the external accretion rate, may influence the accretion disc–corona system, and vice versa. To this end we only consider standard optically thick and geometrically thin accretion discs sandwiched by a patchy magnetic corona, as in the models first proposed by Galeev *et al.* (1979); Haardt *et al.* (1994); Di Matteo *et al.* (1999).

2.2 The structure equations of a disc–corona system

In section 1.2.1 we have seen how to extract algebraic relations among the physical parameters that determine the disc structure from the conservation equations of an accreting flow endowed with angular momentum.

Here we discuss the changes in the disc structure that occur when a magnetic corona is included in the treatment. We will discuss two possibilities for the viscosity law: the *standard* one, in which the magnetic viscosity in the disc is assumed to be proportional to the total pressure (Eq. 1.9), and the *modified* one, in which the disc viscosity is proportional to the gas pressure only, so that

$$\rho W_{R\phi} = \alpha_{\rm v} P_{\rm gas}. \tag{2.1}$$

As in Svensson and Zdziarski (1994), we assume that all angular momentum transport takes place in the cold disc and that all accretion takes place there. A fraction, f, of the power release associated with the angular momentum transport is stored in some form (possibly magnetic field loops or tubes or hydromagnetic waves) that can be transported vertically in a dissipationless fashion inside the disc and finally dissipated above the disc surface.

2.2.1 The standard viscosity law case

Only one modification to the equations (1.3-15) is needed to properly take into account the effect of the corona on the disc structure, namely the heating–cooling balance inside the disc (Eq. 1.15) becomes

$$Q_{-} = \int_{-H}^{+H} F(z)dz \equiv F_0 = (1-f)Q_{+}. \tag{2.2}$$

Then we obtain, for the radiation pressure dominated solution, the following expressions for disc scaleheight, pressure, density (both calculated at the disc mid-plane), temperature and ratio of the radiation to gas pressure, respectively:

$$\begin{aligned}
h &\equiv \frac{H}{R_{\rm S}} \simeq 10.6\dot{m}J(r)(1-f) && (2.3)\\
P &\simeq 3.58\times 10^{15}(\alpha_{\rm v}m)^{-1}r^{-3/2}(1-f)^{-1}\ \text{dyne} && (2.4)\\
\rho &\simeq 1.42\times 10^{-7}(\alpha_{\rm v}m)^{-1}r^{3/2}[\dot{m}J(r)]^{-2}(1-f)^{-3}\ \text{g cm}^{-3} && (2.5)\\
T &\simeq 3.45\times 10^{7}(\alpha_{\rm v}m)^{-1/4}r^{-3/8}(1-f)^{-1/4}\ \text{K} && (2.6)\\
\frac{P_{\rm rad}}{P_{\rm gas}} &\simeq 4.36\times 10^{6}(\alpha_{\rm v}m)^{1/4}r^{-21/8}[\dot{m}J(r)]^{2}(1-f)^{9/4}. && (2.7)
\end{aligned}$$

In the gas pressure dominated part of the disc, instead we have:

$$\begin{aligned}
h &\simeq 2.02\times 10^{-2}\xi^{-3/32}(\alpha_{\rm v}m)^{-1/10}r^{21/20}[\dot{m}J(r)]^{1/5}(1-f)^{1/10} && (2.8)\\
P &\simeq 1.88\times 10^{18}\xi^{3/32}(\alpha_{\rm v}m)^{-9/10}r^{-51/20}[\dot{m}J(r)]^{4/5}(1-f)^{-1/10}\ \text{dyne} && (2.9)\\
\rho &\simeq 20.3\xi^{11/32}(\alpha_{\rm v}m)^{-7/10}r^{-33/20}(1-f)^{-3/10}[\dot{m}J(r)]^{2/5}\ \text{g cm}^{-3} && (2.10)\\
T &\simeq 5.6\times 10^{8}\xi^{-1/4}(\alpha_{\rm v}m)^{-1/5}r^{-9/10}[\dot{m}J(r)]^{2/5}(1-f)^{1/5}\ \text{K} && (2.11)\\
\frac{P_{\rm rad}}{P_{\rm gas}} &\simeq 1.31\times 10^{2}\xi^{-35/32}(\alpha_{\rm v}m)^{1/10}r^{-21/20}[\dot{m}J(r)]^{4/5}(1-f)^{9/10}. && (2.12)
\end{aligned}$$

Once again, the value $\xi \simeq 1/3$ can be found by imposing continuity of all physical quantities at the boundary between the two regions, which can then be found by solving for r in the equation

$$\frac{r}{J(r)^{16/21}} \simeq 350\alpha_{\rm v}^{2/21}m^{2/21}\dot{m}^{16/21}(1-f)^{6/7}. \tag{2.13}$$

The presence of the corona, reducing the amount of energy dissipated in the disc, makes the disc itself thinner and denser, increasing the gas pressure with respect to the radiation one. The effects of these changes on the accretion disc quasi-thermal spectra will be discussed in section 4.3.

2.2.2 The modified viscosity law case

Regardless of the nature of the magnetic field saturation mechanism inside the disc (§2.1), as discussed in Stella and Rosner (1984), magnetic field amplification is likely to be limited to values such that the magnetic pressure is at most equal to the local *gas* pressure, even in its inner, radiation pressure-dominated parts. This led to the suggestion that a modified viscosity law might be more appropriate to describe accretion discs where magnetic turbulence is ultimately responsible for transporting angular momentum. According to such a law, the stress tensor is proportional to the gas pressure, and not to the total pressure as in the standard Shakura-Sunyaev prescription (Eq. 2.1). With such a scaling for the viscosity, the inner radiation pressure dominated part of the accretion disc is stable both to secular and thermal instability (Stella and Rosner, 1984).

In this case, Eq. 1.6 for the angular momentum conservation becomes

$$P_{\rm gas} = \frac{\dot{M}\Omega J(r)}{4\pi\alpha_{\rm v}H}. \tag{2.14}$$

Obviously, the gas pressure dominated part of the solution is left unchanged, while we obtain, for the radiation pressure dominated solution, the following expressions for disc scaleheight, pressure, density (both calculated at the disc mid-plane), temperature and ratio of the radiation to gas pressure, respectively:

$$h \simeq 10.6\dot{m}J(r)(1-f) \tag{2.15}$$
$$P \simeq 7.14\times10^{20}(\alpha_{\rm v}m)^{-4/5}r^{-18/5}[\dot{m}J(r)]^{8/5}(1-f)^{4/5}\ {\rm dyne} \tag{2.16}$$
$$\rho \simeq 2.94\times10^{-2}(\alpha_{\rm v}m)^{-4/5}r^{-3/5}[\dot{m}J(r)]^{-2/5}(1-f)^{-6/5}\ {\rm g\ cm^{-3}} \tag{2.17}$$
$$T \simeq 7.30\times10^{8}(\alpha_{\rm v}m)^{-1/5}r^{-9/10}[\dot{m}J(r)]^{2/5}(1-f)^{1/5}\ {\rm K} \tag{2.18}$$
$$\frac{P_{\rm rad}}{P_{\rm gas}} \simeq 2.01\times10^{5}(\alpha_{\rm v}m)^{1/5}r^{-21/10}[\dot{m}J(r)]^{8/5}(1-f)^{9/5}. \tag{2.19}$$

In Section 2.5 the relationship between coronal magnetic power and the accretion disc structure equations in the case of a modified viscosity law will be explored in more detail. Before that, in the next two sections, a physical model of a structured magnetic corona will be outlined, firstly with the help of a simple energetics argument (§2.3), then with a more thorough discussion of the radiation mechanisms involved and of the expected spectral properties (§2.4).

2.3 Energetics of the observed accretion disc coronae

The relevance of the magnetic field for the emission processes in accretion disc coronae, first introduced in a seminal paper by Galeev *et al.* (1979), has already been considered in detail in Burm and Kuperus (1988); Di Matteo *et al.* (1997a,b); Di Matteo (1998); Di Matteo *et al.* (1999); Wardziński and Zdziarski (2000). They all *assume* that a magnetic corona is the region where a significant fraction of the total accretion power is dissipated and consequently work out the strength of the magnetic field, and the importance of the related radiative processes (cyclo-synchrotron emission in particular). These predictions were in turn compared with the observed luminosities and spectra in order to assess the viability of any such model. In this section, instead, it will be demonstrated, with a simple energetics argument centered on the small thermal energy content of any plausible corona, that a strong magnetic field in the coronal region of black hole accretion discs (both stellar and supermassive) is *required* by the existing data. In particular, we will show that the measured thermal energy of the Comptonizing flow is far too small to explain the observed hard X-ray luminosities without postulating that the flow itself is a *magnetic reservoir*: the magnetic field dominates the energy balance in the corona and act as an *in situ* reservoir of energy that powers the high energy emission.

Let us consider a black hole of mass $M = mM_{\odot}$ and hard X-ray luminosity $L_{\rm H} = 1.3 \times 10^{38} f_{\rm H} \dot{m} m$ ergs s^{-1}, where $\dot{m}$ is the accretion rate in units of the Eddington one and $f_{\rm H}$ is simply the fraction of the total luminosity emitted in hard X-rays (which should be related, but not identical, to the fraction f of the gravitational power dissipated above the disc as defined in the previous section).

Observed galactic black hole candidates whose mass has been reliably estimated, show that, if the source is not in quiescence, the value of the product $f_H \dot{m}$ ranges between 0.001 and 0.1, approximately.

To be fairly general, let us consider the thermal energy content of the hot electrons in a hard X-rays emitting region of size $R = rR_S$, where $R_S = 2GM/c^2$ is the Schwarzschild radius of a black hole of mass M. We have

$$E_{\rm th} \simeq \pi \frac{\tau}{\sigma_T} R^2 kT_e \simeq 5.8 \times 10^{28} \tau T_9 r^2 m^2 \ \ \text{ergs}, \tag{2.20}$$

where σ_T is the Thomson scattering cross section and coronal electron temperature is $T_e = T_9 \times 10^9$ K.

Thus, for even a local equilibrium, the electrons must be heated on a timescale

$$t_{\rm heat} = \frac{E_{\rm th}}{L_{\rm H}} \simeq 3.9 \times 10^{-10} \tau T_9 r^2 m (f_H \dot{m})^{-1} \ \ \text{s}. \tag{2.21}$$

If the energy has to be supplied to the hot electrons from an external heating source, and no reservoir of stored energy is present where the the hot electrons are, then the light crossing time of such region, $t_{\rm cross} = R/c \simeq 10^{-5} mr$ (which is the shortest timescale over which energy can be transferred there), has to be shorter than the heating time. This translates into a condition on the total size of the hard X-rays emitting region:

$$r > 2.5 \times 10^4 \frac{f_H \dot{m}}{\tau T_9}, \tag{2.22}$$

independent of the black hole mass.

For the vast majority of radio-quiet Seyfert 1s and GBHCs in their hard state, we deduce from observations that the hot flow is optically thin ($0.1 \lesssim \tau \lesssim 1$) and has typical temperatures of the order of $1 \lesssim T_9 \lesssim 3$ (Gierlinski *et al.*, 1997; Poutanen and Coppi, 1998; Zdziarski *et al.*, 1998; Zdziarski, 1999; Petrucci *et al.*, 2000; Done *et al.*, 2000), implying a typical dimension of the Comptonizing region of the order of thousands Schwarzschild radii: we have, for example, $r > 1250$ for the set of fairly typical values $\tau \simeq 0.6$, $T_9 = 1.6$ (corresponding to $kT_e \simeq 100$ keV) and $f_H \dot{m} = 0.05$.

Such a large coronal region is not physically plausible, for a number of reasons. First of all, it is far too large to explain the fastest observed variability, both for galactic black hole candidates (Poutanen and Fabian, 1999; Maccarone *et al.*, 2000) and active galactic nuclei (Lee *et al.*, 2000). Strongly variable emission is clearly indicative of an emission cycle made of an energy storage phase followed by an energy release phase. Thus, the corona cannot be a uniform continuous medium, unless it is geometrically thin (sheet-like; see Celotti *et al.*, 1992) so that the crossing time in one direction is orders of magnitude shorter that that in the other direction. Secondly, spectral evidence of a strong reflection component and broadened iron Kα emission lines in Seyfert 1s can be explained only assuming localized hard X-rays emitting regions shining above the very inner part of the accretion disc, and not at a distance of thousands of Schwarzschild radii. Also, the different ratios of accretion disc (blackbody-like) to hard X-ray luminosity observed in different sources, or in the same source at different times, imply that the geometry of the coronal plasma cannot be a slab one, but is rather made up of a number of distinct active regions (Haardt *et al.*, 1994). Furthermore, if the external source of energy is the underlying accretion disc, the amount of energy deposited in the corona is proportional to the local disc viscous power, which is a strong function of the radial distance and decays rapidly outwards, so that almost all the energy is concentrated in the few inner tens of Schwarzschild radii. Further spectral evidence against a uniform corona extending out to thousands of R_S for GBHC can be found in Zdziarski *et al.* (1998); Done and Zycki (1999); Gilfanov *et al.* (1999).

The simplest solution to these problems is to assume that the corona is a collection of N small ($\sim$ few R_S, at most) active regions, whose thermal electron energy is just a fraction of the total. We envisage the magnetic field energy $B^2/8\pi$ as the main reservoir in the Comptonizing region. Thus, the condition $t_{\rm heat} > t_{\rm cross}$ for a magnetically-dominated coronal active region, translates into a condition on the magnetic field there (Di Matteo *et al.*, 1997a):

$$B_{\rm c} > \frac{5.8 \times 10^8}{r} \left(\frac{f_H \dot{m}}{f_{\rm cross} N m} \right)^{1/2} {\rm G}, \tag{2.23}$$

where we have introduced the factor $f_{\rm cross} = v_{\rm A}/c = B/c\sqrt{(}4\pi\rho)$ in order to take into account the fact that in a magnetically-dominated active region the effective velocity for energy transfer is the Alfvèn one, $v_{\rm A}$, which is, under typical coronal conditions, unlikely to exceed the value $v_{\rm A} \sim 0.3c$.

On the other hand, the strength of the magnetic field that rises buoyantly from the disc is in principle limited only by equipartition with the disc pressure (Galeev *et al.*, 1979). Following Wardziński and Zdziarski (2000), we calculate the maximum value of the magnetic field inside the disc (assuming equipartition) and obtain, for the disc region dominated by gas pressure,

$$B_{\rm d} \simeq \frac{3.4 \times 10^8 \dot{m}^{2/5}}{(\alpha_{\rm v} m)^{9/20}(1-f_H)^{1/20}} {\rm G}, \tag{2.24}$$

where $\alpha_{\rm v}$ is the viscosity parameter, and

$$B_{\rm d} \simeq 5.2 \times 10^7 \left[\alpha_{\rm v} m(1-f_H)\right]^{-1/2} {\rm G} \tag{2.25}$$

for a disc region dominated by radiation pressure.

To be self-consistent, we need $B_{\rm d} > B_{\rm c}$, which implies, for the two cases (gas and radiation pressure dominated discs), respectively (note that, again, the limits below depend only very weakly on the black hole mass)

$$r > 1.7 f_H^{1/2}(1-f_H)^{1/20} \alpha_{\rm v}^{9/20} m^{-1/20} \dot{m}^{1/10} (f_{\rm cross} N)^{-1/2}, \tag{2.26}$$

and

$$r > 11 \left(\frac{f_H(1-f_H)\alpha_{\rm v}\dot{m}}{f_{\rm cross} N} \right)^{1/2}. \tag{2.27}$$

As opposed to the case of a thermally dominated corona, Eq. (2.22), the sizes of magnetically dominated coronal region implied by Eqs. (2.26) and (2.27), are perfectly consistent with the various spectral and temporal constraint discussed above, and can thus be regarded as a self-consistency argument in favour of the patchy magnetic corona scenario.

Nevertheless, a number of questions still remain to be answered, which affect the estimates of the energy balance in the hot coronal plasma. It is still controversial whether the magnetic field is amplified in the disc up to equipartition with the gas or the total pressure, and this controversy also affects the nature of the disc viscosity law, with interesting consequences for the issue of stability (see e. g. Nayakshin *et al.*, 2000) . Also uncertain is whether the magnetic energy in a reconnection site is mainly dissipated into electrons or protons. In the latter case, as shown by Di Matteo *et al.* (1997b), given the low Coulomb transfer rate between protons and electrons in the optically thin coronal plasma, it is quite likely that the corona at the equilibrium is a two-temperature flow (Janiuk and Czerny, 2000; Różańska and Czerny, 2000). Thus, the ions could be another energy reservoir, sharing with the magnetic field most of the energy content in the corona (Di Matteo *et al.*, 1997b) and acting as mediators between the magnetic field and the radiating electrons. However, they would also be likely heated to supervirial temperature in the inner region, evaporating part of the accretion disc and causing the the coronal flow to become effectively an outflow (Meyer at al., 2000; Spruit & Haardt, 2000; Spruit and Deufel, 2001; see also Section 2.5). In general, we have to consider the possibility that part of the energy dissipated via magnetic reconnection is converted into kinetic energy, causing bulk motion of the flaring material (Beloborodov, 1999), analogous of the Coronal Mass Ejection events observed in the Sun (Ciaravella *et al.*, 1999, 2000). Bulk motion may indeed be another means of storing energy within the corona. Finally, it is not clear what is the fraction of non-thermal particles produced by

MHD shocks associated with a magnetic reconnection site, and how they contribute to the observed spectral energy distribution (Poutanen and Coppi, 1998; Wardziński and Zdziarski, 2001).

Regardless of the above listed important open issues, we have shown that a strong magnetic field is a key element for explaining the energetics of accretion flows around black holes. From the spectral point of view, the presence of such magnetic field requires the inclusion of cyclo-synchrotron emission processes in models, as we shall see in the following section. The relative importance of this process with respect to inverse Comptonization and bremsstrahlung will in general depend on the geometry, on the interaction between the two flow components and on the relativistic non-thermal particle fraction (Celotti *et al.*, 1992; Di Matteo *et al.*, 1997a; Wardziński and Zdziarski, 2000).

Our result emphasizes the need for energy storage in the corona, with magnetic fields likely to be the dominant repository, although mildly relativistic bulk motion and a two temperature plasma may also share part of the energy content of the region, particularly once it has become active. When the magnetic energy in a particular region has been mostly dissipated, the activity must switch on elsewhere, unless the geometry is extremely sheet-like. Stochastic variability, as observed in both galactic black hole candidates and AGN, is thus a likely consequence of a magnetically-dominated corona, as will be shown in §5. The picture we envisage for the accretion disc coronae is of a spread of active regions, of which only a few are large and dominate at any given time. Short-lived flares may occur within an active region, which may itself last for the duration of many such (possibly correlated) flares. The detailed geometry and motions of the X-ray emitting plasma are expected to be complicated, as indicated by observations of the Sun. The implication of such a picture for the expected observable spectra will be discussed in the following section.

2.4 The spectrum of a structured magnetic corona

2.4.1 Structured coronae and thermal Comptonization

Let us assume that the X-ray spectrum is produced by thermal Comptonization in spherical active regions of size $R_a = r_a R_{\rm S}$, lifted above the disc to a height $H_a = h_a R_{\rm S}$ (Di Matteo *et al.*, 1999), and permeated by a magnetic field with intensity B. The seed photons for Comptonization are both synchrotron ones, produced locally by the interaction between the hot electrons and the magnetic field, and black-body ones coming from the underlying cold disc.

An active region illuminates the cold disc: part of the flux is reflected and part is absorbed and reprocessed. The geometry of the active region plays a crucial role in determining the comptonized spectrum: if $L_{\rm H}(r)$ is the luminosity of an active region, we have, for the reprocessed luminosity that returns to the active region and is comptonized there (Beloborodov, 1999; Malzac *et al.*, 2001),

$$L_{\mathrm{rep}}(r) = L_{\mathrm{H}}(r)(1-a)(1-\mu_0)/2, \tag{2.28}$$

where a is the disc albedo (that will be kept fixed to the value of 0.15 throughout this work), and μ_0 is a geometrical factor which regulates the feedback mechanism. As in Di Matteo *et al.* (1999), we define a circular area of radius $R_{\mathrm{hot}} = r_{\mathrm{hot}} R_{\mathrm{S}}$ in the accretion disc heated by an active region up to a temperature that depends on the illuminating flux, and define

$$\mu_0 = h_a/(r_{\mathrm{hot}}^2 + h_a^2)^{1/2} \tag{2.29}$$

as the angular size of that circle measured from the center of the active region (at height h_a). As a typical relevant radius, we take that one at which the temperature has decreased by a factor of 2, and we have $r_{\mathrm{hot}} \simeq 2.3 h_a + r_a$.

If most of the accretion power is dissipated in the corona, and the reprocessed radiation is the dominant source of soft photons for Comptonization, the ratio h_a/r_a determines the amplification factor, $A(r_a)$, and the active region temperature ($\Theta = kT_{\mathrm{e}}/m_{\mathrm{e}}c^2$): $A(r_a) = L_{\mathrm{H}}/L_{\mathrm{rep}} = 1 + 4\Theta + 16\Theta^2$. The resulting spectrum can be approximated as a power-law, with photon index, Γ, that can be related to A by the approximate expression (Beloborodov 1999a,b) $\Gamma \approx 2.33(A-1)^{-\delta}$, where $\delta \approx 1/6$ for BHC and $\delta \approx 1/10$ for AGNs. Clearly, for very large active regions ($h_a/r_a \to 0$), the amplification factor has a minimum and the spectrum is softer.

In a more general situation, the dominant source of soft photons can be determined by comparing the local energy densities of the synchrotron radiation and of the thermal emission emerging from the disc, both from intrinsic dissipation and reprocessed radiation. As already discussed by Di Matteo *et al.* (1997a, 1999) and Wardziński and Zdziarski (2000), the relevance of synchrotron emission in a magnetically dominated active region decreases with increasing central source mass (so it is less important in AGN) and is a strong function of the temperature (the hotter the corona the more it is important). Therefore, in the coronal flow around an active galactic nucleus, synchrotron radiation is likely to be relevant only for very compact active regions.

2.4.2 The X-ray spectrum

For each active region size r_a, we calculate the spectrum self-consistently: given a hard luminosity $L_{\mathrm{H}}(r_a)$, we assume that the energy density of the magnetic field is in (almost) equipartition with that of the local radiation:

$$\frac{B^2}{8\pi} = \frac{3\epsilon_{\mathrm{M}} L_{\mathrm{H}}(r_a) t_0}{4\pi (r_a R_{\mathrm{S}})^3}, \tag{2.30}$$

where ϵ_{M} is the equipartition factor, of the order of unity, and $t_0(R_a) = R_a/v_{\mathrm{diss}}$ is the dissipation time. The dissipation velocity v_{diss} depends on the uncertain nature of the heating process. For magnetic reconnection models it is related to the Alfvén speed v_{A} and to the magnetic Reynolds number R_{m} (which is very large in the low resistivity coronal plasma) and ranges from $v_\mathrm{A}/\sqrt{R_\mathrm{m}}$, in Sweet-Parker reconnection models (Sweet, 1958; Parker, 1979), to $v_\mathrm{A}/\ln R_\mathrm{m}$, in Petschek reconnection models (Petschek, 1964). On the basis of time variability argument, we can infer that v_diss cannot be larger than a few percent of the speed of light (see Section 5.2.4).

In the following calculations of our fiducial model we will fix the overall normalization constants $M_\mathrm{BH} = 10^7 M_\odot$, $\dot{m} = 0.1$ and $f_\mathrm{H} = 0.7$. Furthermore, we neglect radial dependence of the energy output and consider only the coronal flow above the inner, more luminous part of the accretion disc.

In the hot ($T \sim 50-200$ keV), highly magnetized, coronal plasma the majority of the electrons are thought to be quasi-thermally distributed (Ghisellini *et al.*, 1988) and are expected to produce synchrotron emission, and Compton scatter the softer photons produced both by dissipation in the underlying accretion disk and by the synchrotron processes themselves. In a thermal plasma, optically–thin synchrotron emission rises steeply with decreasing frequency. Under most circumstances the emission becomes self-absorbed and gives rise to a black-body spectrum below a critical frequency (Wardziński and Zdziarski, 2000):

$$\nu_\mathrm{c} \approx 2.7 \times 10^{14} \tau^{0.05} \left(\frac{T}{10^9\mathrm{K}}\right)^{0.95} \left(\frac{B}{10^6\mathrm{G}}\right)^{0.91} \mathrm{Hz} \tag{2.31}$$

where T is the coronal temperature and τ the scattering optical depth. Above this frequency, which is right in the optical/UV band for typical parameters of X-ray transient sources and magnetic fields $B \sim 10^6 - 10^7$ G, the cyclo-synchrotron emission decays exponentially as expected from a thermal plasma, due to the superposition of cyclotron harmonics.

The intrinsic disc luminosity is simply $L_\mathrm{int} = \dot{m}(1-f)L_\mathrm{Edd}$, where $\dot{m}$ is the accretion rate in units of the Eddington one, f is the fraction of the accretion power dissipated in the corona (see section 2.2) and $L_\mathrm{Edd} = 4\pi G M m_\mathrm{p} c/\sigma_\mathrm{T} = 1.3 \times 10^{38} M/M_\odot$ is the Eddington luminosity. Finally, the reprocessed luminosity, $L_\mathrm{rep}(r_a)$, is calculated from Eq. (2.28). For the two corresponding thermal soft photon fluxes from the disc $F_\mathrm{bb,i}$ and $F_\mathrm{bb,r}$, we assume black-body spectra, with temperatures θ_in and θ_re, respectively. They are given by:

$$\theta_\mathrm{in} = \left(\frac{k}{m_\mathrm{e}c^2}\right)\left(\frac{L_\mathrm{int}}{\sigma_\mathrm{B} 4\pi R_\mathrm{disc}^2}\right)^{1/4} \tag{2.32}$$

$$\theta_\mathrm{re} = \left(\frac{k}{m_\mathrm{e}c^2}\right)\left(\frac{L_\mathrm{rep}(r_a)}{\sigma_\mathrm{B} 4\pi R_\mathrm{hot}^2}\right)^{1/4}. \tag{2.33}$$

Comparing the energy densities of the three photon fields inside each active region, we determine the coefficients c_s, c_i and c_r, with $c_\mathrm{s} + c_\mathrm{i} + c_\mathrm{r} = 1$, that fix the relative contribution of synchrotron, intrinsic and reprocessed radiation as soft photons sources for Comptonization, respectively. This is illustrated in Fig. 2.1 for our fiducial model parameters and $\epsilon_\mathrm{M} = 0.1$. It is evident that for $r_a > 0.1 h_a$ the contribution of synchrotron radiation to the cooling luminosity is negligible, in particular for the high optical depth (lower temperature) cases.

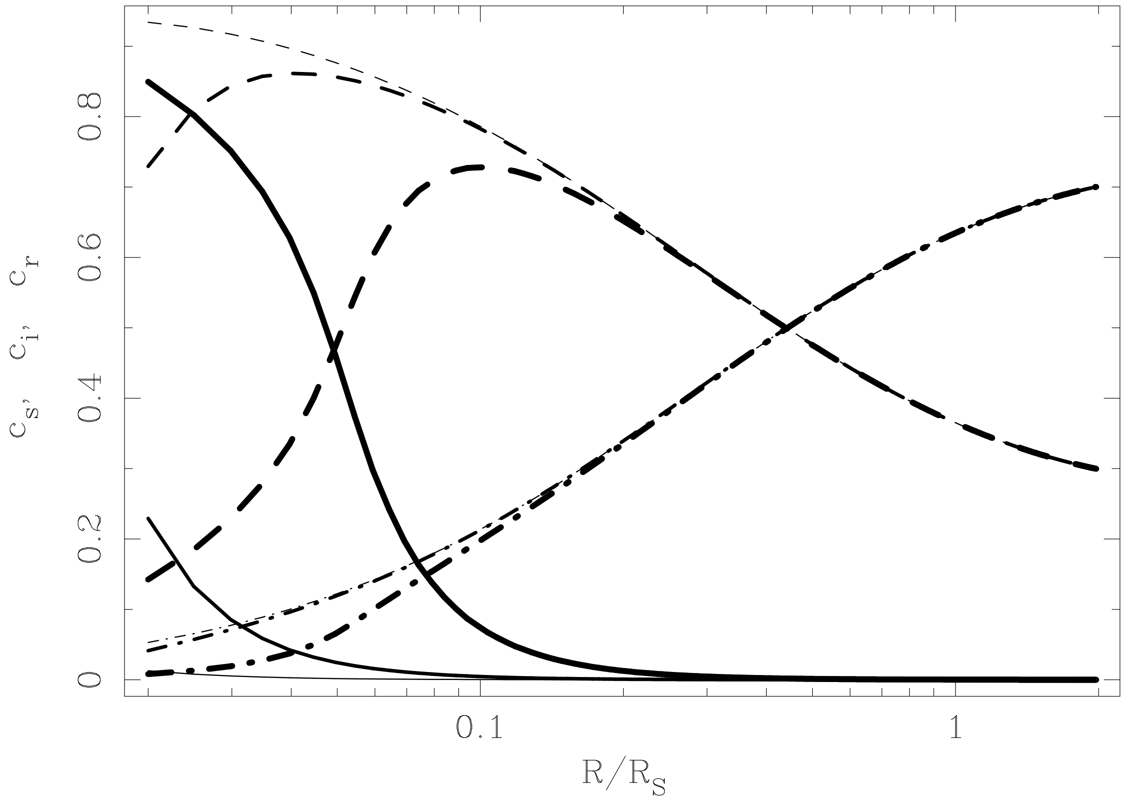

Figure 2.1: The relative contribution to the cooling luminosity from synchrotron radiation ($c_{\rm s}$, solid lines), intrinsic dissipation in the accretion disc ($c_{\rm i}$, dashed lines) and from reprocessed radiation ($c_{\rm r}$, dot-dashed lines), as functions of an active region size $r_a = R/R_{\rm S}$. The energy densities are calculated for a fixed height above the disc $H_a = 1R_{\rm S}$ in the case of an AGN with $M_{\rm BH} = 10^7 M_{\odot}$ accreting with $\dot{m} = 0.1$, $f = 0.7$ and $\epsilon_{\rm M} = 0.1$. The thickness of the lines indicates the optical depth: in order of decreasing thickness we have $\tau_{\rm T} = 0.5, 1, 2$. Clearly synchrotron radiation is important only for the more compact sources with the lowest optical depth, which are hotter and produce an harder spectrum, as shown also in Figure 2.2. Reprocessed radiation energy density, instead, always dominates as a source of soft photons for Comptonization for large enough active regions. Such behaviour is common for all values of the parameters; as a rule, the reprocessed radiation is more important for higher values of the fraction of power dissipated in the corona f.

The luminosity due to the scattered photons can be approximated as a sum of a cut-off power-law and Wien component (Wardziński and Zdziarski, 2000),

$$L_{\rm C} = N_{\rm P} \left(\frac{x}{\Theta}\right)^{-\alpha} \exp^{-x/\Theta} + N_{\rm W} \left(\frac{x}{\Theta}\right)^{3} \exp^{-x/\Theta}, \tag{2.34}$$

where $x = h\nu/m_{\rm e}c^2$ is a dimensionless photon energy, $N_{\rm P}$ and $N_{\rm W}$ are the normalizations of the power-law and Wien tail, respectively, and are related by the ratio (Zdziarski, 1985)

$$\frac{N_{\rm W}}{N_{\rm P}} = \frac{\Gamma_{\rm E}(\alpha)}{\Gamma_{\rm E}(2\alpha+3)} P_{\rm sc}, \tag{2.35}$$

where $\Gamma_{\rm E}(x)$ is Euler's Gamma function.

The scattering probability averaged over the source volume, $P_{\rm sc}$, depends on the coronal optical depth only, and determine the emerging spectral index:

$$\alpha = -\frac{\ln P_{\rm sc}}{\ln A}. \tag{2.36}$$

In spherical geometry (Osterbrock, 1974),

$$P_{\rm sc} = 1 - \frac{3}{8\tau_{\rm T}^3}\left[2\tau_{\rm T}^2 - 1 + \exp^{-2\tau_{\rm T}}(2\tau_{\rm T}+1)\right]. \tag{2.37}$$

Finally, we have for the power-law normalization

$$N_{\rm P} = 4\pi r^2 \phi \left[c_{\rm i} F_{\rm bb,i}(\theta_{\rm in}) \left(\frac{2.78\theta_{\rm in}}{\Theta}\right)^{\alpha} + c_{\rm r} F_{\rm bb,r}(\theta_{\rm re}) \left(\frac{2.78\theta_{\rm re}}{\Theta}\right)^{\alpha} + c_{\rm s} F_{\rm s} \left(\frac{x_{\rm t}}{\Theta}\right)^{\alpha}\right], \tag{2.38}$$

where the self-absorbed synchrotron flux is $F_{\rm s} = 2\pi m_{\rm e} c^3 \Theta x_{\rm t}^2/\lambda_{\rm c}^3$ and $x_{\rm t} = h\nu_{\rm c}/m_{\rm e}c^2$ is the turnover energy (in units of $m_{\rm e}c^2$) of the self-absorbed synchrotron radiation, that has been calculated as in Di Matteo *et al.* (1997a). The factor $\phi \approx (1+4\Theta^2)/(1+40\Theta^2)$ approximates the relative normalization of the power-law extrapolation and the soft photon input peak flux, and is derived form a phenomenological analysis (Zdziarski, 1986).

To finally compute the emerging spectrum, we fix the coronal optical depth, $\tau_{\rm T}$, the active region size r_a and its luminosity $L_{\rm H}(r_a)$, and calculate the temperature by imposing that the total luminosity of the active region (synchrotron plus inverse Compton emission) equals $L_{\rm H}(r_a)$.

In Fig. 2.2 we plot the coronal temperature, Θ, and the slope of the comptonized continuum, α, emerging from each active region as functions of an active region size, for different values of the optical depth. As anticipated, larger and more luminous regions are cooler, and henceforth softer, due to the larger reprocessed soft radiation they intercept. Although calculated for a spherical active region, for the sake of consistency we have checked that, in the limits $h_a/r_a \to \infty$ and $f \to 1$, our results agree with the prediction of Haardt and Maraschi (1993) for a slab corona in energy equilibrium above a cold accretion disc.

Application of the spectral model we have outlined here will be presented in the following section, and in section 5.2 within a time dependent generalization of the model.

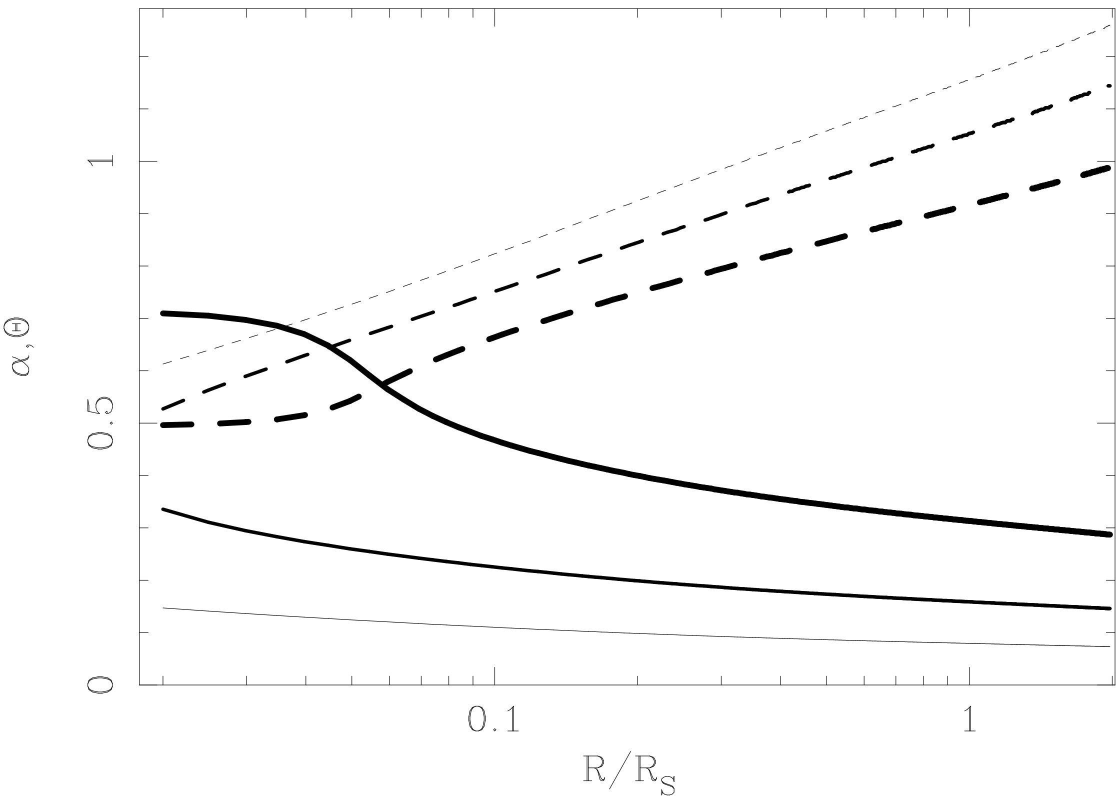

Figure 2.2: The equilibrium temperature ($\Theta = kT/m_e c^2$, solid lines) and spectral index $\alpha = \Gamma - 1$ (dashed lines) of an active region as a function of its size, for a fixed height $H_a = 1R_S$ and different optical depths, calculated for $C = 10^{-3}$ and $D = 1$ (see section 5.2). In order of decreasing line-thickness, the different curves correspond to $\tau_T = 0.5, 1, 2$. Due to the increased reprocessed radiation that is intercepted in the larger regions, the temperature drops with increasing r_a, and the emerging spectrum is softer. The shoulder at low values of R_a for the $\tau_T = 0.5$ case is due to the increased importance of synchrotron emission as a source of soft photons (see also Fig. 2.1).

2.5 Coronal outflow dominated accretion discs

In Section 1.3.2 we have mentioned the observational similarities between the SED of the black hole sources thought to accrete at low rates: black hole candidates in their low/hard state and low luminosity AGN. Here we would like to discuss a possible answer to the following question: what is the common accretion mode for low-luminosity black holes?

Since their rediscovery in recent years (Narayan and Yi, 1994), radiatively inefficient, optically thin, advection dominated accretion flows (see §1.2.3) have been regarded as natural solutions. They can explain the absence of the quasi-thermal hump, the low X-ray luminosities and the observed spectral slopes. When tested against the best data for GBHC in their Low/Hard state, though, as in the case of XTE J1118+480 (Esin *et al.*, 2001) or Cygnus X-1 (Esin *et al.*, 1998), ADAF models alone cannot work. A transition between an inner ADAF and an outer Shakura Sunyaev disc is needed, with $R_{\rm tr} \approx 10 - 100 R_{\rm S}$, as can also be inferred from studies of X-ray reflection components (Done, 2001, and reference therein). Detailed spectral fits to the broadband SED of the nearby LLAGNs M81 and NGC 4579 (Quataert *et al.*, 1999) lead to similar conclusions. The physics of such a transition, which may be taking place through a gradual evaporation of the disc as proposed by Meyer and Meyer-Hofmeister (1994) or via turbulent diffusive heat transport in the radial direction (Honma, 1996), is not included in the ADAF models, so that $R_{\rm tr}$ is usually treated as a free parameter in the spectral fit procedure. Furthermore, the low energy part of the SED is also difficult to reconcile with the standard ADAF picture, that in general predicts highly inverted spectra, instead of the observed flat ones. In fact, morphology and spectral indices of the compact radio cores require additional outflows from the central inner part in order to be consistent with the prediction of an adiabatic flow (Di Matteo *et al.*, 2001b). Finally, we recall that radiatively inefficient flows are subject to strong convective instabilities, but are in general unable to generate strong outflows (although, see Misra and Taam, 2001), unless the viscosity is very high.

Flat or slightly inverted radio spectra from very compact sources are generally associated with jet models (Blandford and Konigl, 1979; Reynolds, 1982). This has prompted the alternative view that spectra of LLAGN are essentially jet-dominated (Falcke, 2001). In particular, detailed spectral jet models have been demonstrated to successfully reproduce the SED of Sgr A* (Falcke and Markoff, 2000). Interestingly, this might also be the case for the X-ray transient XTE J1118+480 (Markoff *et al.*, 2001; §6), which, as will be discussed in details in Chapter 6, has provided us with unprecedentedly good SED and is therefore regarded as a key object for models of the *low/hard* state. Also, the presence of a relativistic jet in the black hole candidate Cygnus X-1 in the *low/hard* state has been recently confirmed by milliarcsecond resolution VLBA observations (Stirling *et al.*, 2001), confirming the general trend. In fact, Fender (2001), on the basis of the observational evidence of strong radio compact jet correlating with hard X-ray emission in GBHC in the *low/hard* state (Fender *et al.*, 1999), concludes that the jet power in these sources is at least comparable with the accretion one.

Here we explore further this latter hypothesis from the point of view of the standard accretion disc theory. We shall propose a possible new model for low-luminosity black holes, in which a standard geometrically thin, optically thick disc at low accretion rates dissipates a large fraction of its gravitational energy in a magnetic corona. We shall outline the reasons why energetically dominant coronae are the ideal site for launching powerful jets/outflows, and discuss the expected spectral properties of such accretion flows. The important conclusion we reach is that if the jet/outflow is radiatively inefficient, then so is the source overall.

2.5.1 Coronal strength at low accretion rates

The fraction f of power dissipated in the corona can be expressed as the ratio of the magnetic Poynting flux in the vertical direction to the locally dissipated energy flux in the disc:

$$f = \frac{F_{\rm P}}{Q} = \frac{P_{\rm mag} v_{\rm P}}{Q}, \tag{2.39}$$

where $F_{\rm P}$ is the vertical Poynting flux and Q is the dissipation rate of gravitational energy per unit surface area, and we have defined the velocity $v_{\rm P}$ with which the magnetic flux is transported in the vertical direction. From the standard equations of geometrically thin accretion discs with modified viscosity law we have

$$Q = \frac{3}{2}\alpha_{\rm v} v_{\rm K} \left(\frac{H}{R}\right) P_{\rm gas} = \frac{3}{2}\alpha_{\rm v} c_{\rm s} P_{\rm gas}, \tag{2.40}$$

where $v_{\rm K}$ is the Keplerian velocity, $c_{\rm s} = \sqrt{P_{\rm tot}/\rho}$ the isothermal sound speed and $P_{\rm gas}$ is the gas pressure in the disc mid-plane.

The main source of uncertainties lies in the complex process of vertical transport of magnetic flux tubes in the body of the accretion disc, and therefore on the value of the velocity $v_{\rm P}$ (see Coroniti 1981, Stella & Rosner 1984, Vishniac 1995a,b for a more thorough discussion). Here we will assume that the rise speed of the magnetic tubes is essentially given by their internal Alfvén speed (which is the case for extremely evacuated tubes), and consequently scales as $v_{\rm P}/c_{\rm s} = b\beta^{-1/2}$, where $\beta = P_{\rm tot}/P_{\rm mag} = 8\pi P_{\rm tot}/B^2$ is the standard plasma parameter, and b is related to the efficiency of buoyant transport of magnetic structure in the vertical direction inside the disc.

Equation (2.39) then becomes

$$f \simeq \frac{2b}{3}\beta^{-1/2}, \tag{2.41}$$

where we have made use of the relation $\alpha_{\rm v} \simeq P_{\rm mag}/P_{\rm gas}$.

The fraction f can then be calculated for any given accretion rate and at any given radius if we further assume that, in steady state conditions, the magnetic field inside the disc is amplified up to (quasi-)equipartition with the local gas pressure, so that

$$\beta = (1/\alpha_{\rm v})(1 + P_{\rm rad}/P_{\rm gas}). \tag{2.42}$$

If the mass of the central black hole is $M = mM_\odot$ and the radial distance from the central source is expressed in units of Schwarzschild radii $r = R/R_\mathrm{s} = Rc^2/2GM$, from (2.41), (2.42) and the equations for the ratio $P_\mathrm{rad}/P_\mathrm{gas}$ with modified viscosity law we obtain the following implicit equation for f in the radiation and gas pressure dominated zones of the disc, respectively (cfr. Eqs. 2.12 and 2.19)

$$\frac{Kf^{-2}-1}{(1-f)^{9/5}} = 2.01\times 10^5(\alpha_\mathrm{v} m)^{1/5} r^{-21/10}[\dot{m}J(r)]^{8/5} \tag{2.43}$$

$$\frac{Kf^{-2}-1}{(1-f)^{9/10}} = 1.31\times 10^2(\alpha_\mathrm{v} m)^{1/10} r^{-21/20}[\dot{m}J(r)]^{4/5}. \tag{2.44}$$

The numerical factor $K = (2\alpha_\mathrm{v} b/3)^2$ contains the unknown quantities in our treatment. As we shall see, the value of K is related to the maximal fraction of power released in the corona. It is evident that high magnetic viscosities and/or high vertical rise speeds (that are associated with the presence of very low-β, strongly evacuated, magnetic filaments in the disc) are needed in order for the corona to be powerful.

The fraction of power dissipated in the corona is higher when gas pressure dominates over radiation pressure inside the disc (see Eq. 2.42). This happens over an increasingly larger portion of the disc as the accretion rate decreases. The radial boundary between the two solutions is found when the fraction of power released in the corona is $f = \sqrt{K/2}$, and can be calculated by solving the equation

$$\frac{r}{J(r)^{16/21}} \simeq 350(\alpha_\mathrm{v} m)^{2/21}\dot{m}^{16/21}(1-\sqrt{K/2})^{6/7}. \tag{2.45}$$

The left hand side has a minimum at $r = 5.72$, therefore, for accretion rates smaller than a critical value, $\dot{m}_\mathrm{cr} \simeq 0.016(\alpha_\mathrm{v} m)^{-1/8}(1-\sqrt{K/2})^{-9/8}$, the disc is gas pressure dominated even in its inner part.

Equations (2.43) and (2.44) can be solved numerically to calculate the disc structure at every radius and for every accretion rate. A global value of f can then be obtained by integrating over all the disc area. In Figure 2.3 we plot such global value of f as a function of the total accretion rate for two different values of K (0.99 and 0.1) for typical stellar mass and supermassive black holes.

The maximum coronal dominance is attained for the lowest values of the accretion rate, and is roughly equal to $K^{1/2}$. If $K > 1$, then Eqs. (2.43) and (2.44) do not admit a solution with $f < 1$ over a wide range of radii. This might correspond to a situation in which the magnetic field is so strong and/or the vertical transport of magnetic flux tubes is so efficient that the standard accretion disc – corona configuration in no longer stable and the accretion disc, which cannot maintain its Keplerian profile, is effectively fragmented by the magnetic field into a number of disconnected rings (Heyvaerts and Priest, 1989). Also, very low-β discs are qualitatively different in terms of angular momentum transport processes. In fact, in such cases the magneto-rotational instability is suppressed and magnetic stresses at the disc–corona interface may be the primary angular momentum vehicle (Blandford and Payne, 1982) and the standard disc

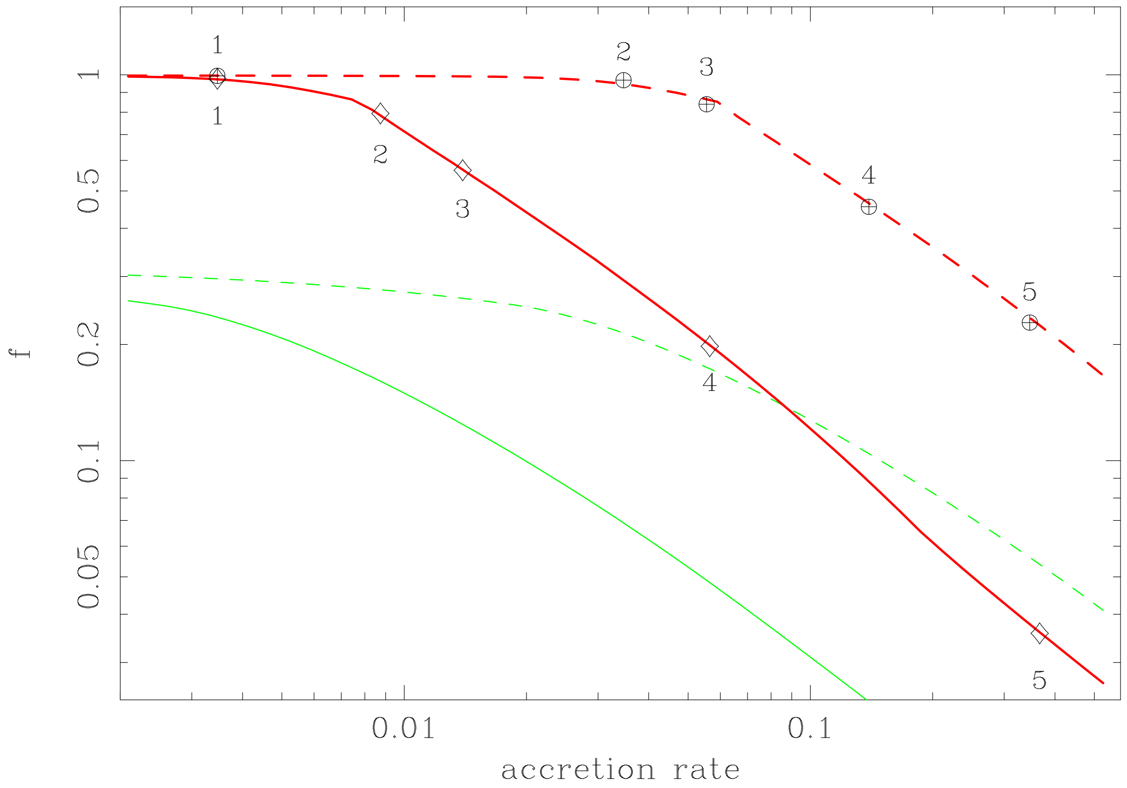

Figure 2.3: The integral fraction of accretion power dissipated into the corona as a function of the accretion rate for $\alpha_{\rm v} = 0.3$ and for two different values of central black hole mass: $M = 10^8 M_\odot$ (solid lines) and $M = 10 M_\odot$ (dashed lines), and of the coefficient K: thicker lines corresponds to $K = 0.99$ and thinner ones to $K = 0.1$. The maximal coronal strength is reached for the smallest accretion rates, and is roughly equal to $K^{1/2}$. The marked numbers on the $K = 0.99$ curves correspond to the spectral energy distributions shown in Figures 2.7 and 2.8.

structure we have assumed may not be appropriate. We therefore did not investigate such a case further, restricting ourselves to the stable case in which $K < 1$.

To summarize, in accretion discs where angular momentum is transported either by magnetic turbulence, or stresses, magnetic coronae may be dominant at low accretion rates, and their strength depends upon the nature of magnetic dissipation inside the disc. Furthermore, magnetic coronae are stronger in stellar mass black holes than in AGN (see also Fig. 2.6 below).

2.5.2 The fate of the coronal energy: coronal heating and Jet launching mechanisms

What is the fate of the energy deposited in the corona by the magnetic structures that emerge from the disc when f is large? If the current paradigm for high energy emission from black holes is correct, involving inverse Compton scattering of soft photons on a population of thermal electrons at temperatures $T_{\rm e} \sim 10^9$K, then part of this energy must be used to heat the corona, most likely via magnetic reconnection (Di Matteo, 1998). On the other hand, because Compton cooling is so efficient in the radiation field of an accretion disc, the energy densities of the thermal electrons and of the hard X-ray radiation are likely to be only a small fraction of the total energy stored in the corona, whose dominant contribution should come from stored magnetic field (see Section 2.3) and possibly hot ions, if the corona is two-temperature (Di Matteo *et al.*, 1997b). In such a situation, the condition can be favourable for the occurrence of strong coronal outflows.

To be fairly general, we consider that the total coronal power generated by the accretion disc, $L_{\rm c} = f\dot{m}L_{\rm Edd}$, can be either dissipated locally to heat the corona, and ultimately radiated away as hard X-ray radiation with a luminosity $L_{\rm H} = (1-\eta)L_{\rm c}$, or used to launch a jet with power $L_{\rm j} = \eta L_{\rm c}$. In the following, we will investigate the dependence of the parameter η on the disc–corona parameters.

The coronal magnetic field intensity depends on the dissipation rate and on the field geometry. Here we assume, on the basis of the strong spectral and variability arguments (Haardt *et al.*, 1994; Di Matteo *et al.*, 1999), that the corona is structured and the magnetic field concentrated in a number of small active regions (where dissipation occurs). The size, height and distribution of such regions determines the details of the spectral and temporal properties of the high energy emission in these sources (see Section 2.4 and 5.2). Here it will suffice to notice that a relatively small number ($N \sim 10$) of spherical active regions of size and height of the order of a few Schwarzschild radii ($R_a \sim H_a \sim 1R_{\rm S}$) is what is needed to reproduce the average properties of the hard X-rays emission of GBHC in their hard state and of Seyfert 1s and low luminosity AGN, namely a spectral index $\Gamma \sim 2$, high energy cut-off around 100 keV and strong variability.

We therefore assume that the magnetic energy density in the corona is (see Eq. 2.30)

$$\frac{B^2}{8\pi} = \frac{3L_{\rm H}}{4\pi R_a^2 Nc}\left(\frac{c}{v_{\rm diss}}\right), \tag{2.46}$$

where we have assumed $\epsilon_{\rm M} = 1$, and where $v_{\rm diss}$ is the dissipation velocity and depends on the uncertain nature of the reconnection process (Di Matteo, 1998; see also section 5.2), and can be assumed to be of the order $v_{\rm diss} \sim 0.01c$.

In the following, we will try to give an estimate of the jet/wind power expected from a corona with the above properties. As we do not discuss either the collimation mechanism or the final velocities of the outflowing gas, but only the power channeled in such a jet/outflow, we do not make any distinction between jets and outflows, and use the two terms indifferently.

The jet power. I. MHD launching mechanisms

Here we discuss the most general mechanisms by which a coronal magnetic field can power strong outflows (either in the form of Poynting flux or in the form of a magnetically driven material wind). Models and simulation of jet production (Blandford and Znajek, 1977; Blandford and Payne, 1982; Meier, 1999) show that it is the *poloidal* component of the magnetic field which mainly drives the production of powerful jets, and the output power[1] can be expressed as (Livio *et al.*, 1999)

$$L_{\rm j} = \left(\frac{B_{\rm p}^2}{8\pi}\right) 2\pi R_{\rm cor}^2 R_{\rm cor} \Omega. \qquad (2.47)$$

Here $R_{\rm cor}$ is the distance from the central black hole where most of the coronal power is dissipated and Ω is the typical angular velocity of the magnetic field lines. Maximally rotating central black holes may be important in this context more for their deeper potential wells and the larger rotational velocities that the accreting gas can attain (see also Meier 2001) than for the extraction of rotational energy from the black hole itself.

The magnetic field that emerges from the disc into the corona must be mainly azimuthal, as simulations also suggest (Miller and Stone, 2000; Machida *et al.*, 2000). If the disc is not threaded by any external large scale poloidal field, as it is likely to be in the case of central black holes, the strength of the poloidal field component depends on the typical scaleheight of a coronal magnetic flux tube and on the capability of reconnection events to create larger and larger coherent structures. Tout and Pringle (1996) have proposed numerical and analytic models in which stochastic reconnection above and below an accretion disc creates magnetic loops on all scales, with a power-law distribution. Analogously here, as the jet-launching region is identified with the corona itself, we consider the constraints put on the poloidal field by the coronal geometry, rather than the disc one.

A magnetic flux tube emerging from the disc should have a cross section of the order of the disc thickness (Galeev *et al.*, 1979). Nonetheless, the strong differential

[1]Based on the conclusion of the analysis presented in Livio, Ogilvie & Pringle (1999), we will neglect the contribution to the total power output from the energy extracted from the black hole via the Blandford–Znajek effect (BZ, Blandford & Znajek 1977). If the angular momentum of the central black hole is high enough, and a large scale poloidal field is generated and sustained in the ergosphere, the BZ power could contribute substantially to the final jet/outflow power, but the main conclusion of our investigation, namely the dependence of the jet power on the disc accretion rate would remain unchanged (see e. g. Meier 2001).

rotation at the tube footpoints causes a twisting of the tube magnetic field and increase its tension, counterbalancing its sideways expansion (see Parker 1979, §9.1, 9.6). As both theoretical arguments and numerical simulations have shown (Aly, 1990a,b; Amari *et al.*, 1996; Romanova *et al.*, 1998), the net effect of this energy injection in the magnetic coronal loops is therefore a rapid loop expansion, followed by reconnection (at a height H_a *much larger* than the disc thickness) and opening of the field lines. Therefore, if H_a is the typical coronal flux tube scaleheight (height of a reconnection site), we have

$$\frac{B_{\rm p}}{B} \simeq \frac{H_a}{R_{\rm cor}}. \tag{2.48}$$

From Eqs. (2.46), (2.47) and (2.48) we then obtain

$$L_{\rm j} = \frac{3}{2} L_{\rm H} \left(\frac{c}{v_{\rm diss}}\right) \left(\frac{H_a}{R_{\rm cor}}\right)^2 \left(\frac{R_{\rm cor}\Omega}{c}\right), \tag{2.49}$$

which in turn gives, for the fraction of coronal power that goes into the MHD jet/outflow

$$\eta_{\rm MHD} = \left(1 + \frac{2}{3}\left(\frac{v_{\rm diss}}{c}\right)\left(\frac{R_{\rm cor}}{H_a}\right)^2 \left(\frac{c}{R_{\rm cor}\Omega}\right)\right)^{-1}. \tag{2.50}$$

By inspection of Eq.(2.50) we can conclude that the jet/outflow power is stronger if:

(a) The dissipation speed is low. In this case magnetic field does not dissipate effectively via reconnection and can reach high intensities, favouring MHD outflow launching;

(b) The coronal scaleheight is large with respect to the distance from the central source. This would help in increasing the relative strength of the poloidal component of the magnetic field, that is the one ultimately responsible for the powering of the jet;

(c) The rotational velocity of the field lines is high. This is related to the gravitational potential of the central black hole (maximally rotating Kerr holes can increase the angular velocity of field lines relative to a distant observer due to the strong frame dragging effect, see e.g Meier 2001), and to the typical radius of maximal coronal dissipation.

As an example, for $v_{\rm diss} \simeq 0.01c$, $R_{\rm cor} \sim 7$, $H_a \sim 2R_{\rm S}$ and $\Omega = \Omega_{\rm K}(R_{\rm cor})$, we obtain $\eta_{\rm MHD} \simeq 0.55$: the MHD jet can carry away a substantial fraction of the coronal power.

The jet power. II. Thermally driven outflows

As discussed in Di Matteo *et al.* (1997b), magnetic dissipation in the corona may more effectively energize protons than electrons. Furthermore, given the high electron cooling rate in the corona, due to the presence of luminous sources of soft photons (either the accretion disc emitting quasi-thermally or the reconnection sites emitting synchrotron radiation), a two-temperature equilibrium situation is easily established if electrons and ions only couple via Coulomb interaction, even if a large fraction of magnetic energy were dissipated directly into the electrons (Shapiro *et al.*, 1976; Di Matteo *et al.*, 1997b).

Let us therefore consider the case of a two-temperature corona (see also Janiuk & Czerny, 2000; Różańska & Czerny, 2000) and assume that all the dissipated magnetic energy is dumped into the protons

$$\left(\frac{d\epsilon_B}{dt}\right)_- = \frac{B^2}{8\pi}\frac{v_{\rm diss}}{R_a} = \left(\frac{d\epsilon_i}{dt}\right). \tag{2.51}$$

The protons exchange energy with the electrons only via Coulomb collision, so that, in a steady state,

$$\left(\frac{d\epsilon_{\rm i}}{dt}\right) = \left(\frac{d\epsilon_{\rm e}}{dt}\right)_+, \tag{2.52}$$

where $(\frac{d\epsilon_{\rm e}}{dt})_+$ is the rate of energy transfer from ions to electrons due to Coulomb collisions between populations with Maxwellian distributions, calculated using the Rutherford scattering cross section (Stepney and Guilbert, 1983):

$$\left(\frac{d\epsilon_{\rm e}}{dt}\right)_+ = \frac{3}{2}\frac{m_{\rm e}}{m_{\rm p}}\frac{n_e n_i \sigma_{\rm T}(kT_{\rm i}-kT_{\rm e})c}{K_2(1/\theta_{\rm e})K_2(1/\theta_{\rm i})}\ln\Lambda f(\theta_{\rm e},\theta_{\rm i}), \tag{2.53}$$

where $T_{\rm e,i}$ are the electrons and ions temperatures, respectively, $\theta_j = kT_j/m_jc^2$ $(j = {\rm e,i})$ are dimensionless temperatures, $\ln\Lambda \approx 20$ is the Coulomb logarithm, Ks are the modified Bessel functions and

$$f(\theta_{\rm e},\theta_{\rm i}) = \left[\frac{2(\theta_{\rm e}+\theta_{\rm i})^2+1}{\theta_{\rm e}+\theta_{\rm i}}K_1\left(\frac{\theta_{\rm e}+\theta_{\rm i}}{\theta_{\rm e}\theta_{\rm i}}\right) + 2K_0\left(\frac{\theta_{\rm e}+\theta_{\rm i}}{\theta_{\rm e}\theta_{\rm i}}\right)\right]. \tag{2.54}$$

In order to calculate the electron temperature, we equate the electron heating rate with the total cooling rate $q_{\rm cool} = q_{\rm Comp}+q_{\rm synch}+q_{\rm CS}$, which includes inverse Compton scattering of both disc photons and self-absorbed synchrotron emission produced in the active region itself (see e.g Section 2.4).

Once the heating rate of ions and electrons is specified via Eqs. (2.46), (2.51) and (2.53), and the geometry of the corona is fixed, determining the cooling rate $q_{\rm cool}$, we can calculate electron and ion temperatures, if the coronal optical depth is known. Observationally, both black hole candidates in their Low/Hard state and AGN have similar values of τ, lying in a narrow range around $\tau \sim 1$ (Gierlinski *et al.*, 1997; Zdziarski, 1999). As an illustrative example, we made here the assumption that, for each value of the central source mass, M, the coronal optical depth is proportional to the accretion disc surface temperature. In particular, for gas pressure dominated solution appropriate for low accretion rates, we have chosen $\tau \simeq 4\dot{m}^{2/5}(1-f)^{1/5}$. Therefore τ is smaller for smaller accretion rates ($\tau \sim 0.2$ for $\dot{m} = 0.005$) and we have $\tau \sim 1$ for $\dot{m} = 0.05 - 0.08$, depending on the black hole mass. The dependence of τ on the accretion rate for central black holes of masses $m = 10$ and $m = 10^8$ is shown in Fig. 2.4. It is important to stress that the specific dependence of τ on the disc parameters we have assumed here

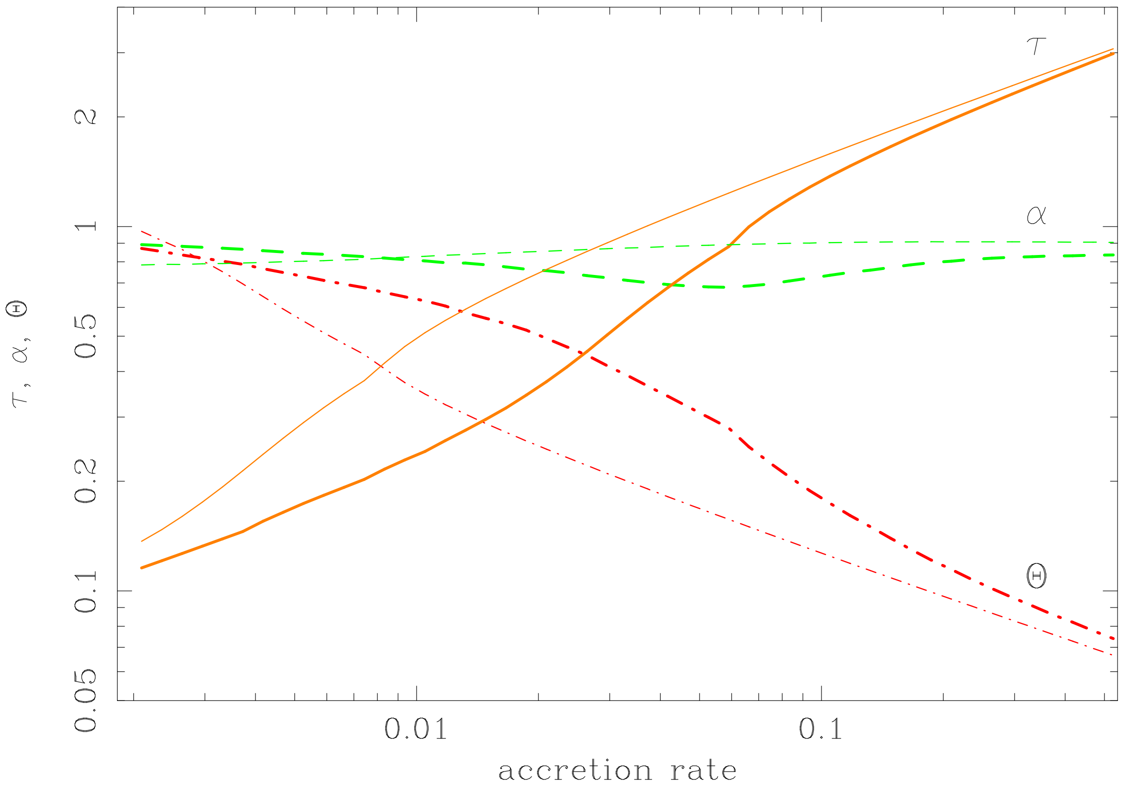

Figure 2.4: Variation of the electron temperature in the corona ($\Theta = kT_{\rm e}/m_{\rm e}c^2$, dot-dashed lines) and of the X-ray spectral index (α, dashed lines) as functions of the accretion rate, calculated for the optical depth profile shown (τ, solid lines). Thicker lines correspond to a central black hole mass $m = 10$, thinner lines to $m = 10^8$.

has been chosen only for illustrative purposes: the results we present on the strength of thermally driven outflows would be qualitatively the same for any physical situation in which colder and denser accretion discs were sandwiched by lower optical depth coronae (as would be the case, for example, if the coronal optical depth depend, instead, on the accretion disc ionization parameter $\xi = L_{\rm H}/nH_a^2$).

Once a value for the coronal optical depth is fixed, for each value of the accretion rate we can then calculate magnetic field intensity, electron and proton temperatures and the overall emitted spectrum by solving the equation for the cooling and heating rate, adopting an analytic approximation for the emissivities described in Section 2.4.2. In Figure 2.4 we also show, as functions of the accretion rate, the calculated values of the electron temperature $\Theta = kT_{\rm e}/m_{\rm e}c^2$ and spectral index α of the hard X-rays produced by inverse Compton scattering on the hot coronal electrons.

We stress that the values of the electron temperature depends also on the detail of the coronal geometry, namely, on the size, height and number of magnetic regions reconnecting in the corona at any time (Stern *et al.*, 1995; Di Matteo *et al.*, 1999). This is an inherently time dependent problem (see e.g. Poutanen & Fabian, 1999; §5.2) and here we have chosen average values for the coronal geometric parameters ($H_a = R_a = 1R_{\rm S}$) that ensure that the value of the spectral index is close to the observed

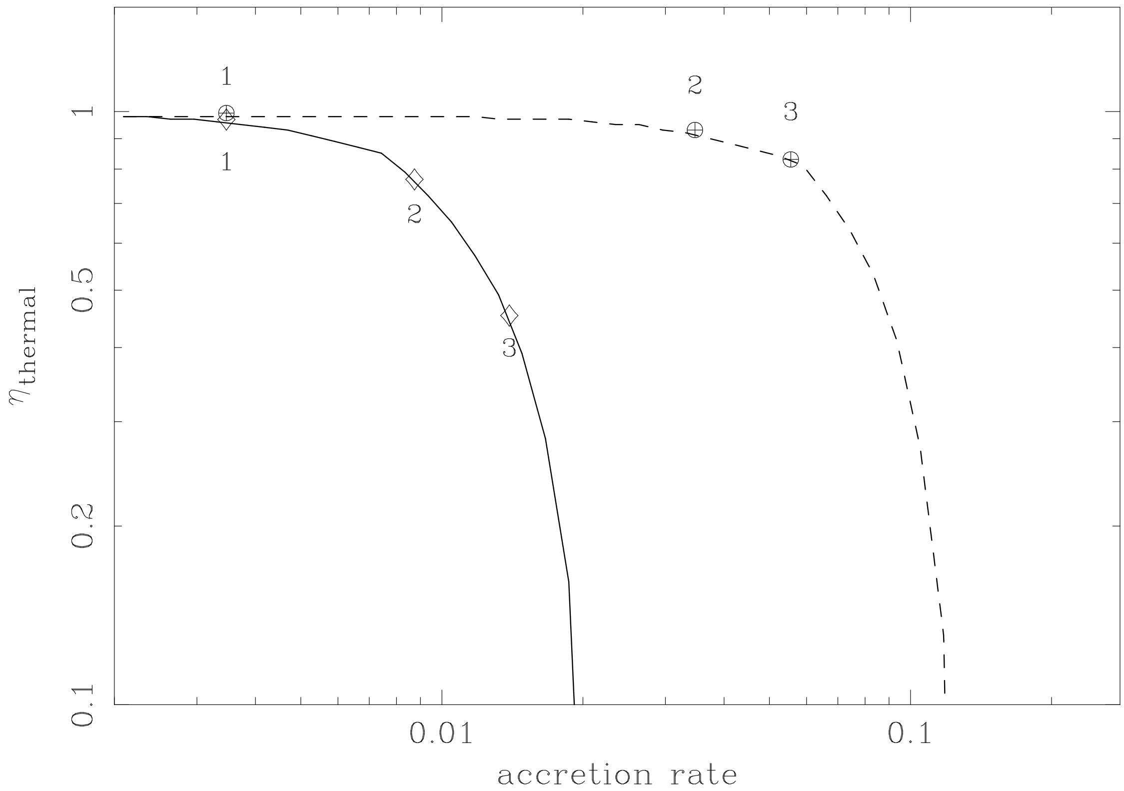

Figure 2.5: The relative strength of thermally driven coronal outflow as a function of the accretion rate for two different values of the central black hole mass: $M = 10^8 M_\odot$ (solid line) and $M = 10M_\odot$ (dashed line). We have imposed maximal coronal strength by taking $K = 0.99$. At the lowest accretion rates, where $f \rightarrow \sqrt{K}$ we have $\eta_{\text{thermal}} \simeq 0.98$.

one, and we are not interested in detailed spectral modeling of the X-ray emission.

If the coronal density is low enough, and if the power dissipated in the corona high (and both conditions are more likely in low accretion rate discs, as we have shown in Section 2.5.1), the protons can be heated up to temperatures higher than the virial one $T_{\text{vir}} = GMm_{\text{p}}/6kR_*$ (here we may take as R_* the radius at which the coronal dissipation is higher). In this case the corona is likely to drive powerful jets/outflows (Piran, 1977; Lin *et al.*, 2001). A fraction η of the coronal power is advected by the outflow in the form of bulk kinetic energy and the heating rate of the protons is therefore reduced. In such cases we may estimate a value for the parameter η simply by looking for the minimal value of η for which the protons are at the virial temperature. The resulting values for such η_{thermal} as a function of the accretion rate for $\alpha_{\text{v}} = 0.3$, $K = 0.99$ and two different black hole masses are shown in Figure 2.5. The outflow/jet power (kinetic energy plus Poynting flux) decreases sharply as the accretion rate increases and is negligible as soon as the temperature up to which the protons are heated in the corona drops below the virial one.

The coronal and jets strengths depend weakly on the central source mass, as implicitly shown in Eq. (2.43) and (2.44). In Fig. 2.6 we show explicitly the values of the accretion rate for which $f > 0.5$ ($\dot{m}_{5,\text{f}} \propto M_{\text{BH}}^{-0.124}$, filled circles, solid line) or

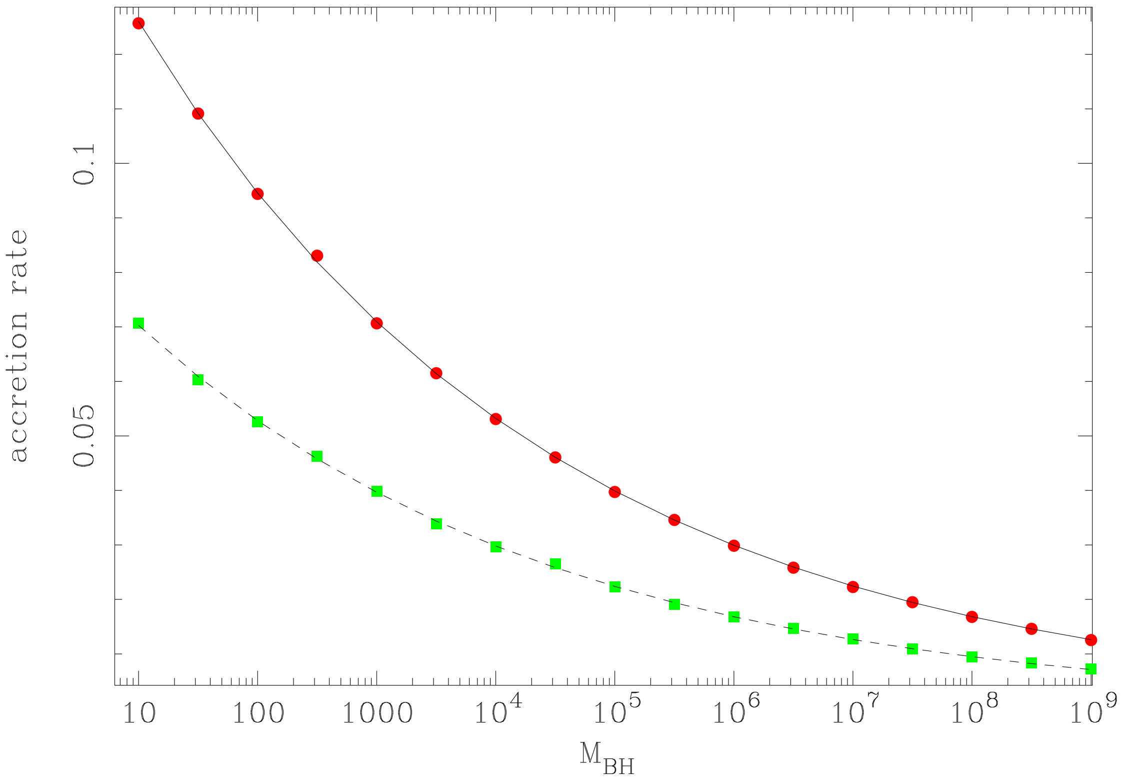

Figure 2.6: As a function of the central black hole mass, we plot the value of the accretion rate for which: (a) the dissipation in the corona is more than three times the internal disc one ($f > 0.5$, filled circles) and (b) the thermally driven jet power is more than three times the sum of the radiative corona plus disc output ($f\eta > 0.5$, filled squares). Also shown are the best power-law fits to the two functions (see text).

$f\eta > 0.5$ ($\dot{m}_{5,\mathrm{jet}} \propto M_{\mathrm{BH}}^{-0.125}$, filled squares, dashed line). Ghisellini & Celotti (2001b), by studying the dividing line between FR I and FR II radio-galaxies (which correspond approximately to low and high radio–power galaxies, respectively) in the radio–host galaxy luminosity plane conclude that such dividing line correspond to an approximately universal (independent on the black hole mass) transition value of $\dot{m} \simeq 0.06$, remarkably close to the values we found.

2.5.3 Predicted spectra

Let us consider now the case in which the outflow is thermally driven, and discuss the expected spectral properties from the system at different accretion rates. For small and intermediate values of f (therefore for $\dot{m} \gtrsim 0.1$ or $\dot{m} \gtrsim 0.01$ for $m = 10$ and $m = 10^8$, respectively) the seed soft photons for Comptonization come from the quasi-thermal accretion disc emission (either intrinsic or reprocessed). Then, the coronal cooling decreases when the accretion rate decreases, and the X-ray spectrum gets harder, as can be seen if Fig. 2.4. The hardest spectra are obtained for $f \to 1$ and $\eta < 0.9$. At this point inverse Compton scattering on synchrotron photons produced in the corona dominates the cooling. Finally, as the ions become supervirial, more and more power is carried away in the form of a powerful jet/outflow and the coronal heating is reduced more rapidly than the cooling due to synchrotron emission and the spectrum gets slightly softer again.

This is illustrated in Fig. 2.7 and 2.8, which show a sequence of spectral energy distributions for the stellar mass and supermassive black hole cases, respectively.

We do not attempt to model the emission from the jet/outflow. Given the high brightness temperatures measured in the cores of some LLAGN, we indeed expect self-synchrotron Compton emission to be important at low $\dot{m}$. Also, the high energy spectrum would be modified by even a small fraction of non-thermal electrons in the corona and/or in the outflow (see e. g. Poutanen & Coppi 1998; Wardziński & Zdziarski 2001).

2.5.4 ADAFs or Jets?

The scenario we have presented for low-luminosity accreting black holes is an alternative to the current ADAF/CDAF one. The main testable difference between the two models is the presence of a geometrically thick, cold, accretion disc in the inner part of the flow. In the magnetic corona scenario, even at the lowest accretion rates, when most of the accreting power is dissipated in the corona, the presence of the disc in the inner part of the flow would manifest itself by reprocessing coronal radiation and producing both a thermal and a reflection components (see §3). Nonetheless, it is well known that if the coronal luminosity is so high that the inner part of the accretion disc is fully ionized, the reflection features are so weak that it is difficult to distinguish between a truncated disc and an ionized one (Done and Nayakshin, 2001; Ballantyne *et al.*, 2001). Furthermore, when the corona is so powerful that it produces relativistic outflows, the bulk motion of the coronal outflowing material reduces the amount of high energy radiation impinging on the disc, thus reducing the strength of the reprocessed components (Beloborodov, 1999; Malzac *et al.*, 2001).

Our coronal outflow dominated solutions are both thermally and viscously stable, as in general are all standard Shakura–Sunyaev accretion disc solution in the gas pressure dominated regime. Rapid and dramatic variability in the observed high-energy flux is nevertheless expected, as X-rays are produced by coronal structures that are the eventual outcome of the turbulent magnetic field generation inside the disc. The geometry of these structures (open vs. closed field lines, for example) plays a very important role and may be such that, at times, parts of the corona become temporarily radiatively efficient. This could explain, for example, the rapid X-ray flaring episode observed recently in the galactic centre (Baganoff *et al.*, 2001). During such sudden rapid flaring episodes in the X-ray energy band would be possible to analyse the reflection spectral component and ultimately determine the inner disc geometry, therefore discriminating between a coronal outflow dominated accretion disc and an advective flow.

At the low accretion rates we are considering, both our corona dominated solution for a standard thin disc and ADAF/CDAF solution are admitted. A 'strong ADAF

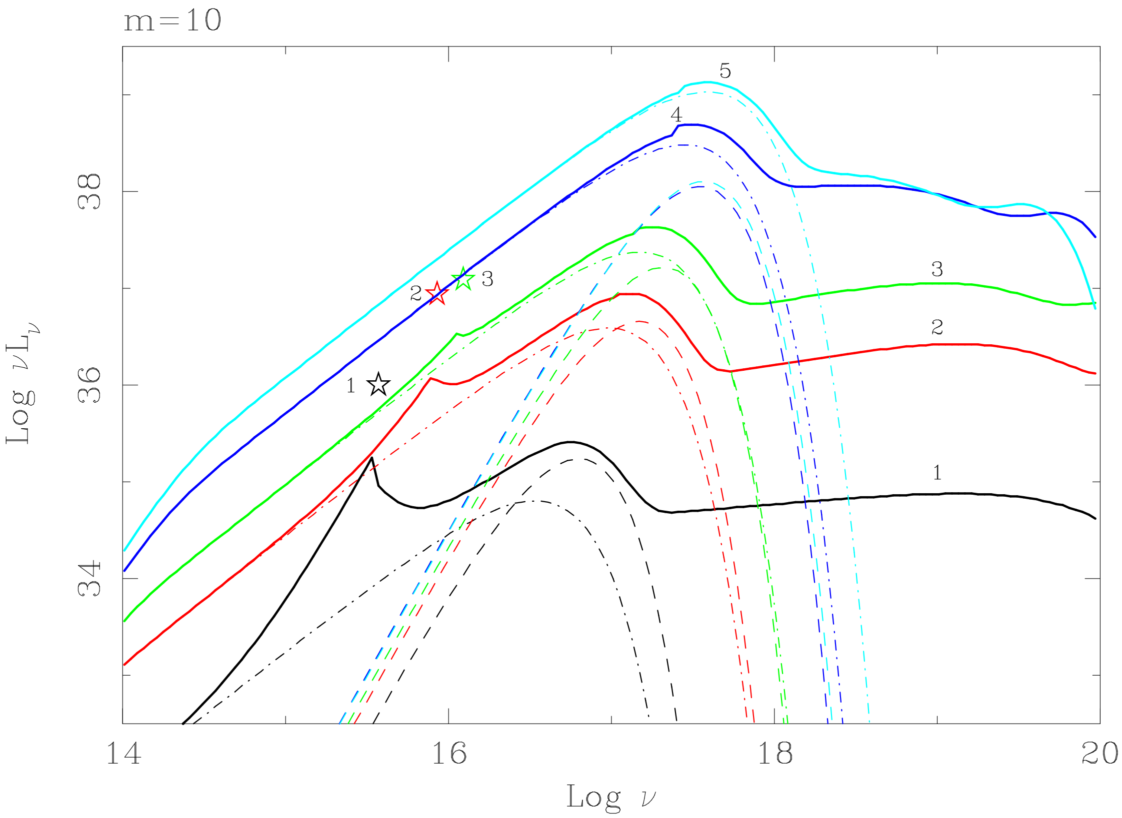

Figure 2.7: The spectral energy distributions calculated for our thermally driven jet model for $m = 10$ (see text for details). The five spectra correspond to the five points marked with open circles in Fig. 2.3. Solid lines show the total emerging spectra, while dashed lines show the contribution of thermal reprocessed radiation from the disc and dot-dashed lines the intrinsic multicolor disc emission (with outer radius $R_{\rm out} = 2 \times 10^5 R_{\rm S}$). The strong peak at $10^{15} - 10^{16}$ Hz represent the self absorbed synchrotron emission from the active coronal regions: for spectra 1 and 2 ($\dot{m} \simeq 0.003, 0.03$) it clearly represents the main source of seed photons for Comptonization. The open stars mark the level of total jet luminosity with the assumption of a 10 per cent radiative efficiency. If the jet spectrum is flat ($L_\nu \propto \nu^\gamma$ with $\gamma \sim 0$), and extends up to the frequency of coronal synchrotron self-absorption, the stars mark the peak of the compact jet spectral component. No optically thin emission from the jet is included. Also neglected is the reduction of the thermal reprocessed hump (dashed lines) that can be expected if the X-ray emitting coronal active regions also move with the outflow at relativistic speeds (Beloborodov 1999).

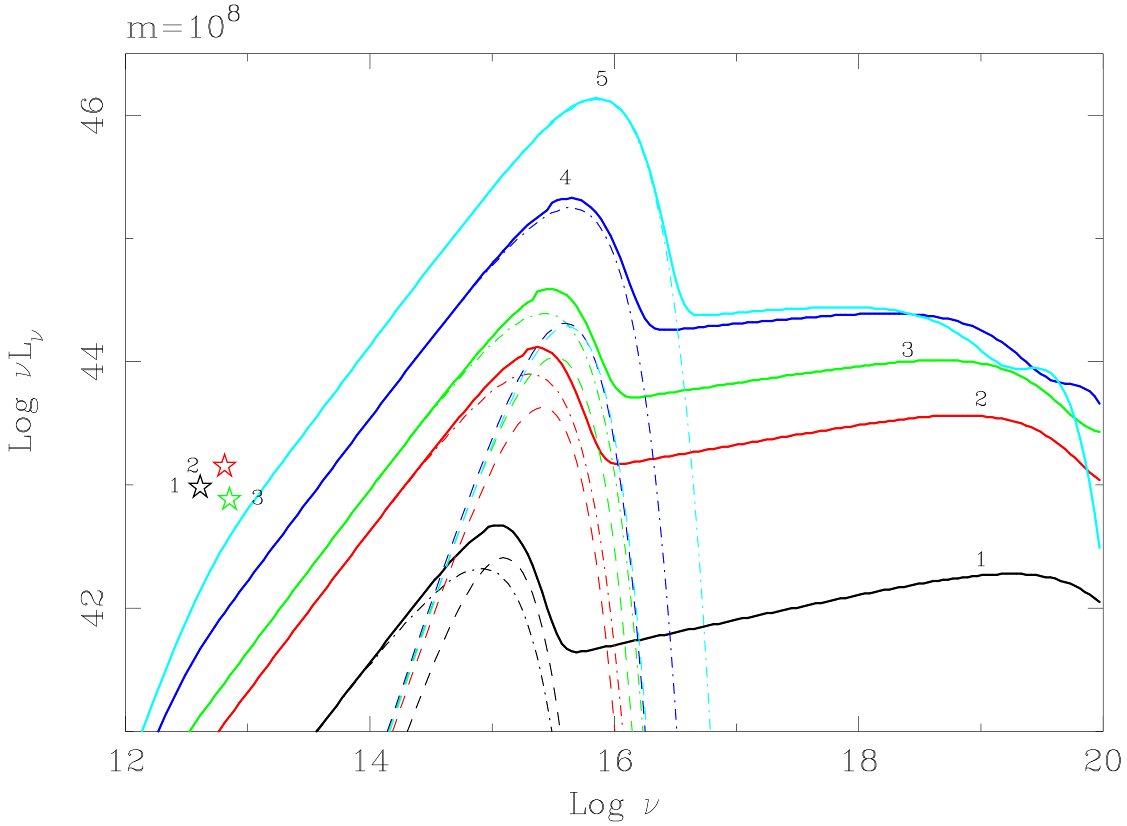

Figure 2.8: The spectral energy distributions calculated for our thermally driven jet model for $m = 10^8$ (see text for details). Symbols and line styles are the same as in Figure 2.7. Here direct synchrotron radiation is always dominated by the quasi-thermal disc component, due to the decreased value of the coronal magnetic field ($B \propto m^{-1/2}$). At accretion rates lower than what shown by curve 1 ($\dot{m} < 0.003$) the shape of the SED does not change any longer, the overall luminosity being simply reduced.

principle' has been advocated (Narayan and Yi, 1995b) to ensure that the real systems will tend to chose the ADAF/CDAF branch whenever possible. Here we have explored the possibility that such a strong ADAF principle does not hold, and studied the expected properties (spectral and energetic) of an alternative accretion mode. Nonetheless, there are admittedly some similarities between the powerful outflow-dominated, radiatively-inefficient coronae that we found here at the lowest accretion rates and a classical ADAF, and we might well be exploring a region of the accretion flow parameter space where the two accretion modes are bridged together (in this case mainly by virtue of strong magnetic field generation, rather than evaporation; cfr. Meyer & Meyer-Hofmeister, 1994). In fact, from our study we expect strong coronal outflows at high values of the viscosity parameter $\alpha_{\rm v}$ similar to what is predicted by the theory of advective flows (Igumenshchev and Abramowicz, 2000).

When $f \rightarrow 1$ and $\eta \rightarrow 1$, the radiative efficiency of a coronal outflow dominated flow depends on the radiative efficiency of the outflow itself. However, unless $1-\eta \sim 10^{-3}$, we cannot achieve the extremely low efficiencies ($\epsilon \lesssim 10^{-5}$) required to explain some nearby LLAGN (Di Matteo *et al.*, 2001a). Such estimates, though, are based on the Bondi accretion rates estimated at relatively large distances from the source. It is plausible that the strong outflows we envisage, by interacting with the intergalactic medium, would stifle accretion through the inner part of the disc (an effect analogous to that of the ADIOS solution of Blandford and Begelman, 1999, in the advective case), reducing the value of the accretion rate through the inner disc that we are considering here and alleviating the need for too low a radiative efficiency (see also discussion in Di Matteo *et al.*, 2001).

An important issue concerns the fate of the cold thin disc when we extrapolate our solution at extremely low accretion rate. Is it disrupted when the fraction of the power dissipated in the corona approach unity, or does it survive, extremely thin and cold? Very strong outflowing coronae might have relevant effects on the nature of the angular momentum transport in the flow, and therefore on the disc structure. The constant improvement of numerical simulations in recent years, make us believe that the relevance of the solutions we describe here will be assessed in the near future. At present, numerical simulations of MRI unstable accretion discs with sufficient extension in the vertical direction seem able to generate only modestly powerful coronae ($f \sim 0.2$, Miller and Stone, 2000). The inclusion of radiation in the MHD codes (Turner and Stone, 2001), and a detailed study of the dependence of the solution on the accretion rate will prove crucial to settle the issue. We remark, however, that *observationally* the presence of strong coronae is a fact (see e.g. Cygnus X-1 in its low/hard state) we are confronted with.

We have discussed separately two different outflow mechanisms. Clearly both may be at work at the same time, and influence each other. For example, when the conditions for MHD jet launching are favourable, and a larger number of open field lines thread the inner part of the corona, then, depending on the inclination angle of the field lines, a larger mass can be channeled into the outflow, reducing the coronal density and therefore the Coulomb cooling of the hot ions and enhancing the thermally driven jet power as well.

Radiatively inefficient flows are also expected at very high accretion rates, as discussed in Section 1.2.4. We just remark here that observationally, black holes believed to accrete at super-Eddington rates bear many similarities with their low-accretion rate counterparts. This class of object may include GBHC in the very high state (see Done, 2001 and references therein), whose X-ray spectra show a power-law component usually as strong as the quasi-thermal one; the microquasar GRS 1915+105 (Belloni *et al.*, 2000b); broad line radio galaxies (BLRG, see e. g. Zdziarski 1999 and reference therein); powerful blazars (see in particular Ghisellini and Celotti, 2001, where it is shown how the relativistic jet in these sources may dominate the total output power); and possibly, narrow line Seyfert 1s (NLS1, Mineshige *et al.*, 2000). Most likely, newly formed supermassive black holes at the epoch of galaxy formation and quasars in their early evolutionary stages might be fed at super-Eddington rates, therefore a better understanding of accretion flows and jet/outflow production in these sources will shed light on the processes of galaxy formation and evolution (Fabian, 1999).

2.6 Summary and conclusions

In this chapter we have discussed many aspects of the physics of the hot, rarefied part of the accretion flow, the so-called corona, which is responsible for the hard X-ray power-law emission observed in the spectra of almost all black hole powered sources. After a discussion of the structure equation of the accretion disc–corona system (§2.2), in Section 2.3, by comparing the thermal energy content of the corona, deduced from the observed spectra, with the observed X-ray luminosity, we have shown that the corona is likely to be patchy, and energetically dominated by a magnetic field. Then (§2.4), we have illustrated the generic model for the X-ray spectrum produced by a structured magnetic corona via inverse Compton scattering, of both thermal photons from the accretion disc and synchrotron ones produced locally in the coronal active regions, on the hot coronal electrons. Finally, in Section 2.5, we have studied the energetics and power output of the coronae generated by geometrically thin, optically thick accretion discs at low accretion rates. We have assumed that angular momentum transport in the disc is due to magnetic turbulent stresses and that both magnetic energy density and effective viscous stresses inside the disc are proportional to the gas pressure. In this case, we have shown that the relative strength of the corona, generated via amplification and expulsion of the turbulent disc magnetic field, increases as the accretion rate decreases. The rarefied corona, heated by the dissipating field (via magnetic reconnection and/or shock heating) up to temperature of few tens of keV, is the ideal site for launching an outflow, either magnetically or thermally. We assessed the relevance of the various mechanisms that can generate such powerful outflows from the coronal region. We have shown that, depending on the actual coronal field geometry, MHD launching mechanisms can indeed produce strong outflows, whose power is of the order of the radiated one. Moreover, if the corona is two-temperature, a thermally driven outflow can easily dominate the power output from the source at low accretion rates. Thus, if the jet/outflow do not radiate efficiently, the whole system can be very under-luminous compared to a standard radiatively efficient accretion disc.

Chapter 3

The effects of a Comptonizing corona on the observed reflection component in black hole spectra

3.1 Introduction

In the previous chapter we have addressed in some detail the issue of the mechanisms by which the so-called primary continuum of black hole emission is produced, with particular emphasis on the physics of the hot corona that is responsible for the ubiquitous hard X-ray power-law in the observed spectra.

The presence of secondary components in the spectra of Seyfert galaxies and galactic black hole candidates, such as the fluorescent iron Kα line at $\sim$6.4 keV and a reflection hump between 10 and 50 keV, superimposed on the primary X-ray continuum, is now well established observationally (Nandra and Pounds, 1994). Discovered in the late eighties with the *GINGA* satellite (Matsuoka *et al.*, 1990; Pounds *et al.*, 1990), they are signatures of reprocessing of the primary X-ray emission in surrounding cold ($T \leq 10^5 K$) and optically thick matter accreting onto the central engine. Indeed, part ($\sim 10\%$) of the primary X-ray radiation may be Compton reflected at the gas surface, producing the observed secondary features (Bai and Ramaty, 1978; Lightman and White, 1988; George and Fabian, 1991; Matt *et al.*, 1991; Magdziarz and Zdziarski, 1995). The remaining incident flux is reprocessed in the UV/Soft X-ray band and is believed to form part of the UV–soft X–ray excess (the so-called UV bump) generally observed in this class of objects.

These reflections features are of great importance in testing theoretical models of the high energy emission in compact objects, since they give crucial (while indirect) constraints on the geometry and on the nature of the emitting regions.

As we have seen in Section 2.4, Compton scattering of the soft photons emitted by the cold, optically thick matter on a population of hot thermal electrons (the corona) is the best model to date for the primary high energy emission in these objects. Indeed, if we assume radiative equilibrium between the thermal comptonizing plasma and the underlying cold matter (generally an accretion disc), we can naturally account for the average properties of the X-ray emission of black holes accretion flows (Haardt and Maraschi, 1991). Also, as we have already discussed in chapter 2, it has been shown that a patchy geometry, where the corona is disrupted in localized blobs, appears to be in better agreement with the spectral variability and L_{UV}/L_X ratios observed, for example in Seyfert galaxies (Haardt *et al.*, 1994; Stern *et al.*, 1995). However, the real geometry of the corona–disc configuration is relatively difficult to constrain in the framework of this class of models and the reflection features can give some important clues in this respect. An alternative model for the high energy emission in black hole spectra consists of an advection–dominated accretion flow (ADAF) near the central engine (see Section 1.2.3).

The amount of reflection is expected to be different in these different scenarios. For instance, in a disc–corona configuration we expect a reflection fraction of the order of unity, since the reflecting disc, as seen by the hot corona, subtends a solid angle of 2π. On the other hand, in the case of a truncated disc–ADAF model, the solid angle would be smaller due to the lack of reflecting matter in the central regions. For the same reason, we expect narrower iron Kα fluorescent lines since relativistic effects, which are stronger in the vicinity of the black hole, are negligible in the ADAF configuration.

That is why it is generally expected that the properties of the reflected spectrum could provide a strong observational test to discriminate between different accretion modes. However, many secondary effects may complicate the situation. For instance, the complex ionization state of the reflector's skin can strongly mask and/or modify the reflection features that we expect in the case of a simple neutral reflector, or even of a single–zone ionization model. Done and Nayakshin (2001) and Ballantyne *et al.* (2001) have recently shown that, if the accretion disc is highly ionized, single–zone ionization models can severely underestimate the reflection normalization. They could even give rise to an apparent correlation between the reflection normalization and the spectral photon index similar to that reported by Zdziarski *et al.* (1999) in a sample of Seyfert galaxies and galactic black hole candidates. The presence of a dynamic hot corona (Reynolds and Fabian, 1997; Beloborodov, 1999; Malzac *et al.*, 2001) will also strongly modify the reflection spectrum, due to the anisotropic illumination produced by relativistic motions of the active regions. Finally, it is quite possible that the surface of a turbulent disc (the disc–corona interface) is far from smooth. A wrinkled, fractal-like surface might have a very different (lower) albedo from what is usually assumed in the case of a regular (analytic) surface, and therefore reduce the amount of reflected radiation observed in the outgoing spectrum.

In this chapter we will discuss in some detail another important effect, which will also modify the appearance of the reflected spectral components. In a disc–corona configuration, we expect that part (or even all, depending on the coronal covering fraction) of the reflection features cross the comptonizing plasma before being observed. In this case, the reflected photons are also Compton scattered in the corona and the shape

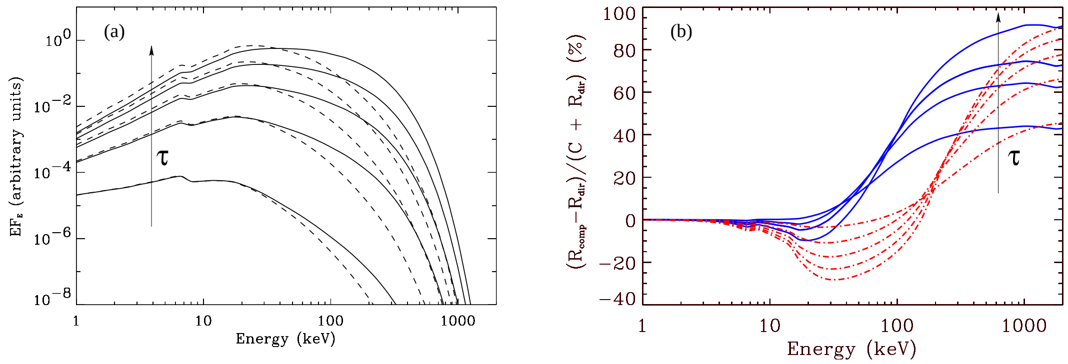

Figure 3.1: (a) The comptonized (solid lines) and uncomptonized (dashed lines) reflection humps, $R_{\rm comp}$ and $R_{\rm dir}$, for different values of the coronal optical depth, the temperature being fixed to $kT_{\rm e}$=50 keV. From bottom to top, τ=0.1, 0.3, 0.5, 0.7 and 0.9. (b) Deviations (in %) between the outgoing spectra. The solid line and dot-dashed lines correspond to $kT_{\rm e}$ = 50 keV and 350 keV respectively.

of the secondary spectral components may be significantly modified as compared to the one expected when no Comptonization in the corona is taken into account.

The effects of the hot corona on the appearance of the reflection component have been already pointed out by some authors (Haardt *et al.*, 1993). The aim of the work presented in this section is to study more precisely the dependence of such effects on the physical (temperature and optical depth) and geometrical (inclination angle) parameters of the hot corona. Also, we are interested in the consequences of these effects in the analysis and the interpretation of real spectral data. We mainly focus on the slab geometry, where the effects are expected to be large since the corona completely covers the reflecting material, but our treatment can be applied to patchy corona models, too, for large enough active regions. In such a case, although the total covering fraction of the corona may be quite small, still the reflected radiation coming from the cold disc will be largely comptonized in the corona, as it is produced right underneath the active regions themselves.

3.2 The model

We use the thermal Comptonization code of Haardt (1994, hereafter H94). The code computes the angle–dependent spectrum of the disc–corona system in a slab configuration using an iterative scattering method, where the scattering anisotropy is taken into account only up to the first scattering order. It also computes, separately, the reflection components obtained either including or neglecting the effect of Comptonization in the corona. They will be denoted $R_{\rm dir}$ and $R_{\rm comp}$, respectively, in the following. The continuum will be simply called C.

The reflection component $R_{\rm dir}$ is computed following White *et al.* (1988) and Lightman and White (1988); thus, the spectral shape of the reflected radiation is averaged over angles. It is well-known that the actual shape of the reflection component does indeed depend on the viewing angle, especially at high energy. Such angular distortion is relatively complex and is a function of the photon energy. The main effects occur in the hard X-ray and soft γ-ray bands, where the reflected spectra strongly harden with increasing viewing angle (Hua and Lingenfelter, 1992; Magdziarz and Zdziarski, 1995). We have checked *a posteriori* (cfr. Section 3.3.2 and Fig. 3.3) that the effects of such an angular dependence are always smaller than the ones we discuss here. Consequently, in the rest of the chapter, we will normalize the spectrum at different viewing angles by just multiplying the reflection component by the angular function

$$\begin{aligned} f(\mu) &= \frac{3\mu}{4}\left[(3-2\mu^2+3\mu^4)\ln\left(1+\frac{1}{\mu}\right)+\right. \\ &\quad \left.(3\mu^2-1)\left(\frac{1}{2}-\mu\right)\right], \end{aligned} \tag{3.1}$$

where μ is the cosine of the inclination angle i, neglecting any energy dependence (see Ghisellini *et al.*, 1994, for details)[1].

The effect of Comptonization on the reflection component will depend mainly on three physical parameters: the temperature $kT_{\rm e}$ and the vertical optical depth τ of the corona and the inclination angle i. The last two parameters may be combined to give an "effective"optical depth $\tau_\mu = \tau/\mu$, which is the line-of-sight optical depth that a photon, emitted at the surface of the disc, has to cross in order to escape from the corona without being comptonized and reach an observer at the viewing angle i.

The soft temperature of the cold matter $kT_{\rm bb}$, does not play an important role in the problem we study here. In fact, in an anisotropic geometry, as the one we are dealing with, the spectrum emitted by the corona depends on such temperature because of the presence of an anisotropy break (Stern *et al.*, 1995; Svensson, 1996; Haardt *et al.*, 1997; Petrucci *et al.*, 2000). Such a break is due to the reduced contribution of the first Compton scattering order, mainly emitted backward towards the disc, to the outgoing flux. The spectrum is then better approximated by a convex broken power law where the break energy depends mainly on $kT_{\rm e}$ and $kT_{\rm bb}$. Changing $kT_{\rm bb}$ will thus modify the shape of the X-ray spectrum impinging on the cold matter and consequently the shape of the reflection components $R_{\rm dir}$ and $R_{\rm comp}$. However, we have checked that these effects are negligible in comparison to the ones we are looking at. We will thus fix $kT_{\rm bb}$ to a constant value of 10 eV in the following.

3.3 Comptonization effects on the reflection hump shape

3.3.1 Dependence on the physical parameters of the corona

In this section we will firstly discuss the effect of the Comptonization in the corona on the *shape* of the reflection component, when varying the optical depth and/or

[1] It is worth noting that the shape of the reflection component averaged over angles is very similar to the real shape expected with an inclination angle of 60°.

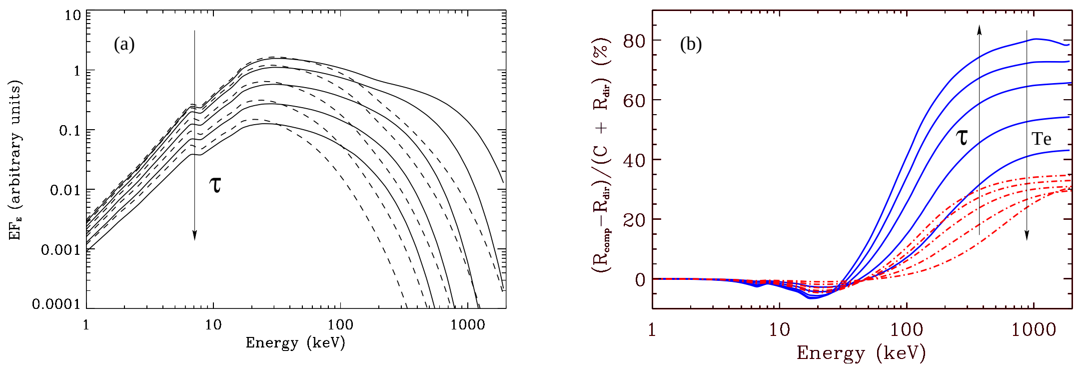

Figure 3.2: (a) As in Fig. 3.1a, but for a constant Compton parameter y equal to 0.6, i.e. consistent with a slab corona in radiative equilibrium above a passive accretion disc. From bottom to top τ=0.1, 0.2, 0.35, 0.5 and 0.64 and kT_e=240, 150, 90, 65 and 50 keV. (b) As in Fig. 3.1b but for a constant Compton parameter y equal to 0.6 (solid line) and 2 (dot-dashed lines). The latter case is consistent with a hemispherical corona in radiative equilibrium above a passive accretion disc.

the temperature of the corona, but keeping fixed the viewing angle (here μ = 0.9). According to thermal Comptonization theory, the temperature of the corona is directly related to the average fractional energy change that a photon undergoes per scattering, whereas τ gives an estimate of the mean number of scattering events. Both parameters play thus a major role in the Comptonization process.

Varying τ at fixed coronal temperature

We will first assume that the temperature of the corona is fixed, equal to 50 keV, while τ varies. In Figure 3.1a we have plotted the shapes of the reflection humps $R_{\rm dir}$ and $R_{\rm comp}$ (in dashed and solid line, respectively) for different values of the coronal optical depth τ. The increase of the optical depth hardens the X-ray primary spectrum, thus modifying the intrinsic shape of the reflection component. It thus explains the hardening of the uncomptonized reflection $R_{\rm dir}$ between τ=0.1 and τ=0.9. Increasing τ also magnifies the effect of Comptonization. The larger τ, the larger the probability of a photon to be comptonized. In this process, the reflected photons are shifted towards higher energies and an increasing deviation between $R_{\rm dir}$ and $R_{\rm comp}$ is observed for increasing τ.

The optical depth of the corona also controls the relative intensity of the different Compton scattering orders. The larger τ, the higher the intensity of the different orders producing a hardening of the comptonized shape at high energy (above ~10–30 keV) as observed in Fig. 3.1a.

To estimate quantitatively such effects on the overall outgoing spectrum, we have plotted in Fig. 3.1b (solid lines) the deviations (in %) between the total spectrum expected if all the reflected photons cross the comptonizing corona before being observed, $(C + R_{\rm comp})$, and the one predicted when the Comptonization of the reflection hump is

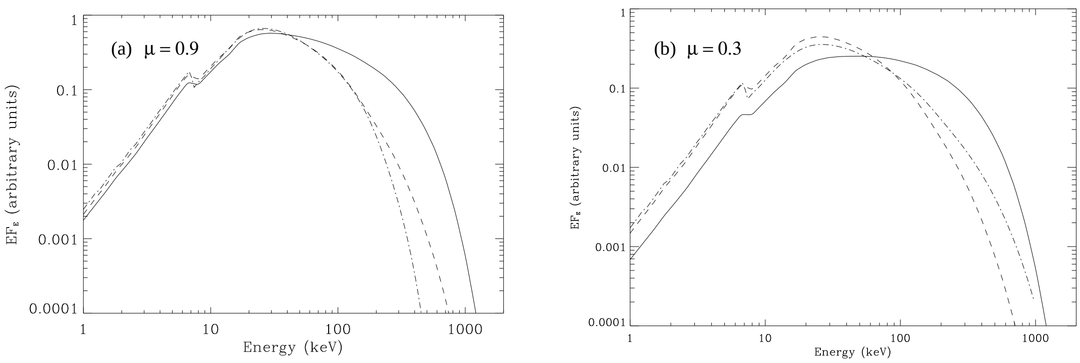

Figure 3.3: Plots of $R_{\rm comp}$ (solid line), $R_{\rm dir}$ (dashed line) and $R_{\rm pexrav}$ (dot-dashed line) at two different viewing angles: (a) μ=0.9 and (b) μ=0.3.

not taken into account, $(C + R_{\rm dir})$. The most important effects (variations of $> 50\%$) occur at very high energies (above 100 keV). They are due to the hardening of $R_{\rm comp}$ for large optical depths. For the larger optical depth case considered ($\tau = 0.9$), a factor of $\sim$2 is expected near 1 MeV. At these energies, $R_{\rm comp}$ tends to have the same shape as the primary continuum and the fractional deviations between the two spectra attain a maximum.

Comptonization in the corona also produces smaller ($< 10\%$) differences between $R_{\rm dir}$ and $R_{\rm comp}$ near 10 keV. The larger one is still produced in the high optical depth case, as expected. It is worth noting that the X–ray detectors are generally well sensitive in the 10–20 keV energy range, which can help constraining the degree of Comptonization.

Also plotted in Fig. 3.1b are the results obtained for a coronal temperature of 350 keV (dot-dashed lines). We can still observe differences between $R_{\rm dir}$ and $R_{\rm comp}$ below and above $\sim kT_{\rm e}$. However, such deviations are larger than in the previous case, at least at low energy (below 100 keV), since the average fractional energy change of a scattering photon increases with $kT_{\rm e}$. These deviations reach $\sim$40% near 20-30 keV for $\tau = 0.9$. Above 100 keV, they roughly behave as in the small temperature case.

Varying τ and $T_{\rm e}$ at fixed Compton parameter

In the case of a disc–corona system, such as the one we are dealing with, we expect the comptonizing region and the source of soft photons to be *coupled*, as the optically thick disc necessarily reprocesses and re-emits part of the comptonized flux as soft photons which are the seeds for Comptonization. In this case, the system can only be in equilibrium if temperature and optical depth satisfy a precise relation (Haardt and Maraschi, 1991). That, in turn, corresponds to roughly constant Compton y parameter, defined as:

$$y = 4\left(\frac{kT_{\rm e}}{m_{\rm e}c^2}\right)\left[1 + 4\left(\frac{kT_{\rm e}}{m_{\rm e}c^2}\right)\right]\tau(1+\tau), \tag{3.2}$$

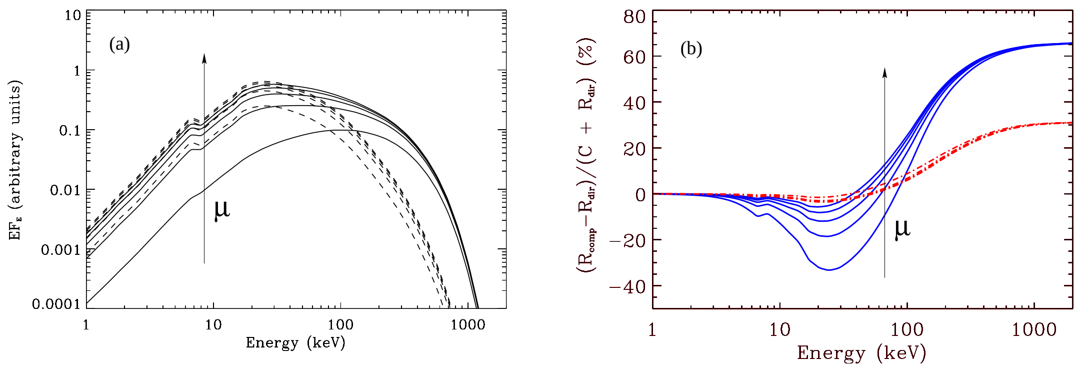

Figure 3.4: (a) The comptonized (solid lines) and uncomptonized (dashed lines) reflection humps, $R_{\rm comp}$ and $R_{\rm dir}$, for different viewing angles. From bottom to top μ=0.1, 0.3, 0.5, 0.7 and 0.9. The optical depth and temperature of the corona are fixed to 0.35 and 90 keV respectively. (b) Deviations (in %) between the outgoing spectra. In dot-dashes line the case of an hemispherical corona with τ=0.35 and $kT_{\rm e}$=200 keV.

which is about 0.6 in a slab geometry when all the accretion power is released in the corona (Haardt and Maraschi, 1993; Stern *et al.*, 1995; Svensson, 1996).

In the case of a constant Compton parameter, changes in τ will be necessarily accompanied by changes in $kT_{\rm e}$, namely, a larger optical depth will require a smaller coronal temperature. This results in three effects: first, the photon index of the primary continuum correlates with τ (Haardt *et al.*, 1997), whereas these two parameters are anti-correlated if the temperature is kept fixed (see section 3.3.1). Second, the variation of the coronal temperature modifies the high energy cut–off of the primary continuum, which scales roughly as $2kT_{\rm e}$. Consequently, it slightly modifies the high energy part of the reflection component $R_{\rm dir}$. Finally, the change of $kT_{\rm e}$ modifies the mean photon energy gain per scattering.

These different effects produce a hardening of $R_{\rm comp}$ at high energies when τ decreases as can be seen in Fig. 3.2a. Such a behaviour is thus opposite to that predicted when the temperature is fixed. However, as shown in Fig. 3.2b (solid lines), the deviations between the outgoing spectra closely resemble those shown in Fig. 3.1b, becoming larger for larger optical depth (i.e. smaller temperature) and reaching a plateau at high energies (above 200 keV). For comparison, we have also plotted the deviation curves obtained in the case of a hemispherical geometry in radiative equilibrium (dot-dashed lines). In this case, the Compton parameter is of the order of 2 (if all the accretion power is released in the corona, see Stern *et al.*, 1995). We see that the differences are smaller than in the slab case, by about a factor of 2. This is simply due to the fact that in hemispherical geometry, the corona does not cover all the cold disc. Consequently, only a part of the reflected photons have to cross the comptonizing plasma before being observed, reducing the effects of Comptonization.

3.3.2 Dependence on the inclination angle

In this Section we keep the temperature and optical depth of the corona fixed to 90 keV and 0.35 respectively[2], and we focus on the dependence of the Comptonization effects on the inclination angle.

As already mentioned in the introduction to this chapter, the actual shape of the reflection hump depends on μ in a relatively complex manner, which is a function of the photon energy. We recall that such an angular dependence is neglected in our computation of $R_{\rm dir}$, whose shape is constant and corresponds to the angular averaged one. In Figures 3.3a and 3.3b we have plotted the spectral energy distribution of the reflection component $R_{\rm dir}$, computed with our code (dashed line), and the one computed following Magdziarz and Zdziarski (1995), obtained with the PEXRAV model of XSPEC ($R_{\rm pexrav}$, dot-dashed line), for two different inclination angles $\mu = 0.9$ (Fig. 3.3a) and $\mu = 0.3$ (Fig. 3.3b). $R_{\rm pexrav}$ is computed using angle dependent Green functions and takes properly into account the angular distortion of the Compton reflection. The continuum assumed to compute $R_{\rm pexrav}$ corresponds to the best cut-off power law fit of the spectrum emitted by our slab corona model, that has a photon index $\Gamma \simeq 2.2$ and a high energy cut–off $E_c \simeq 250$ keV. Therefore, the primary spectra impinging on the disc are roughly similar in the two models. Inspection of Fig. 3.3a and 3.3b shows that the main differences between $R_{\rm dir}$ and $R_{\rm pexrav}$ appears above 10 keV. Also, $R_{\rm pexrav}$ hardens at larger inclination angles, i, (i.e. smaller μ). For comparison, in the same Figures we have plotted the comptonized reflection $R_{\rm comp}$ computed with our model. It is evident that the effects of the Comptonization on the reflection hump are generally more important than the intrinsic angular distortion, especially at high energies. Therefore, in the following, we will simply use Eq. (3.1) to rescale the amplitude of the reflection component as a function of μ.

Keeping in mind the limitations of the above approximation, we have plotted in Fig. 3.4a, the different shapes of $R_{\rm comp}$ and $R_{\rm dir}$ for different values of the viewing angles. Because an increase of i will correspond to an increase of the effective optical depth τ_μ, we expect to observe, for increasing i, the same effects we observed for increasing τ (cfr. section 3.3.1). However, in this case the shape of the primary spectrum impinging on the accretion disc is constant.

The differences between $R_{\rm comp}$ and $R_{\rm dir}$ are relatively strong (see Fig. 3.4a). The effective optical depth, τ_μ, can easily reach values of the order of 2 or 3 for large inclination. It thus results in large mean photon energy shifts and hardening of $R_{\rm comp}$ at high energy. The deviations between $R_{\rm dir}$ and $R_{\rm comp}$ are reported in Fig. 3.4b. They may be as large as $\sim$30% in the 10–50 keV range for μ=0.1 whereas they are of the order of a few for nearly face-on configuration.

Above 100 keV the different shapes overlap near $2kT_{\rm e}$, the larger energy that a photon may reach by Comptonization in the corona. It is worth noting that such an

[2]Those values correspond to a Compton parameter y close to 0.6, i.e. consistent with a slab corona in radiative equilibrium above a passive accretion disc (see previous section).

overlapping is a direct consequence of our treatment of the angular dependence of the reflection hump. Actually, the reflection shapes for different inclination angles would be different, particularly at high energies. The differences, however, would not depend strongly on the real reflection shape, and are of the order of 60% near 300 keV for a slab geometry.

As a final remark, we note that the most evident effects, those at energies beyond $\sim$ 100 keV, may not be easily detected. Firstly, because the high energy instruments are generally not very sensitive beyond $\sim$ 100 keV, thus preventing any firm constraint on the spectral shape to be put. Secondly, any deviations from the ideal case studied here, as, for instance, a stratified temperature corona, may distort the derived reflected shape, especially at high energy, and complicate the spectral analysis. The effects of Comptonization at lower energies (near $\sim$ 20 keV, where the instrumental sensitivity is very good), although less dramatic, would certainly be more valuable for any estimation of the physical parameters of the corona.

3.4 Comptonization effects on the iron line

The equivalent width (EW) of the fluorescent Fe Kα line produced by cold matter surrounding the hot corona depends on different parameters, as the elemental abundance of the reflecting matter, its inclination angle as seen by the observer, and the ionization state of the reflecting surface layers (see Fabian *et al.*, 2000, for a review). It also depends on the geometry of the corona–cold matter configuration (i.e. on the solid angle subtended by the cold matter as seen by the X–ray source). The Comptonization of the iron line is another process which may affect the measurement of the EW, as already pointed out by Haardt *et al.* (1993) and discussed by Matt *et al.* (1997).

Assuming a slab coronal geometry above an accretion disc of neutral matter and solar abundance, the dependence of the EW on μ can be approximated by the simple formula:

$$\begin{aligned} EW_{\rm comp}(\mu) &= \frac{EW_{\rm dir}(\mu=1)}{\ln 2}\mu \ln\left(1+\frac{1}{\mu}\right) e^{-\tau_\mu} \\ &= EW_{\rm dir}(\mu) e^{-\tau_\mu}. \end{aligned} \tag{3.3}$$

The term before the exponential is an approximated one, given by Ghisellini *et al.* (1994), for the angular dependence of the equivalent width due to limb darkening, $EW_{\rm dir}(1)$ corresponding to the face-on EW of the uncomptonized line. The exponential term $e^{-\tau_\mu}$ gives the probability that a line photon cross the corona and reach an observer at the viewing angle i without being comptonized. The comptonized ones will be scattered around in the underlying continuum and will not contribute to the line flux anymore.

We have plotted in Fig. 3.5 the reduced equivalent width $EW_{\rm comp}(\mu)/EW_{\rm dir}(\mu = 1)$ as a function of the optical depth of the corona and for different viewing angles. The effects of Comptonization are very strong, especially at large inclination angles. For $\mu = 0.9$ the EW is reduced by a factor $\sim$3 when τ varies between 0 and 1, whereas it

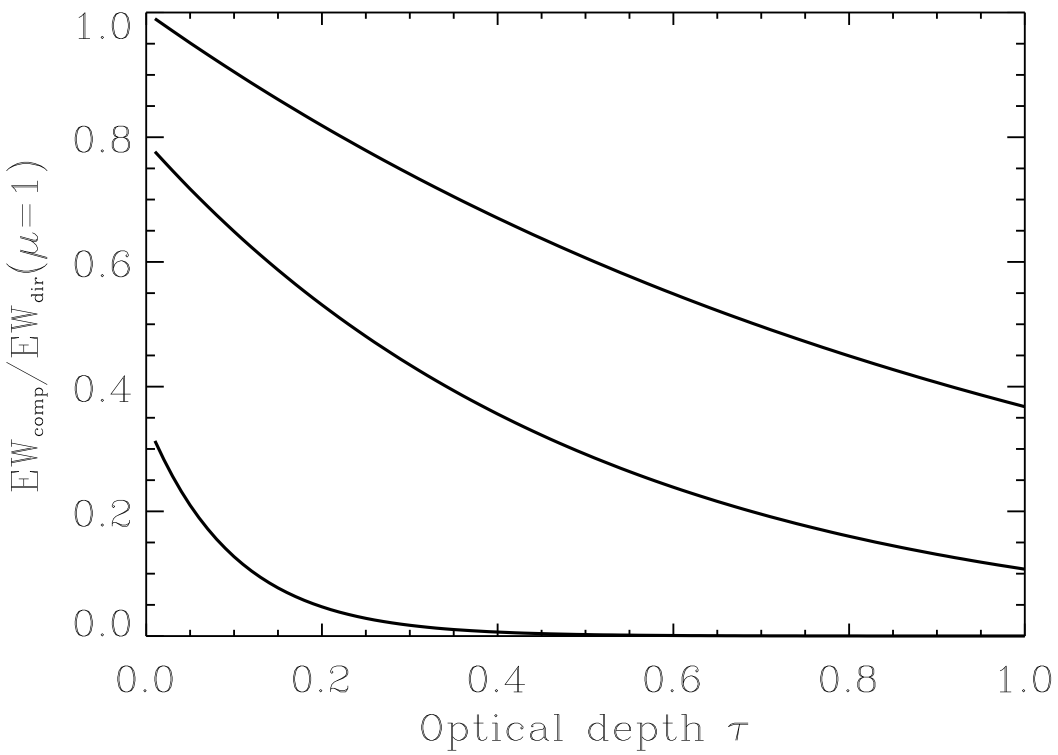

Figure 3.5: Reduced equivalent width $EW_{\rm comp}(\mu)/EW_{\rm dir}(\mu = 1)$ of the comptonized iron line in function of the optical depth of the corona for different inclination angles. From top to bottom $\mu = 1$, 0.5 and 0.1

becomes rapidly negligible for $\tau > 0.5$ if $\mu = 0.1$. We thus expect that such modifications of the iron line EW be more easily observable than the spectral changes of the reflection hump detailed in Section 3.3

3.5 Application to fitting procedures

In Section 3.3 we have discussed the changes in the observable reflection hump due to the presence of a comptonizing corona above the cold reflector (the accretion disc). Here we will try to give a more quantitative estimate of such an effect. To do so, we have to rely on some simple and straightforward measure of the reflection component strength, and compare such a measure in the two cases of a bare disc and of a disc engulfed in a hot, optically thin corona.

The most widely used model to fit the hard X-ray continuum of Seyfert galaxies and GBHC comprises a cut–off power law and an uncomptonized reflection (the so-called PEXRAV model of XSPEC, Magdziarz and Zdziarski, 1995). Such a model is known to be a poor approximation to the true Compton continuum, since it does not reproduce the (possible) anisotropy break (§3.2) and gives a poor representation of the high energy cut–off shape. However, it can help in quantifying the effects of a comptonizing corona on the appearance of the hard X-ray continuum. For this purpose we have proceeded in the following way. We have first created two sets of simulated spectra using the thermal Comptonization code of H94 in a slab geometry. In the first set we have properly taken into account the Comptonization of the secondary components in the corona, while in the second one we have neglected such effect. Then we have fitted our simulated spectra between 1 and 500 keV with the PEXRAV model. We have computed the simulated spectra for different viewing angles and different values for coronal temperature and optical depth, chosen as to keep $y = 0.6$. For every simulated spectrum, our fitting procedure gives the best fit value of the spectral index, the high energy cut-off and the reflection fraction. We will denote R_1 and $E_{c,1}$, respectively, the value of the reflection fraction and of the high energy cut-off obtained for the comptonized model, and R_2 and $E_{c,2}$ the ones obtained for the uncomptonized case. The ratio R_1/R_2 and $E_{c,2}/E_{c,1}$ can then help to *quantitatively* estimate the modifications to the best fit parameter values due to the Comptonization effects.

In Fig. 3.6 we show the ratio R_1/R_2 as a function of the optical depth and for different viewing angles i. As expected, due to the smoothing effect of the comptonizing corona on the reflection shape, R_1 is always smaller than R_2, because the fitting procedure requires smaller reflection normalization to fit the comptonized component. Furthermore, their ratio decreases with increasing i and/or optical depth in the corona. This is in agreement with the results of Section 3.3.

The shifting of the reflection hump $R_{\rm comp}$ towards high energies (as discussed in Section 3.3) as a consequence of the Comptonization, modifies also the high energy part of the spectra and the estimate of the high energy cut–off, so that it is always larger for the comptonized case. The amount of such shift depends on the temperature and optical

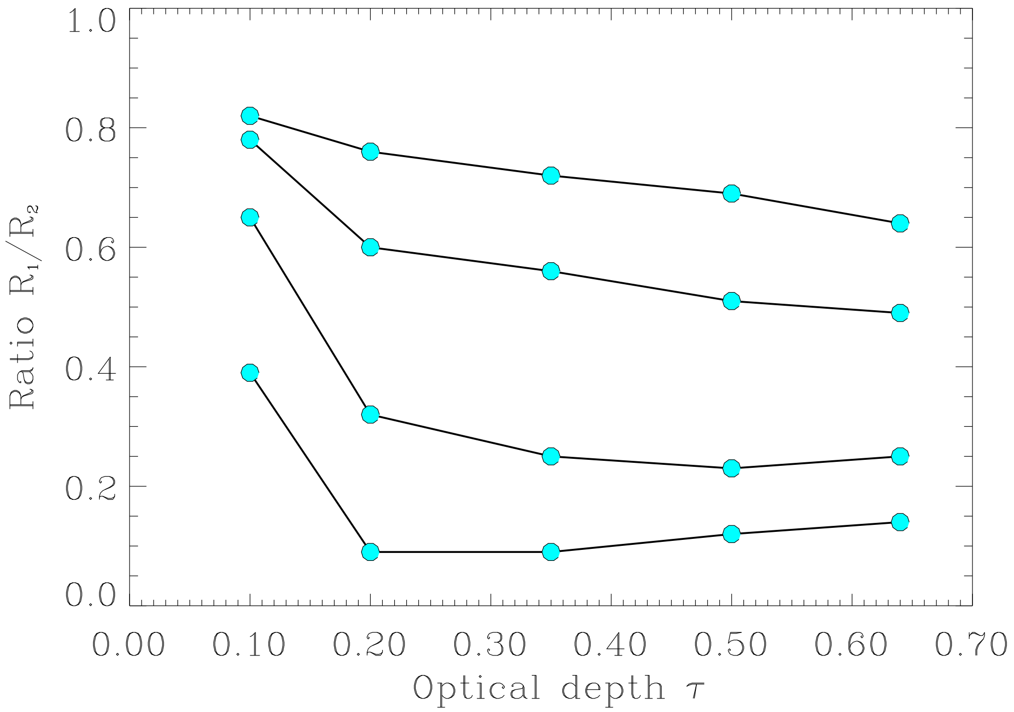

Figure 3.6: Ratio R_1/R_2 as a function of the coronal optical depth for different viewing angles at constant Compton parameter $y = 0.6$. From top to bottom μ=0.9, 0.5, 0.2 and 0.1

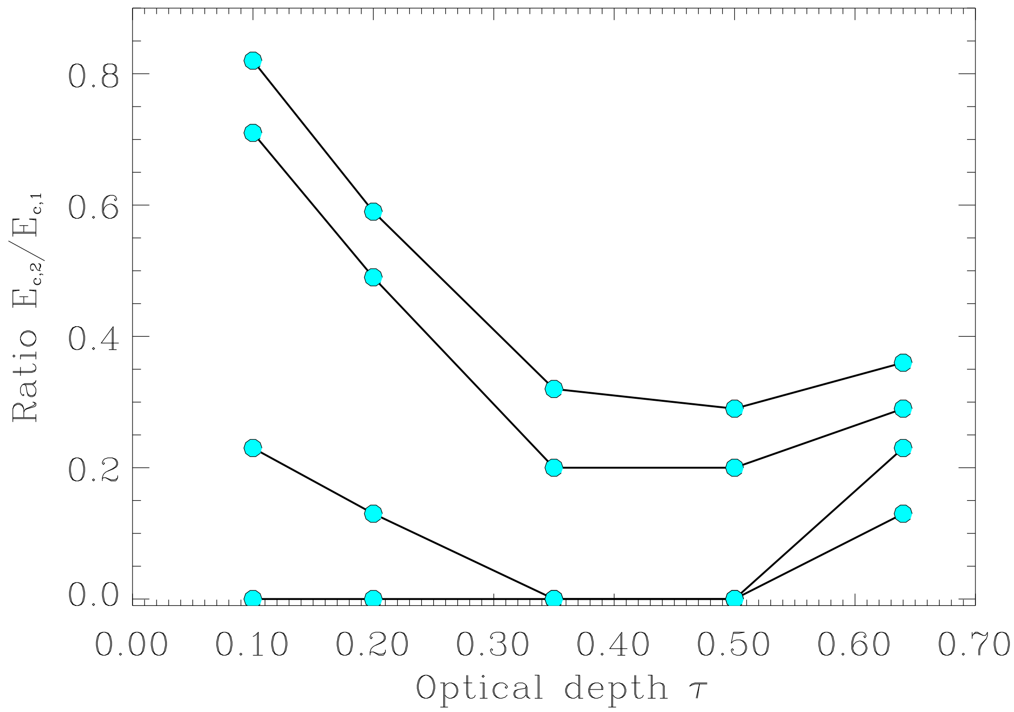

Figure 3.7: Ratio $E_{c,2}/E_{c,1}$ versus the coronal optical depth, for different values of μ. From top to bottom μ=0.9, 0.5, 0.2 and 0.1.

depth of the corona (cfr. Fig. 3.2a): the higher the temperature, the higher the energy of the scattered photons. At the same time, however, in our simulations, given that higher coronal temperature correspond to lower optical depth, the effect of the anisotropy break has to be properly taken into account. When trying to fit the curved spectrum with a cut-off power-law, we obtain a lower value of the spectral index and, consequently, a lower cut-off energy. The net result is shown in Fig. 3.7, where we have plotted the ratio $E_{c,2}/E_{c,1}$ of the measured cut-off energies as functions of the optical depth for different viewing angles. The ratio has a minimum for $\tau \simeq 0.4$. At the highest inclination angle (μ=0.1–0.2) we are unable to constrain the high energy cut-off in the comptonized case $E_{c,1}$, below 500 keV, so we report for the ratio $E_{c,2}/E_{c,1}$=0.

The main *qualitative* conclusion of this section is that fitting simulated spectra, in which the effects of Comptonization on the reflection component have been properly taken into account, with the usual cut–off power law plus uncomptonized reflection models (e.g. PEXRAV), leads to underestimate the reflection normalization and to overestimate the high energy cut–off. Quantitatively, these effects will of course strongly depend on the quality of the data, especially at high energy (above 100 keV).

3.6 Observational consequences

3.6.1 The case of NGC 4258

From the X–ray point of view, the nearby bright galaxy NGC 4258 possesses the general characteristic of the Seyfert class, that is: a power law primary continuum with a photon index $\Gamma \simeq 2$, a relatively large amplitude variability in the 3-10 keV band on time scales of a few tens of thousands of seconds and smaller ones (~20%) on time scales of the order of an hour (Reynolds *et al.*, 2000, hereafter R00; Fiore *et al.*, 2001, hereafter F01) and the presence of a (narrow) iron line near 6.4 keV with an equivalent width measured by *ASCA* of 107^{+42}_{-37} eV (R00). The *BeppoSAX* observation gives a more poorly constrained value for the EW of 85±65 eV. Moreover, as discussed in R00, a broad iron line with an EW < 200–300 eV may still be consistent with the *ASCA* data. On the other hand, the bad signal to noise above 10–20 keV has prevented any good detection of a possible reflection hump.

NGC 4258 is well known for the detection, from high resolution observations, of a water maser. It is expected to be produced by the accreting gas spiraling down to the central engine (Claussen *et al.*, 1984; Watson and Wallin, 1994; Miyoshi *et al.*, 1995). The combination of the central mass estimate (deduced from the water maser properties, Herrnstein *et al.*, 1999; Miyoshi *et al.*, 1995), and the NIR-to-X–ray luminosity suggest that NGC 4258 is an AGN in a low state with an accretion rate $\dot{m} \simeq 0.0002$ (F01). The presence of an ADAF seems however to be ruled out by the recent *BeppoSAX* observations, on the base of both the measured X-ray spectral shape and X-ray variability, and the most natural explanation of the X-ray luminosity of this source may be in terms of Comptonization of soft photons in a hot corona (F01). The inclination of the disc is large and very well constrained $i = 82 \pm 1$ degrees (Herrnstein *et al.*, 1999). We thus expect the Comptonization effects on the reflection components coming from the disc to be relatively important.

What constraints can be put on the origin of the reflection features detected in this object? To answer this question, we have first tried to estimate the physical parameters (temperature and optical depth) of the the corona. We have thus fitted the *BeppoSAX* data (downloaded from the *BeppoSAX* archive) with the code H94, assuming an inclination angle of 82° (i.e. $\mu = 0.14$). Since the intensity of the hard component is strongly reduced by photo-electric absorption below 2–3 keV, we only fit the data above 2.5 keV. Due to the low signal–to–noise ratio of the spectrum, particularly at high energy, and the lack of data to constrain the soft photon temperature $kT_{\rm bb}$, τ and $kT_{\rm e}$ are badly constrained, τ being smaller than 1 at the 90% confidence level for 2 parameters, with a best fit value of 0.05.

These large uncertainties still enable us to make some interesting comments. First, let us assume, as R00 did, that the narrow iron line observed in NGC 4258 is produced by the accretion disc. Then it has to originate at relatively large radii ($R_{K\alpha} >$ 100 Schwarzschild radii) in order to have the observed small width. In this case, and

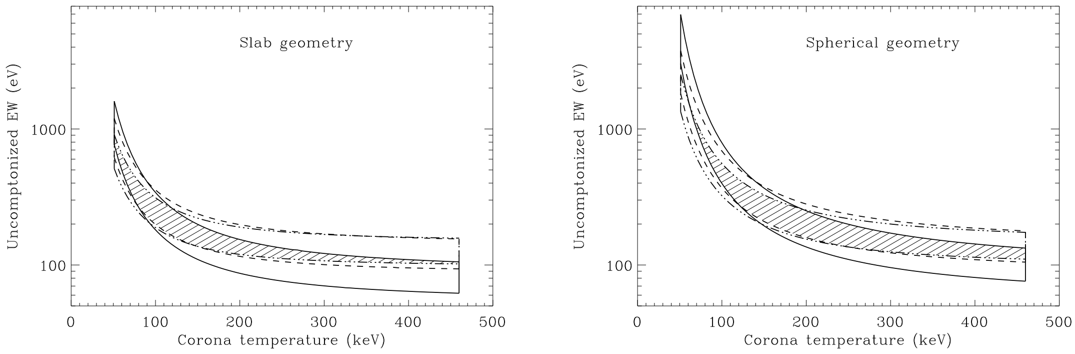

Figure 3.8: The solid, dashed and dotted-dashed lines are the 90% envelopes of the uncomptonized iron line EW computed for the three spectral indexes reported by LZ00, i.e. Γ =1.62, 1.82 and 1.94 respectively. The hatched area correspond to the intersection of the three envelopes. For any fixed value of $EW_{\rm dir} \gtrsim 100$ eV, this area delimits the range of acceptable common values of the coronal temperature in the three samples. Alternatively, for any fixed value of $kT_{\rm e}$, the hatched area corresponds to the acceptable range for the broad line equivalent widths. The left and right plots show the case of a slab and spherical geometry respectively.

since the inclination angle of the disc is large (we assume that the inclination of the inner part of the disc is also of 82°, i.e. the disc is not strongly warped) we expect part of the iron line photons to be comptonized in the corona. Thus, as shown in section 3.4, the EW of the iron Kα line should be significantly reduced with respect to what we can expect without a comptonizing corona. Let us suppose that all iron line photons have to cross the corona before being observed (this would be the case if the coronal dimension D is large i.e. $D > R_{K\alpha}$, as noted by R00): the observed EW of 100 eV would then correspond to an actual uncomptonized face–on line equivalent width (the $\mathrm{EW_{dir}}(\mu = 1)$ parameter in Eq. 3.3) larger than 300 eV (∼500 eV for τ=0.05 and ∼40 keV for $\tau = 0.5$!). Recent estimates of the average narrow iron line equivalent width observed in Seyfert 1 galaxies rather suggest a value of the order ∼ 100 eV (Matt, 2000; Lubiński and Zdziarski, 2001). This would corresponds to an $\mathrm{EW_{dir}}(\mu = 1)$ of ∼200 eV for τ=0.5 and a viewing angle of 30° (as estimated by Nandra *et al.*, 1997, for Seyfert 1). These (admittedly qualitative) computations rather suggest that the narrow iron line in NGC 4258 *does not suffer Comptonization.* The most simple explanation, with the assumption that the X–ray emitting region has a disc–corona configuration, is that the narrow iron line preferentially originates from matter not associated with the accretion disc.

In this case, and following R00, we can also set an upper limit on the equivalent width of the uncomptonized broad iron line consistent with its non detection by ASCA. R00 have estimated that the corresponding face–on EW of a possible broad line has to be smaller than ∼ 200–300 eV to be consistent with the data. This estimate takes into account the limb darkening and relativistic bending effects but not the Comptonization of the iron line photons in the corona. If such an effect is also taken into account (and still assuming an inclination of 82°), the limits are less strict and a broad line with a face–on uncomptonized EW$\sim$0.8–1.2 keV (for $\tau \sim$0.05–0.1) would still be consistent with the ASCA data. Thus, if there were a broad line present at the level seen in most other AGN ($\sim$100–300 eV, Nandra *et al.*, 1997; Lubiński and Zdziarski, 2001), we should not expect to detect it. The data thus do not require that the inner part of the accretion disc be truncated as suggested in R00.

3.6.2 Correlations between reflection features and X-ray spectral slope

The Comptonization effects we have discussed so far may influence the apparent correlation we observe between the reflection features characteristics (broad Fe line equivalent width, reflection normalization) and the other parameters of the high energy continuum.

In a recent paper, Lubiński and Zdziarski (2001, hereafter LZ01) have analyzed the complete available ASCA database to re–examine the issue of the strength and width of the Fe Kα line in Seyfert galaxies. An interesting results they report is an apparent correlation between the broad iron line EW and the spectral index in this class of objects. The correlation is actually observed in the average spectra of Seyfert galaxies grouped according to their spectral hardness. As underlined by the authors, this correlation may be naturally explained in the framework of thermal Comptonization model. Indeed, in this case, the power law slope of the X–ray/γ–ray spectrum emitted by the hot comptonizing corona is related to the rate of cooling by incident soft photons. Then the spectral slope will be correlated with the broad line EW, provided that the main source of the cooling photons is emitted by the same material that is responsible for the observed reflection. Furthermore, such an interpretation is consistent with the Γ–R correlation observed by Zdziarski *et al.* (1999) in a sample of Seyfert and galactic black hole candidates (see also Gilfanov *et al.*, 1999; Matt, 2000).

We show here that the Comptonization effects in coronae of different intrinsic properties (i.e. different temperature and optical depth) may also contribute to produce this kind of correlation, without the need to postulate a change of the geometry of the inner accretion disc.

In thermal Comptonization theory, τ and $kT_{\rm e}$ are related to the X–ray spectra photon index Γ through the approximate relation (Osterbrock, 1974; Pozdniakov *et al.*, 1976; Zdziarski, 1985):

$$\Gamma - 1 = -\frac{\ln P_{\rm sc}}{\ln A}. \tag{3.4}$$

In this equation, $P_{\rm sc}$ is the average scattering probability, its expression depending on the coronal geometry, and $A = 1 + 4\frac{kT_{\rm e}}{m_{\rm e}c^2} + 16\left(\frac{kT_{\rm e}}{m_{\rm e}c^2}\right)^2$ is the average photon energy amplification per scattering. In the following, we only treat the cases of slab and spherical geometry. The expression of $P_{\rm sc}$ in these cases can be found in Zdziarski *et al.* (1994) and Wardziński and Zdziarski (2000) respectively.

For a given value of the photon index, we can then use Eq. (3.4) to compute the coronal optical depth τ for different values of $kT_{\rm e}$. Assuming that the broad iron lines observed by LZ01 have been comptonized in the corona, we can then compute the EW of these lines *before* Comptonization, $EW_{\rm dir}$, by inverting Eq. 3.3 (we fix the inclination angle to 45 degrees, which is the best fit value obtained by LZ01). In Fig. 3.8a and 3.8b (corresponding to a slab and a spherical geometry, respectively) we have plotted the 90% confidence envelopes for $EW_{\rm dir}$ and $kT_{\rm e}$ obtained for each of the three average values of the spectral indexes reported by LZ01, i.e. Γ= 1.62, 1.82 and 1.94 (solid, dashed and dotted-dashed envelopes, respectively). These envelopes have been computed by taking into account the 90% errors of the photon index and of the observed EW reported by LZ01. The hatched surfaces correspond to the region of the parameter space where the equivalent width of the broad lines before Comptonization, computed for the different photon index classes, are equal within the errors.

Interestingly, the values of $EW_{\rm dir}$ are consistent with each other (within the errors) for a relatively large range of coronal temperatures and optical depths, particularly for the spherical geometry case, where $EW_{\rm dir} \simeq$ 100–150 eV for $kT_{\rm e} \gtrsim 150$ keV and $\tau \lesssim 0.6$. In the slab geometry case, $EW_{\rm dir} \simeq$ 100–150 eV for $100 \lesssim kT_{\rm e} \lesssim 250$ keV and $0.6 \gtrsim \tau \gtrsim 0.1$. These results thus show that the presence in different objects, all having broad lines with similar EW (before Comptonization), of hot coronae with different physical characteristics (i.e. different τ and $kT_{\rm e}$), may result in an apparent EW–Γ correlation (as observed by LZ01).

It is worth noting that the main implication of this interpretation is that the coronae producing the harder spectra (smaller Γ) must also have the larger optical depth. Such behaviour necessarily requires a change of the Compton y parameter (i.e. a change of the geometrical and/or energetic properties of the corona), since for constant y a correlation between τ and Γ is expected (Haardt *et al.*, 1997).

We note that, in this picture, we also expect a correlation between the observed reflection normalization R and the photon index Γ. Indeed, as shown in Section 3.5, for larger optical depths the Comptonization effects smooth the reflection hump so that fitting with an uncomptonized reflection gives smaller R. This goes in the sense of the results of Zdziarski *et al.* (1999), although, as shown in Section 3.5, we do not expect strong effects ($\lesssim$ 30% for inclination angles smaller than 60°) on the reflection normalization.

Thus, we can conclude that the effects of Comptonization in different objects, whose coronae possess different physical parameters, may have some influence to produce and/or emphasize the observed correlations between the reflection features and X-ray slope.

3.6.3 Consequences for the X-ray background

After the most recent X-ray surveys carried out by *Chandra* and *XMM Newton* (Mushotzky *et al.*, 2000; Hasinger *et al.*, 2001) there is now a tantalizing evidence that the X-ray Background (XRB) is mainly produced by the integrated emission of single sources, i.e. AGNs lying at cosmological distances. All the spectral models for the XRB assume that the intrinsic AGN spectrum (before any absorption in a putative large scale molecular torus) is the sum of a power-law continuum and an uncomptonized reflection. We expect that the effects described here can be of some relevance for any detailed fitting model for the XRB. Indeed, in all current models (Madau *et al.*, 1994; Wilman and Fabian, 1999; Gilli *et al.*, 2001), for an average continuum slope of $\Gamma \sim 2$, the peak of the XRB (in νF_ν) is associated with the peak of the reflection hump and interestingly, there is evidence that the observed peak of the XRB is located at slightly higher energies than those predicted by the standard models that neglect the effect of Comptonization in the corona.

In Fig. 3.9 we show, as an illustrative case, an angle averaged reflection hump calculated for $kT_\mathrm{e} = 90keV$ and $\tau = 0.35$ (corresponding to $y = 0.6$) for both the comptonized (solid line) and uncomptonized (dashed line) case. Although many uncertainties come into the exact determination of the possible consequences of such effect on the XRB shape, as the temperature and optical depth distribution in the different sources or the total coronal covering fraction, the work we have presented in this chapter should indicate that Comptonization of the reflection component in the corona have to be taken into account when dealing with accurate spectral fitting of the X-ray background.

3.7 Summary and conclusions

In this chapter, we have shown that the effects of a comptonizing corona on the appearance of the reflection components in the spectra of accreting black holes may be relatively important, modifying the shape of the observed reflection hump and the measured iron line equivalent width. We have studied in detail the dependence of these effects on the physical (i.e. the electron temperature T_e and optical depth τ) and geometrical (i.e. the inclination angle) parameters of the corona, mainly focusing on the case of a slab geometry. This is an extreme case since the corona covers all the reflecting material and consequently the Comptonization effects are large. The results of this study can be summarized as follows:

- Due to the smoothing and shifting towards high energies of the comptonized reflection hump, the main effects on the emerging spectra appear at energies below and above $\sim T_\mathrm{e}$.

- They are larger for larger optical depth of the corona and/or larger inclination angle of the corona–disc configuration.

- Fitting Comptonization models that take into account comptonized reflection by means of the usual cut–off power law plus uncomptonized reflection models, leads to an underestimation of the reflection normalization and an overestimation of the high energy cut–off.

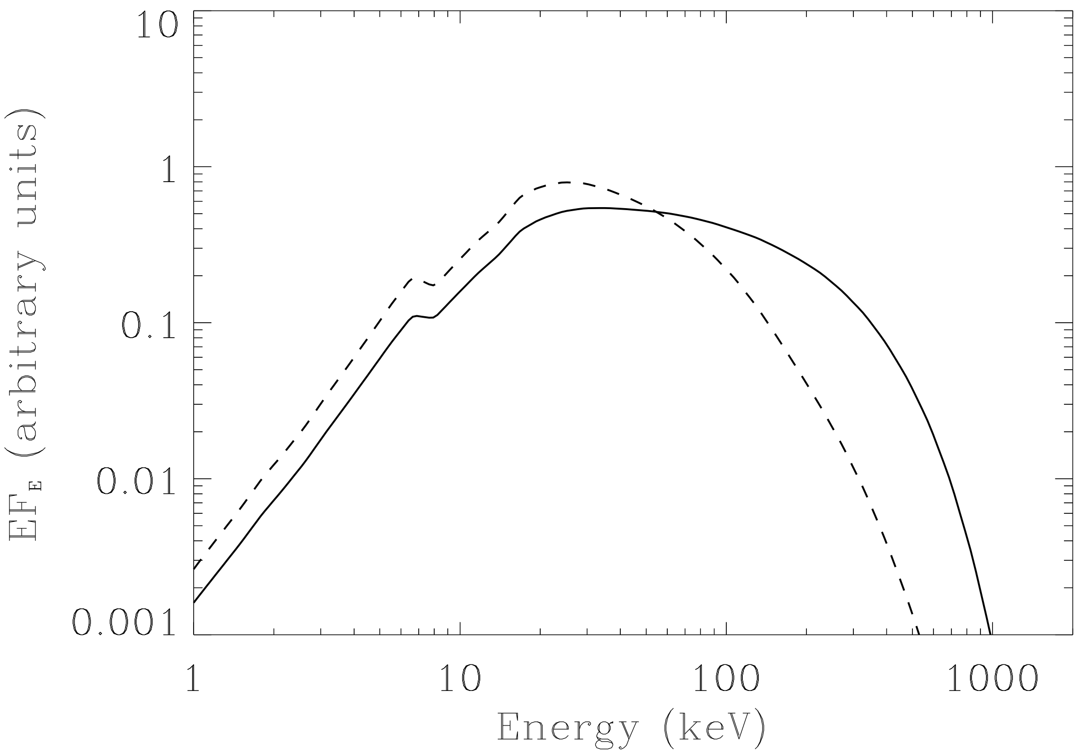

Figure 3.9: An angle-averaged reflection hump calculated for $kT_e = 90keV$ and $\tau = 0.35$ (corresponding to $y = 0.6$). The solid line represents the comptonized reflection, the dashed the direct one. The slight shift of the peak energy of the hump is an indication of the predicted effect of the Comptonizing corona on the location of the peak energy in the X-ray background.

- The Comptonization effects may strongly reduce the equivalent width of the observed iron line, especially at large inclination angles.

These effects may have important consequences on the physical interpretation of the observed reflection features in astrophysical objects. As an example, we have studied the case of the galaxy NGC 4258: with the assumption that the X–ray emitting region has a disc–corona configuration and given the high inclination angle of the accretion disc in this source, proper evaluation of the Comptonization effects enabled us to find less strict limits on the EW of a putative broad iron Kα line, thus explaining its non-detection. Besides, according to this picture, the narrow iron line observed in this object is believed to originate from matter not associated with the accretion disc since, otherwise, it would require an uncomptonized (i.e. before Comptonization) line with too large an equivalent width.

We also find that the presence of a comptonizing corona can produce and/or emphasize the correlations between the reflection features (iron line equivalent width or covering fraction) and the X–ray spectral index. Then, similarly to the effects produced by a bad representation of the complex ionization pattern expected at the surface of the X-ray–irradiated reflecting material, these different effects are to be properly taken into account to correctly interpret these correlations.

Finally, we underline the possible importance of Comptonization effects on the reflection shape when dealing with accurate spectral fitting of the X-ray background. Indeed, there is evidence that the observed peak of the X-ray background is located at slightly higher energies than those predicted by the standard models that neglect the effect of Comptonization in the corona.

Chapter 4

The spectrum of an accretion disc

4.1 Introduction: Theoretical models for optically thick accretion discs

As we have discussed in Section 1.3, the observed spectra from sources thought to be powered by accretion onto a black hole are complex and in general comprise different components. After having explored in detail the physics of the hot corona considered both as a source of the primary X-ray power-law emission (§2), and as the medium where the secondary reflection component of the spectrum are comptonized, in this chapter we focus on the quasi-thermal continuum component associated with the emission from the accretion disc itself.

The local radiation spectrum is formed in the disc upper layers and depends not only on the distance from the central source or on the accretion rate, but also, crucially, on the vertical structure of the disk and its temperature profile along the z axis. Here we briefly summarize the main spectral properties of the different regions of a standard accretion disc, referring the reader to the works of Shakura and Sunyaev (1973), Pringle (1981), Frank *et al.* (1992), Papaloizou and Lin (1995) for a thoroughly discussion of the subject.

Local thermodynamic equilibrium is established in the innermost layers of the disc up to the 'thermalization depth', where the effective optical depth for absorption is equal to unity,

$$\tau_*(\nu) = \sqrt{3\tau_{\rm ff}(\nu)(\tau_{\rm T} + \tau_{\rm ff}(\nu))} = 1 \qquad (4.1)$$

where $\tau_{\rm T}$ is the Thomson depth below the surface, and $\tau_{\rm ff}(\nu)$ is the optical depth due to free-free absorption. It is at this depth that a typical escaping photon is created before emerging from the surface. Then the nature of the spectral energy distribution depends crucially on the physical properties of such a upper layer.

Only in the outermost parts of an accretion disc, when absorption dominates scattering ($\bar{\kappa}_{\rm ff} \gg \bar{\kappa}_{\rm es}$) the local emission will be blackbody, at a temperature equal to the local effective surface temperature

$$T_{\rm s} \simeq 1.16 \times 10^8 m^{-1/4} r^{-3/4} [\dot{m} J(r)]^{1/4}. \tag{4.2}$$

The integrated emission from this region produces radiation whose spectral index γ ($F_\nu \propto \nu^\gamma$) is equal to 1/3, which is usually considered the standard signature of an accretion disc in the optical/UV band.

Closer in, where electron scattering dominates absorption, the effect of Comptonization have to be taken into due account. These effects are important whenever the Compton parameter (Rybicki and Lightman, 1979)

$$y = \frac{kT}{m_{\rm e}c^2}\tau_{\rm T}^2 \tag{4.3}$$

becomes greater than unity. In fact, in the very innermost part of the disc we have $y > 1$ at the thermalization depth, and therefore Comptonization is 'saturated' and the radiation spectrum has a Wien distribution (Illarionov and Syunyaev, 1972) $F_\nu \sim \nu^3 e^{-h\nu/kT_{\rm Wien}}$, where $T_{\rm Wien}$ corresponds approximately to the temperature of the gas at the depth where $y = 1$ (which is *lower* than the temperature at the thermalization depth).

In the intermediate region, where electron scattering still dominates absorption, but Comptonization is not saturated ($y < 1$ at the thermalization depth) an hybrid spectrum is produced, that depends on the density profile in the surface layer (Shakura and Sunyaev, 1973). Because of the reduced importance of Comptonization the resulting spectrum lacks the Wien tail and is somewhat harder. It can be shown (Shakura and Sunyaev, 1973) that the integrated emission from this region of the disc produce a radiation with a flat spectral index $\gamma \sim 0$.

4.2 The observational perspective: phenomenological models

We have seen in the previous section that the standard theory of geometrically thin and optically thick accretion discs predicts a quite complicated spectral energy distribution, depending on the values of the different physical parameters (accretion rate, mass of the central object, viscosity parameter). On the other hand, when dealing with the limited information provided by the observations (see section 1.3), a simplifying approach is often adopted. Here we discuss at some length the most widely used of such phenomenological models, the so-called Multicolour Disc Model (MCD), aiming in particular at a critical assessment of the claims that have been done in the literature of direct measurements of the inner disc radius, and therefore of the central black hole parameters.

4.2.1 The multicolour disc model

In the zeroth order approximation for describing emission from an accretion disc, not only is the disc assumed to be geometrically thin and optically thick, but also the vertical temperature structure is neglected, as is the effect of Comptonization on the emergent spectrum. Each point of the disc is then assumed to radiate like a blackbody at an effective temperature which scales with the radius as $r^{-3/4}$. This is the so-called *multicolour disc model* (Mitsuda *et al.*, 1984). Such a simple model has the advantage of being easy to use in trying to fit spectral data. It has only two adjustable parameters: a (*colour*) temperature, independent on the source distance, and a normalization factor, which in turn depends on the inner radius of the disc, on the distance of the source and on the inclination of the disc from the line of sight. When these two latter quantities are independently known, or can be reasonably inferred, fitting the ultra-soft component of a GBHC spectrum with the MCD model immediately gives estimates of the temperature in the inner region of the disc and its inner radius.

Given the assumption of local Planckian emission, the observed flux from the disc is approximated by

$$F_d(E) = \frac{8\pi R_{\rm col}^2 \cos i}{3D^2} \int_{T_{\rm out}}^{T_{\rm col}} \left(\frac{T}{T_{\rm col}}\right)^{-11/3} B(E,T) \frac{dT}{T_{\rm col}}, \tag{4.4}$$

where $B(E,T)$ is the Planck function and $T_{\rm out}$ is the temperature at the outer radius of the disc (and it is assumed that $T_{\rm out} \ll T_{\rm col}$). The two fit parameters of the model are the colour temperature of the inner accretion disc ($T_{\rm col}$), in keV, and the normalization factor

$$n = \frac{R_{\rm col}^2 \cos i}{D^2},$$

where $R_{\rm col}$ is expressed in km and the distance D in units of 10kpc.

It is important here to stress that, in fact, the parameter $R_{\rm col}$ is *not* the inner disc radius, nor the so-called 'effective' inner radius, $R_{\rm eff}$ (i.e. the radius at which the temperature of the disc is the highest). As we have shown in Section 4.1, the Comptonization of the emergent spectrum, which is important in the inner region of the disc, forms a Wien peak with characteristic temperature $T_{\rm col} > T_{\rm s}$, where $T_{\rm s}$ is the effective surface temperature (see Eq. 4.2) at the peak of the disc emission. If the ratio $f_{\rm col} \equiv T_{\rm col}/T_{\rm eff}$ (the so called *spectral hardening factor*, Shimura and Takahara, 1995) was constant throughout the disc and did not vary with varying physical parameters, it would still be possible to use the multicolour disc model to infer meaningful disc parameters. In fact, the assumption behind the use of the MCD model is that the Comptonized emergent spectrum can be approximated by a *diluted* blackbody emission:

$$F_\nu = \frac{1}{f_{\rm col}^4} \pi B_\nu(f_{\rm col} T_{\rm s}). \tag{4.5}$$

In this case, the actual inner edge of the disc would be given by

$$R_{\rm in} = \eta R_{\rm eff} = \eta g(i) R_{\rm col} f_{\rm col}^2, \tag{4.6}$$

where η is the ratio of the inner radius of the disc to the radius at which the emissivity actually peaks, typically $\eta \simeq 0.6 - 0.7$ (Shakura and Sunyaev, 1973; Shimura and Takahara, 1995). The factor $f_{\rm col}^2$ comes from the assumed dilution of the blackbody spectrum, while $g(i)$ takes into account general relativistic corrections and is of the order $g \simeq 0.7 - 0.8$ (Ebisawa *et al.*, 1994).

The measurement of the inner radius of an accretion disc, which, in the standard geometrically thick case is almost equal to the radius of the innermost stable orbit of a free particle around a black hole, is clearly a very important astrophysical task, as it could be used to estimate mass and angular momentum of the central black hole. In the following Section, we present a critical analysis of the usual interpretation of the multicolour disc model parameters for black hole candidates in terms of the inner radius and temperature of the accretion disc. We will show that not only do such a model systematically underestimates the value of the inner disc radius, but that when the accretion rate and/or the energy dissipated in the corona are allowed to change, the inner edge of the disc, as inferred from the multicolour model, appears to move even when it is in fact fixed at the innermost stable orbit.

4.3 A critical assessment of the multicolour disc model

We will focus our discussion on the *soft/high* or the *very high* state spectra of galactic black hole candidates (see Section 1.3.1). According to the common paradigm in interpreting the observed spectra, the ultra-soft thermal component which is clearly detected in the observed spectra is the product of the emission from an optically thick accretion disk.

The aim of the work presented in this section is to demonstrate that the values one can obtain with such a fitting procedure, *which is now a standard one*, are *not* in general directly related (or at least not in a reliable way) to the actual geometrical parameters of the accretion disc.

We will use a self-consistent model for the radiative transfer in Shakura-Sunyaev accretion discs, including first-order corrections for gravitational redshift and Doppler blurring, as developed by Ross and Fabian (1996). The observable spectrum is computed for a number of different physical situations, each determined by the values of the viscosity parameter $\alpha_{\rm v}$ and the accretion rate through the disc. We then vary both the external accretion rate, $\dot{m}$, and the fraction f of the accretion power dissipated in the corona. In all the cases we consider, the value of the inner radius of the disc will be kept fixed to that of the innermost stable orbit of a free particle around a non-rotating black hole. Nevertheless, when trying to fit the computed spectra with the MCD model, we will obtain results at variance with this assumption. This is because changes in the normalization factor of the MCD model are produced, in a very complicated way, by variations in the structure of the uppermost disc layer (and hence in the emerging spectrum) induced by variability of the accretion rate and coronal activity.

We assume, as a starting point of our modelisation, the basic structure equations for geometrically thin accretion discs around Schwarzschild black holes given by the standard theory of Shakura and Sunyaev (1973) and presented in Section 1.2.1. The disc is assumed to have a *fixed* inner boundary at the innermost stable orbit at radius $R_{\rm in} = 3R_{\rm S} = 6GM/c^2$. We consider both an inner, radiation pressure dominated region and an outer, gas pressure dominated region of the disc. In determining the structure of the disc, the opacity is assumed to be dominated by Thomson scattering, and the gas is assumed to be composed of fully ionized hydrogen and helium, therefore

$$\bar{\kappa} \approx \kappa_T = 0.2(1+X)\ {\rm cm^2 g^{-1}}, \tag{4.7}$$

where X is the mass fraction of hydrogen. At every given radius R, the density is taken to be uniform in the vertical direction (which is the correct solution for the disc structure when radiation pressure dominates).

Choosing dimensionless parameters

$$m = \frac{M}{M_\odot}, \quad \dot{m} = \frac{\dot{M}}{\dot{M}_{\rm Edd}}, \quad r = \frac{R}{R_S},$$

where $\dot{M}_{\rm Edd} = 3.1 \times 10^{-8} m\ M_\odot\ {\rm yr}^{-1}$ is the Eddington accretion rate for a disk efficiency $\eta = 0.083$, the flux emerging from the surface of the disc is given by

$$F_0 = 1.2 \times 10^{27} m^{-1} r^{-3} [\dot{m} J(r)](1-f), \tag{4.8}$$

with $J(r) = (1 - \sqrt{3/r})$. The radial structure of the disc is summarized by the values of the half-thickness of the disc (in units of the Schwarzschild radius) h and the uniform gas density ρ_0:

1. *Radiation pressure dominated region*

$$h = \frac{H}{R_S} = 5.3(1+X)[\dot{m}J(r)](1-f) \tag{4.9}$$

$$\rho_0 = 1.1 \times 10^{-6}(1+X)^{-3}\alpha_{\rm v}^{-1} m^{-1} r^{3/2} [\dot{m}J(r)]^{-2}(1-f)^{-3} {\rm g\ cm^{-3}} \tag{4.10}$$

2. *Gas pressure dominated region*

$$h = 2.1 \times 10^{-2}(1+X)^{1/10}\alpha_{\rm v}^{-1/10} m^{-1/10} r^{21/20} [\dot{m}J(r)]^{1/5}(1-f)^{1/10} \tag{4.11}$$

$$\rho_0 = 17(1+X)^{-3/10}\alpha_{\rm v}^{-7/10} m^{-7/10} r^{-33/20} [\dot{m}J(r)]^{2/5}(1-f)^{-3/10} {\rm g\ cm^{-3}} \tag{4.12}$$

The radiative transfer and the vertical temperature structure are treated self-consistently at each radius, using the Fokker-Planck/diffusion equation of Ross *et al.* (1978) in plane-parallel geometry:

$$\frac{\partial n}{\partial t} = 0 = \frac{N_{\rm e}\sigma_{rmT}}{m_{\rm e}c}\frac{1}{\epsilon^2}\frac{\partial}{\partial \epsilon}\left\{\epsilon^4\left[n + \left(kT + \frac{7\epsilon^2}{10m_{\rm e}c^2}\right)\frac{\partial n}{\partial \epsilon}\right]\right\} + \frac{\partial}{\partial z}\left(\frac{c}{3\bar{\kappa}}\frac{\partial n}{\partial z}\right) + \frac{j_{\rm ff}h^3c^3}{8\pi\epsilon^3} - c\kappa_{\rm ff}n. \tag{4.13}$$

Here n is the photon occupation number, ϵ is the photon energy, z is the vertical height within the disc, $N_{\rm e}$ is the free-electron number density, T is the gas temperature, $j_{\rm ff}$ is free-free spectral emissivity, $\bar{\kappa}$ is the total opacity (per volume) and $\kappa_{\rm ff}$ is the free-free absorption opacity. The first term on the right hand side of equation (4.13) treats the full effect of incoherent Compton scattering, including the lowest order Klein-Nishina correction to the scattering rate. The remaining terms accounts for vertical diffusion of radiation as well as emission and absorption by free-free processes. The equation is solved in finite-difference form over a rectangular grid of ϵ and z values as described by Ross *et al.* (1978). The outer boundary condition for the radiation emerging from the surface of the disc has been discussed by Foster *et al.* (1986).

As we have already discussed in Section 4.1, incoherent Compton scattering within the accretion disc must be treated properly whenever it has an important effect on the emergent spectrum. The competition between Compton scattering of higher-energy photons and inverse Compton scattering of lower energy photons often results in the emergence of a Wien-law hard tail. For high energy photons the *thermalization depth* (where $\tau_*(\nu) = 1$) can be reached at very high Thomson depths, where the temperature is considerably higher than near the surface. Compton scattering in the outer layers of the disc down-scatters these photons to lower energies and produces a Wien-law tail.

Decreasing the flux emerging from the disc itself, either by lowering the accretion rate ($\dot{m}$) or increasing the fraction (f) of the accretion power dissipated in the corona, results in ever larger regions of very high density, both in the outermost portions of the disc and, for very low fluxes, in the very innermost portions as well. In those cases Comptonization is not complete or 'saturated' because the Compton parameter is less than unity at the thermalization depth. This corresponds to an increased importance of the intermediate spectral region (as defined in section 4.1). In these regions we treat Compton scattering as *coherent*, dropping the Fokker-Planck term in the radiative transfer equation (see discussion in Ross and Fabian, 1996).

In our calculations we fix the value of the black hole mass $m = 10$ and assume a composition $X = 0.71$. Following Ross and Fabian (1996) we divide the region $3 < r < 200$ of the disc into 20 annuli that make comparable contributions to the total luminosity. For each set of the parameters $\alpha_{\rm v}$, $\dot{m}$ and f, we find the radius at which radiation pressure equals gas pressure, which is the root of the equation (2.13)

The typical emergent spectrum from each annulus is calculated and then multiplied by the area of the annulus to find the contribution to the spectral luminosity. The resulting spectra are added together, taking into account blurring due to gravitational redshift and transverse Doppler effect using the method described by Chen *et al.* (1989). Finally, in order to allow direct comparison with observations in which a dramatic change in the inner radius has been reported (GRS 1915+105, see e.g. Belloni *et al.*, 1997), we choose an inclination angle $i = 70^\circ$ and a distance $D = 12.5$kpc.

For each set of parameters the emergent disc spectrum is used as a table model to create a fake set of data (with RXTE response matrix p012_LR1_970804.rsp, integration time 1000 s). These data are then fitted with the standard multicolour blackbody

Table 4.1: Physical parameters of the eleven set of simulated accretion disc spectra.

SET	$\alpha_{\rm v}$	$\dot{m}$	f	$r_{\rm AB}$	$r_{\rm coh}$
S1	0.1	0.3	0.0	100	50
S2	0.1	0.2	0.0	70	36
S3	0.1	0.1	0.0	50	28
S4	0.1	0.2	0.5	50	22
S5	0.3	0.08	0.1	36	22
S6	0.3	0.08	0.2	36	18
S7	0.1	0.1	0.4	28	13
S8	0.1	0.05	0.0	28	13
S9	0.1	0.1	0.5	22	9.6
S10	0.1	0.05	0.5	13	4.6 - 5.2
S11	0.1	0.05	0.8	-	-

model (DISKBB in XSPEC) in the $2-20$ keV band.

4.3.1 Results from simulations

We have simulated disc spectra in eleven different physical situations represented by the sets of parameters S1-S11 (see Table 4.1). The sets are listed in order of decreasing value of the radius $r_{\rm AB}$, the boundary between the radiation pressure and gas pressure dominated regions. Table 4.1 also lists the value of the radial coordinate $r_{\rm coh}$ for the boundary between the regions where Compton scattering is either saturated (inner part) or unsaturated. In the latter case, it has been treated as coherent (see section 4.1). As the power dissipated in the disc decreases and the density increases, from the combined effects of changes in $\dot{m}$ and f, this boundary moves inwards. That is, for an increasing portion of the disc Comptonization is incomplete and the local spectrum will be somewhat harder. For the S10 model, the density in the innermost region of the disc is so high (due to the $J(r)^{-2}$ term) that we have to consider incomplete Compton scattering also in the first inner annuli, where a significant fraction of the X-ray power is emitted. Consequently, for this set of parameters, two values of $r_{\rm coh}$ are listed. Finally, for the model S11, when the disc is entirely gas pressure dominated, we considered incomplete Compton scattering throughout all the disc (but see next section for a caveat on the applicability of our model to this extreme case).

Figure 4.1 shows the spectra emerging from the annulus at $r = 7$ from the S8-S11 sets of parameters. In the first two cases (S8 and S9, dotted and triple-dot-dashed lines, respectively) the power dissipated in the disc ($\propto (1-f)\dot{m}$) is the same, but in the

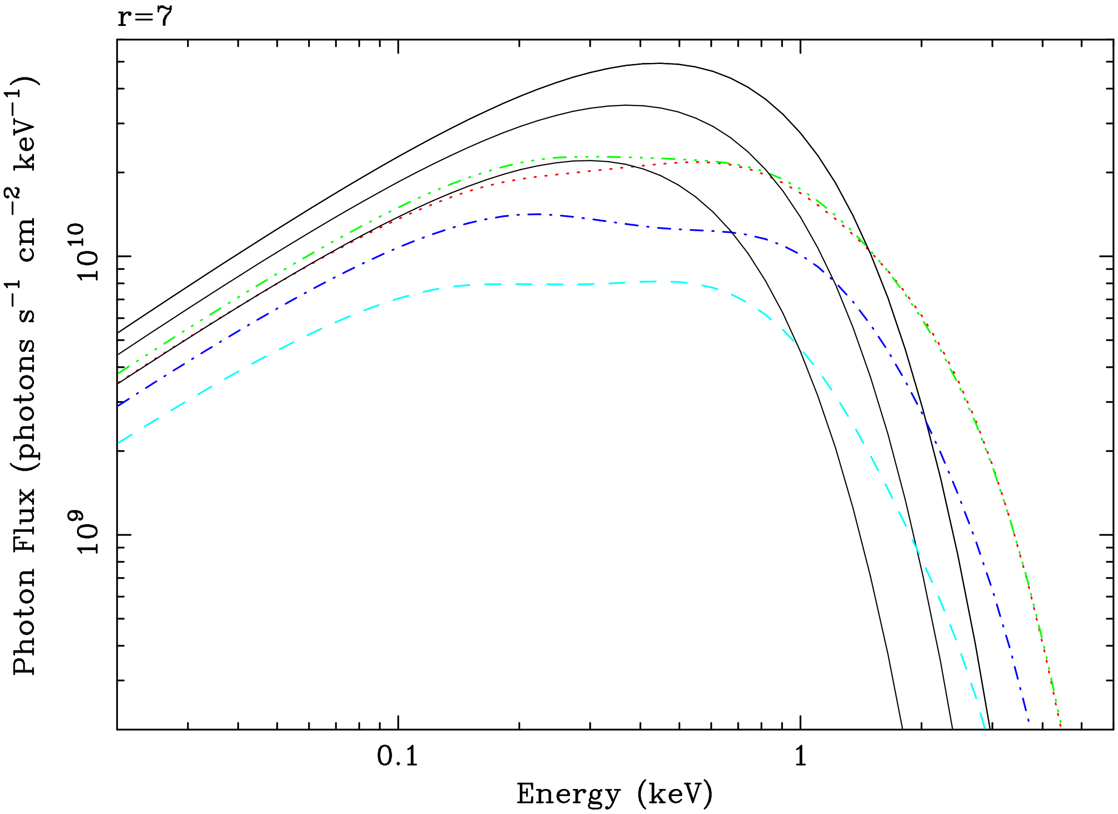

Figure 4.1: The disc spectra emergent at $r = 7$, computed for the parameter sets S8 (dotted line, $\dot{m} = 0.05$, $f = 0$, $\alpha_{\rm v} = 0.1$); S9 (triple-dot-dashed line, $\dot{m} = 0.1$, $f = 0.5$, $\alpha_{\rm v} = 0.1$); S10 (dot-dashed line, $\dot{m} = 0.05$, $f = 0.5$, $\alpha_{\rm v} = 0.1$) and S11 (dashed line, $\dot{m} = 0.05$, $f = 0.8$, $\alpha_{\rm v} = 0.1$). For each of the plots also shown are the spectra that would be observed for a blackbody-emitting annulus (solid lines). As the energy dissipated in the disc decreases, the spectra become increasingly hard.

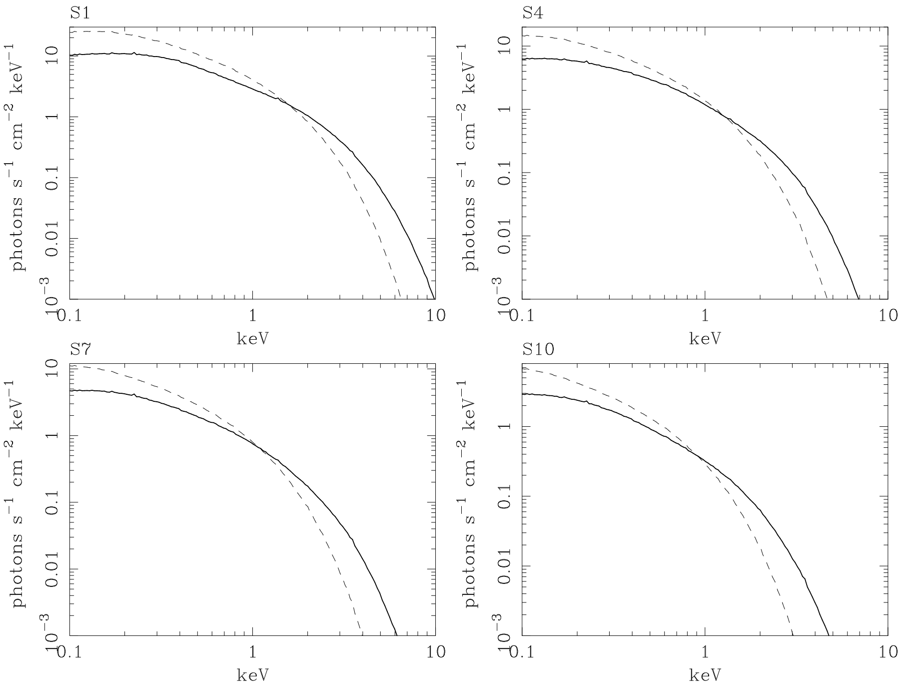

Figure 4.2: The disc spectra (solid lines) computed for the parameter sets S1 ($\dot{m} = 0.3$, $f = 0$, $\alpha_{\rm v} = 0.1$); S4 ($\dot{m} = 0.2$, $f = 0.5$, $\alpha_{\rm v} = 0.3$); S7 ($\dot{m} = 0.1$, $f = 0.4$, $\alpha_{\rm v} = 0.1$) and S10 ($\dot{m} = 0.05$, $f = 0.5$, $\alpha_{\rm v} = 0.1$). For each of the plots also shown are the spectra that would be observed for a blackbody-emitting disc (dashed lines).

former saturated Comptonization is more important, and the Wien shoulder is slightly more prominent. In the S10 case (dot-dashed line), still radiation pressure dominates, but Comptonization in unsaturated, the Wien tail is suppressed and the spectrum is harder. Finally, in the last case (dashed line), in which gas pressure dominates, the spectrum is flat over a large energy interval, and the spectrum is even harder.

Figure 4.2 shows the observed integrated spectra for S1, S4, S7 and S10, taking into account Doppler blurring and gravitational redshift. For comparison, Fig. 4.2 also shows the blurred spectra that would be observed if each point on the surface of the accretion disc emitted a blackbody spectrum at the local effective temperature. The observed spectra are harder than such effective blackbody spectra, and the discrepancy increases as we increase the density of the disc and decrease the power released in the disc itself (going from S1 to S10).

Table 4.2 lists the values of the fit parameters $T_{\rm col}$ and $R_{\rm col}$ for the eleven cases, as well as the corresponding reduced χ^2 of the fits and the spectral hardening factors obtained from Eq. (4.6) by assuming $\eta g(70°) = 0.5$ and $R_{\rm in} = 88.6$ km, as appropriate for the $10 M_\odot$ Schwarzschild black hole we are considering. The results are also shown in Figures 4.3a and 4.3b, where we plot the spectral hardening factor and the colour radius as functions of $\dot{m}(1-f)$, which is a measure of the flux emergent from the disc itself.

Table 4.2: Fit parameters in the range 2-20 keV. All the models refer to a $10M_{\odot}$ black hole with inclination angle and distance set to the values of the black hole candidate GRS 1915+105, namely $i = 70°$ and $D = 12.5$kpc.

SET	$T_{\rm col}$[keV]	$R_{\rm col}$[km]	$\chi^2_{\rm red}$	$f_{\rm col}$
S1	0.98	54.5	47	1.80
S2	0.87	56.9	22	1.76
S3	0.75	53.3	6.0	1.82
S4	0.75	52.1	6.4	1.84
S5	0.70	49.2	2.7	1.90
S6	0.69	49.3	2.5	1.90
S7	0.69	46.5	2.8	1.95
S8	0.68	41.1	1.6	2.08
S9	0.67	41.5	1.5	2.07
S10	0.59	39.0	1.8	2.12
S11	0.55	24.5	0.7	2.68

To check the sensitivity of our results to the energy range fitted, we also fitted the spectra in the $3-10$ keV band. The values obtained for the colour radii were, at most, just one or two kilometers smaller than those obtained in the 2-20 keV band (i.e. a change of about $3-4\%$).

It is clear that the multicolour model gives systematically lower values for the "inner radius" than the actual ones, a point which is well known. More interestingly, our results show that the hardening factor is by no means constant when we change the physical parameters of the disc. For example, assuming the conventional value $f_{\rm col} = 1.7 \pm 0.2$ (Shimura and Takahara, 1995; Sobczak *et al.*, 1999) and taking Doppler blurring and gravitational redshift into account, we would have underestimated the value for the inner disc radius by up to a factor of 2 (S11) using the fits with a multicolour model. On the other hand, the model gives quite stable and acceptable results for high accretion rates and/or lower values of the fraction of the power eventually dissipated in the corona. This in turn can help to understand the cases in which a nearly constant value of $R_{\rm col}$ is observed even when $T_{\rm col}$ varies (Tanaka and Lewin, 1995).

4.4 Summary and conclusions

The multicolour disc model is the most commonly used phenomenological model for the spectrum of a standard geometrically thin and optically thick accretion disc in the analysis of the data from GBHC in their *high/soft* or *very high* states. Taken at face

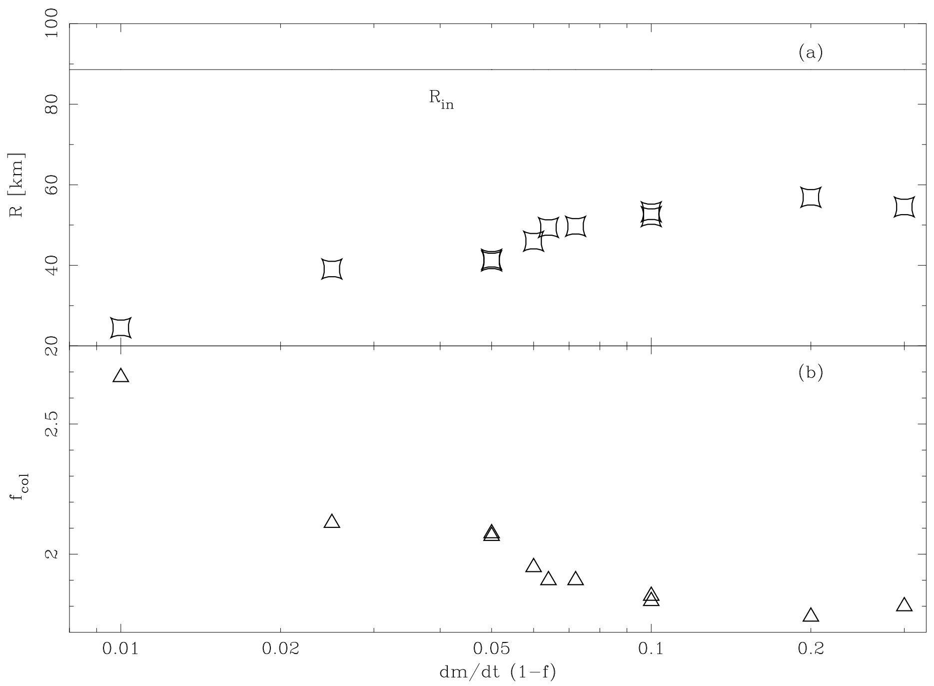

Figure 4.3: (a): Diamonds correspond to the values or $R_{\rm col}$ (in km) plotted as functions of $\dot{m}(1-f)$, which is a measure of the flux emergent from the disc, while the solid line marks the actual inner boundary of the disc, fixed in all our ten simulations. (b): Triangles represent the value of the spectral hardening factor needed to rescale the computed $R_{\rm col}$ to $R_{\rm in}$ (Eq. 4.6).

value, the two fitting parameters of the model allow us to estimate the temperature of the inner disc and its distance from the black hole, thus giving crucial pieces of information on the inner accretion flow geometry and, consequently, on the parameters of the central gravitational source (first and foremost its mass and angular momentum). But can we really trust the inner disc measurements done by fitting accretion disc spectra with such a model? By simulating accretion disc spectra with a more realistic model, that takes into account the temperature stratification in the vertical direction by solving self-consistently the radiative transfer equation using a Fokker-Planck/diffusion approximation, we have shown that MCD models systematically underestimate the value of the inner radius of the accretion disc for a black hole candidate. We also have shown that the spectral hardening factor f_{col}, which is needed to correct the results of the fits with a multicolour model, is not, as is usually assumed, constant when the accretion rate and/or fractional coronal activity change.

Recent observations of galactic black hole candidates seem to point towards an extreme dependence of the observed *colour* radius on f. In the work of Sobczak *et al.* (1999), where the authors report on the RXTE spectral observations of the 1996-97 outbursts of the microquasar GRO J1655-40, a sudden jump inward of the color radius (see their Fig. 7) occurs for the five very high state observations of the source during which the power-law (hard) flux was extremely high and the blackbody–to–total flux ratio was less than 0.5 (see their Fig. 5).

A similar trend has been reported by Muno *et al.* (1999) in the case of the microquasar GRS 1915+105. In their observations, the smallest values of the inner disc radius obtained by fitting the spectrum with the MCD model are associated with the highest values of the power-law–to–blackbody flux ratio, which in turn should be directly related to the value of f. In both these cases the inferred inner disc radii can change by more than a factor of four.

Belloni *et al.* (1997b,a), analyzing RXTE data of GRS 1915+105, interpreted the sudden change measured in the inner colour radius of roughly a factor of four in terms of the rapid disappearance of the whole inner part of the geometrically thin accretion disc. Once again, in that case the inner edge of the disc appears to shrink to its smallest values during an outburst in which the power law flux dominates the blackbody, and the blackbody–to–total flux ratio is less than 0.5.

Such a behaviour is exactly what our results predict we should expect from the MCD model when we increase f and/or reduce the accretion rate. In this case, every time the observations imply that the coronal activity is dominant, the multicolour fits should be corrected with a *varying* hardening factor $1.7 < f_{\mathrm{col}} < 3$ in order to recover the actual value of the inner disc radius.

It should be clear, however, that the issue of determining the exact shape of accretion disc spectra is very complicated and is very sensitive to the actual physical models used to describe it. In particular, key elements are the vertical structure of the disc, its density profile , the relativistic effects on the disc equations themselves (Gierliński *et al.*, 1999) and, to a greater extent, the surface density.

It is quite possible, and perhaps easier to conceive, that dramatic changes in the disc spectrum are produced by changes in the surface properties of the accretion disc, rather than by the disappearance of the entire inner regions. This, unfortunately, is hard to model theoretically. It would be interesting, for example, to assess the problem in the extreme case when almost all the accretion power is dissipated in the corona (i.e. in the limit $f \to 1$). As we believe that even in our most extreme simulation (S11) with $f = 0.8$ the simple treatment of the vertical disc structure we used here can be inadequate, and as this must be true *a fortiori* for larger values of f, we do not push our study further.

To do that we would need to take into account the X-ray reflection spectra of discs illuminated by a hot corona and to model carefully the heating of the disc atmosphere (e.g., see Sincell and Krolik, 1997; Ross and Fabian, 1993, who show how a hard tail in the disc spectrum is produced in this case). It is natural to believe, given the trend we observe in the simulations presented above and the observational results we referred to, that in such a situation the oversimplified multicolour model will give even smaller values of the colour radius.

Chapter 5

Aperiodic time variability in black hole accretion flows

5.1 Introduction

What we have discussed so far mainly concerned time-averaged spectral properties of black hole accretion flows. However, it is well known that the emission from accreting black holes shows highly variable lightcurves, on a wide range of timescales. Together with X-ray spectroscopy, the study of rapid (periodic, quasi-periodic or aperiodic) time variability is the main way to obtain information on the physical environment very close to the accreting source. In this section we will focus on the aperiodic variability, or "noise", leaving aside the issue of quasi-periodic oscillations (QPOs). I will mainly discuss the pieces of information that can be gathered by analysing X-ray lightcurves (that are the most variable) in the frequency domain, in particular by looking at the power density spectrum (PDS) as a function of frequency, $P(f) \propto |S(f)|^2$, where $S(f)$ represent the Fourier transform of the signal $S(t)$ in the time domain.

After a brief outline of the properties of aperiodic variability in active galactic nuclei and galactic black holes, we will present a model, based on a magnetic corona (see §2) for the short-time variability of Seyfert galaxies (§5.2), which nonetheless is general enough to be of interest also for the case of stellar mass black holes. Then, I will present an attempt to use rapid time variability of gamma-ray bursts (GRB) to constrain models of their inner engine, in particular those involving rapid accretion of a neutron torus onto a central black hole.

5.1.1 Variability in AGN

In this section we will briefly outline the main characteristics of the time variability properties of active galactic nuclei. As the variability timescale is shorter for the emission in the X-ray band (McHardy, 1989), we will refer mainly to studies based on observations carried on in this wave-band. A more thorough discussion can be found in the review articles by Mushotzky *et al.* (1993) and Nandra (2001), and in some of the references therein.

The *EXOSAT* satellite demonstrated in the eighties the existence of rapid variability in a number of AGN (Lawrence *et al.*, 1985; McHardy and Czerny, 1987) and allowed the first studies of their PDS. A systematic analysis of those data (Lawrence and Papadakis, 1993; Green *et al.*, 1993) generally found featureless power density spectra, with a steep "red noise" power-law, characterizing the variations. For an assumed power in the form $P(f) = Af^{-\gamma}$, where A is a normalizing constant, the power-law index was found to be $\gamma \sim 1.5$, for almost all the observed sources.

The observed slope of the power density spectra of AGN clearly indicates that there must be a turnover at low frequencies in order for the total power not to diverge. Finding such a "knee" in the PDS requires regular, long-term monitoring of a source, and is indeed a difficult task. However, thanks to observations made with the RXTE satellite, there have been recently a number of convincing reports of observed turnover frequencies in many AGN (McHardy *et al.*, 1998; Edelson and Nandra, 1999; Chiang *et al.*, 2000). Also, at high frequencies, in the absence of relativistic effects, the fastest variability should be determined by the light crossing time of the smallest emission region, and therefore a second break to a steeper power-law is expected in the PDS. Tentative evidence of such a steepening in the PDS of the Seyfert galaxy MCG–6-30-15 has been reported by Nowak and Chiang (2000).

Red noise (also called '$1/f$ noise') is characteristic of many astrophysical systems: solar flares (Lu and Hamilton, 1991), Soft Gamma Repeaters bursts (Göğüş *et al.*, 1999), Gamma-ray bursts (McBreen *et al.*, 1994; Beloborodov *et al.*, 2000), and many others, as well as more familiar, terrestrial ones (tides, earthquakes and even radio broadcasting, see e.g. Press, 1978; Montroll & Shlesinger, 1982), and is intimately related to the turbulent and/or chaotic nature of such non-linear systems. However, the information contained in the PDS alone is not enough to discriminate between different mechanisms that many authors have proposed as the origin of the $1/f$ noise.

In one of such attempts, Mineshige *et al.* (1994) (see also Mineshige & Negoro, 1999) have proposed that black holes accretion flows develop into a state of Self-Organized Criticality (Bak *et al.*, 1987) in which mass accretion occurs in avalanches, whose size is distributed as a power-law: large (and longer) shots contribute to the low-frequency part of the PDS, while small and shorter shots determine the power-law decline at high frequencies.

No consensus has emerged so far as to the physical interpretation of the low and high frequency breaks in the PDS. These features are presumably related either to a physical size in the system, or to some characteristic timescale in the accretion flow. As we shall see in the following section, observation of galactic black hole candidates with the highest time resolution (in particular those performed with the *RXTE* satellite) offers a better chance to study in detail the shape of their PDS and to possibly identify characteristic features (periodic or quasi-periodic) in it.

5.1.2 Variability in GBHC

Rapid variability, on all timescales, down to the millisecond level, is observed in the X-ray binaries thought to harbour a black hole in their center. Broadband noise properties in the frequency domain had been studied for a long time, and the spectral state classification discussed in Section 1.3.1 has in general been corroborated by the study of power density spectra of GBHC at different times. Changes in the X-ray spectra that lead to the so-called state transitions, are paralleled by changes in the rapid X-ray variability, in the following manner.

In the *low/hard* state the power spectra are dominated by a very strong (20 to 50 per cent 'root mean squared' (rms) amplitude) band limited noise (BLN), which follows approximately a power-law $P(f) \propto f^{-\gamma}$ with index $\gamma \sim 1$ at relatively high frequencies (up to abut 10-100 Hz, usually). Below a certain frequency (the so called "break frequency") the PDS flattens out ($\gamma \sim 0$: "white noise"). Above this break frequency a broad bump (sometimes narrow enough to be defined a QPO) is often present. In some sources, a second break is visible in the power density spectrum, above which the power-law index increases to $\gamma \sim 2$ (this is the case of the best studied GBHC, Cygnus X-1, that strongly resemble the observed PDS of the best studied Seyfert 1, MCG–6 -30-15, see Section 5.2).

In the *high/soft* state, the PDS shows only a weak (a few per cent) power-law noise component, while in the *very high* state noise is present similar to either the weak high/soft state noise or the BLN characteristic of the low/hard state (although only with a strength of 1-15 per cent rms).

Such a relatively simple situation is complicated by the ubiquitous presence of quasi-periodic features, both at high ($>$ 100 Hz) and low ($<$ 20 Hz) frequencies, both evolving and stable. This is an extremely interesting and active field of research, that could potentially unveil the properties of the geometry and the dynamics of the innermost parts of accretion flows around black holes, and even be used to test strong-gravity effects in these systems (Cui *et al.*, 1998; Stella and Vietri, 1998; Merloni *et al.*, 1999; Psaltis and Norman, 2000; Psaltis, 2001; Wagoner *et al.*, 2001).

5.2 Spectral variability in Seyfert 1 galaxies: the thundercloud model

As we have just seen, the high energy emission from accreting black holes is extremely variable. Then we may expect that also their spectral properties are not stationary, but vary on timescales comparable to the typical bolometric flux variations. Indeed, time resolved spectral analysis have established that spectral variability on the shortest timescales is important in all these sources. For example, the analysis of average peak aligned shots of the BHC Cygnus X-1 (Li *et al.*, 1999) has shown that, during the *hard* state and the transitions between the two states of the source, the spectrum evolves from hard to soft to hard again as the shot evolves. Such kind of analysis, though, is much better suited for active galactic nuclei. As a matter of fact, the dynamical timescale of a Keplerian accretion flow around a black hole, $t_{\rm dyn} \simeq 9 \times 10^2 \varpi^{3/2} (M_{\rm BH}/10^7 M_{\odot})$ s (where we have introduced the dimensionless radius $\varpi = R/R_{\rm S} = c^2 R/2GM$), is such that it is much easier to perform reliable time resolved spectroscopy for the brightest AGN, where a typical flaring event may last hours or days.

There is in fact growing observational evidence for a number of Seyfert 1s, that during a flare the X-ray spectrum becomes softer as the 2-10 keV flux increases (see e.g. Done *et al.*, 2000; Zdziarski and Grandi, 2001; Petrucci *et al.*, 2001; Vaughan and Edelson, 2001; and Nandra, 2001 for a recent review). More recently, Georgantopoulos and Papadakis (2001) found similar trends in a number of Seyfert 2 galaxies observed with *RXTE*.

Uttley and McHardy (2001) have discovered a remarkable linear correlation between variability and flux in two X-ray binaries (Cygnus X-1 and the millisecond pulsar SAX J1808.4-3658), on all timescales (Uttley, private communication). They have also found that the lightcurves of three Seyfert galaxies are consistent with such relationship and have therefore argued that such behaviour is an universal one in compact accreting systems. Indeed, Edelson *et al.* (2001) have recently found a similar linear relationship between X-ray flux and variability in the Seyfert 1 galaxies Akn 564 and Ton S180, confirming the generality of the correlation.

In this section we propose a simple model of Seyfert 1 high energy emission that combines the basic properties the accretion flows must have to reproduce temporal *and spectral* characteristics of the observed objects. In particular, we will show how it is possible to explain both the two most common and interesting correlations we have mentioned: the flux-spectral slope one and the flux-variability one.

The basic idea of the model is that magnetic reconnection in the accretion disc corona does not occur randomly in time and space, but rather in avalanches of correlated events (Poutanen and Fabian, 1999). This not only affects the properties of the lightcurve, but is responsible for the observed spectral variability. The spectrum produced in region where a large number of heating events take place is different from the spectrum generated by an isolated event, as we discuss in the next section. Furthermore, large avalanches of magnetic flares may obscure the underlying disc as seen from the observer (see §3), and complicates the temporal behaviour of the secondary spectral features (reflection hump and fluorescent lines).

To build a full time-dependent model on the basis of the above ideas, including a detailed treatment of the radiative transfer in the accretion disc – corona system is undoubtedly a formidable task. Here we have chosen to simplify it by adopting an approximate analytic treatment for the spectral generation, as outlined in §2.4. This, we believe, gives a fair representation of the modeled system and enables us to highlight the main prediction of the model in the simplest possible way, allowing us to introduce the time variable, keeping at the same time the problem treatable.

5.2.1 Active regions distribution and luminosity

It is well known that phenomenological shot noise models in their original version (in which the shot duration is fixed) are unable to reproduce the observed power-law slope of the PDS. Whatever the assumed shot profile, such models predict a *minimum* slope of $\gamma = 2$. In general, in order to explain the observed values of $\gamma \sim 1.5$, any model requires individual signals to have a broad range of typical timescales. In this way Poutanen and Fabian (1999) were able to reproduce the properties of the observed Power Spectrum of the BHC Cygnus X-1, using a simple stochastic pulse-avalanche model, originally proposed by Stern and Svensson (1996) to explain γ-ray burst temporal characteristics. In such a model the individual signals correspond to coronal hard X-ray magnetic flares, which possess a range of durations and are capable to trigger larger avalanches.

Magnetic field reconnection of flux tubes in a tenuous corona is in principle capable of producing power-law distribution of active region sizes. In a pioneering work, Tout and Pringle (1996) have demonstrated, both with a simple analytic model and with Monte Carlo simulations, that, if a dynamo-generated magnetic field with a coherence scale of the order of the disc thickness emerges from the accretion disc, then the inverse cascade process of stochastic magnetic reconnection of flux tubes may lead to much larger coherent fields and active regions (see also §2.5.2), with a power-law distribution in size.

In the hot, comptonizing corona the energy input is likely to be provided by a strong, highly intermittent magnetic field (see Section 2.3) amplified in the underlying turbulent disc by a dynamo process generated by the magneto rotational instability (Balbus and Hawley, 1998; Tout and Pringle, 1992). Dissipation is then triggered by magnetic reconnection of flux tubes on the smallest possible scale (given approximately by the disk scaleheight). If these small reconnection sites were distributed randomly in time and space, all with a similar aspect ratio, h_a/r_a, we would observe shot-noise-like variability in the lightcurve and, more importantly, no spectral variability. If, on the other hand, the system is in some kind of critical state, such that each small flare can trigger an avalanche in its immediate neighborhood (i.e. the flares are spatially and temporally correlated), the situation will be qualitatively different. In fact, any such avalanche is effectively a large active region: more luminous (because it contains more reconnection sites), more extended and with a softer spectrum (because h_a/r_a is smaller, see Section 2.4).

As a consequence of such avalanche generation process, at any given time there would be a spread of active regions above the disc, with typical size ranging from the very small micro-flares ($R_a \sim$ disc scaleheight), to the larger avalanches ($R_a \sim$ a few Schwarzschild radii).

Hence, we assume that the luminosity of an active region is determined by the size of the avalanche, and therefore scale as the size of the region itself

$$L(r_a) = c_1 r_a^D. \tag{5.1}$$

Here D may be related to the spatial distribution of the correlated flares (and be regarded as a fractal dimension of the reconnection sites) and/or to the radial dependence of the energy generation in the accretion disc.

On the other hand, because of the stochastic nature of the avalanche generation process, we will assume a *power-law* shape for the time-independent active region size distribution $n(r_a)$ (as also suggested by the shape of the observed power density spectra), such that the number of active regions of size r_a lying in the interval $(r_a, r_a + dr_a)$ is, *at any time*, given by

$$n(r_a)dr = c_2 r_a^{-p} dr. \tag{5.2}$$

The two constants c_1 and c_2 can be fixed imposing the overall normalization for the total corona average covering fraction C and for the average hard luminosity:

$$\begin{aligned} C &= \int_{r_{\min}}^{r_{\max}} n(r_a) \frac{\mathcal{A}(r_a)}{A_{\rm disc}} dr_a & (5.3) \\ L_{\rm hard} &= \dot{m} f_{\rm H} L_{\rm Edd} = \int_{r_{\min}}^{r_{\max}} n(r_a) L(r_a) dr, & (5.4) \end{aligned}$$

where $\mathcal{A}(r_a)$ is the area of the disc covered by an active region of size r and $A_{\rm disc}$ is the total area of the disc.

The basic principle of the model is illustrated schematically in Fig. 5.1, where we show two maps of the inner accretion disc corona ($A_{\rm disc} = \pi(20R_{\rm S})^2$ cm^2) produced by two Monte Carlo realization of our model: they can be regarded as two pictures of the corona, taken from an observer at an inclination angle of 0° at two different times. The figure clearly shows that the more luminous state (right panel, for which the instantaneous covering fraction is ~ 29 per cent), is dominated by active regions with soft spectrum.

To summarize, we model the accretion disc corona as highly inhomogeneous stochastic system, whose basic building blocks, the active regions, can be viewed as 'magnetic thunderclouds', charged by the differential rotation of the underlying disc and/or the turbulent motions in the accretion flow. The sizes of the thunderclouds are distributed as a power-law. The fast energy release, triggered by magnetic reconnection on the smallest scales, heats progressively larger active regions. Each active region (thundercloud) produces the observed rapid flares (X-ray lightning strokes) by inverse Compton scattering soft photons coming mainly from the underlying optically thick accretion disc[1]. Larger active regions are more luminous and have softer spectra. Furthermore, if the coronal optical depth $\tau_{\rm T}$ is high enough, the active regions may obscure the X-ray spectral features produced in the cold disc (in particular the reflection hump

[1]It is interesting here to remark that the analogy between high energy astrophysical processes and terrestrial lightning is not new. McBreen *et al.* (1994) have pointed out the similarity between the log-normal properties of gamma-ray bursts lightcurves and those of terrestrial lightning. In the latter case, the durations, peak currents, intervals between the strokes in the flashes, and the flash charges are log-normally distributed (Berger *et al.*, 1975). When the dispersion of a log-normal distribution is large, the distribution is mimicked by a $1/x$ distribution over a wide range of x, while it can be shown that amplification processes generally relate log-normally distributed variables to power-law tails (Montroll and Shlesinger, 1982).

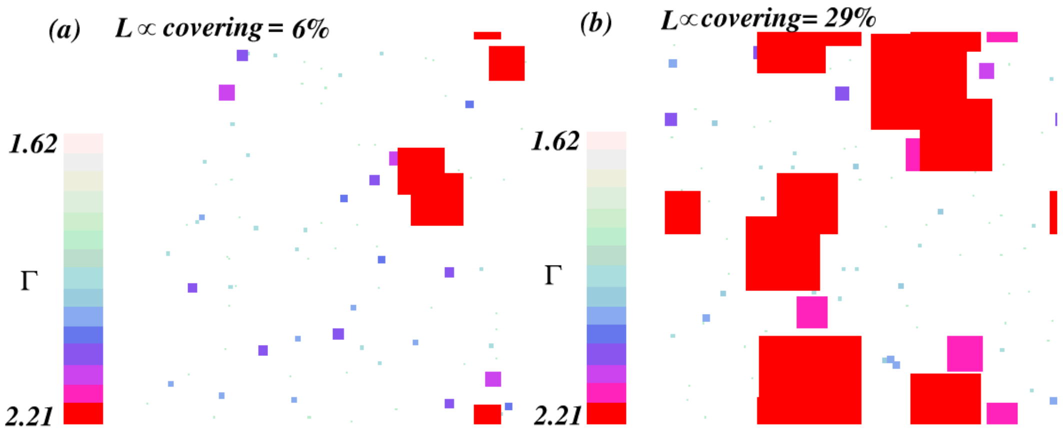

Figure 5.1: The inner accretion disc corona is mapped into a square of 100×100 pixels, so that each pixel represents an area of $\pi(0.2R_{\rm S})^2$ cm^2. For simplicity, we have chosen $D = 2$, so that each pixel have the same luminosity and the overall luminosity is proportional to the covered area. The regions of the corona active at any time are represented by filled squares, whose size is distributed as a power-law, with index $p = 2$ (see text for details). Each region is assumed to have the same height above the disc ($H_a = 1$) and optical depth ($\tau_{\rm T} = 1$). The color code shows the spectral index of the filled active regions, calculated according to the semi-analytic prescription described in Section 2.4, and that goes from $\Gamma = 1.62$ (grey-green) to $\Gamma = 2.21$ (red). Clearly the more luminous state (panel (b), right hand side, for which the instantaneous covering fraction is ~ 30 per cent), is dominated by active regions with soft spectrum.

and the fluorescent lines, see §3) for an observer situated above them (and act therefore as 'Compton clouds').

5.2.2 Time variability and Power Density Spectra

In general, if the heating process is related to the dissipation of the magnetic field in the corona, the dissipation timescale is given by $t_0(r_a) \simeq 10^2 r_a M_7 b$ s, where $M_7 = M_{\rm BH}/10^7 M_\odot$ and $b = c/v_{\rm diss}$ (Haardt *et al.*, 1994). Here we assume that the spectrum is produced instantaneously in every active region, i.e. the timescale over which an active region is heated is longer than the region light-crossing time and $b \gtrsim$ a few. We fix $b = 30$ (see section 5.2.4 for a discussion of this point).

As we have mentioned in the introduction to this chapter, power density spectra of both AGNs and BHCs show a break that separates low-frequency white noise ($P(f) \sim$ constant) from the red noise part of the PDS. Within our model, such a break can naturally be associated with the largest possible active region, and thus fix $r_{\rm max}$.

The slope of the active regions size distribution can in turn be constrained by the observed PDS slope. As a matter of fact, in any stochastic process in which the characteristic durations and amplitudes are distributed as power-laws, we have

$$N(t_0) I^2(t_0) \propto t_0^\beta \ \text{ for } \ t_{0,\rm min} < t_0 < t_{0,\rm max}, \tag{5.5}$$

where $N(t_0)$ is the probability and $I^2(t_0)$ the mean square amplitude of a flare with a duration t_0, and the PDS is approximately given by

$$P(f) \propto f^{-\gamma} \quad \gamma = (3+\beta), \tag{5.6}$$

in the range $(2\pi t_{0,\rm max}) < f < (2\pi t_{0,\rm min})$ (Lochner *et al.*, 1991). Then, according to our model, for which $N(t_0) \propto t_0^{-p}$ and $I(t_0) \propto t_0^D$, the observed slope of the PDS determines the relation between p and D:

$$p = 2D + 3 - \gamma. \tag{5.7}$$

In the following section we present a numerical simulation of the thundercloud model for AGN spectral/temporal variability, keeping fixed $\gamma = 1.5$ (as usually dictated by the observations of AGN), but varying the total corona covering fraction C and the luminosity index D. Also, we will discuss the main observable consequences of the thundercloud model.

5.2.3 The full picture: results from simulated lightcurves

In this section we describe the results we obtained from simulated lightcurves with variable X-ray spectra. To take into account time dependence, we introduce a new distribution $n(r_a, t)$, defined in such a way that the number of active regions of size in the interval $(r_a, r_a + dr_a)$ *generated* in the time bin $(t, t+dt)$ is given by $n(r_a,t)\, dr_a\, dt$. In a stationary state $n(r_a,t)$ does not depend on t, and we assume $n(r_a) = n(r_a,t) t_0(r_a)$, where $t_0(r_a)$ is the total duration of an avalanche (see previous section).

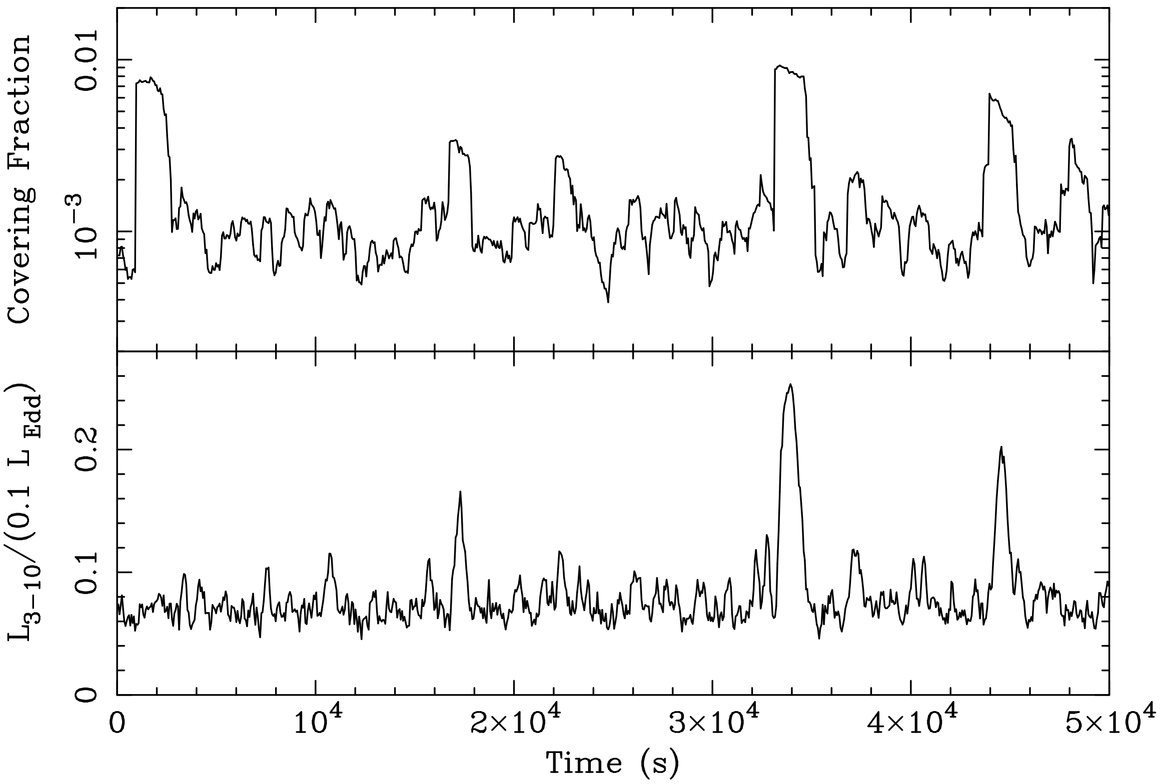

Figure 5.2: A simulated lightcurve (bottom panel) with its corresponding evolution of the covering fraction (top panel), for a $M_{\rm BH} = 10^7 M_\odot$ central black hole accreting at one tenth of the Eddington rate.

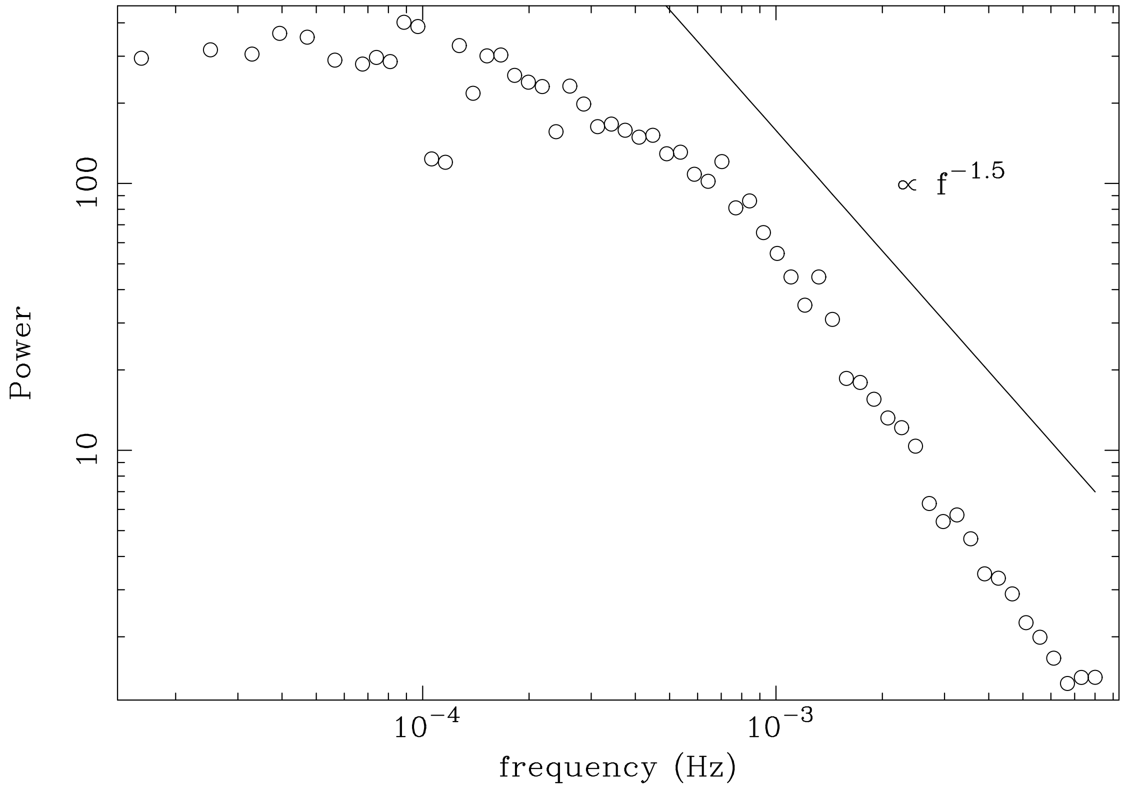

Figure 5.3: Power density spectrum of the simulated lightcurve shown in Fig. 5.2. The indexes of the active region distributions are $D = 1$ and $p = 3.5$. To reduce the scatter the PDS has been obtained averaging the power density spectra of 16 lightcurves of the total duration of 1.2×10^5 seconds each.

A simulated lightcurve (see Fig. 5.2 for an example) is then produced requiring that in any time bin the actual number $\mathcal{N}(r_a, t)$ of avalanches generated with size in the interval $(r_a, r_a + dr_a)$ be picked from a Poissonian distribution with mean $n(r,t)dr$ and then summing over all the active regions generated at any time. For the sake of simplicity, we adopted a triangular shape for the individual flares profile. Because we enforce relation (5.7) for the indexes of the distribution, the final PDS has the correct slope in the red-noise part (see Figure 5.2.3).

The spectrum of each active region is calculated as in §2.4. We have assumed that every active region has the same height above the disc ($H_a = 1$). Its size, R_a, determines its luminosity (Eq. 5.1). Once a value for the coronal optical depth, $\tau_{\rm T}$, is chosen, temperature, magnetic field intensity, synchrotron self-absorption frequency $\nu_{\rm c}$ and power-law index of the comptonized spectrum, α, are calculated self-consistently as in §2.4. The emerging spectrum at any time is then calculated superimposing the contribution from all the flaring regions active at that time. The photon index Γ is calculated for every time bin with a least square fit to the spectrum with a power-law model in the 3-10 keV band.

We have fixed $r_{\rm min} = 0.02$ and $r_{\rm max} = 4$. The average covering factor C, in turn, fixes the total number of active regions and the degree of variability (RMS) of the PDS.

To explore the parameter space, we have simulated AGN light curves of total duration equal to 3×10^6 s, with a temporal resolution of 60 s. We varied the coronal optical depth (in the range $0.5 \leq \tau_{\rm T} \leq 2$), the average covering fraction ($5 \times 10^{-4} \leq C \leq 2 \times 10^{-3}$) and the luminosity scaling index ($0.6 \leq D \leq 1.4$).

The spectral index-luminosity correlation

In Figure 5.4, for $D = 1$ and $C = 10^{-3}$, we plot the photon index Γ of the total emerging spectrum, measured in the 3-10 keV band, as a function of the luminosity in the same band, for three different values of the optical depth. Clearly, the higher the 3-10 keV luminosity, the softer the spectrum in that energy band, as observed. Furthermore, when the largest flares occur, and consequently the instantaneous covering fraction has a maximum (see Fig. 5.2), the $\Gamma - L$ relation tends to saturate to the softest value corresponding to an almost slab-like geometry. This is an intrinsic property of our model, and is due to the fact that larger active regions are cooler because the reprocessed soft luminosity that reenters the blobs (and is comptonized there) is larger.

Overall, we find a spectral variability range $\Delta\Gamma \sim 0.3 - 0.4$ for a change in luminosity of about a factor of four, similar to what is observed in many Seyfert 1 galaxies. It is worth remarking that a similar correlation was indeed predicted by Haardt *et al.* (1997) for the case of a pair dominated corona, but in that case the same $\Delta\Gamma$ was achieved for a luminosity variation of at least two orders of magnitude, which is clearly inconsistent with the observations.

To test the consistency of the model against an observed system, we show in

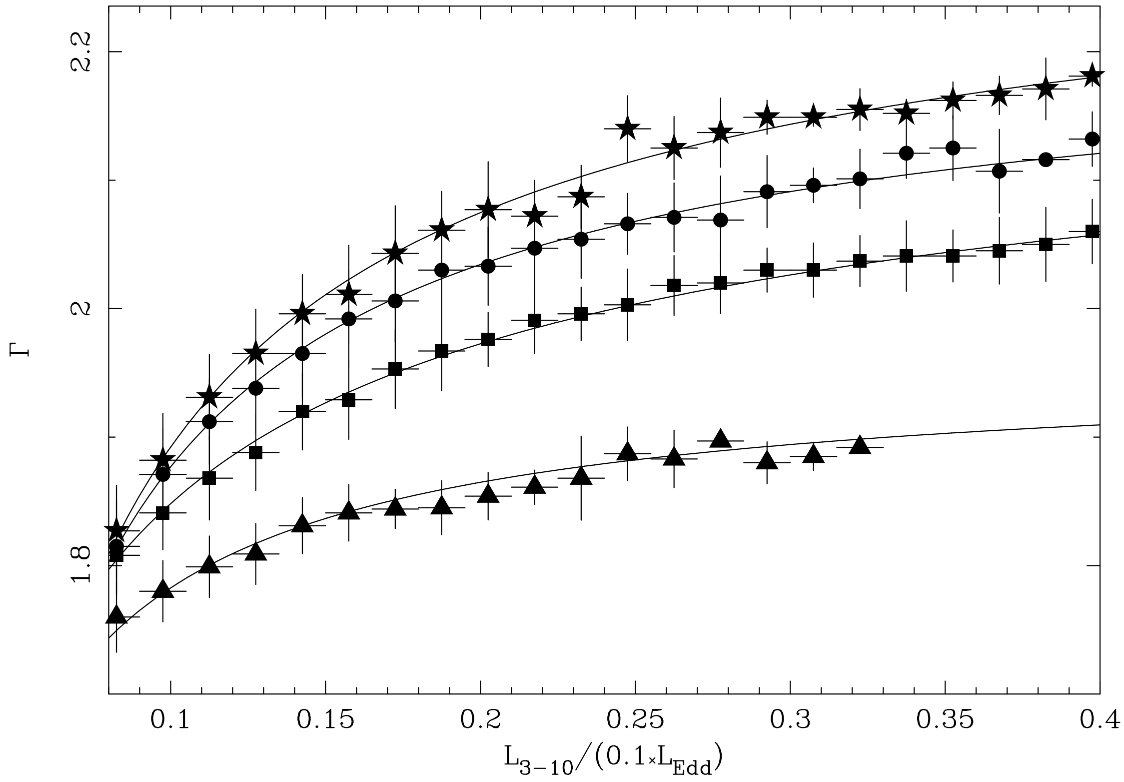

Figure 5.4: The observed photon index in the 3-10 keV band plotted versus the luminosity in the same band (in units of $0.1L_{\rm Edd}$) as obtained from our fiducial simulation for $D = 1$ and $C = 10^{-3}$. The points for all the time intervals have been grouped in luminosity bins and the average gamma has been calculated. The error bars correspond to the weighted statistical uncertainty. Also shown are the best fitting functions (as in Table 1) for each of the four groups. Triangles corresponds to $\tau_{\rm T} = 0.5$, squares to $\tau_{\rm T} = 1$, circles to $\tau_{\rm T} = 1.5$ and stars to $\tau_{\rm T} = 2$.

Fig. 5.5 the observed $\Gamma - L$ correlation for the Seyfert 1 galaxy MCG–6-30-15 (from Vaughan and Edelson, 2001) observed with *RXTE* in 1997 and in Fig. 5.6 the observed correlation extarcted from the 1999 *ASCA* observation of the same source (Shih et al., 2001). For both our simulated lightcurves and the MCG–6-30-15 data we have fitted the Γ-luminosity relation with the function

$$\Gamma = \Gamma_0 - KL^{\delta}. \tag{5.8}$$

In Table 5.1 the values of the three fitting parameters Γ_0, K and δ are listed for our set of simulated lightcurves. The asymptotic value of the photon index, Γ_0, depends mainly on the optical depth, and is larger for larger values of $\tau_{\rm T}$. The exponent δ, instead, which determines the amount of spectral variation for a given increase in luminosity, is mainly dependent on the index D.

For the 1997 data plotted in Figure 5.5 we obtain $\Gamma_0 = 2.30^{+0.63}_{-0.02}$, and $\delta = -1.31^{+0.79}_{-0.79}$, while for the 1999 ones, plotted in Figure 5.6 we obtain $\Gamma_0 = 2.11^{+0.11}_{-0.04}$, and $\delta = -3.9^{+3.8}_{-2.7}$ (the parameter K only reflects the different calibrations of the two satellites). Compared to our model simulations, such a result is a strong indication of a relatively high value for the coronal optical depth ($\tau_{\rm T} \gtrsim 1$) in this source, at least for the observation considered here, with even higher values of $\tau_{\rm T}$ preferred for the 1997 *RXTE* observation. This, in turn, agrees well with the results presented in Guainazzi *et al.* (1999) of the analysis of a *BeppoSAX* observation of the same source: the measured spectral cut-off energy ($E_{\rm c} \simeq 130 \pm 40$ keV for their best-fitting model), in the framework of thermal Comptonization models implies a coronal temperature[2] $\Theta \sim 0.1$, that we obtain for $\tau_{\rm T} \gtrsim 1.5$ (see Fig. 2.2). Although it is more difficult to put tight constraints on the other two model parameters (D and C, but see also the discussion about the variability-luminosity correlation below), nonetheless we may conclude that the observed $\Gamma - L$ correlation in MCG–6-30-15 is consistent with $D \sim 1$ and $C \sim 10^{-3}$. Such a fairly small value for the average covering fraction is indeed required by the observed data: the smaller the covering fraction, the larger the observer variability, and the greater the chance of a large flare to occur. Too a large value of C would therefore drastically reduce the observed spectral variability, as discussed below. For our fiducial case, $D = 1$ and $C = 10^{-3}$, we have $c_1 = 0.16\dot{m} f_{\rm H} L_{\rm Edd}$ and $c_2 = 0.046$. The total number of active regions at any time is on average[3] $\mathcal{N} = \int n(r) dr \simeq 160$.

[2]We note that, usually, an e-folding power-law is not a good approximation for the actual shape of the observed high energy cut-off in many sources, in particular those with the better quality data, see e.g. Frontera *et al.* (2001a). The actual coronal temperature is somewhat model and geometry dependent, and its real value for MCG–6-30-15 may differ from the one we adopt here by a factor of the order of unity, which does not change our main conclusion regarding the source optical depth.

[3]The total number of individual micro-flares that are the fundamental constituents of an avalanche is of course larger, depending on the actual number of events that are contained in any larger active region.

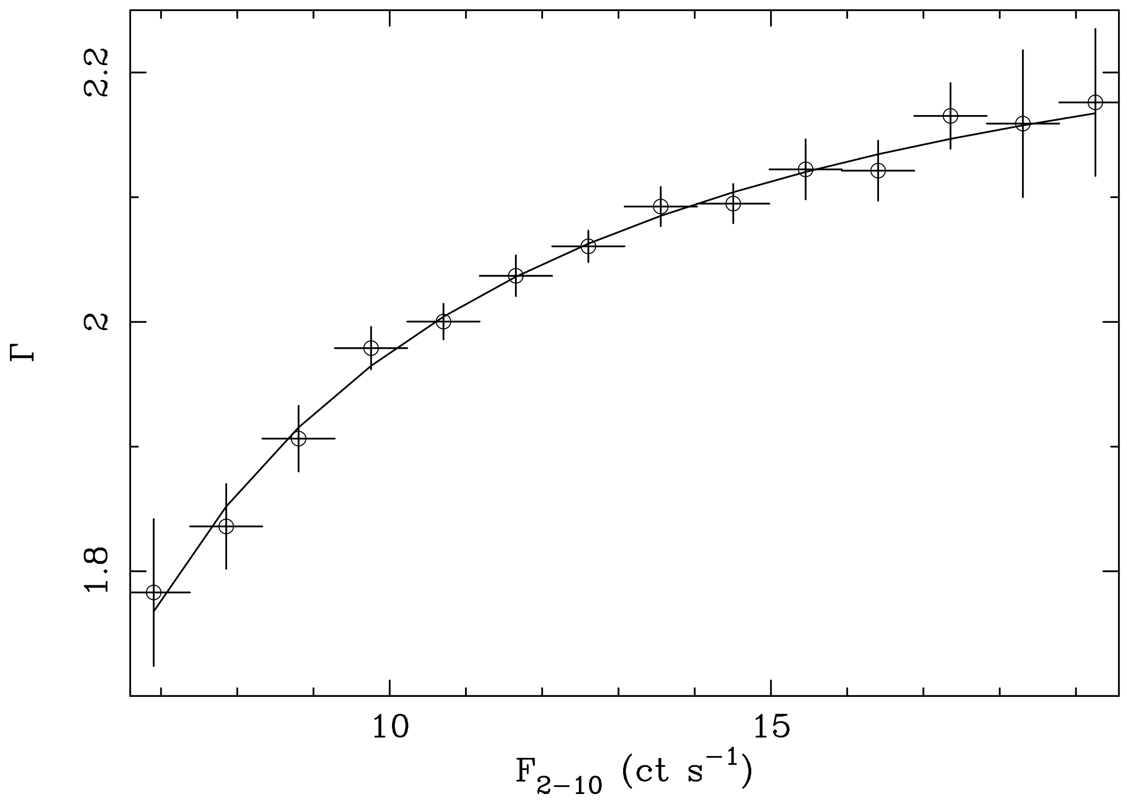

Figure 5.5: The observed photon index in the 2-10 keV band plotted versus the *RXTE* count rate in the same band for the Seyfert 1 galaxy MCG–6-30-15, from the analysis of Vaughan & Edelson (2001) (their Figure 3). The data point have been grouped in flux bins and the errors correspond to the weighted statistical uncertainty on the value of the spectral index. Also shown is the best fitting function of the form $\Gamma = \Gamma_0 - KF^{\delta}$. We obtain $\Gamma_0 = 2.30^{+0.63}_{-0.02}$, $K = 6.8^{+20.8}_{-4.5}$ and $\delta = -1.31^{+0.79}_{-0.79}$.

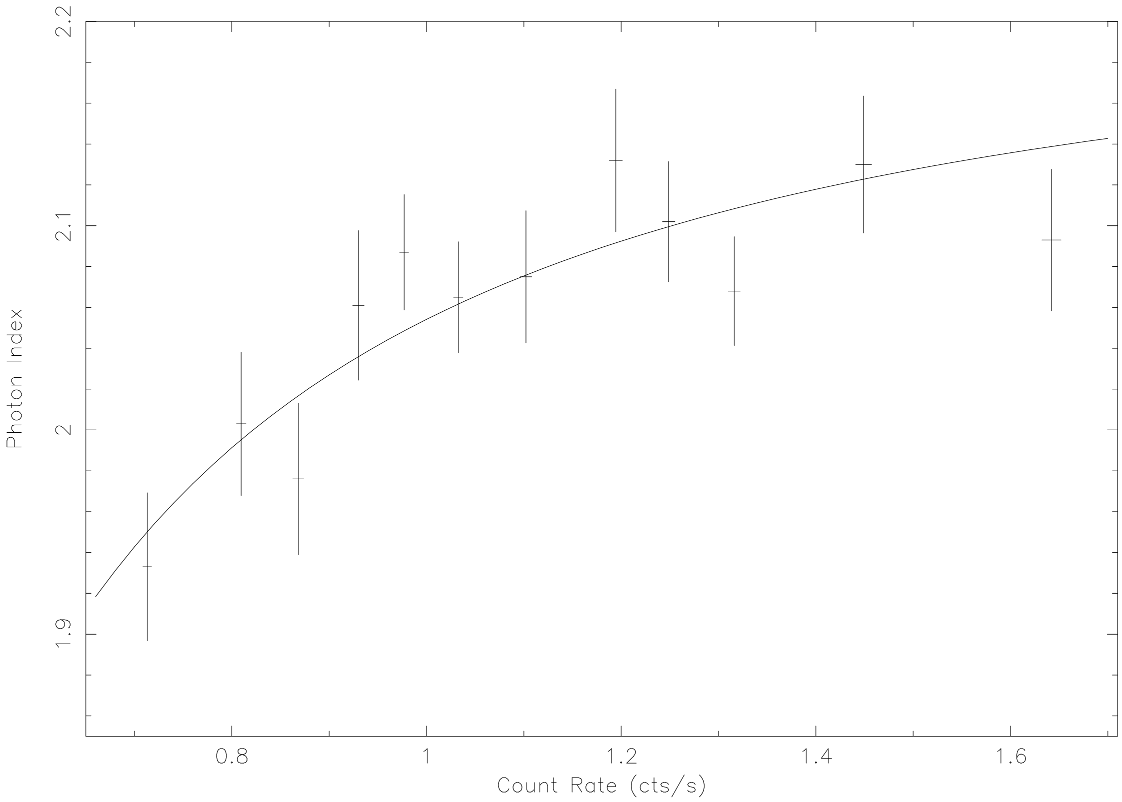

Figure 5.6: The observed photon index in the 3-10 keV band plotted versus the *ASCA* count rate in the same band for the Seyfert 1 galaxy MCG–6-30-15, from the analysis of Shih et al. (2001). The data point have been grouped in flux bins and the errors correspond to the weighted statistical uncertainty on the value of the spectral index. Also shown is the best fitting function of the form $\Gamma = \Gamma_0 - KF^{\delta}$. We obtain $\Gamma_0 = 2.11^{+0.11}_{-0.04}$, $K = 0.05^{+0.12}_{-0.04}$ and $\delta = -3.9^{+3.8}_{-2.7}$.

Table 5.1: Results from simulations and best fit parameters for the Γ-luminosity relation. We fitted a function of the form $\Gamma = \Gamma_0 - KL^{\delta}$.

Model parameters			Fit parameters		
C	D	τ_T	Γ_0	K	δ
0.0005	0.6	0.5	$2.01^{+0.04}_{-0.02}$	$0.050^{+0.041}_{-0.019}$	$-0.55^{+0.20}_{-0.20}$
0.0005	0.6	1.0	$2.21^{+0.11}_{-0.04}$	$0.08^{+0.12}_{-0.03}$	$-0.49^{+0.23}_{-0.22}$
0.0005	0.6	1.5	$2.30^{+0.01}_{-0.02}$	$0.058^{+0.019}_{-0.013}$	$-0.65^{+0.11}_{-0.11}$
0.0005	0.6	2.0	$2.34^{+0.01}_{-0.01}$	$0.030^{+0.011}_{-0.008}$	$-0.93^{+0.13}_{-0.14}$
0.0005	1.0	0.5	$2.07^{+0.01}_{-0.02}$	$0.11^{+0.45}_{-0.07}$	$-0.37^{+0.23}_{-0.41}$
0.0005	1.0	1.0	$2.21^{+0.18}_{-0.06}$	$0.10^{+0.25}_{-0.05}$	$-0.56^{+0.26}_{-0.26}$
0.0005	1.0	1.5	$2.32^{+0.13}_{-0.05}$	$0.10^{+0.01}_{-0.003}$	$-0.62^{+0.22}_{-0.22}$
0.0005	1.0	2.0	$2.32^{+0.01}_{-0.01}$	$0.040^{+0.013}_{-0.009}$	$-1.00^{+0.11}_{-0.12}$
0.0005	1.4	0.5	$1.96^{+0.01}_{-0.01}$	$0.019^{+0.072}_{-0.009}$	$-0.89^{+0.68}_{-0.92}$
0.0005	1.4	1.0	$2.09^{+0.01}_{-0.01}$	$0.010^{+0.012}_{-0.009}$	$-1.28^{+0.63}_{-0.64}$
0.0005	1.4	1.5	$2.15^{+0.35}_{-0.05}$	$0.085^{+0.43}_{-0.005}$	$-1.44^{+1.22}_{-1.70}$
0.0005	1.4	2.0	$2.38^{+0.02}_{-0.02}$	$0.070^{+0.01}_{-0.003}$	$-0.81^{+0.50}_{-0.79}$
0.001	0.6	0.5	$2.09^{+0.31}_{-0.07}$	$0.13^{+0.30}_{-0.05}$	$-0.35^{+0.22}_{-0.22}$
0.001	0.6	1.0	$2.20^{+0.10}_{-0.05}$	$0.075^{+0.096}_{-0.035}$	$-0.62^{+0.24}_{-0.24}$
0.001	0.6	1.5	$2.36^{+0.05}_{-0.06}$	$0.13^{+0.05}_{-0.005}$	$-0.46^{+0.10}_{-0.19}$
0.001	0.6	2.0	$2.36^{+0.05}_{-0.02}$	$0.081^{+0.052}_{-0.030}$	$-0.63^{+0.15}_{-0.16}$
0.001	1.0	0.5	$1.96^{+0.02}_{-0.01}$	$0.024^{+0.003}_{-0.005}$	$-0.88^{+0.77}_{-0.76}$
0.001	1.0	1.0	$2.21^{+0.34}_{-0.05}$	$0.11^{+0.06}_{-0.02}$	$-0.54^{+0.30}_{-0.31}$
0.001	1.0	1.5	$2.23^{+0.02}_{-0.02}$	$0.048^{+0.030}_{-0.022}$	$-0.86^{+0.49}_{-0.48}$
0.001	1.0	2.0	$2.32^{+0.14}_{-0.08}$	$0.071^{+0.15}_{-0.046}$	$-0.79^{+0.29}_{-0.30}$
0.001	1.4	0.5	$2.04^{+0.08}_{-0.03}$	$0.019^{+0.072}_{-0.009}$	$-0.89^{+0.68}_{-0.92}$
0.001	1.4	1.0	$2.17^{+0.01}_{-0.02}$	$0.010^{+0.012}_{-0.009}$	$-1.28^{+0.63}_{-0.64}$
0.001	1.4	1.5	$2.22^{+0.09}_{-0.09}$	$0.085^{+0.43}_{-0.005}$	$-1.44^{+1.22}_{-1.70}$
0.001	1.4	2.0	$2.34^{+1.43}_{-0.16}$	$0.057^{+0.051}_{-1.196}$	$-0.85^{+0.70}_{-0.72}$
0.002	0.6	0.5	$1.92^{+0.02}_{-0.02}$	$0.0011^{+0.001}_{-0.0005}$	$-2.1^{+0.3}_{-0.4}$
0.002	0.6	1.0	$2.17^{+0.14}_{-0.05}$	$0.077^{+0.133}_{-0.042}$	$-0.63^{+0.29}_{-0.29}$
0.002	0.6	1.5	$2.32^{+0.01}_{-0.01}$	$0.13^{+0.03}_{-0.01}$	$-0.52^{+0.71}_{-0.67}$
0.002	0.6	2.0	$2.39^{+0.14}_{-0.06}$	$0.11^{+0.13}_{-0.04}$	$-0.61^{+0.22}_{-0.22}$
0.002	1.0	0.5	$1.96^{+0.07}_{-0.02}$	$0.010^{+0.006}_{-0.003}$	$-1.19^{+0.59}_{-0.62}$
0.002	1.0	1.0	$2.11^{+0.03}_{-0.01}$	$0.006^{+0.002}_{-0.001}$	$-1.6^{+0.40}_{-0.40}$
0.002	1.0	1.5	$2.17^{+0.11}_{-0.04}$	$0.016^{+0.001}_{-0.0005}$	$-1.26^{+0.58}_{-0.59}$
0.002	1.0	2.0	$2.67^{+0.35}_{-0.14}$	$0.29^{+0.35}_{-0.12}$	$-0.43^{+0.19}_{-0.19}$
0.002	1.4	0.5	$1.92^{+0.05}_{-0.03}$	$0.015^{+0.035}_{-0.014}$	$-1.21^{+0.68}_{-0.69}$
0.002	1.4	1.0	$2.01^{+0.02}_{-0.01}$	$0.002^{+0.001}_{-0.004}$	$-1.75^{+0.76}_{-0.70}$
0.002	1.4	1.5	$2.46^{+1.21}_{-0.16}$	$0.21^{+0.92}_{-0.05}$	$-0.43^{+0.32}_{-0.30}$
0.002	1.4	2.0	$2.21^{+0.17}_{-0.06}$	$0.025^{+0.096}_{-0.018}$	$-1.04^{+0.45}_{-0.46}$

Variability properties

As shown in Section 5.2.2, the requirement that the shape of the power density spectrum be similar to the observed one fixes both the relation between the parameters D and p and the size of the largest active region. Furthermore, we have seen in the previous section how it is possible to use the Γ-luminosity correlation to put constarints on the coronal optical depth.

On the other hand, the absolute level of variability (variance), namely the normalization of the PDS, does not depend on $\tau_{\rm T}$, but it is fixed by D and C, and can be used to further constrain these two parameters.

The fractional rms, which correspond to the variance of the lightcurve divided by its mean, has been calculated for ten segments of a lightcurve of duration 3×10^4 s (and resolution of 60 s) and then averaged, for fixed $\tau_{\rm T} = 1.5$ and for different values of C and D. The fractional rms is shown in Table 5.2. It decreases with increasing covering fraction, as is expected, because in any shot-noise-like model the rms $\propto N^{-1/2}$, where N is the number of shots, which here is proportional to C. Also, the fractional rms decreases with increasing D. The reason for this is that long and short flares contribute differently to the total rms: large flares, being more luminous, contributes more. Smaller D implies a larger number of long flares, and therefore, for any given covering fraction, a larger variability.

The influence of the covering fraction on the PDS is shown in Figure 5.7, where we plot the average PDS of ten segments of lightcurve, each 3×10^4 seconds long, calculated for $D = 1$ and different values of the covering fraction.

We can compare these results with the 1999*ASCA* observation of MCG–6-30-15. For that observation, the fractional rms has been estimated to lie between 20% and 30% (Shih et al., 2001). Given the above mentioned degeneracy between the C and D parameters in determining the rms, such a value corresponds to a line in the $C - D$ plane that pass through our fiducial values $C = 0.001$ and $D = 1$, and extend towards the high-C, low-D direction and vice versa (for example the fractional rms is equal to 32% for $C = 0.01$ and $D = 0.4$, and to 28% for $C = 0.0001$ and $D = 3.0$). On the other hand, too high values of D, although consistent with the observed rms, gives unrealistic-looking lightcurves and PDS. Indeed, if D is too high, the number of large flares is drastically suppressed, and the break in the PDS moves to higher and higher frequencies, and can be undetectable. The corresponding lightcurve would resemble a white noise, with only very rare high luminosity flares. Therefore an upper limit on D (and a lower limit on the covering fraction) can be placed, based on simultaneous considerations about the shape and normalization (or rms level) of the PDS. For the 1999 long *ASCA* observation, these limits can be safely placed at $D < 1.5$ and $C > 0.0002$.

The variability-luminosity correlation

As already mentioned in the introduction, recent analysis of time variability properties of X-ray binaries and AGN (Uttley and McHardy, 2001) have highlighted an

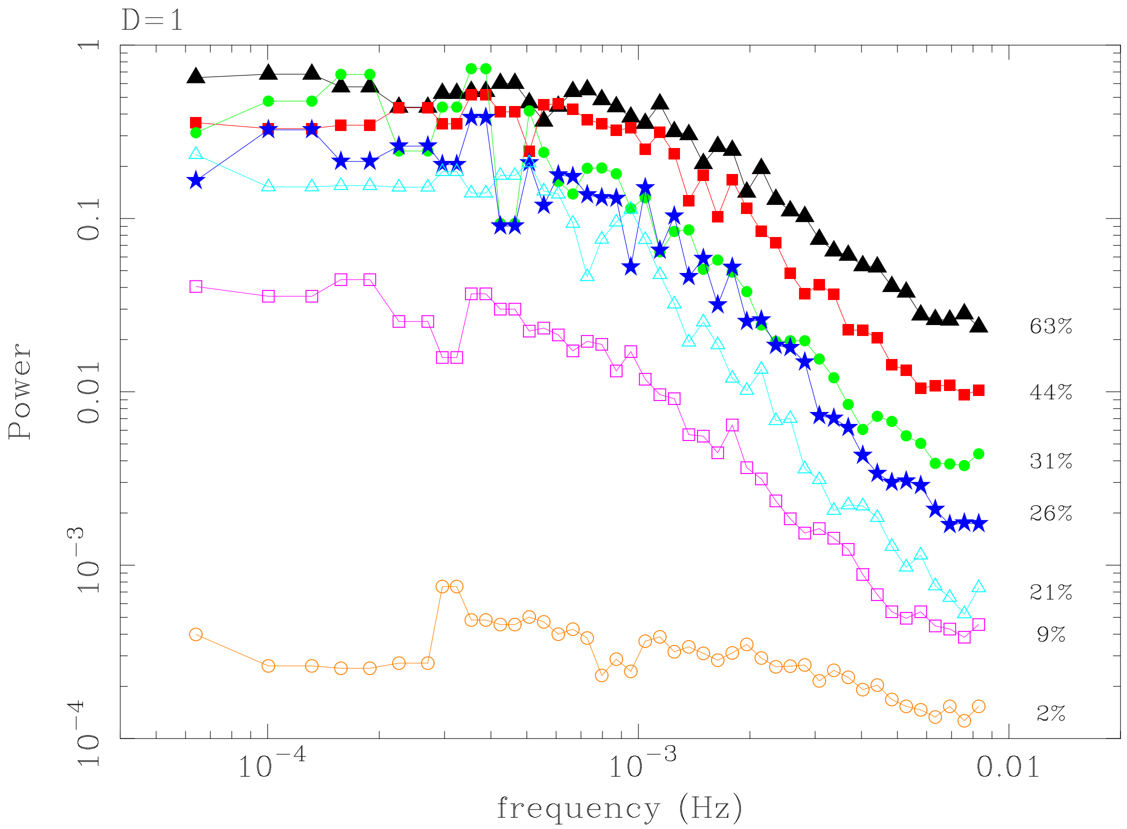

Figure 5.7: Average power density spectra of ten segments of a simulated lightcurve (each 3×10^4 seconds long), for fixed $\tau = 1.5$ and $D = 1$. From bottom to top the different curves correspond to $C = 0.03$ (orange, open circles), $C = 0.01$ (purple, open squares), $C = 0.005$ (cyan, open triangles), $C = 0.002$ (blue, filled stars), $C = 0.001$ (green, filled circles), $C = 0.0003$ (red, filled squares) and $C = 0.0001$ (black, filled triangles). On the right, close to each curve, the corresponding fractional rms is reported.

Table 5.2: Values of fractional rms, calculated from simulated lightcurves of duration 3×10^4 s, as a function of the covering fraction C and of the index D, with fixed $\tau = 1.5$.

C	D	rms (%)
0.0003	0.6	82
0.0005	0.6	61
0.001	0.6	46
0.002	0.6	39
0.005	0.6	29
0.0003	0.8	48
0.0005	0.8	54
0.001	0.8	44
0.002	0.8	33
0.005	0.8	24
0.0003	1.0	45
0.0005	1.0	43
0.001	1.0	31
0.002	1.0	26
0.005	1.0	21
0.0003	1.2	38
0.0005	1.2	24
0.001	1.2	25
0.002	1.2	19
0.005	1.2	15
0.0003	1.4	28
0.0005	1.4	27
0.001	1.4	21
0.002	1.4	17
0.005	1.4	13

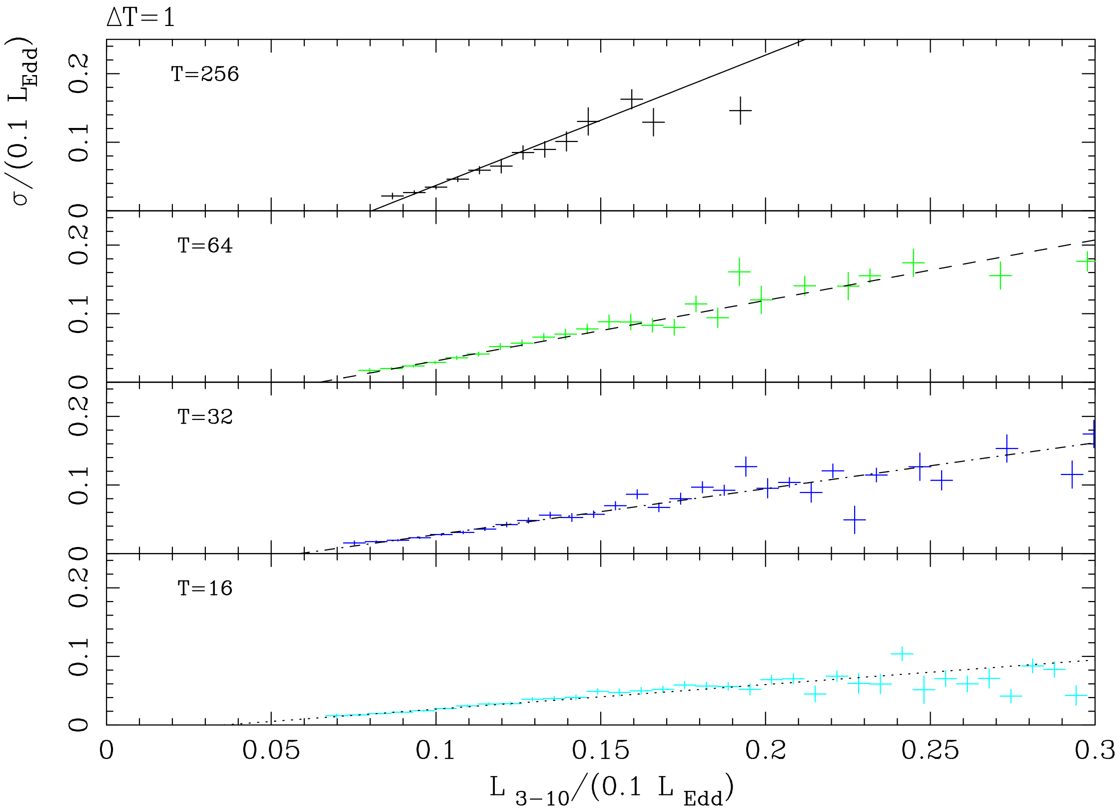

Figure 5.8: Luminosity dependence of the variance calculated for segments of a simulated lightcurve ($D = 1$, $C = 10^{-3}$ and $\tau_{\mathrm{T}} = 1.5$) with a fixed temporal resolution of 60 seconds. The duration of the different segments (in minutes) is written in each panel The fitting functions are of the form $\sigma = k(L_{3-10} - L_0)$, with k and L_0 constants.

intrinsic property of broadband noise variability in accreting compact objects, namely the strong linear correlation between RMS variability and flux.

We have analysed a simulated lightcurve in order to look for a similar correlation. With the parameters D and C fixed to the values of 1 and 0.001, respectively, we have produced a lightcurve of the total duration of about 3×10^6 s, with resolution of 1 minute.

Then, keeping fixed the time resolution, we calculated the mean $\mu = (1/N)\Sigma_i l_i$ and variance $\sigma = (1/(N-1))\Sigma_i (l - I - \mu)^2$ for segments of different length. The results, binned in luminosity intervals, are shown in Fig. 5.8, where the length of the segments T is measured in minutes. The variance corresponds to the integral of the PDS shown in Fig. 5.2.3 from frequencies $1/(T \times 60)$ to $1/60$ (Hz).

A clear correlation is evident in all cases, consistent with a linear one with an offset. We fitted a function of the form $\sigma = k(L_{3-10} - L_0)$, with k and L_0 constants. In Table 5.3 the values of the fitting parameters k and L_0 for the different durations considered are reported.

Finally, we have considered segments of fixed length (equal to 512 minutes) and calculated the variance with different time resolutions ΔT. This correspond to integrating the PDS of Fig. 5.2.3 from frequencies $1/(512 \times 60)$ to $1/(\Delta T \times 60)$ Hz. The

Table 5.3: Results from simulations and best fit parameters for the σ-luminosity relation for segments of different duration T (in minutes), with the same time resolution $\Delta T = 1$ minute. We fitted a function of the form $\sigma = k(L - L_0)$. Both σ and L are in units of a tenth of the Eddington luminosity. The thundercloud model parameters are fixed to $C = 0.001$, $D = 1$ and $\tau = 1.5$.

T (minutes)	k	L_0
16	1.90	0.079
32	0.88	0.064
64	0.67	0.058
256	0.35	0.034

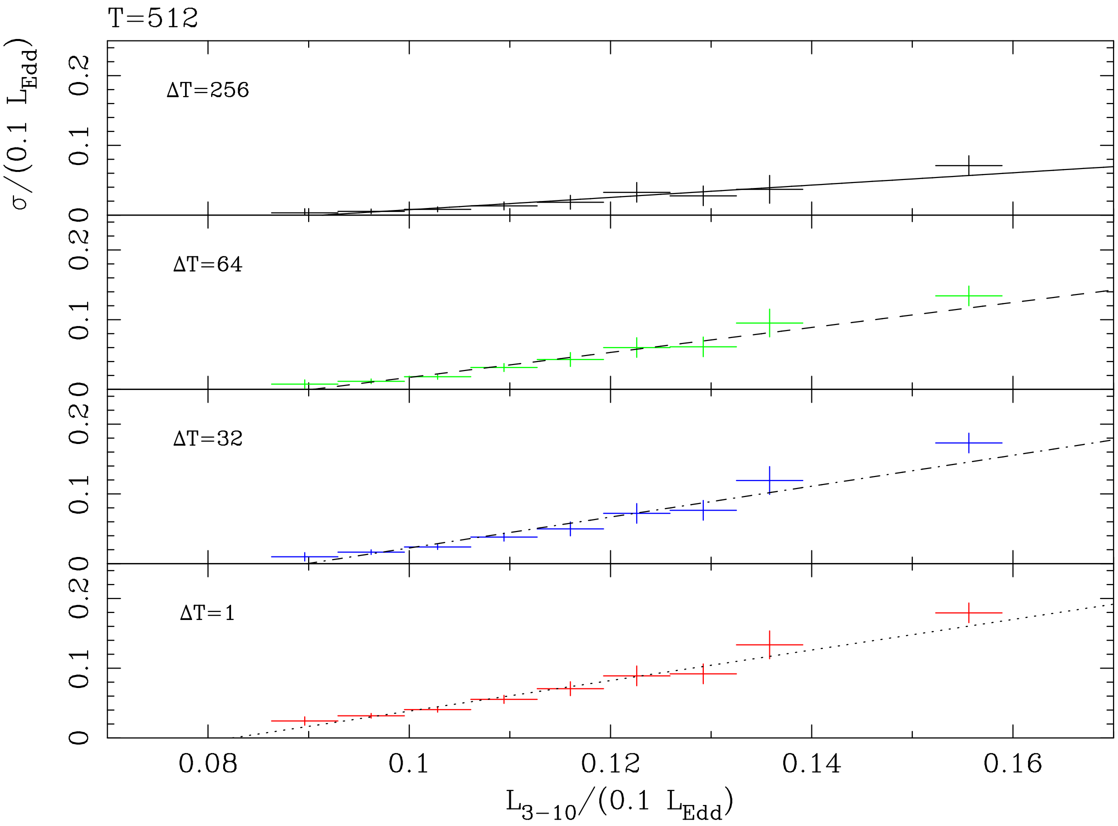

Figure 5.9: Luminosity dependence of the variance calculated for segments of a simulated lightcurve ($D = 1$, $C = 10^{-3}$ and $\tau_T = 1.5$) with a fixed duration (512 minutes). The time resolution of the different segments (in minutes) is written in each panel The fitting functions are of the form $\sigma = k(L_{3-10} - L_0)$, with k and L_0 constants.

results for these cases are shown in Fig. 5.9. Also in these cases, the linear plus constant fits are acceptable even at high ΔT. The fit parameters are listed in Tab. 5.4.

Uttley and McHardy (2001) argues that the correlation they found between the

Table 5.4: Results from simulations and best fit parameters for the σ-luminosity relation for segments of different time resolution ΔT (in minutes), with the same duration $T = 512$ minutes. We fitted a function of the form $\sigma = k(L - L_0)$. Both σ and L are in units of a tenth of the Eddington luminosity. The thundercloud model parameters are fixed to $C = 0.001$, $D = 1$ and $\tau = 1.5$.

ΔT (minutes)	k	L_0
256	0.88	0.092
64	1.79	0.089
32	2.21	0.090
16	2.19	0.090

variability and flux at all timescales, rules out any possible shot noise model, still, we are able to reproduce it within our thundercloud model, which a generalized shot noise model. One possible explanation for this lies in the way the lightcurve is 'randomized' (Timmer and Koenig, 1995). Once we have fixed the average covering fraction C and the distributions indexes D and p, the total expected number of active region expected at any time $N_{\rm tot}(t)$ is calculated, then the actual number $\mathcal{N}_{\rm tot}(t)$ is picked from a poissonian distribution that has $N_{\rm tot}(t)$ as its mean. Then, starting from the smallest flares, we calculate in similar fashion the number of active regions of every size in such a way as to ensure that the total number is exactely $\mathcal{N}_{\rm tot}(t)$. Therefore, random variations in $\mathcal{N}_{\rm tot}(t)$ (which correspond to random variations in the covering fraction C, as shown in Fig. 5.2) are transferred to flares of all sizes, and of all timescales, thus enforcing a correlation between the overall flux level and the amount of variability on all time-scales.

5.2.4 Discussion

Coronal scaleheight

In the above calculations we have kept fixed the value of the height of the flares above the accretion disc. In fact, as long as the main source of soft photons for Comptonization is the reprocessed radiation from the disc itself (as in the case of our fiducial model for which $c_{\rm r} > c_{\rm i} \gg c_s$, see Section 2.4), what matters for the spectral properties of the source is the ratio h_a/r_a of an active region height over its size. Then, in order for the model to accommodate spectral variations as large as those observed in many Seyfert 1 galaxies, we need $r_{\rm min} \ll h_a \ll r_{\rm max}$.

If the small-scale flux loops are generated by a self-sustaining magnetic dynamo operating inside the disc, it is natural to identify the size of the smallest active regions emerging from the disc, i.e. the micro-flares that trigger the larger avalanches, with the accretion disc thickness (Tout and Pringle, 1996; Galeev *et al.*, 1979; Nayakshin and

Kazanas, 2001). Thus, the observed spectral variability implies that the average elevation of a reconnection site is larger (and perhaps much larger) than the disc scaleheight, as firstly proposed by Di Matteo (1998).

It is interesting that full MHD simulations of magneto rotational instability in weakly magnetized accretion discs indeed show the formation of a strongly magnetized corona, considerably more extended in the vertical direction than the disc itself (Miller & Stone, 2000; see also discussion in section 2.5). Moreover, in the framework of a model similar to the one we present here, Di Matteo *et al.* (1999) studied observations of the GBH GX 339-4 in different spectral states to place limits on the model parameters, and in particular on the flare height. They conclude that the X-ray emission from galactic black holes in their *hard* state is more likely a result of inverse Compton scattering of soft photons in hot magnetic flares triggered high above the accretion disc.

The analytic treatment of Svensson and Zdziarski (1994) of the accretion disc–corona system allows us to give an estimate of the ratio of the coronal to disc scaleheight in the inner, radiation pressure dominated, part of the disc. From such a calculation, we can conclude that indeed, given the observed coronal temperatures, whenever most of the accretion power is released in the corona (say, $f_{\rm H} \gtrsim 0.7$), the corona is much more extended in the vertical direction than the underlying disc. We have

$$\begin{aligned} \frac{H_{\rm c}}{H_{\rm d}} &= \left(\frac{m_{\rm e}}{m_{\rm p}}\right)^{1/2} \frac{4}{9} \varpi^{3/2} \Theta^{1/2} \dot{m}^{-1} J(\varpi)^{-1} (1-f_{\rm H})^{-1} \\ &\gtrsim 16 \left(\frac{\Theta}{0.1}\right)^{1/2} \left(\frac{\dot{m}}{0.1}\right)^{-1} \left(\frac{(1-f_{\rm H})}{0.1}\right)^{-1}, \end{aligned} \tag{5.9}$$

where ϖ is the radial disc coordinate in units of Schwarzschild radii, $J(\varpi) = 1 - \sqrt{3/\varpi}$, and the last inequality is obtained taking the minimum of $\varpi^{3/2}/J(\varpi)$.

In the case of a structured corona the situation ought to be more complicated: if the flux tubes emerging from the disc carry a magnetic field with strength comparable to the equipartition with the internal disc pressure, they will tend to expand (reducing the strength of the magnetic field) in the less pressurized coronal atmosphere (Parker, 1979, §8.4). However, if the flux tubes are twisted, as is likely to be the case if they are anchored in the differentially rotating disc underneath, their sideways expansion is counterbalanced by the generation inside the flux tube itself of an azimuthal field component, with a net increase of its total magnetic energy content. The flux rope will rise buoyantly (Parker, 1979, §9.1, 9.6), keeping a much lower aspect ratio (defined as the ratio of the loop length over its diameter). To conclude, given the major uncertainties on the magnetic flux tube dynamics in the disc-corona interface, we believe that it is not unlikely for the height of the magnetic flares in the corona to be much larger than the disc thickness[4], as envisaged in our model, and, indeed, needed to explain the large observed spectral variability.

[4]As a final remark, we note that a puzzling characteristic of solar coronal loops, so often invoked in analogy with accretion disc coronal ones, is their tendency to have a nearly uniform thickness, instead of being substantially wider at their tops than at their foot-points, as expected from a straightforward application of the force-free assumption (Klimchuk *et al.*, 2000).

The magnetic field

Within the framework of active coronal models for the hard X-ray emission of black hole accretion flows, the exact nature of the heating process remains the most elusive issue. Here, as throughout most of this thesis, we have assumed that the magnetic field is the main repository of the energy in the corona and that the active regions are heated by the dissipation of such energy, probably via magnetic reconnection.

Although there is a growing consensus on the dynamical importance of magnetic fields in accretion discs, mainly driven by recent progresses in numerical MHD simulation of accretion flows and magneto–rotational instability, the detailed topology of the magnetic field is far beyond the reach of our current theoretical understanding. The solar analogy has provided theorists with ideas and inspiration, if not with quantitative insight, but it is wise to bear in mind that although we are able to actually image magnetic structures in our nearest star, even the heating of the solar corona is still not well understood.

With these *caveats* in mind, we discuss here some of the implications of our stochastic model for the accretion disc corona on the strength of the magnetic field and on the heating mechanism.

The ratio of magnetic to thermal energy in an active region is given by

$$\begin{aligned} E_{\rm mag}/E_{\rm th} &\simeq \frac{\epsilon_{\rm M} c_1 r^D \dot{m} f_{\rm H} L_{\rm Edd} t_0 \sigma_{\rm T}}{\pi \tau_{\rm T} R^2 k T_{\rm e}} \\ &\sim 5\times 10^3 \frac{\epsilon_{\rm M}\dot{m} f_{\rm H} b}{\tau_{\rm T}\Theta} c_1 r^{D-1}. \end{aligned} \tag{5.10}$$

For the standard set of physical parameters we have adopted, as long as the energy in the magnetic field is more than a few percent of the equipartition with the emitted radiation field, we have $E_{\rm mag} \sim 10^2 r^{D-1} E_{\rm th}$ and the active regions are indeed magnetically dominated. In fact, the magnetic field intensity can be estimated as

$$B \simeq 1.6\times 10^7 \tau^{1/2} r^{(D-1.5)} \left(\frac{m}{10}\right)^{-1/2} \left(\frac{b}{30}\right)^{1/2} \;\mathrm{G}. \tag{5.11}$$

Furthermore, from the above equation we have $v_{\rm A}/c \simeq 0.03 r^{D-1} b^{1/2}$. It is evident that the slow Sweet-Parker reconnection model is not compatible with the above scenario, because it would lead to too large a magnetic field accumulated in the corona. Our adopted value of the parameter b, is instead more appropriate for a relatively fast reconnection, as in the Petschek-type model. This translates into $v_{\rm A}/c \simeq 0.1 r^{2(D-1)/3} (\ln R_{\rm m})^{1/3}$. In principle, the value of the ratio $b = c/v_{\rm diss}$ could be inferred from temporal studies, if the physical characteristic size of an emitting region was known independently, as its value affects primarily the timescale of the individual flares.

To conclude, as already discussed in section 2.4, we would like to remark on the fact that synchrotron radiation is hardly important as source of seed photons for Comptonization in AGN, but for the hardest, compact short lived flares. However, direct synchrotron light at frequencies near the self-absorption cut-off could be observed in sources where the direct emission from the accretion disc is strongly suppressed (as may be the case of LLAGN, see §2.5 or of the X-ray binary XTE J1118+480, see §6).

Iron line variability

The X-ray spectra of accreting black holes, and those of Seyfert 1s in particular, often show a clear sign of reflected radiation in the form of a prominent fluorescent iron Kα line. This spectral component is sensitive to the geometry of the disc–corona system and can be then used to place more firm constraints on it (§3). Often such lines are Doppler and gravitationally broadened, suggesting that the cold material within which they are produced is moving at relativistic speeds in the deep potential well of the central black hole (Fabian *et al.*, 2000). In the standard picture in which the reflection features are produced by the accretion disc illuminated by the hard X-rays coming from the active regions, the strong observed continuum variability should drive the line variability with a short time-lag.

This simple picture, though, is challenged by the observations, which seem to indicate that, although the iron line does indeed vary with the varying flux, its flux is not correlated with the changes of the continuum intensity or of its slope (Vaughan and Edelson, 2001).

In the framework of the thundercloud model, such complicated behaviour can be explained by the fact that the observed line at any time is the super-position of different features produced by active regions illuminating the disc with different spectral shape and intensity. The ionization properties of the surface of the accretion disc, which in turn determine the line characteristics, are strongly dependent on the illuminating continuum properties (Nayakshin *et al.*, 2000a; Done and Nayakshin, 2001; Ballantyne *et al.*, 2001; Ballantyne and Ross, 2001). Therefore the observed iron line is expected to be complex, and variable on a wide range of timescales in a complicated way.

Furthermore, as the coronal optical depth becomes larger the reflection features are strongly suppressed by Compton scattering in the corona itself (Matt *et al.*, 1997), as illustrated in Chapter 3. This effect becomes more important the larger the active region. Analogously to what is discussed by Malzac *et al.* (2001), we define a geometrical parameter that determines the fraction of reflected luminosity that reenters an active region, $\mu_s = h_a/\sqrt{4r_a^2 + h_a^2}$. Then, we can quantify the effect of an obscuring thundercloud by estimating the iron Kα line luminosity produced by any given illuminating spectrum of an active region in the following way:

$$L_{K\alpha} = (L_{7-20}/2)a[\mu_s + (1-\mu_s)(1-P_{\rm sc}(\tau_{\rm T}))], \tag{5.12}$$

where $L_{7-20}/2$ is an estimate of the luminosity above the iron Kα edge emitted towards the disc and $P_{\rm sc}$ is the scattering probability in an active region (see section 2.4.2). A fraction μ_s of the reflected X-rays reaches the observed directly, while a fraction $(1-\mu_s)P_{\rm sc}$ suffers further Compton scattering in the corona and is therefore scattered

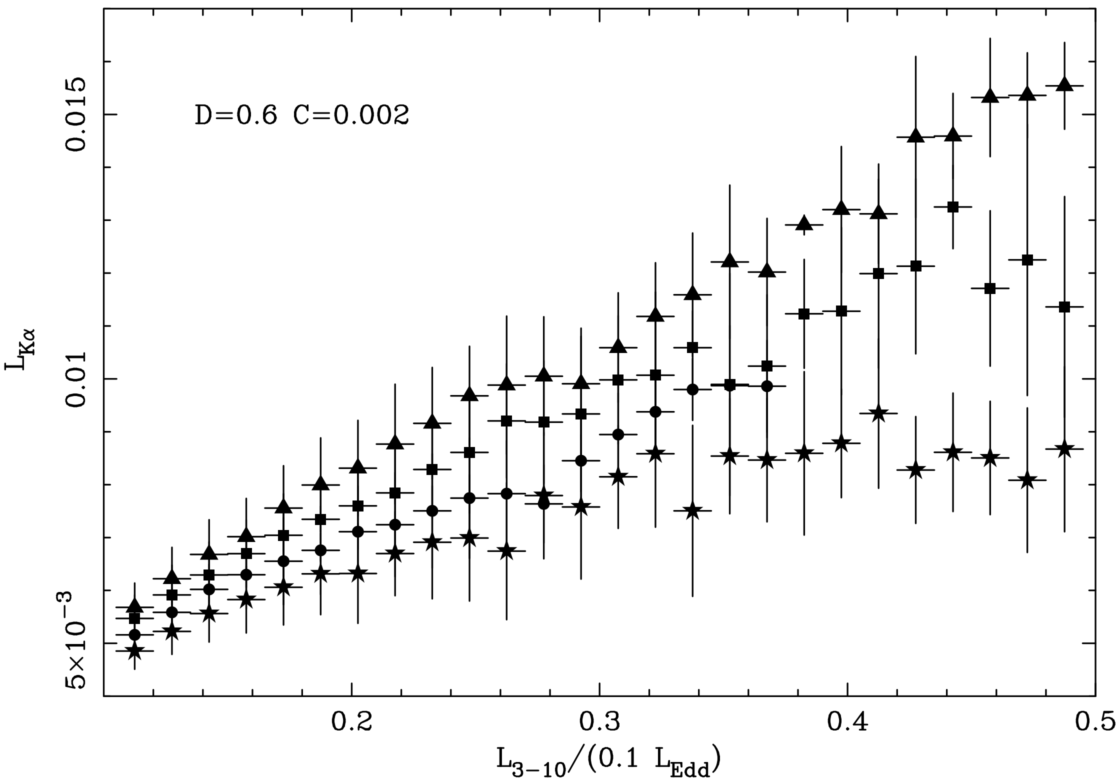

Figure 5.10: The estimated iron line luminosity, as calculated in Eq. (5.12) as a function of the observed flux in the 3-10 keV band (in units of $0.1L_{\rm Edd}$) for the simulation with $D = 0.6$ and $C = 0.002$. The points for all the time intervals have been grouped in luminosity bins and the average line flux has been calculated. The error bars correspond to the weighted statistical uncertainty. Triangles corresponds to $\tau_{\rm T} = 0.5$, squares to $\tau_{\rm T} = 1$, circles to $\tau_{\rm T} = 1.5$ and stars to $\tau_{\rm T} = 2$.

out of the line, reducing its absolute flux. We note here that the above expression may be in fact underestimating the amount of cloud obscuration because the optical depth $\tau_{\rm T}$ that enters in the determination of $P_{\rm sc}$ is the one calculated from the center of an active region and is smaller than that seen by the photons coming from the underlying disc.

In Figure 5.10 we show the estimated total Fe Kα line luminosity produced by all the simultaneous active regions for a thundercloud model simulation with $C = 0.001$ and $D = 1$, plotted as a function of the total observed 3-10 keV luminosity. Clearly, in the case of high coronal optical depth ($\tau_{\rm T} \gtrsim 1.5$), although still mildly correlated with the observed continuum at low luminosity (small flares and small timescales), the line variability is strongly suppressed at high luminosity (larger flares and longer timescales), to the extent that for a variation of a factor of three in the 3-10 keV flux, the line flux may increases only by about 50%.

In general, even for less dramatic cases, we expect the line equivalent width $W_{K\alpha}$ to decrease with the increasing flux. For example, in the simulation presented in Fig. 5.10, for $\tau = 1.5$, we have $W_{K\alpha} \sim 300$eV for $L_{3-10} \simeq 0.1$ and $W_{K\alpha} \sim 200$eV for $L_{3-10} \simeq 0.3$. Such an high value for the unattenuated iron line equivalent width (compared to the expected value of ~ 100 eV; George and Fabian, 1991) can be consistent with a static corona model if the iron is overabundant with respect to the solar value, as indeed has been shown to be required to explain the reflection features of MCG–6-30-15 (Lee *et al.*, 1999).

A full simulation of the temporal behaviour of the iron line, which is clearly beyond the scope of this work, will involve a full treatment of the ionization state of the accretion disc atmosphere below different active regions (with different illuminating spectra) *and* of the obscuring effects of the corona itself. Similarly, the effect of Comptonization in the corona on the shape and intensity of the reflection hump may reveal themselves in time-resolved spectral analysis of the hard X-ray emission, though this may prove a difficult task for the existing instruments capabilities.

5.2.5 Conclusions

In this section we have presented a model for spectral and temporal variability of the X-ray emission from accretion disc coronae around black holes. Thermal Comptonization has been assumed as the main radiation mechanism to produce the observed X-ray continuum. The cooling radiation comes either from the intrinsic dissipation of gravitational energy in the underlying accretion disc, or from the reprocessed radiation in the cold disc or from synchrotron radiation produced locally in the magnetically dominated corona. For the case of a typical AGN of $10^7 M_{\odot}$, accreting at ten percent of the Eddington ratio and for which most of the power is dissipated in the corona ($f_{\rm H} \gtrsim 0.7$), reprocessed radiation is usually the main source of soft photons but from the case of more compact and hot active regions, where the contribution from synchrotron radiation is important. Nonetheless, the magnetic field in the corona acts as the main energy reservoir and dominates the local energy budget.

The basics geometric properties of the coronal flow assumed in our model and, we believe, required to explain the observed spectral and temporal variability of AGN are the following:

- The corona must not be uniform, but structured and heated intermittently (see section 2.3);
- The fundamental heating event, a flare likely caused by magnetic reconnection, must be compact, with typical size comparable to the accretion disc thickness;
- The height of the reconnection site must be at least an order of magnitude larger than its size;
- The spatial and temporal distribution of the flares are not random, but proceed in correlated trains of events in an avalanche fashion;
- The size of the avalanches determines the size of the active regions and their luminosity, and is distributed as a power-law.

We have simulated X-ray lightcurves of AGN and studied the correlation between the photon index and the X-ray luminosity. By comparing our simulations with observation of the best studied Seyfert 1 galaxy MGC–6-30-15 we conclude that the model is able to reproduce the observed Γ-luminosity correlation and to put some constraints on the model parameter. In particular, to explain the trend observed in the 1997 *RXTE* observations analysed by Vaughan and Edelson (2001) and in the 1999 *ASCA* observation analysed by Shih et al. (2001), we need a fairly high coronal optical depth ($\tau_{\rm T} \gtrsim 1.5$), a small *average* covering fraction ($\sim 10^{-3}$) and a scaling index for the active region luminosity $D \sim 1$. Furthermore our model naturally explains the linear correlation between luminosity and rms variability (at different epochs in the same source), recently discovered by Uttley and McHardy (2001) in a number of accretion-powered compact objects.

The thundercloud model does not include other important geometrical or dynamical parameters that may vary on timescales much longer than that over which the corona is heated (which is close to the dynamical one) and may indeed be relevant to determine the average long-term spectral properties of these sources. In fact, our model does not reproduce the observed correlation between the spectral index and the reflection features (Zdziarski *et al.*, 1999; Lubiński and Zdziarski, 2001). Indeed, no 'static' corona does, as demonstrated by Malzac *et al.* (2001). If the corona instead is in stable relativistic bulk motion (i.e. is the base of a jet/outflow), and the outflow velocity changes with time, or from source to source, then we do expect the average spectral index to correlate with the amount of reflection (Beloborodov, 1999; Malzac *et al.*, 2001), as observed. Then our model would be applicable as it is only to the sources with the softest spectra (and indeed the spectral parameters of MCG–6-30-15 correspond to negligible bulk coronal velocity in the model of Beloborodov, 1999a).

On the other hand, such a correlation has not yet been proved to hold on the short timescales we focused our attention on. The short-time variability should bear information on some fundamental properties of any accreting system in which an optically thick and geometrically thin disc coexist with a hot comptonizing medium heated by dissipation of a structured magnetic field. A dynamic corona, where the reconnection sites moves with relativistic velocities and generate an outflow whose global properties evolve on timescales much longer than the dynamical one (see Section 2.5), is a straightforward generalization of the thundercloud model we have presented here, and should be consider in order to better constrain the geometry and dynamics of the inner accretion flow around black holes.

Thus, detailed analysis of time-averaged spectra will help determining the value of the parameter that is ultimately responsible for the long-term variability and therefore for the Γ-R correlation (such as the bulk outflow velocity, for example), while spectral and temporal variability on short timescales will ultimately probe the physics of coronal heating and magnetic reconnection, providing a test for the model we have illustrated in this section.

5.3 Quiescent times in gamma-ray bursts

5.3.1 Introduction

In this final section of the chapter, we leave the study of active galactic nuclei and galactic black hole candidates, and we move to the very different subject of γ-ray bursts (GRBs). Although the very nature of the astrophysical objects that are responsible for GRBs is still far from clear, nevertheless the temporal analysis we present here is intimately related to the broader subject we dealt with at length in this chapter, as it involves a model of γ-ray bursters as stellar mass black holes accreting, at super-Eddington rates, matter at nuclear density, likely in the form of an accretion disc or torus. The stochastic variability associated with turbulent accretion flows, that we have invoked to explain the X-ray lightcurve of Seyfert 1 galaxies, should manifest itself also in the very high energy lightcurves of GRBs.

The study of γ-ray bursts has undergone a revolution since the the first fading sources at X-ray (Costa *et al.*, 1997), optical (van Paradijs *et al.*, 1997) and radio (Frail *et al.*, 1997) wavelengths were discovered, making them the most powerful photon-emitters known in the Universe. Although much attention has been devoted to the late afterglow emission since then, the prompt γ-ray emission still has to be understood. Many issues remain unsolved, regarding the nature of the central engine, the different scenarios giving rise to this prompt emission, and the radiation mechanisms.

The data collected by the *Burst and Transient Source Experiment*, *BATSE*, have provided us with a great wealth of information, especially about rapid time variability in the γ-ray lightcurve. Nonetheless, gamma-ray bursts are so complicated and diverse in the time domain that, at first sight, their behaviour obeys no simple rule.

One of the main issues that has remained largely unexplained is what determines the characteristic durations of the bursts, that typically range between 10^{-2} and 10^3 seconds[5]. Observationally (Kouveliotou *et al.*, 1993) the short ($\lesssim 2s$) and long ($\gtrsim 2s$) bursts appear to represent two distinct subclasses. While numerical simulations have shown that Neutron Star-Neutron Star (NS-NS) coalescence could only explain the very short class of bursts, there is a growing consensus that the long bursts might be produced by the collapse of a massive star (*collapsars*), that at some stage during the disruptive event evolve into a configuration composed by a black hole and an accretion disc/torus around it (Woosley, 1993; Paczynski, 1998; MacFadyen and Woosley, 1999).

One striking feature of the observed gamma-ray burst light-curves is their enormous diversity. Beside the well established bimodality of durations (Kouveliotou *et al.*, 1993), they seem to obey no rule. Bursts have been observed with very complex and irregular light-curves, made of many different pulses, or with a single, smooth pulse, or even with mixed in-between properties. On the other hand, when observed in the Fourier domain, long bursts exhibit a simple behaviour: their average PDS is a power-

[5]The definition of the burst duration is not unique. The *BATSE* team characterizes it using T_{90} (T_{50}): the time needed to accumulate from 5% to 95% (from 25% to 75%) of the counts in the 50-300 keV band (Meegan *et al.*, 1996). For the purpose of our analysis, we used T_{90} as a measure of burst duration.

law, with the slope of the Kolmogorov law for homogeneous turbulence ($\alpha \sim -5/3$) and with superimposed standard statistical fluctuation Beloborodov *et al.* (2000).

Here we focus our attention on another striking property of long burst light-curves, namely their extremely large amplitude variation, such that different emission episodes in the same burst may appear separated by intervals during which the count-rate in the gamma-ray band drops to the background level. The very existence of such quiescent times in GRB light-curves poses severe restrictions on any emission model: it is well known, for example, that in the external shock scenario it is almost impossible to reproduce this property, as it would require the presence in the interstellar medium of coherent structures as large as 10^{16} cm (Fenimore and Ramirez-Ruiz, 1999).

5.3.2 Observational results: a new correlation between the duration of different emission episodes

In an earlier report, Koshut *et al.* (1995) found that about 3% of bursts show signs of *precursor* activity, with a peak intensity lower than the main burst, separated from the remaining emission by a background interval that is at least as long as the rest of the burst. *BATSE* burst 2156, shown in the upper panel of Figure 5.11, falls into this category. However, the above definition singles out a data set with rather extreme properties. Several time profiles show periods of quiescence without having precursor activity. See, as an example, BATSE burst 3067, which is shown in the lower panel of Fig. 5.11. For this reason, in order to study the periods of quiet emission, we adopted more general selection criteria. Here, we allowed multiple pairs of successive events separated by a quiescent time within a single burst and we did not impose requirements on the relative intensities or on the time interval separating any two emission episodes. The periods of emission occurring before and after the quiescent time are therefore referred to as *prequiet* and *afterquiet* time, respectively.

For the purpose of our analysis, we have used all 94 bursts from the 4B *BATSE* catalog longer than 5s ($T_{90} > 5s$) and brighter than 5 photons^{-1} cm^{-2} (*BATSE* peak photon flux in the 256 ms time-scale). We have used the *BATSE* 64 ms four-channel data (i.e., from 25 to $\sim$ 800 keV). A background model was created for each energy channel by fitting user-defined background intervals with a second-degree polynomial and interpolating this fit across the source interval. We subtracted the background model from the observed count rates in each energy channel. This then gave us the total source count rates as a function of time. In order to be selected, a burst must have at least one quiescent period in its time history. The selection was accomplished by calculating the total number of counts, over the entire energy range, recorded in a temporal window sliding along the time axis. The width of the window was set to 5% of the duration of the burst. Thus, the width of the window varied from burst to burst, allowing us to avoid bias against quiescent times with duration less than some arbitrary window width. We define a drop to the background level whenever the number of net counts in a window is smaller than the 2σ level in the corresponding background counts.

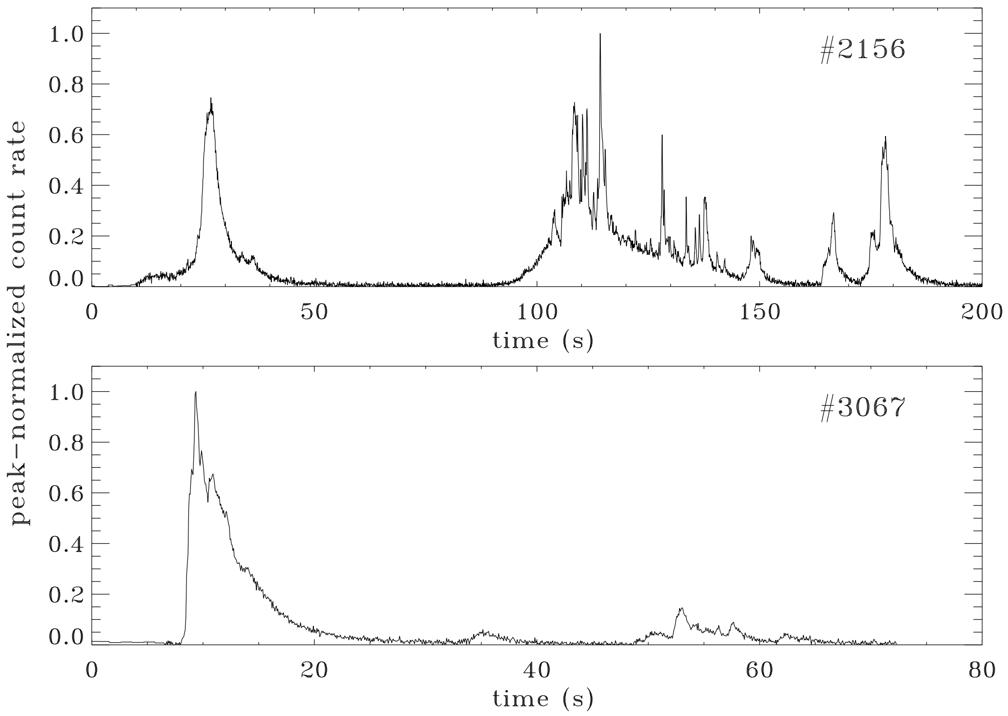

Figure 5.11: Time profiles observed with BATSE (at energies > 20keV) that contain periods of quiet emission. Upper panel: BATSE burst #2156 have a very strong main burst after a long quiet emission period. Lower panel: BATSE burst #3067 have a very strong main burst before the count rate drops to the background level.

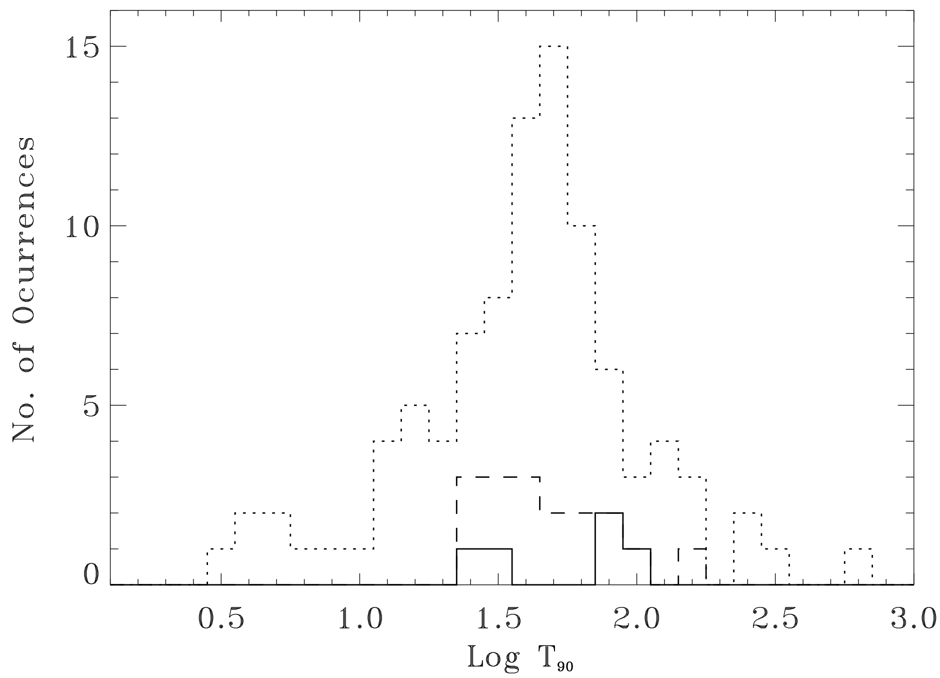

Figure 5.12: Distribution of GRB durations. The dotted line is the distribution of all bright bursts that were longer than 5s and brighter than 5 photons^{-1} cm^{-2}, the dashed one represents the bursts which show at least one quiescent time and the solid one the bursts with more than one quiescent interval.

We have used this absolute test, rather than a relative limit (e.g., a fixed fraction of the highest number of counts in any given window), to try to avoid the possibility of the existence of source emission below our detection level, during any time interval in any burst.

We found that $\sim 15\%$ of the analysed long and bright bursts contain at least one quiescent interval in their time history (of duration $\gtrsim 0.05 T_{90}$) and $\sim 25\%$ of these have more than one. Figure 5.12 illustrates the distribution of durations for, respectively, all bursts in the sample (dotted line), the subset of those that contain at least one quiescent period (dashed line), and the bursts with two or more quiet emission intervals (solid line).

Fig. 5.12 shows that the distribution of durations for the subset of bursts that contained quiet emission periods is consistent with the sample distribution. We find no significant evidence that the presence of quiescent times is preferentially found in longer or shorter bursts within our sample. Some limitations are necessarily inherent in our approach and data selection: the conclusions we reach are based on measurements of a subset of the bursts detected with *BATSE*; we analyse relatively bright bursts with durations greater than ~ 5 s, recorded with 64 ms temporal resolution and four channel spectral resolution. Analysis of quiescent times in shorter bursts will be more difficult due to the fact that few short bursts are brighter than 5 photons^{-1} cm^{-2}. The selection of a high brightness sample is appropriate in order to avoid the systematic effects that might change the observed time histories with different statistics. The time histories of dim events would be more randomized by fluctuations than the time histories of bright bursts. Using other GRB samples with a high signal to noise level ($\gtrsim 3$ photons^{-1} cm^{-2}) gives similar results.

We have searched for correlations between the temporal properties of the different emission periods. Any correlation will provide strong constraints on various burst models. In particular, we have investigated the dependence of the duration of the quiescence period on the duration of the following (*afterquiet*) and the preceding (*prequiet*) emission episodes. It is worth stressing that, by comparing time intervals within each burst, we eliminate the distance dependence (or time dilation effects) that would arise if we compared, for example, total number of counts of an emission episode with the duration of the quiescence period. We find no evidence for a correlation between quiescent times and prequiet burst times, as seen in Figure 5.13a. However, a strong one-to-one correspondence seems to exist between quiescent times and afterquiet burst durations, at about 4σ confidence level ($r_s \sim 0.89$). Stated otherwise, we found that, in our time histories sample, the longer the quiescent time the longer the duration of the following emission period, as shown in Figure 5.13b.

The existence of a correlation between the duration of the quiescent time and the *total energy* of the afterquiet burst would of course reveal very interesting properties of GRB sources. However, to characterize the total energy of a burst, we would need information about the distance of the event[6]. Without this information, looking for any correlation between the total number of counts (and hence energy) of the afterquiet emission and the duration of the quiet period in different events will be misleading.

Nonetheless, one could expect a correlation between the duration of an emission episode and the total energy radiated. If this is the case, the correlation between times we found should simply reflect a correlation between the burst strength and the time elapsed since the previous emission episode.

5.3.3 Discussion

All the bursts analysed here are long and structured. Clearly in these cases the central engine has to be active for a period extremely long compared to the typical dynamical time-scale ($\sim$ milliseconds) for stellar-mass compact objects. Thus, the central engine has to evolve into a configuration which is stable enough to survive the violent gravitational instabilities associated with the merging/collapse of compact objects, while

[6] At the moment, there is only one *BATSE* event (7560) with periods of quiet emission in its light-curve and for which a redshift measurement has been done (GRB 990510).

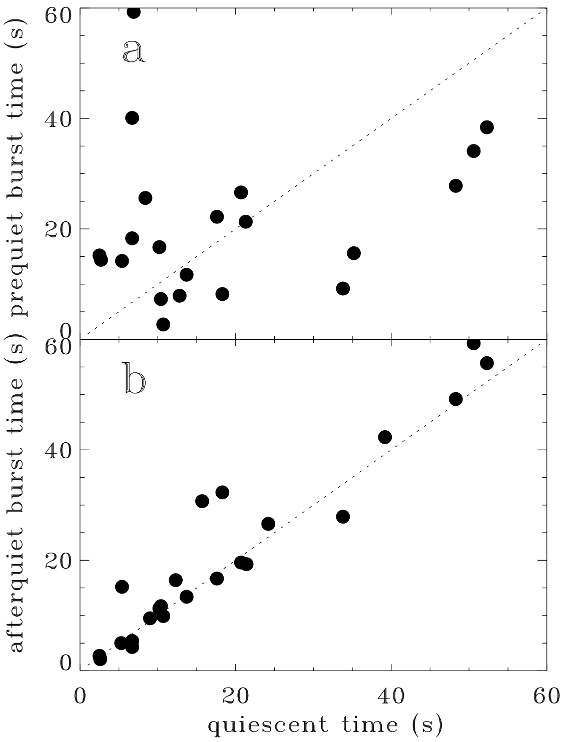

Figure 5.13: Correlations between the temporal properties of the different emission periods. In panel (a) we plot the duration of an emission episode (*prequiet burst time*) against the duration of the following quiescent time. No clear correlation is found in this case. In panel (b) we plot the duration of an emission episode (*afterquiet burst time*) against the duration of the previous quiescent time. There is a clear trend: the longer the quiescent time, the longer the duration of the following emission period.

still keeping enough binding energy to power the burst. A thick torus (or an advective, optically thick accretion disk) accreting at a rate of 0.01 to 10 $M_{\odot}\mathrm{yr}^{-1}$ (Popham *et al.*, 1999, hereafter PWF), is a key ingredient for achieving this. The system also needs to be highly unstable to produce the extremely varied light curves we observe (Stern, 1999), and this requirement is even stronger for the bursts exhibiting quiescent times.

Of the two more popular mechanisms that have been proposed to explain the GRBs energy release (neutrino annihilation and conversion of Poynting flux into a magnetized wind), the first seems unable to produce the longer, more energetic and variable bursts (Popham *et al.*, 1999; Rees, 1999). As PWF have shown, the efficiency of such a process is highly variable and extremely sensitive to the accretion rate: higher accretion rates lead to higher efficiencies. They conclude that neutrino annihilation in hyper-accreting black hole systems can explain bursts of isotropic equivalent energy up to 10^{52}ergs.

The other popular scenario, the conversion of Poynting flux into a magnetized wind, requires, in order to liberate the observed amount of energy, a magnetic field $\gtrsim 10^{15}$ G (Rees, 1999, and references therein). Such a high field is not unphysical. First, because it is about two orders of magnitude smaller than the virial limit; second, because it has possibly been observed in some peculiar neutron stars (the so called *magnetars*; see e.g. Duncan and Thompson, 1992; Kouveliotou *et al.*, 1998, and references therein).

A neutron torus, with its huge amount of differential rotation, is a natural site for the onset of a dynamo process that winds up the field to the required intensity (Kluźniak and Ruderman, 1998), provided that a fluid element is able to complete a sufficient number of orbits around the hole. This number, in turn, depends on the viscosity inside the disk, $N \sim \alpha_{\rm v}^{-1}$, where $\alpha_{\rm v}$ is the standard Shakura-Sunyaev viscosity.

The actual properties of the expected variability depend on the details of the configuration of the disc corona generated by the magnetic field, which is removed from the disc interior via turbulent flux buoyancy Araya-Gòchez (1999). This is a very complicated (and almost unaddressed; but see Tout & Pringle, 1996) issue, on which some insight can come from observations such as the one we present here.

In order to extract as much information as possible from the correlation we found, and to gain more insight into the dynamics of GRB central sources, we need first to understand the physical processes responsible for the production of quiescent times. The fundamental issue to tackle is whether the gaps in the γ-ray light-curves are produced by a turning-off central engine or by a structure in the relativistic outflow velocity space, due possibly to its interactions with the ambient medium it propagates into. In the former case, the flow will be discretised in a number of thick shells, each one of size roughly comparable to the duration of the emission episodes observed at the detector. In the latter, instead, the flow could be regarded as a single shell whose thickness is related to the total burst duration.

Let us consider first the former scenario. If the gaps reflect a period of inactivity of the central source, the correlation hints at the following general scenario.

The system builds up its energy (via an MHD instability driven dynamo, for example) and reaches a near critical, or *meta-stable* state. Any local instability can, by definition, cause a rapid dissipation of all the stored energy through an avalanche of dissipation events analogous to the one responsible for the stochastic variability in GBHC and AGN (see §5.2). The system will tend to return to a more stable configuration, characterized by a certain threshold energy E_0, or a sub-critical coronal magnetic field configuration. The source then becomes quiescent. If the lifetime of the accreting torus is long enough, and depending on the rate at which the energy is actually extracted from the disc (or from the black hole) and deposited into the external magnetic field, the system can undergo another episode of strong emission. As we can assume E_0 to be fixed by the geometry and by the physical parameters of the black hole–accretion disc system, the longer the quiescent time, the higher will be the stored energy above the threshold available for the next episode. Such a situation will give rise to the observed correlation[7].

It is also important to note that the threshold energy E_0 above which the system is in a meta-stable state is not directly related to the intensity of the seed magnetic field inside the neutron torus. It is instead most likely related to the intensity and the topological configuration of the amplified field which emerges from the torus.

Finally, we would like to point out the suggestive analogy with the microquasar GRS 1915+105, a galactic black hole candidate which exhibits a strikingly similar (even quantitatively) correlation between the duration of a quiescent time and that of the following burst (Belloni *et al.*, 1997a). This source is believed to accrete at a rate very close to (or maybe higher than) the Eddington limit, which is also the case for the configuration suggested for gamma-ray bursters discussed above.

We do not speculate further on the physical nature of such meta-stable configuration, and on the alternative possibility that it be associated to the complex interaction of the relativistic jet that powers the burst with its environment (particularly for the Super/Hyper/Supra-nova scenarios; see e.g. Ghisellini *et al.*, 2000). Instead, in order to explore the alternative possibility that the quiescent episodes in the γ-ray lightcurves are *not* produced by an intermittent central engine, but by a modulation of the relativistic outflow, we studied in a recent work (Ramirez-Ruiz *et al.*, 2001) various different mechanisms that can give rise to the observed quiescent times in the framework of the internal shocks model for GRB (Rees and Meszaros, 1994), trying to assess their relative likelihood. The conclusion that can be drawn from such a study are the following:

- Internal shocks can produce significantly long periods of quiescence with an opportune modulation of a continuous relativistic wind: for example, when the wind ejecta have a constant (or progressively decreasing) Lorentz factor for a long enough time, the relativistic shells will not catch up with each other and the emission from the internal shocks may be delayed or shifted to lower energy bands.

[7]We stress that this is the opposite to what expected from a relaxation oscillator, in which the accumulation time depends on the amount of energy previously dissipated. This produces a correlation between the quiescent time and the duration of the *previous* emission episode (as, e.g., in the case of the Rapid Burster Lewin *et al.*, 1976) that is clearly ruled out by the observations.

- Consequently, a measurement in a single energy channel is inadequate for the correct identification of a complete turn-off of the central engine.

How is it possible to discriminate between a central engine turning-off and a continuous, modulated outflow?

First of all, we stress the importance of simultaneous, high temporal resolution multiwavelength observations of GRBs. In particular, cross-correlating X/γ-rays light-curves will probe the velocity structure of the relativistic outflow responsible for the internal shocks (Ramirez-Ruiz *et al.*, 2001). The newly launched *HETE-2* satellite, with its large bandwidth (from $\sim$1 to 400 keV) and high temporal resolution (of the order of a millisecond) is the ideal instrument to accomplish this task.

Furthermore, we suggest that the prompt afterglow emission from the reverse shock, that strongly depends on the wind dynamics (Sari and Piran, 1999), is best suited to discriminate between these cases. In particular, the time delay of the prompt afterglow peak with respect to the main γ-ray event, will be much shorter in the case of a discontinuous wind. Thus, a very rapid optical follow-up of the long bursts exhibiting periods of quiescence would be crucial to distinguish between the two possibilities. This will help us to extract physical informations from the observed correlation and give us a hint of the properties of the central engine.

5.4 Summary and conclusions

This chapter has been devoted to the discussion of different aspects of the aperiodic time variability in sources powered by accretion onto a central black hole. In Section 5.2 a model (the 'thundercloud model') for the temporal and spectral short-time variability produced by a structured magnetic corona has been presented. The model explains the correlations between X-ray flux and spectral slope and between X-ray-flux and rms variability, observed in a number of Seyfert galaxies and galactic black hole candidates on timescales comparable to the dynamical one. It represents an attempt to bridge together the pieces of information on the inner accretion flow, and in particular on the geometry and physical state of the hot comptonizing component of the flow (the corona), provided separately by spectral and temporal analysis. We have neglected in our discussion the role of the quasi-periodic variability in accreting black holes, that, especially in the case of GBHC, could indeed provide us with valuable clues on the nature of the accretion flow in its innermost part. Nonetheless, the analysis of the broad band variability component (noise) of the observed power density spectra of such sources, and in particular of the spectral variability on the very short timescales that we can probe with the X-ray emission of AGN, has allowed us to put new constraints on the geometry (in particular on the typical height of a coronal active region and on the total average covering fraction), optical depth, and temperature of the corona for the case of one of the best studied Seyfert 1 galaxies, MCG–6-30-15.

The final section of the chapter (§5.3), instead, dealt with a new discovery regarding the aperiodic time variability of γ-ray bursts, namely a correlation between the duration of the periods of quiescence, sometimes found in long bursts, and the duration of the following emission episodes. Although our theoretical understanding of the central engines of GRBs is still far from complete, we have discussed here how our findings could be used to discover and elaborate new paradigms for the emission mechanisms of γ-ray bursts, in the framework of models that envisage a stellar mass black hole accreting at very high rates from a nuclear torus as the power-house of GRBs. Indeed, we argue that the wealth of information contained in the complicated temporal structure of the longer bursts bear many analogies with that contained in the lightcurve of 'standard' accreting black holes. Such information could be used to probe the accretion flow itself, the viscous mechanisms by which the angular momentum is transported outwards, the magnetic field involved in this process and the energetics of the corona produced by the flow.

Chapter 6

The case of the X-ray transient XTE J1118+480

6.1 Introduction: a key object in the X-ray sky

In this final chapter we apply many of the considerations presented throughout this thesis on the nature of accretion disc coronae and of the role of the magnetic field in the inner part of the accretion flows to the recently discovered X-ray transient XTE J1118+480. This source, likely the first black hole candidate in the galactic halo, which was in the low/hard state throughout all its outburst in the year 2000, has been considered a key object, for the unprecedented quality of its observed spectral energy distribution and the many peculiarities of its variability properties. In this respect it represents a formidable test for any theoretical model of accretion flows.

6.2 Review of the observations

The transient X-ray source XTE J1118+480 was discovered with the *RXTE* All-Sky Monitor (ASM) on March 29, 2000 (Remillard *et al.*, 2000) as a weak (~ 40 mCrab) X-ray source at high galactic latitude ($b \simeq 62^o$). The source was also detected in the 20-100 keV band with the *CGRO*/BATSE experiment (Wilson and McCollough, 2000). Subsequent *RXTE* pointed observations revealed an energy spectrum typical of black hole candidates in their *low/hard* state, showing a prominent power-law component with a photon index $\Gamma \simeq 1.8$ up to at least 30 keV. Also, the source has been the subject of a target of opportunity observation with the Narrow Field Instruments (0.1-200 keV) of the *BeppoSAX* satellite (Frontera *et al.*, 2001a) that has confirmed the power-law nature of the spectrum (photon index $\Gamma \simeq 1.7$), although modified by an ultrasoft X-ray excess and a high-energy cutoff above ~ 100 keV.

A variable radio counterpart was discovered by Pooley and Waldram (2000) on March 31, with a flux density of 6.2 mJy at 15 GHz. Also, the source was detected in the optical and near infrared bands (Garcia *et al.*, 2000; Chaty *et al.*, 2000; Wren and McKay,

2000) with magnitudes of 12.12, 11.75 1nd 11.06 in the J, H and K bands, respectively, on April 4.2. The 13th magnitude optical counterpart, discovered by Uemura *et al.* (2000), exhibited a spectrum reminiscent of X-ray Novae in outburst (Garcia *et al.*, 2000). Observations performed with the *Hubble Space Telescope* (Haswell *et al.*, 2000a) on April 8, 2000, showed an Hα absorption line with FWHM corresponding to radial velocities likely $> 10^4$ km s^{-1}, which are suggestive of a massive accretor.

More recently, dynamical measurements by two different groups (McClintock *et al.*, 2001a; Wagner *et al.*, 2001), based on optical spectra taken near the source's quiescent state, have established that XTE J1118+480 has a very large mass function, which sets a hard lower limit of $6M_\odot$ on the mass of the compact X-ray source. This value greatly exceeds the maximum allowed stable mass of a neutron star in general relativity (Rhoades and Ruffini, 1974), and thus makes XTE J1118+480 one of the most firmly established black holes in the Galaxy.

The most peculiar property of XTE J1118+480 is its location at high galactic latitude (Mirabel *et al.*, 2001), and its corresponding very low reddening. This made it a perfect target for multi-wavelength campaigns (Hynes *et al.*, 2000; McClintock *et al.*, 2001b). In particular, the near-simultaneous observations centered on April 18th carried out by the 3.8m *United Kingdom Infrared Telescope* (UKIRT), *Hubble Space Telescope* (HST), *Extreme Ultraviolet Explorer* (EUVE), the *Chandra X-ray Observatory* and by *RXTE*, as reported in McClintock *et al.* (2001b), have allowed $\sim 80\%$ of the electromagnetic spectrum, from the infrared to the hard X-rays, to be covered with unprecedented sensitivity. Results from such campaigns, and their implications for theoretical models of black hole accretion flows will be discussed in Section 6.4.

From the variability point of view, beside the established orbital periodicity of 4.08 hrs, a strong QPO feature with a frequency $\nu \sim 0.1$ Hz has been found in the X-ray power density spectrum (PDS) of the source in the first month of the outburst (Revnivtsev *et al.*, 2000; Wood *et al.*, 2000). More surprisingly, the optical lightcurves also showed strong flickering on timescales of a few seconds or faster and a prominent quasi periodic feature with frequency in agreement with that of the X-ray QPO. Subsequent *HST*, *RXTE*, *ASCA* and *USA* observations in the optical/UV and X-ray bands respectively, have also shown that the QPO drifted to higher frequencies systematically in both bands (see Fig. 6.1), from $\nu \sim 0.08$ Hz to $\nu \sim 0.13$ Hz during the course of the outburst (Haswell *et al.*, 2000; Yamaoka *et al.*, 2000; Wood *et al.*, 2000; Patterson private communication).

The strikingly similar variability properties observed in both bands, and the fact that the fractional rms of the quasi-periodic oscillation is higher in the optical than in the X-rays ($\sim 30\%$ and $< 10\%$, respectively), disfavour reprocessing as the origin of the optical emission, and suggests that at least a fraction of the optical/UV flux from the object should be produced in the same region of the accretion flow where the X-rays are produced and hence represent a different aspect of the same phenomenon. This implies that the modulated optical/UV flux cannot be produced by thermal emission from the accretion disc itself; the optical/UV flux from a stellar mass black hole arises from the

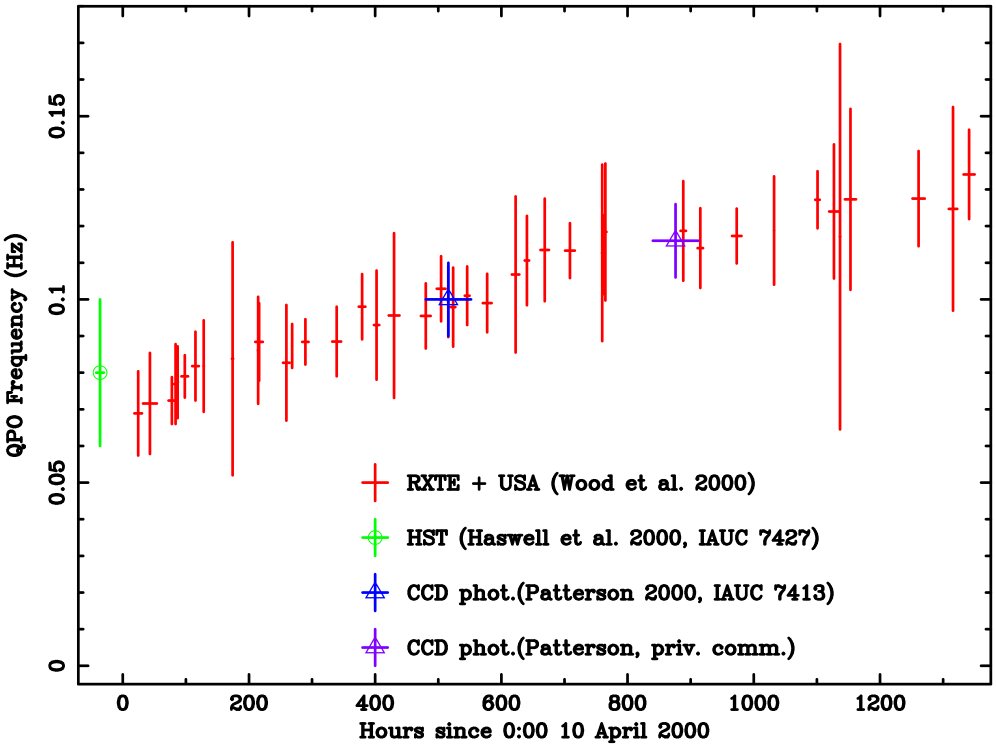

Figure 6.1: The time evolution of the low frequency QPO during the outburst of the X-ray transient XTE J1118+480, as observed simultaneously in the X-rays (red crosses, from Wood et al, 2000) and in the optical/UV (green,blue and purple points).

outer region of the disc (radii greater than hundreds of Schwarzchild radii) where the X-ray emission is negligible. Such a conclusion is also confirmed by the NIR aperiodic variability, which is even larger that the optical one (Chaty *et al.*, 2000).

Here we show that the presence of such a peculiar optical/UV variability of XTE J1118+480, together with its broad band spectral properties, argues for significant synchrotron radiation from a magnetically dominated corona (as described in Chapter 2), or possibly from an advection dominated accretion flow, ADAF, occupying the inner parts of the flow (Esin *et al.*, 2001)[1].

6.3 Cyclo-synchrotron emission from a magnetic corona

In an active region above an accretion disc, the relative importance of the cyclo-synchrotron emission (and its Comptonization) as opposed to the Comptonization of the external photon field has to be estimated by comparing the relevant timescales for the processes (see Section 2.4.2). As the synchrotron emission is heavily self-absorbed, we can set an upper limit to the ratio of the internal energy density of the synchrotron radiation $U_{\mathrm{rad,int}} < B^2/8\pi$ to the 'external' energy density, $U_{\mathrm{rad,ext}}$ of the radiation emerging from the disc (both intrinsic and reprocessed). Here we adopt the simplified spectral model described in Sections 2.4 and 2.5, namely we neglect the details of temporal variability and of the possible distribution of active region sizes as in the thundercloud model of Section 5.2. We assume that the total number of active regions is N, that they have an average size R_a, and an average height H_a. Also, a fraction η of the power dumped into the corona, instead of being dissipated there, is advected in an outflow (see Section 2.5). Then, from Eq. (2.46), we can set an upper limit on the energy density of the synchrotron radiation

$$U_{\mathrm{rad,int}} \lesssim \frac{B^2}{8\pi} = \frac{3f(1-\eta)\dot{m}L_{\mathrm{edd}}}{4\pi R_a^2 N c}\left(\frac{c}{v_{\mathrm{diss}}}\right). \tag{6.1}$$

On the other hand, the total energy density of the radiation coming from the disc is given by the sum of the intrinsic and of the reprocessed radiation energy densities

$$U_{\mathrm{rad,ext}} = \frac{\dot{m}L_{\mathrm{Edd}}}{4\pi c}\left[\frac{(1-f)}{R_{\mathrm{disc}}^2} + \frac{2f(1-a)(1-\mu_0)}{R_{\mathrm{hot}}^2}\right], \tag{6.2}$$

where a is the disc albedo, $R_{\mathrm{hot}} \simeq 2.3H_a + R_a$ and $\mu_0 = (H_a/R_{\mathrm{hot}})(1 + H_a^2/R_{\mathrm{hot}}^2)^{-1/2}$ (see Eq. 2.29).

Interestingly, when $f \to 1$, as we argue is indeed the case of BHCs in the low/hard state and of XTE J1118+480 in particular, the relative importance of the synchrotron emission depends crucially on the dissipation velocity v_{diss}, on the total number of active regions N and on the ratio H_a/R_a, but not on f itself. In fact, for

[1]The only other object ever observed to show similar short timescale variability, in both the optical and X-ray bands, is the black hole candidate GX 339-4 in its hard state (Motch *et al.*, 1983). For the case of GX 339-4, typically brighter than XTE J1118+480 in X-rays, it was also suggested that thermal synchrotron emission should provide a significant contribution to the optical band (Fabian *et al.*, 1982; Di Matteo *et al.*, 1999).

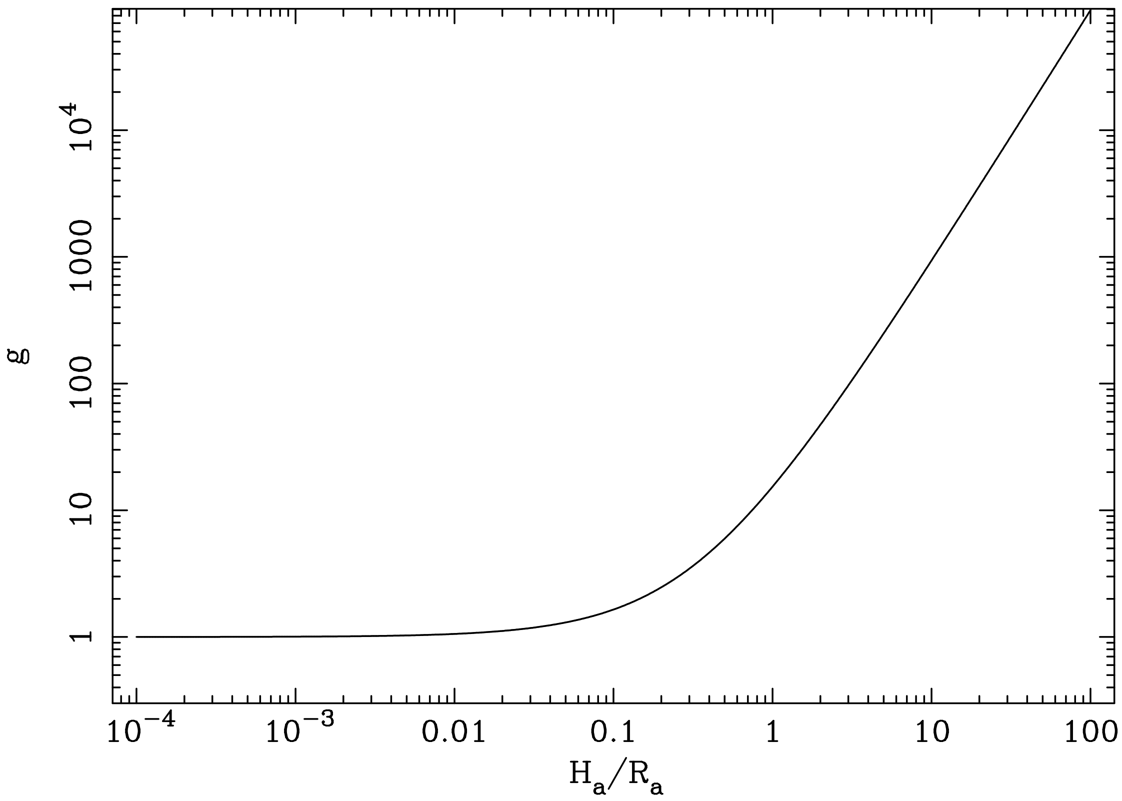

Figure 6.2: The geometrical factor g, that determines the ratio of the synchrotron radiation energy density to the external radiation energy density, plotted as a function of the height over radius ratio for a coronal active region.

large f the intrinsic disc dissipation does not contribute to the external radiation energy density (we can neglect the first term in the squared bracket in Eq. 6.2). Thus, we have (for a fixed disc albedo $a = 0.15$)

$$\frac{B^2}{8\pi U_{\mathrm{rad,\,ext}}} = 0.11 \left(\frac{1-\eta}{0.2}\right)\left(\frac{100}{N}\right)\left(\frac{c}{30 v_{\mathrm{diss}}}\right) g(H_a/R_a), \tag{6.3}$$

where

$$g(H_a/R_a) = \frac{\left(1 + 2.3\frac{H_a}{R_a}\right)^2}{\left[1 - \frac{H_a}{R_{\mathrm{hot}}}\left(1 + \frac{H_a^2}{R_{\mathrm{hot}}^2}\right)\right]} \tag{6.4}$$

is a geometrical factor that depends only on the average aspect ratio of an active region. In Fig. 6.2 we plot the dependence of such factor on H_a/R_a. When $H_a \gtrsim R_a$, the magnetic energy density in the corona becomes equal to the energy density of the 'external' soft radiation field, and the ratio of the two energy densities increases rapidly with the increase of H_a/R_a.

This is analogous to what was already discussed in the context of MHD driven outflows from the corona (§2.5): qualitatively, we can say that whenever the conditions are favourable for a magnetically driven jet to be launched from the corona, then the synchrotron emission is likely to be a relevant (or dominant) source of soft photons for

Comptonization, even neglecting any non thermal component of the electron distribution (Wardziński and Zdziarski, 2001). Furthermore, as we shall see in detail in the following sections, for black holes in the low/hard state, the disk blackbody component, which dominates the X-ray emission in the soft state, often disappears or cools down significantly, and the synchrotron component is likely to contribute significantly to the observed emission in the optical/UV band.

6.4 Models for the broad-band spectrum

6.4.1 The ADAF model

The spectral energy distribution of XTE J1118+480 as obtained from the multi-wavelength campaign described in McClintock *et al.* (2001b) shows no sign of a soft blackbody-like disc component in the X-rays, while it exhibits a very steep soft component in the EUV. If, as is very plausible, this spectral component is the Wien tail of the quasi-thermal emission from the accretion disc, a very stringent upper limit on the inner disc temperature can immediately be placed. Based on this argument, Esin *et al.* (2001) have proposed a model for the spectrum of XTE J1118+480 in which a standard geometrically thin and optically thick accretion disc is truncated at a distance, $R_{\rm tr}$, of a few tens of Schwarzschild radii from the central black hole and an ADAF occupies the inner part of the flow. The data, together with two different ADAF models proposed by Esin *et al.* (2001) are shown in Fig. 6.3, where the model parameters are shown as well.

Beside the already mentioned constraints on the inner disc temperature implied by the *Chandra/EUVE* data, there are three points worth stressing concerning such ADAF models. First, there is a clear excess of emission in the optical/IR with respect to the predicted multicolour disc component. This, we argue, is a clear sign of synchrotron emission, especially when considered alongside the peculiar variability properties of the optical/IR emission and the flat radio spectrum (not shown in Fig. 6.3), which possibly extends up to IR data points (Fender *et al.*, 2001). Secondly, the high energy emission can be fitted only by requiring an uncomfortably high value of the plasma parameter β, the ratio of the gas to total (gas plus magnetic) pressure in the ADAF, in order to increase the electron temperature (Esin *et al.*, 2001). Such a low magnetic field, although possible, is very different to the one needed in the ADAF modeling of Cygnus X-1 in the hard state (Esin *et al.*, 1998), which has, on the other hand, very similar physical parameters to the one inferred for XTE J1118+480. Finally, as shown in the inset of Fig. 6.3, such models leave unexplained the broad dip in the data centered around 0.3 keV. This has prompted Esin *et al.* (2001) to suggest that a warm absorber model, similar to what usually observed in the spectra active galactic nuclei, might be applied to this source. Their proposed toy model ascribes the absorption features to gas expelled from the system in previous outbursts and accumulated at a distance of about 10^{15} cm, with a column density $N_{\rm H} \simeq 2 \times 10^{21}$ cm^{-2}. However, as note of caution concerning the warm absorber interpretation, we wish to stress that the *BeppoSAX* observation

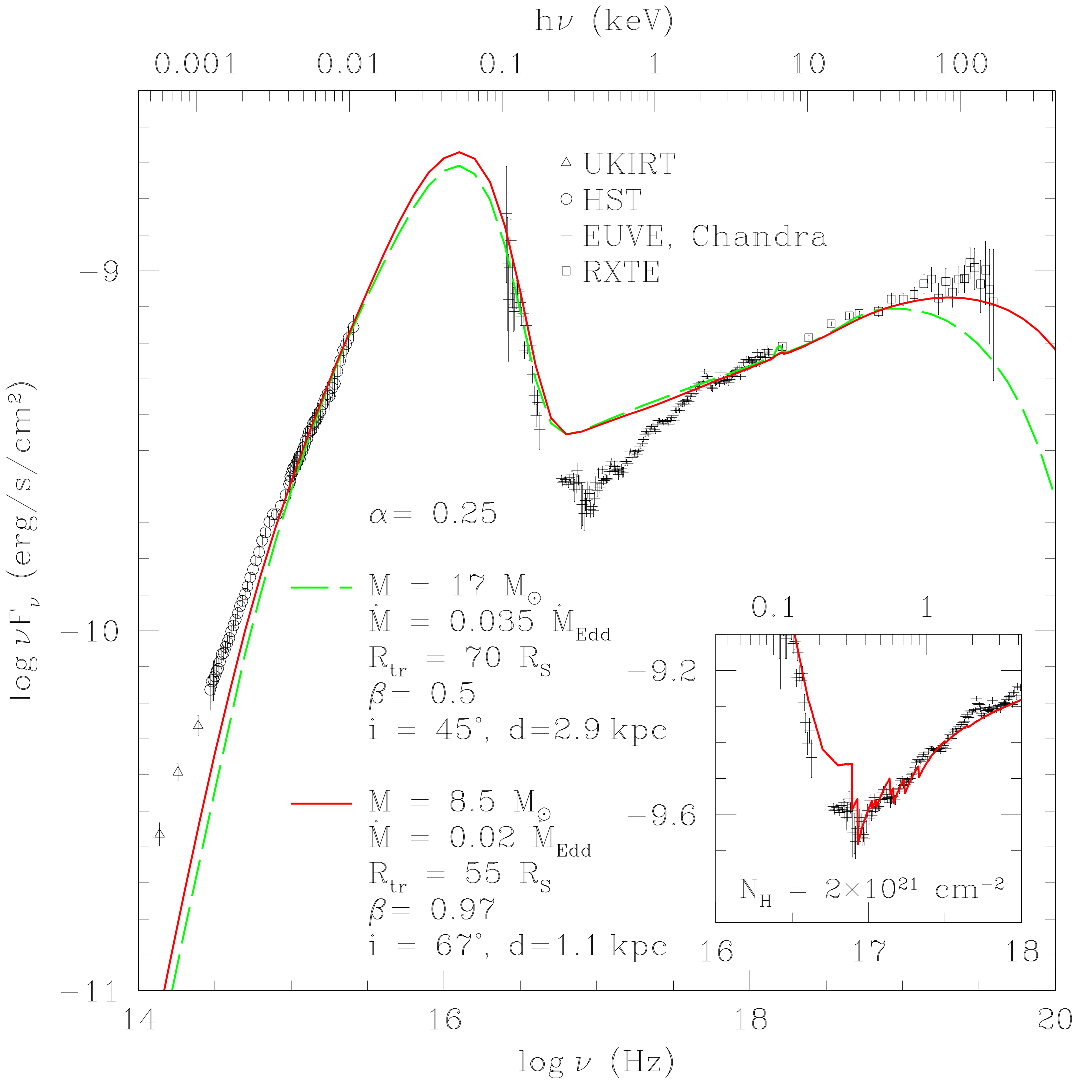

Figure 6.3: Multi-wavelength observations of XTE J1118+480 on April 8, 2000 (points; different symbols correspond to different instruments, as labeled in the figure) together with two ADAF model spectra (dashed and solid lines, from Esin *et al.*, 2001). The model in the inset incorporates phenomenologically the effects of a warm absorber. For more details see discussion in Esin *et al.* (2001). Courtesy of Ann Esin.

reported in Frontera *et al.* (2001a) does not show such strong features and that cross calibration uncertainties among the different instruments used to produce the SED shown in Fig. 6.3 could be responsible for at least part of the absorption dip. If, instead, the warm absorber interpretation is correct, a self-consistent model for the absorbing gas should be considered, and the effect of such gas on the EUV data taken into account: the estimate of the inner disc radius may be affected by the putative warm absorber, as we shall see in section 6.4.4.

6.4.2 The coronal outflow model

In this section we explore the alternative hypothesis that the SED of XTE J1118+480 reveals an accretion flow at very low $\dot{m}$ (few times 10^{-3}), in which the corona is a dominant repository of the gravitational power, and a powerful outflow is produced in the corona, as in the scenario discussed in section 2.5.

Hubble Space Telescope observations of XTE J1118+480 (Haswell *et al.*, 2000a), made at the end of the rising phase of the outburst, indicate a flux density at 1500Å of 3×10^{-13}ergs cm^{-2}s^{-1}Å^{-1} and a spectrum between 1200 and 8000 Å flatter than $F_\nu \propto \nu^{1/3}$. On the other hand, unfiltered CCD fast photometry (Haswell *et al.*, 2000b; Patterson *et al.*, 2000) has revealed optical flickering of ± 0.2 mag on timescales of seconds, which correspond to $\sim$ 25 per cent of the optical flux. As the optical variability is strongly modulated by a QPO with the same frequency of the X-ray one (as shown in Fig. 6.1), the emission in the two bands is clearly correlated.

Let us assume that such rapid variability is due to self absorbed cyclo-synchrotron (CS) emission. To explicitly show the various parameter dependences of the synchrotron emission we write the flux at the peak frequency ν_c as (Di Matteo *et al.*, 1997a)

$$
\begin{aligned}
F_{\rm CS} &= 2\pi m_e \nu_c^3 \theta r_a^2 N \left(\frac{R_{\rm S}}{D}\right)^2 \left[\frac{1}{1+t_{\rm CS}/t_{\rm iC}}\right] \qquad (6.5)\\
&\simeq 7.7\times 10^{-13}\theta r_a^2 N \left(\frac{\nu_c}{10^{15}}\right)\left(\frac{m}{7}\right)^2\left(\frac{1.9\rm kpc}{D}\right)^2 \times \left[\frac{1}{1+3.2\times 10^2 \tau U_{\rm rad}\left(\frac{10^{15}}{\nu_c}\right)^3}\right],
\end{aligned}
$$

where we have fixed the black hole mass and distance to the values $M = 6.9 M_\odot$ and $D = 1.9$ kpc (Wagner *et al.*, 2001), the dissipation velocity $v_{\rm diss} = c/20$, and $\theta = kT/m_e c^2$ is the dimensionless temperature, $U_{\rm rad} = U_{\rm rad,int} + U_{\rm rad,ext}$. The ratio of the relevant timescales for the cyclo-synchrotron and inverse Compton emission determines which process dominates in an active region (see section 2.4.2). Electron temperature and optical depth in the corona are constrained by the observed slope of the power-law in the X-ray spectrum ($\alpha \simeq 0.7-0.8$), from the relation $\alpha \simeq -\ln(P_{\rm sc})/\ln(A)$, where $P_{\rm sc}$ is the scattering probability and A is the average photon energy amplification per scatter.

We model the spectrum of the source following our discussion of Section 2.5. The value of the fraction of the gravitational power dissipated in the corona, f, is calculated as a function of the accretion rate from Eq. (2.44) with a value of $K = 0.99$. Also, a fraction η of the power dissipated in the corona is assumed to be advected away in the form of a jet/outflow, with 10% radiative efficiency and a flat spectrum extending up to the self-absorption synchrotron cutoff ν_c corresponding to the value of the magnetic field in the corona.

Reprocessing of coronal radiation in the accretion disc in considered not only according to the active blob size but also according to their height above the disc. Once we fix the coronal optical depth τ, the number of active regions N, their average size R_a and height H_a, the spectrum is calculated self-consistently taking into account all the relevant radiative processes (cyclo-synchrotron emission and its Comptonization; inverse Compton scattering of disc photons on the hot coronal electrons; thermal emission from intrinsic dissipation in the accretion disc and from the reprocessed radiation) opportunely rescaled according to the ratios of their typical cooling timescales, which are obtained by integrating each spectral component. In all cases we postulate that the accretion disc extends down to the innermost stable orbit of a non-rotating black hole ($R_{\rm in} = 3R_{\rm S}$). The number of active regions should depend on their size and distribution, as discussed in §5.2. For simplicity, here we will assume that, although the time variability properties of the observed lightcurves require the application of the full thundercloud model, the spectral properties can still be modeled fairly well by assuming a fixed number N of active region, with $N \sim 100$ (see Section 5.2.3).

In Figure 6.4 we show an illustration of two model spectra for the multi-wavelength observations of XTE J1118+480. The stars connected by the blue line represent the observations from radio wavelength (VLA and Ryle Telescope; Fender et al. 2001) through sub-millimeter (*SCUBA* instrument on JCMT; Fender et al. 2001) and infrared (UKIRT; Hynes et al. 2000) to the optical/UV observed with HST (Hynes *et al.*, 2000). All these observations have been performed almost simultaneously in the rising phase of the April 2000 outburst. The X-ray points (see inset in Fig. 6.4) come from two different sets of data. The open squares mark the simultaneous *Chandra* and *RXTE* observations of April 18, 2000, discussed in McClintock *et al.* (2001b), while the open triangles mark the data from the *BeppoSAX* observations of April 14-15, 2000 (Frontera *et al.*, 2001a). The red lines represents two predicted SED from our magnetic corona model; the solid one represent a model for the *BeppoSAX* data, while the dashed one a model for the *Chandra-RXTE* data. They are not to be regarded as detailed fits to the data, rather as indicative of the physical properties of the source implied by the model. The parameters of the model in the two cases are listed in table 6.1.

As expected from the simple scaling arguments of Eq. (6.5), we obtain a relatively low accretion rates ($\dot{m} \simeq 0.004$) and a high value of the fraction of the power dissipated in the corona ($f \simeq 0.99$), both consistent with the source being in its *hard* state. Also, a fraction $\eta = 0.8$ of coronal power to be advected in a jet/outflow is needed. We have assumed that such an outflow has a radiative efficiency of 10 % and that its optically thick synchrotron emission produces a flat spectrum ($F_\nu \propto \nu^0$; see Markoff, Falcke & Fender, 2001) up to the synchrotron turn-over frequency $\nu_{\rm c}$ corresponding to the value of the magnetic field in the corona (that is regarded then as the base of the jet). This jet-corona emission represent the bulk of the infrared-optical emission, possi-

Table 6.1: Model parameters for the two predicted SED of XTE J1118+480 shown in Fig. 6.4. N is the total number of active regions, H_a and R_a the average height and size of each active region, respectively, $\dot{m}$ is the accretion rate, η the fraction of coronal power that goes into the outflow and τ the coronal optical depth. The asterisks mark the three *dependent* parameters (the fractional coronal power f, the electron temperature in the corona θ and the slope of the comptonized X-ray spectrum Γ) that are calculated self-consistently from the others in the model.

Parameter	*BeppoSAX*	*Chandra-RXTE*
N	100	150
H_a	$5R_{\rm S}$	$5R_{\rm S}$
R_a	$0.7R_{\rm S}$	$0.7R_{\rm S}$
$\dot{m}$	0.0038	0.0047
η	0.79	0.80
τ	0.37	0.215
f^*	0.989	0.989
θ^*	0.54	0.70
Γ^*	1.71	1.79

bly with some additional contribution from the reprocessed black-body component, that, in a more realistic situation, will emit as a multicolor disc, rather than the monochromatic one we have assumed here. The radio and sub-millimeter data points suggest that the spectral slope of the jet emission changes from flat to inverted ($F_\nu \propto \nu^{0.5}$) at low frequencies, and this may constrain the jet length, as illustrated by Markoff *et al.* (2001).

A strong constraint on the model comes from the absence of a soft excess below 0.3 keV. At the low accretion rate and the high value of f we found, the intrinsic disc dissipation (green lines in Figure 6.4) is much reduced, but the reprocessed one (blue lines in Figure 6.4) still contributes substantially in the EUV band. For our best parameter, $R_a = 0.7$, we have to allow the reconnection sites to be above the accretion disc at a height of $5R_{\rm S}$. The need for such aspect ratio of the active region is just an indication that the soft radiation field seen by the flaring region is relatively cooler, which is a peculiarity also of any truncated disc model for GBHC in their *low/hard* state. From Figure 6.2 we can see that, for $H_a/R_a = 7.14$ we have $g \simeq 500$ and $B^2/8\pi U_{\rm rad,\,ext} \simeq 50$.

The X-ray part of the spectrum is used to fix the coronal parameter and the accretion rate. The main source of soft photons for Comptonization is, in both cases, synchrotron coronal emission. When this is the case, an increase in the coronal optical depth determines a decrease in the coronal temperature and an hardening of the spectrum

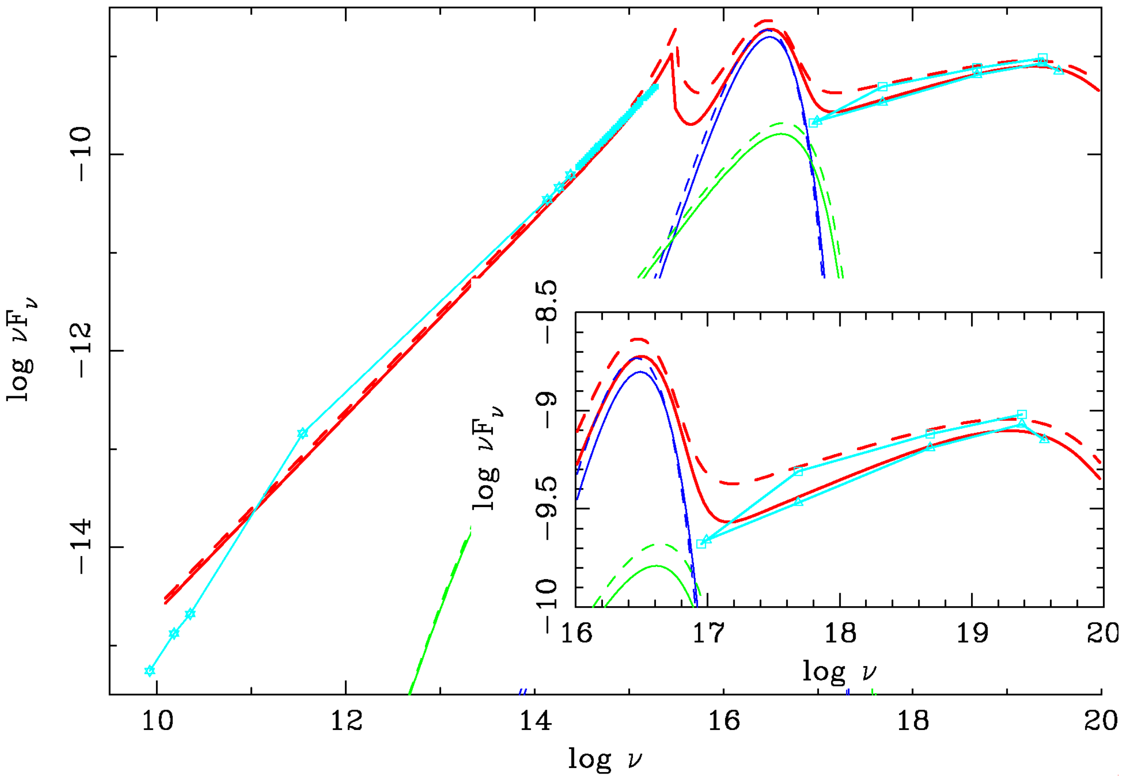

Figure 6.4: Representative model predictions for the spectral energy distribution of XTE J1118+480. The stars connected by the cyan line represents the observations from radio wavelength (VLA and Ryle Telescope; Fender et al. 2001) through sub-millimeter (*SCUBA* instrument on JCMT; Fender et al. 2001) and infrared (UKIRT; Hynes et al. 2000) to the optical/UV observed with HST (Hynes *et al.*, 2000). All these observations have been performed almost simultaneously in the rising phase of the April 2000 outburst. The X-ray points (see inset) come from two different sets of data. The open squares mark the simultaneous *Chandra* and *RXTE* observations of April 18, 2000, discussed in McClintock *et al.* (2001b), while the open triangles mark the data from the *BeppoSAX* observations of April 14-15, 2000 (Frontera *et al.*, 2001a). The red lines represents two predicted SED from our outflow dominated magnetic corona model. The parameters for the two cases are listed in table 6.1. Solid lines correspond to the model for the *BeppoSAX* X-ray observation, while dashed ones to the model for the *Chandra-RXTE* one. Blue lines correspond to reprocessed thermal emission from the accretion disc, green ones to the intrinsic multicolor disc emission.

(see e.g. Figs. 2.2 and 2.4). The spectrum was harder during the Frontera *et al.* (2001a) observation, when the flux was lower, and a lower high-energy cut-off was tentatively found. This can be reproduced by our model with a higher optical depth and lower $\dot{m}$ in the *BeppoSAX* observation, which results in a lower temperature and harder spectrum (see Table 6.1).

6.4.3 Jet power and magnetic field intensity

From Eq. (6.1) and the set of parameters corresponding to the two solutions of Tab. 6.1, we find, for the magnetic field intensity, the values $B \simeq 2.5 \times 10^7$ G and $B \simeq 2.3\times 10^7$ G, for the *BeppoSAX* and *Chandra-RXTE* observations, respectively. As we have neglected any contribution from a non-thermal tail in the electron distribution, which would lower the value of the magnetic field needed to produce the observed synchrotron radiation (Wardziński and Zdziarski, 2001), the values we found are consistent with the constraints discussed in Frontera *et al.* (2001a) ($10^7 \lesssim B \lesssim 10^8$) for the synchrotron process to be the dominant source of seed photons.

Furthermore, we can check the self-consistency of our treatment by calculating the expected strength of a magnetically driven outflow, as in Section 2.5. We recall that in general the relative strength of an MHD driven coronal outflow is given by

$$\eta_{\rm MHD} = \left(1 + \frac{2}{3}\left(\frac{v_{\rm diss}}{c}\right)\left(\frac{R_*}{H_a}\right)^2\left(\frac{c}{v_{\rm K}(R_*)}\right)\right)^{-1}, \tag{6.6}$$

where we have expressed the rotational velocity of the coronal magnetic field lines in terms of the Keplerian velocity $v_{\rm K}$ at the typical magnetic loop location in the disc, R_*.

The value of $\eta = 0.8$ we obtain from the model applied to XTE J1118+480 is compatible with the above estimate, if we take $R_* \simeq 7R_{\rm S}$, which means that the location of the maximal coronal outflow strength roughly corresponds to the location of the maximal intrinsic disc dissipation, as expected if the coronal field is ultimately generated by the differential velocity of the underlying cold disc.

6.4.4 The warm absorber

Both the model SEDs for the multi-wavelength spectra of XTE J1118+480 that we have shown in Fig. 6.4 do over-predict the soft excess below ~ 0.5 keV. As already mentioned, in their ADAF model for the multi-wavelength spectrum of XTE J1118+480 Esin *et al.* (2001) interpret the observed dip around 0.4 keV as due to a warm absorber. Here we just want to stress that, if indeed absorption is important in the spectrum, this will affect the estimates of the inner disc radius obtained from the inferred temperature of the disc blackbody. To illustrate further this point, we have taken the two continua from our outflow dominated magnetic corona model (Fig. 6.4) and calculated the absorption from a shell of constant density n and width ΔR, placed at distance R_0 from the source, using the CLOUDY photo-ionization code (Ferland *et al.*, 1998). As already discussed in Esin *et al.* (2001), if indeed we interpret the observed dip as due to absorption, the lack of a prominent Oxygen K edge around 0.7 keV requires that the O abundance be less than solar. XTE J1118+480 is probably a halo source (Mirabel *et al.*, 2001), and we can expect its metallicity to be substantially lower than solar (Frontera *et al.*, 2001a), nonetheless, the strong putative C edge observed in the *Chandra* data, if real, requires a relatively high Carbon abundance. Here we do not attempt a detail fit of the absorption features, but we just study the effects of a warm absorber on the broadband spectral

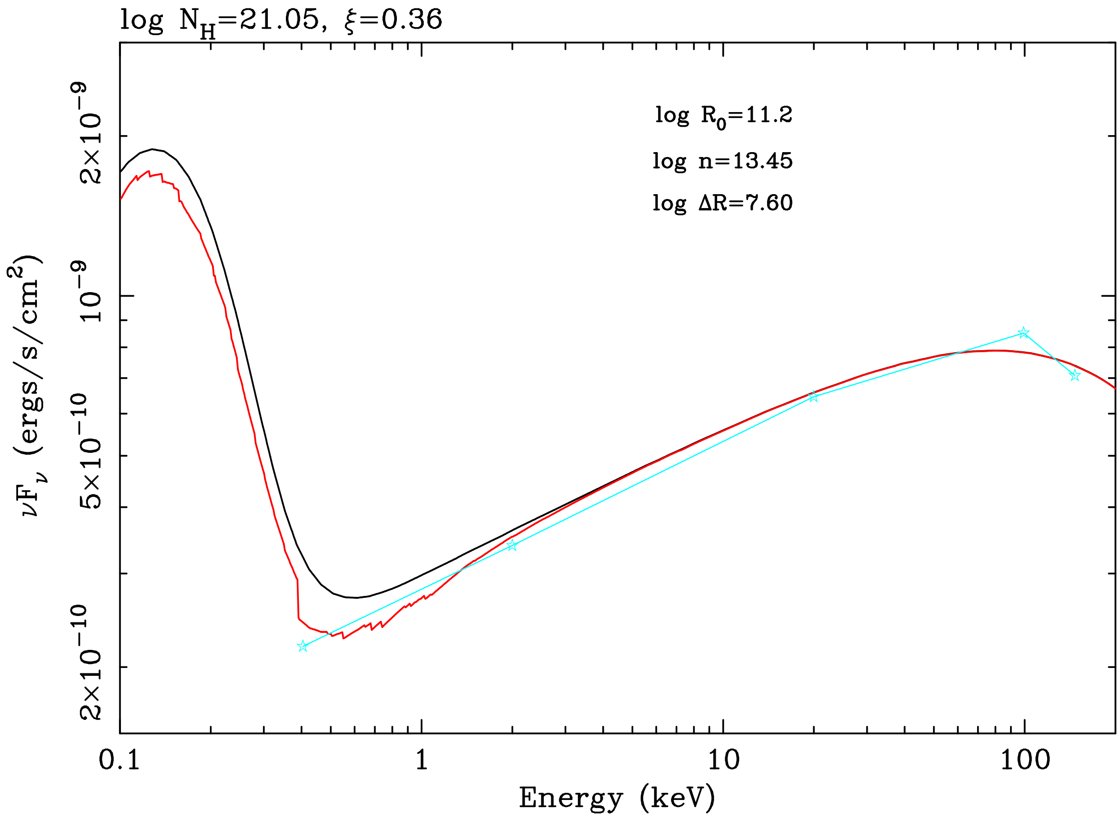

Figure 6.5: Input spectrum (black line) from our coronal outflow dominated model and result from a constant density CLOUDY simulation for the warm absorber (red line) for the high energy SED of XTE J1118+480 observed by *BeppoSAX* on April 14-15, 2000. The three independent model parameters are the distance from the illuminating source R_0, the density of the absorber n and the thickness of the absorbing shell ΔR. The resulting column density and ionization parameter are shown in the header.

shape. We therefore assume that all the elements have solar abundance apart from O, for which we reduce the abundance by a factor of two. We apply the CLOUDY model to both the *BeppoSAX* and *Chandra-RXTE* sets of data, and show the results in Figures 6.5 and 6.6, respectively.

Given the two different illuminating spectra, consistency with the observed data can be obtained if the absorption seen in the *Chandra-RXTE* data comes from a closer in (and therefore denser) shell ($R_0 = 8.9 \times 10^{10}$ cm, $n = 8.9 \times 10^{13}$ cm^{-3}) with respect to the one responsible for the very weak absorption features possibly seen in the *BeppoSAX* data ($R_0 = 1.58 \times 10^{11}$ cm, $n = 2.8 \times 10^{13}$ cm^{-3}). Such values for R_0 correspond to approximately $4 \times 10^4 R_{\rm S}$, a distance similar to the expected outer accretion disc radius estimated using Paczyński's (1971) formula $R_{\rm out} = 3 \times 10^4 R_{\rm S}(10/m)^{2/3}$. The shell thickness is very low, possibly suggesting a low covering fraction of the absorber (as is the covering fraction of the corona in the thundercloud model, see section 5.2.3). Also, the presence of a warm absorber clearly reduces the observed EUV flux between 0.1 and 0.3 keV (see Fig. 6.5 and 6.6), thus demonstrating the need for a fully self-consistent

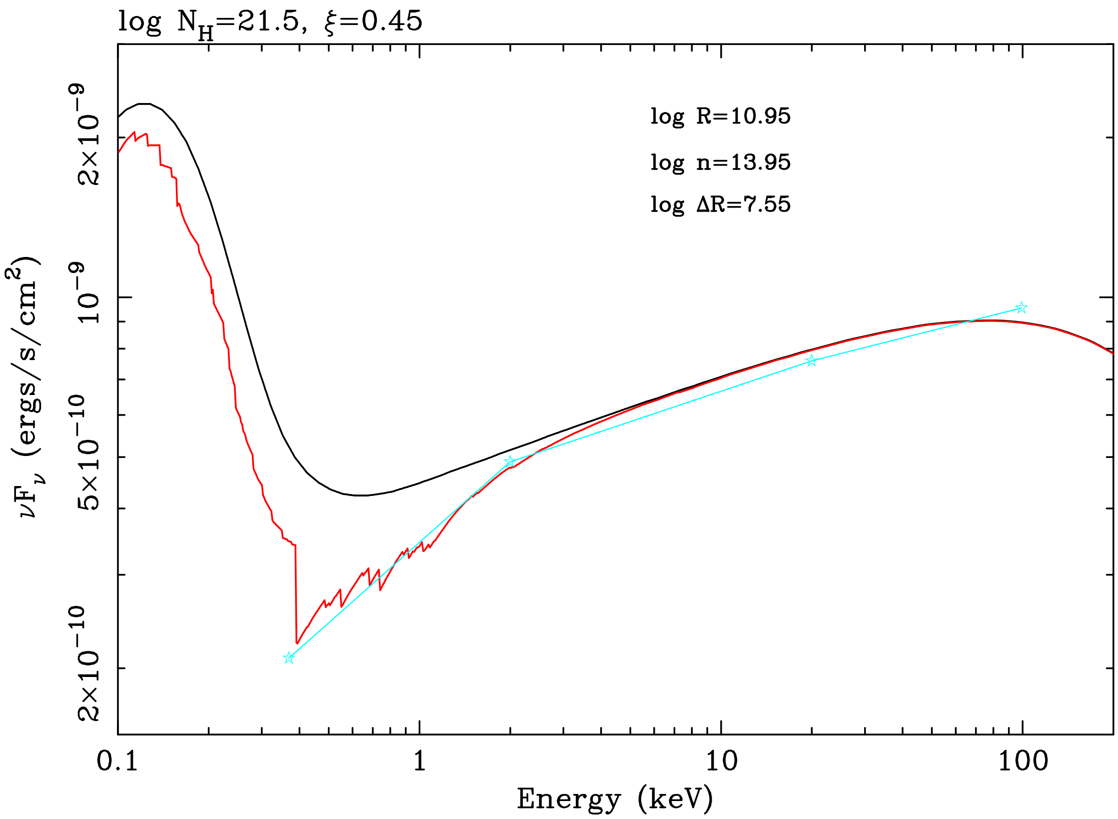

Figure 6.6: Input spectrum (black line) from our coronal outflow dominated model and result from a constant density CLOUDY simulation for the warm absorber (red line) for the high energy SED of XTE J1118+480 observed by *Chandra-RXTE* on April 18, 2000. The three independent model parameters are the distance from the illuminating source R_0, the density of the absorber n and the thickness of the absorbing shell ΔR. The resulting column density and ionization parameter are shown in the header.

spectral model (including, when needed, absorption and emission features) before any firm conclusion about the location of the inner disc could be drawn.

For example, here we can conclude that in both cases the absence of any prominent soft excess in the X-ray band is ultimately a combined effect of the low accretion rate, of the strong outflowing corona with high H_a/R_a ratio and (possibly) of a warm absorber. In fact, the inner disc radius has always been kept fixed to the innermost stable orbit of a Schwarzschild black hole for all the models we have presented here. Finally, we would like to note that, if the tentative evidence for a warm absorber will be confirmed, it is quite likely that it will turn out to be variable on the timescales (3-4 days) we have tested here. Strong differences in the emerging spectra could be explained with relatively small variations in the absorbing material, in particular if the low covering fraction we have suggested is to be trusted.

6.5 The evolution of the ~ 0.1 Hz QPO and the inner disc

The spectral analysis presented in the previous section, by leaving effectively open both the possibility of an ADAF or a coronal dominated outflow, is not conclusive regarding the issue of the location of the inner disc radius. The information provided by temporal studies are then crucial for constraining the geometry of the inner disk, in particular optical-X-rays cross-correlation and time lag analysis for the QPO component.

In two recent papers Psaltis *et al.* (1999) and Wijnands and van der Klis (1999) have suggested that the frequencies of the periodic features in the PDS of black hole candidates (which can appear more or less broadened) follow a quite tight correlation that encompasses also neutron star sources, and therefore has to be related to the properties of the accretion flow. More recently Psaltis and Norman (2000) have proposed a model in which the QPOs are produced in a narrow ring in the accretion disc where a discontinuity in some properties of the flow occurs. The frequencies themselves are essentially determined by the relativistic proper frequencies of the system (Stella *et al.*, 1999; Merloni *et al.*, 1999). Assuming such a model, the data can be used to constrain the position of the flow discontinuity (di Matteo and Psaltis, 1999).

The published PDS of XTE J1118+480 Revnivtsev *et al.* (2000) strongly resembles that of GX 339-4 in the *hard* state (see Nowak, 2000, for a discussion of the various variability components). Apart from the strongly peaked QPO at 0.08 Hz, it exhibits a broader feature around 1 Hz. Plotted one against the other, these frequencies fall remarkably well on the correlation presented by Psaltis *et al.* (1999). This would suggest that the low frequency QPO is analogous to the horizontal branch oscillation (HBO) in neutron stars and is related to twice the nodal precession general-relativistic frequency of a perturbed orbit around the compact object. The value of the transition radius, where the modulation is produced, depends on the spin of the black hole, but is limited in the range $25 \gtrsim R_t/R_\mathrm{S} \gtrsim 6$ for a $10\,\mathrm{M}_\odot$ black hole with dimensionless angular momentum $0.99 \gtrsim a \gtrsim 0.01$. This provides an upper bound for the inner extent of the geometrically thin accretion disc, which is in conflict with the limits derived from

EUVE observations (Hynes *et al.*, 2000) and significantly reduces the relevance of a central ADAF component, favoring instead models like the one discussed in Section 6.4.2. We note, however, that if the observed QPO is associated with the HBO frequency of neutron stars, it is not clear why the expected modulation at the keplerian frequency at the same radius (with frequency $\nu_{\rm Kep} \sim 30$ Hz) is not directly observed, even though it should have a higher quality factor (although, see e.g. Nowak 2000).

Alternatively, we can ignore the very broad feature in the PDS at ~ 1 Hz and consider the sharp low frequency QPO as due to Keplerian modulation of the flow far away from the source. This would imply a transition radius $R_t \simeq 500 R_{\rm S}$. This interpretation for the observed variability is less plausible, and is also in disagreement with the ADAF prediction for the EUV flux, that places $R_t \simeq 60 R_{\rm S}$. Also, in this case it remains to be explained how the modulation propagates inward in the advective flow without loss of coherence, given that, in the ADAF model, the bulk of the optical and X-ray are produced in the inner part of the flow, where the magnetic field is high enough ($B_{ADAF} \sim 10^7 \alpha_{\rm v,0.1}^{-1/2} m_{10}^{-1/2} \dot{m}_{0.01}^{1/2} r_3^{-5/4}$ G) to power the cyclo-synchrotron emission, which is then Componized to give rise to the high energy spectrum (see e. g. Narayan and Yi, 1995; Quataert and Narayan, 1999).

6.6 Discussion

We have applied a model for the emission from a highly magnetic, structured corona to the multi-wavelength observations of the newly discovered X-ray transient XTE J1118+480, and compared our model for the SED with the ADAF one (Esin *et al.*, 2001).

This source is unique for a number of reasons. It is located at high galactic latitude and therefore suffers for very little galactic extinction, thus allowing almost full spectral coverage from the FIR to the hard X-rays with unprecedented sensitivity. It also has a peculiarly high optical-to-X-ray flux ratio. The source is observed in the typical black hole candidates low/hard state (photon index $\Gamma \simeq 1.8$, see Section 1.3.1).

According to our model, XTE J1118+480 reveals an accretion flow at very low $\dot{m}$ ($\sim 4 \times 10^{-3}$), in which the corona is a dominant repository of the gravitational power, and a powerful outflow is produced in the corona. By fitting the complete SED, we have derived constraints for the approximate number, size, elevation, optical depth and magnetic field strengths of the coronal active regions.

The main point of our work is that the simultaneous presence of a strong quasi periodic feature in the optical and X-ray lightcurves clearly suggests that the fluxes in the two bands both originate from the same region in the inner part of the accretion flow. Self-absorbed cyclo-synchrotron emission is the natural candidate to explain the optical variability. Such emission is expected in any magnetic corona model, and the inferred magnetic field value ($B \approx 2.5 \times 10^7$ G) is the one predicted to arise when the source is in the *hard* state (low value of $\dot{m}$ and high value of f).

Independently of the dominant source of soft photons for Comptonization, we expect that any (small) variation in the physical parameters characterizing the active coronal regions (either in temperature or optical depths) driven by a flow discontinuity in the disk should modulate the emission simultaneously in the optical (via the CS emission) and in the X-ray band (via inverse Compton emission). In particular, any increase (at a level of 20 per cent or so, as required) in temperature or density in the corona will cause an increase in the cyclo-synchrotron component at optical frequencies, while at the same time it will make the X-ray spectrum harder. From any such model we then expect a correlation between the optical and hard X-ray variability but an anticorrelation between optical and soft X-rays (this has been observed for the case of GX 339-4; see Motch *et al.*). Our model also predicts optical variability on flaring timescales ($\sim$ tens of milliseconds), with a PDS similar to the one observed in X-rays. Indeed, such rapid optical flaring has been observed (Kanbach *et al.*, 2001), correlated with the X-ray emission on timescales from 20msec to several seconds, ruling out effectively reprocession as the main source of the optical light.

As for the origin of the QPO itself, if it is to be associated with any proper frequency of the accretion flow at a specific distance from the source, as in relativistic precession models (Stella *et al.*, 1999; Psaltis and Norman, 2000; Psaltis, 2001), then Lense-Thirring precession frequency, excited relatively close to the black hole ($25 \gtrsim R_t/R_{\rm S} \gtrsim 6$), is preferred to Keplerian rotation at a grater distance ($R_t/R_{\rm S} \sim 500$).

Chapter 7

Conclusions and future work

The work presented in this thesis has focussed on the study of spectral and temporal properties of accretion flows onto black holes. Great emphasis has been given to the study of two-phase accretion flow in which a geometrically thin and optically thick accretion disc coexist in the inner region with a hot comptonizing corona.

The main conclusion of this work are summarized below.

- *Chapter 2: The physics of magnetic accretion disc coronae.* In this Chapter the fundamental properties of magnetic accretion disc coronae have been studied. First (§2.3), by comparing the thermal energy content of the corona, deduced from the observed spectra of GBHC in their low/hard state and of Seyfert galaxies, with the observed X-ray luminosities, we have shown that the corona is likely to be patchy, and energetically dominated by a magnetic field. Then (§2.4), we have shown how the observed X-ray spectra can be reproduced by a generic model for a structured magnetic corona emitting hard X-ray photons via inverse Compton scattering of both thermal photons from the accretion disc and synchrotron ones produced locally in the coronal active regions. Finally, in Section 2.5, we have studied the energetics and power output of the coronae generated by geometrically thin, optically thick accretion discs at low accretion rates. We have assumed that angular momentum transport in the disc is due to magnetic turbulent stresses and that both magnetic energy density and effective viscous stresses inside the disc are proportional to the gas pressure. In this case, we have shown that the relative strength of the corona, generated via amplification and expulsion of the turbulent disc magnetic field, increases as the accretion rate decreases. Furthermore, we have shown that the rarefied corona, heated by the dissipating field (via magnetic reconnection and/or shock heating) up to temperature of few tens of keV, is the ideal site for launching an outflow. We assessed the relevance of the various mechanisms that can generate such powerful outflows from the coronal region, either magnetic or thermal. We have shown that, depending on the actual coronal field geometry, MHD launching mechanisms can indeed produce strong outflows, whose power is of the order of the radiated one. Moreover, if the corona is two-temperature, a thermally driven outflow can easily dominate the power output from the source at low accretion rates. Thus, if the jet/outflow do not radiate efficiently, the whole system can be very under-luminous compared to a standard radiatively efficient accretion disc.

- *Chapter 3: The effect of the corona on the reflected spectral components.* In this Chapter, we have shown that the effects of a comptonizing corona on the appearance of the reflection components in the spectra of accreting black holes may be relatively important, modifying the shape of the observed reflection hump and the measured iron line equivalent width. We have studied in detail the dependence of these effects on the physical (i.e. the electron temperature $T_{\rm e}$ and optical depth τ) and geometrical (i.e. the inclination angle) parameters of the corona, mainly focusing on the case of a slab geometry. Due to the smoothing and shifting towards high energies of the comptonized reflection hump, the main effects on the emerging spectra appear at energies below and above $\sim kT_{\rm e}$; they are larger for larger optical depth of the corona and/or larger inclination angle of the corona–disk configuration. Fitting Comptonization models that take into account comptonized reflection by means of the usual cut–off power law plus uncomptonized reflection models, leads to an underestimation of the reflection normalization and an overestimation of the high energy cut–off. Moreover, the Comptonization effects may strongly reduce the equivalent width of the observed iron line, especially at large inclination angles.

  These effects may have important consequences on the physical interpretation of the observed reflection features in astrophysical objects. As an example, we have studied the case of the galaxy NGC 4258: with the assumption that the X–ray emitting region has a disk–corona configuration and given the high inclination angle of the accretion disk in this source, proper evaluation of the Comptonization effects enabled us to find less strict limits on the EW of a putative broad iron Kα line, thus explaining its non-detection. Besides, according to this picture, the narrow iron line observed in this object is believed to originate from matter not associated with the accretion disk since, otherwise, it would require an uncomptonized (i.e. before Comptonization) line with too large an equivalent width.

  We also find that the presence of a comptonizing corona can produce and/or emphasize the correlations between the reflection features (iron line equivalent width or covering fraction) and the X-ray spectral index. Then, similarly to the effects produced by a bad representation of the complex ionization pattern expected at the surface of the X-ray–irradiated reflecting material, these different effects are to be properly taken into account to correctly interpret these correlations.

  Finally, we underline the possible importance of Comptonization effects on the reflection shape when dealing with accurate spectral fitting of the X-ray background. Indeed, there is evidence that the observed peak of the X-ray background is located at slightly higher energies than those predicted by the standard models that neglect the effect of Comptonization in the corona.

- *Chapter 4: Spectral models for the cold accretion disc.* In this Chapter we have studied the spectrum emitted from a standard, geometrically thin and optically thick accretion disc. In particular, we have focussed our study on the interpretation of the multicolour disc (MCD) spectral model. It is the most commonly used phenomenological model for the spectrum of a standard accretion disc in the analysis of the data from GBHC in their *high/soft* or *very high* states. Taken at face value, the two fitting parameters of the model allow us to estimate the temperature of the inner disc and its distance from the black hole, thus giving crucial pieces of information on the inner accretion flow geometry and, consequently, on the parameters of the central gravitational source (first and foremost its mass and angular momentum). By simulating accretion disc spectra with a more realistic model, that takes into account the temperature stratification in the vertical direction by solving self-consistently the radiative transfer equation using a Fokker-Planck/diffusion approximation, we have shown that MCD models systematically underestimate the value of the inner radius of the accretion disc for a black hole candidate. We also have shown that the spectral hardening factor $f_{\rm col}$, which is needed to correct the results of the fits with a multicolour model, is not, as is usually assumed, constant when the accretion rate and/or fractional coronal activity change. In the light of our findings, it is quite possible that dramatic changes in the disc spectrum, such as those associated with state transitions in GBHC, are produced by changes in the surface properties of the accretion disc, rather than by the disappearance of the entire inner regions. This, unfortunately, is hard to model theoretically. It would be interesting, for example, to assess the problem in the extreme case when almost all the accretion power is dissipated in the corona (i.e. in the limit $f \rightarrow 1$). To do that we would need to take into account the X-ray reflection spectra of discs illuminated by a hot corona and to model carefully the heating of the disc atmosphere.

- *Chapter 5: Aperiodic time variability in black hole accretion flows.* This chapter has been devoted to the discussion of different aspects of the aperiodic time variability in sources powered by accretion onto a central black hole. In Section 5.2 a model (the 'thundercloud model') for the temporal and spectral short-time variability produced by a structured magnetic corona has been presented. The model explains the correlations between X-ray flux and spectral slope and between X-ray flux and rms variability, observed in a number of Seyfert galaxies and galactic black hole candidates on timescales comparable to the dynamical one. It represent an attempt to bridge together the pieces of information on the inner accretion flow, and in particular on the geometry and physical state of the hot comptonizing component of the flow (the corona), provided separately by spectral and temporal analysis. The analysis of the broad band variability component (noise) of the observed power density spectra of such sources, and in particular of the spectral variability on the very short timescales that we can probe with the X-ray emission of AGN, has allowed us to put new constraints on the geometry (in particular on the typical height of a coronal active region and on the total average covering fraction), optical depth, and temperature of the corona for the case of one of the best studied Seyfert 1 galaxies, MCG–6-30-15. The final section of the chapter (§5.3), instead, dealt with a new discovery regarding the aperiodic time variability of γ-ray bursts, namely a correlation between the duration of the periods of quiescence sometimes found in long bursts and the duration of the following emission episodes. Although our theoretical understanding of the central engines of GRBs is still far from complete, we have discussed here how our findings could be used to discover and elaborate new paradigms for the emission mechanisms of γ-ray bursts, in the framework of models that envisage a stellar mass black hole accreting at very high rates from a nuclear torus as the power-house of GRBs. Indeed, we argue that the wealth of information contained in the complicated temporal structure of the longer bursts bear many analogies with that contained in the lightcurve of 'standard' accreting black holes. Such information could be used to probe the accretion flow itself, the viscous mechanisms by which the angular momentum is transported outwards, the magnetic field involved in this process and the energetics of the corona produced by the flow.

- *Chapter 6: A powerful magnetic corona in the black hole candidate XTE J1118+480.* In this final chapter we have applied the model for the emission from a highly magnetic, structured corona developed in the previous chapters to the multi-wavelength observations of the newly discovered X-ray transient XTE J1118+480. This source is unique for a number of reasons. It is located at high galactic latitude and therefore suffers for very little galactic extinction, thus allowing almost full spectral coverage from the FIR to the hard X-rays with unprecedented sensitivity. According to our model, XTE J1118+480 reveals an accretion flow at very low $\dot{m}$ ($\sim 4 \times 10^{-3}$), in which the corona is a dominant repository of the gravitational power, and a powerful outflow is produced in the corona. By fitting the complete SED, we have derived constraints for the approximate number, size, elevation, optical depth and magnetic field strengths of the coronal active regions. Another peculiarity of this source is the simultaneous presence of a strong quasi periodic feature in the optical and X-ray lightcurves. This clearly suggests that the fluxes in the two bands both originate from the same region in the inner part of the accretion flow. Self-absorbed cyclo-synchrotron emission is the natural candidate to explain the optical variability. Such emission is expected in any magnetic corona model, and the inferred magnetic field value ($B \approx 2.5 \times 10^7$ G) is the one predicted to arise when the source is in the *hard* state (low value of $\dot{m}$ and high value of f).

7.1 Future work

7.1.1 Coronal outflows

In Section 2.5 we have explored a new idea regarding the role of a magnetic corona in launching the powerful jets/outflows observed in many accreting black holes. The basic energetics of the coronal region we have discussed, suggest that indeed the dynamical role of the magnetic field in that region is a key ingredient to link accretion disc and jet physics, and I intend to pursue the research to understand this link in the future. Possible lines of future research include: a study of the magnetic field configuration in the inner corona, to assess the relative occurrence of either open closed field lines and their relevance for the jet production; a study of the relationships between the inner accretion flow geometry and the kinematics of the coronal outflow, aimed at understanding the differences between highly relativistic collimated jets and slower outflows and the velocity structure of such outflows in the polar direction; more sophisticated spectral modeling, which includes non-thermal electron distribution in the corona produced at the reconnection sites, where the magnetic field is dissipated; an assessment of the influence of the outflowing coronae on the inner cold accretion disc structure in order to evaluate the extent to which the disc itself may be disrupted (or evaporated) by the corona; study of the disc–corona interaction at high accretion rates in order to better understand the accretion/outflow geometry of GBHC in the *very high* state.

7.1.2 Magnetic flare models and X-ray spectral variability

Magnetic flares models, as the thundercloud one (§5.2) can be refined to gain more insight into the emission processes of AGNs, and their spectral variability. For example, a time-dependent model for the corona such as the one we have presented in this thesis could be matched with a photoionization code (Ballantyne *et al.*, 2001) to compute the temporal evolution of the accretion disc atmosphere and of the reflection features it gives rise to. In fact, one of the most puzzling spectral variability patterns observed recently in AGN light-curves is the lack of clear correlation between the X-ray continuum and the fluorescent iron Kα line. Indeed, in the framework of the thundercloud model, such complicated behaviour can be explained by the fact that the observed line at any time is the super-position of different features produced by active regions illuminating the disc with different spectral shape and intensity. The ionization properties of the surface of the accretion disc, which in turn determine the line characteristics, are strongly dependent on the illuminating continuum properties. Therefore, the observed iron line is expected to be complex, and variable on a wide range of timescales in a complicated way.

7.1.3 Models for the accretion disc spectra

The work presented here in §4 has been done for non-rotating black holes in the Newtonian approximation, but can be extended in order to include rapidly rotating black holes in a fully relativistic treatment. Such a study will be relevant to the understanding of the Ultra-Luminous X-ray sources (ULXs) in nearby galaxies in the light of the results from the new X-ray satellites *Chandra* and *XMM-Newton*. These sources are dominated by a strong thermal disk-like component Makishima *et al.* (2000), and our model could help in better constrain the central source parameters.

7.1.4 Time variability in galactic black hole candidates

It will be important also to assess the role of the magnetic field on the black hole time variability. In particular, in a magnetically dominated, patchy corona a whole spectrum of oscillation should be excited, as in the solar corona, whose frequencies depends both on the strong gravitational potential of the central source and on the magnetic field strength. The ultimate goal of such a study would be to be to find a way to distinguish in the time variability data, the signatures of both general relativistic effects and strong magnetic fields.

7.1.5 Internal shock and temporal structures in gamma-ray bursts

The physics of Gamma-ray bursts is intertwined with that of black holes, and indeed many physical processes are thought to be at work in both classes of sources, as we have discussed in §5.3. Thus, I consider GRBs astrophysics as an active field of my future research work, that could involve a number of open issues as the nature of the central engine, the rapid variability in the γ-ray lightcurve and the relevance of synchrotron and inverse Compton processes in determining the bursts spectral properties.

Bibliography

Abramowicz, M. A. (1998). Physics of black hole accretion. In *Theory of Black Hole Accretion Disks*, page 50.

Abramowicz, M. A., Chen, X., Kato, S., Lasota, J., and Regev, O. (1995). Thermal equilibria of accretion disks. *ApJ*, **438**, L37–L39.

Abramowicz, M. A., Lasota, J., and Igumenshchev, I. V. (2000). On the absence of winds in advection-dominated accretion flows. *MNRAS*, **314**, 775–781.

Aly, J. J. (1990a). *Comp. Phys. Comm.*, **59**, 13.

Aly, J. J. (1990b). Storage and release of magnetic energy in a force-free field. In *IAU Symp. 142: Basic Plasma Processes on the Sun*, volume 142, page 313.

Amari, T., Luciani, J. F., Aly, J. J., and Tagger, M. (1996). Very fast opening of a three-dimensional twisted magnetic flux tube. *ApJ*, **466**, L39.

Antonucci, R. (1993). Unified models for active galactic nuclei and quasars. *ARA&A*, **31**, 473–521.

Araya-Gòchez, R. A. (1999). Hydromagnetic energy conversion and prompt collimation in mildly advective, Kerr black holes. *MNRAS, submitted. astro-ph/9912324*.

Armitage, P. J. and Natarajan, P. (1999). The Blandford-Znajek mechanism and the emission from isolated accreting black holes. *ApJ*, **523**, L7–L10.

Baganoff, F. K., Bautz, M. W., Brandt, W. N., Chartas, G., Feigelson, E. D., Garmire, G. P., Maeda, Y., Morris, M., Ricker, G. R., Townsley, L. K., and Walter, F. (2001). Rapid X-ray flaring from the direction of the supermassive black hole at the Galactic Centre. *Nature*, **413**, 45–48.

Bai, T. and Ramaty, R. (1978). Backscatter, anisotropy, and polarization of solar hard X-rays. *ApJ*, **219**, 705–726.

Bak, P., Tang, C., and Wiesenfeld, K. (1987). Self-organized criticality - An explanation of $1/f$ noise. *Physical Review Letters*, **59**, 381–384.

Balbus, S. A. and Hawley, J. F. (1991). A powerful local shear instability in weakly magnetized disks. I - Linear analysis. II - Nonlinear evolution. *ApJ*, **376**, 214–233.

Balbus, S. A. and Hawley, J. F. (1998). Instability, turbulence, and enhanced transport in accretion disks. *Rev. Mod. Phys.*, **70**, 1–53.

Ballantyne, D. R. and Ross, R. R. (2001). The responce of the Fe Kα line to changes in the X-ray illumination of accretion discs. *MNRAS, submitted.*

Ballantyne, D. R., Ross, R. R., and Fabian, A. C. (2001). Ionized iron lines in X-ray reflection spectra. *MNRAS, in press. astro-ph/0102040.*

Bardeen, J. M. and Petterson, J. A. (1975). The Lense-Thirring effect and accretion disks around Kerr black holes. *ApJ*, **195**, L65.

Begelman, M. C. and Chiueh, T. (1988). Thermal coupling of ions and electrons by collective effects in two-temperature accretion flows. *ApJ*, **332**, 872–890.

Begelman, M. C. and Meier, D. L. (1982). Thick accretion disks - Self-similar, supercritical models. *ApJ*, **253**, 873–896.

Belloni, T., Mendez, M., King, A. R., van der Klis, M., and van Paradijs, J. (1997a). A unified model for the spectral variability in GRS 1915+105. *ApJ*, **488**, L109.

Belloni, T., Mendez, M., King, A. R., van der Klis, M., and van Paradijs, J. (1997b). An unstable central disk in the superluminal black hole X-ray binary GRS 1915+105. *ApJ*, **479**, L145.

Belloni, T., Klein-Wolt, M., Méndez, M., van der Klis, M., and van Paradijs, J. (2000a). A model-independent analysis of the variability of GRS 1915+105. *A&A*, **355**, 271–290.

Belloni, T., Migliari, S., and Fender, R. P. (2000b). Disk mass accretion rate and infrared flares in GRS 1915+105. *A&A*, **358**, L29–L32.

Beloborodov, A. M. (1998). Super-Eddington accretion discs around Kerr black holes. *MNRAS*, **297**, 739–746.

Beloborodov, A. M. (1999). Plasma ejection from magnetic flares and the X-ray spectrum of Cygnus X-1. *ApJ*, **510**, L123–L126.

Beloborodov, A. M., Stern, B. E., and Svensson, R. (2000). Power Density Spectra of Gamma-ray bursts. *ApJ*, **535**, 158–166.

Berger, K., Anderson, R. B., and Kröninger, H. (1975). *Electra*, **80**, 23.

Bisnovatyi-Kogan, G. S. and Lovelace, R. V. E. (1997). Influence of Ohmic heating on advection-dominated accretion flows. *ApJ*, **486**, L43.

Björnsson, G. and Svensson, R. (1992). Hot pair-dominated accretion disks. *ApJ*, **394**, 500–514.

Björnsson, G., Abramowicz, M. A., Chen, X., and Lasota, J. (1996). Hot accretion disks revisited. *ApJ*, **467**, 99.

Blackman, E. G. (1996). Overcoming the backreaction on turbulent motions in the presence of magnetic fields. *Phys. Rev. Lett.*, **77**, 2694–2697.

Blandford, R. D. and Begelman, M. C. (1999). On the fate of gas accreting at a low rate on to a black hole. *MNRAS*, **303**, L1–L5.

Blandford, R. D. and Konigl, A. (1979). Relativistic jets as compact radio sources. *ApJ*, **232**, 34–48.

Blandford, R. D. and Payne, D. G. (1982). Hydromagnetic flows from accretion discs and the production of radio jets. *MNRAS*, **199**, 883–903.

Blandford, R. D. and Znajek, R. L. (1977). Electromagnetic extraction of energy from Kerr black holes. *MNRAS*, **179**, 433–456.

Brandenburg, A. (1998). Disc turbulence and viscosity. In *Theory of Black Hole Accretion Disks*, page 61.

Brandenburg, A., Nordlund, A., Stein, R. F., and Torkelsson, U. (1995). Dynamo-generated turbulence and large-scale magnetic fields in a Keplerian shear flow. *ApJ*, **446**, 741.

Burm, H. and Kuperus, M. (1988). Accretion disk coronae and the contribution to angular-momentum transport in the disk. *A&A*, **192**, 165–169.

Campana, S. and Pardi, M. C. (1993). Do molecular clouds contain accreting black holes? *A&A*, **277**, 477.

Capetti, A., de Ruiter, H. R., Fanti, R., Morganti, R., Parma, P., and Ulrich, M.-H. (2000). The HST snapshot survey of the B2 sample of low luminosity radio-galaxies: a picture gallery. *A&A*, **362**, 871–885.

Carter, B. (1968). Global structure of the Kerr family of gravitational field. *Phys. Rev.*, **174**, 1559.

Celotti, A., Fabian, A. C., and Rees, M. J. (1992). Dense thin clouds in the central regions of active galactic nuclei. *MNRAS*, **255**, 419–422.

Chandrasekhar, S. (1960). *Proc. Nat. Acad. Sci. USA*, **46**, 253.

Charles, P. (1998). Black holes in our Galaxy: observations. In *Theory of Black Hole Accretion Disks*, page 1.

Chaty, S., Haswell, C. A., Smith, G. P., Smail, I., and Hynes, R. I. (2000). XTE J1118+480. *IAU Circular*, **7394**, 3.

Chen, K., Halpern, J. P., and Filippenko, A. V. (1989). Kinematic evidence for a relativistic Keplerian disk - ARP 102B. *ApJ*, **339**, 742–751.

Chen, X., Abramowicz, M. A., Lasota, J., Narayan, R., and Yi, I. (1995). Unified description of accretion flows around black holes. *ApJ*, **443**, L61–L64.

Chiaberge, M., Capetti, A., and Celotti, A. (1999). The HST view of FR I radio galaxies: evidence for non-thermal nuclear sources. *A&A*, **349**, 77–87.

Chiang, J., Reynolds, C. S., Blaes, O. M., Nowak, M. A., Murray, N., Madejski, G., Marshall, H. L., and Magdziarz, P. (2000). Simultaneous EUVE/ASCA/RXTE Observations of NGC 5548. *ApJ*, **528**, 292–305.

Ciaravella, A., Raymond, J. C., Strachan, L., Thompson, B. J., Cyr, O. C. S., Gardner, L., Modigliani, A., Antonucci, E., Kohl, J., and Noci, G. (1999). Ultraviolet and optical observations of a coronal transient with SOHO. *ApJ*, **510**, 1053–1063.

Ciaravella, A., Raymond, J. C., Thompson, B. J., van Ballegooijen, A., Strachan, L., Li, J., Gardner, L., O'Neal, R., Antonucci, E., Kohl, J., and Noci, G. (2000). Solar and Heliospheric Observatory observations of a helical coronal mass ejection. *ApJ*, **529**, 575–591.

Claussen, M. J., Heiligman, G. M., and Lo, K. Y. (1984). Water-vapor maser emission from galactic nuclei. *Nature*, **310**, 298–300.

Costa, E., Frontera, F., Heise, J., Feroci, M., in 't Zand, J., Fiore, F., Cinti, M. N., dal Fiume, D., Nicastro, L., Orlandini, M., Palazzi, E., Rapisarda, M., Zavattini, G., Jager, R., Parmar, A., Owens, A., Molendi, S., Cusumano, G., Maccarone, M. C., Giarrusso, S., Coletta, A., Antonelli, L. A., Giommi, P., Muller, J. M., Piro, L., and Butler, R. C. (1997). Discovery of an X-ray afterglow associated with the gamma-ray burst of 28 February 1997. *Nature*, **387**, 783–785.

Crawford, C. S., Gandhi, P., Fabian, A. C., Wilman, R. J., Johnstone, R. M., Barger, A. J., and Cowie, L. L. (2001). Multi-wavelength observations of serendipitous Chandra X-ray sources in the field of A2390. *MNRAS, submitted. astro-ph/0106067*.

Cui, W., Zhang, S. N., and Chen, W. (1998). Evidence for frame dragging around spinning black holes in X-ray binaries. *ApJ*, **492**, L53.

della Ceca, R., Lamorani, G., Maccacaro, T., Wolter, A., Griffiths, R., Stocke, J. T., and Setti, G. (1994). The properties of X-ray selected active galactic nuclei. 3: The radio-quiet versus radio-loud samples. *ApJ*, **430**, 533–544.

Dermer, C. D. (1997). Accreting isolated black holes and the unidentified EGRET sources. In *AIP Conf. Proc. 410: Proceedings of the Fourth Compton Symposium*, page 1275.

Di Matteo, T. (1998). Magnetic reconnection: flares and coronal heating in active galactic nuclei. *MNRAS*, **299**, L15.

di Matteo, T. and Psaltis, D. (1999). Quasi-periodic variability and the inner radii of thin accretion disks in galactic black hole systems. *ApJ*, **526**, L101–L104.

Di Matteo, T., Celotti, A., and Fabian, A. C. (1997a). Cyclo-synchrotron emission from magnetically dominated active regions above accretion discs. *MNRAS*, **291**, 805.

Di Matteo, T., Blackman, E. G., and Fabian, A. C. (1997b). Two-temperature coronae in active galactic nuclei. *MNRAS*, **291**, L23–L27.

Di Matteo, T., Celotti, A., and Fabian, A. C. (1999). Magnetic flares in accretion disc coronae and the spectral states of black hole candidates: the case of GX339-4. *MNRAS*, **304**, 809–820.

Di Matteo, T., Johnstone, R. M., Allen, S. W., and Fabian, A. C. (2001a). Accretion onto Nearby Supermassive Black Holes: Chandra Constraints on the Dominant Cluster Galaxy NGC 6166. *ApJ*, **550**, L19–L23.

Di Matteo, T., Carilli, C. L., and Fabian, A. C. (2001b). Limits on the accretion rates onto massive black holes in nearby galaxies. *ApJ*, **547**, 731–739.

Done, C. (2001). Galactic black hole binary systems. In *Proc. of the 33rd COSPAR Scientific Assembly. Warsaw, Poland.* To appear in Advances for Space Research. astro-ph/0012380.

Done, C. and Nayakshin, S. (2001). Observational signatures of X-ray–irradiated accretion disks. *ApJ*, **546**, 419–428.

Done, C. and Zycki, P. T. (1999). Relativistic distortions in the X-ray spectrum of CYG X-1. *MNRAS*, **305**, 457–468.

Done, C., Madejski, G. M., and Życki, P. T. (2000). The relativistic iron line profile in the Seyfert 1 galaxy IC 4329A. *ApJ*, **536**, 213–224.

Duncan, R. C. and Thompson, C. (1992). Formation of very strongly magnetized neutron stars – Implications for gamma-ray bursts. *ApJ*, **392**, L9–L13.

Ebisawa, K., Ogawa, M., Aoki, T., Dotani, T., Takizawa, M., Tanaka, Y., Yoshida, K., Miyamoto, S., Iga, S., Hayashida, K., Kitamoto, S., and Terada, K. (1994). Spectral evolution of the bright X-ray nova GS 1124-68 (Nova MUSCAE 1991) observed with GINGA. *PASJ*, **46**, 375–394.

Edelson, R. and Nandra, K. (1999). A cutoff in the X-ray fluctuation power density spectrum of the Seyfert 1 Galaxy NGC 3516. *ApJ*, **514**, 682–690.

Edelson, R., Turner, T. J., Pounds, K., Vaughan, S., Markowitz, A., Marshall, H., Dobbie, P., and Warwick, R. (2001). X-ray spectral variability and rapid variability of the soft X-ray spectrum Seyfert 1 galaxies Ark 564 and Ton S180. *ApJ, in press. astro-ph/0108387.*

Elvis, M., Wilkes, B. J., McDowell, J. C., Green, R. F., Bechtold, J., Willner, S. P., Oey, M. S., Polomski, E., and Cutri, R. (1994). Atlas of quasar energy distributions. *ApJS*, **95**, 1–68.

Esin, A. A., Narayan, R., Cui, W., Grove, J. E., and Zhang, S. (1998). Spectral transitions in Cygnus X-1 and other black hole X-ray binaries. *ApJ*, **505**, 854–868.

Esin, A. A., McClintock, J. E., Drake, J. J., Garcia, M. R., Haswell, C. A., Hynes, R. I., and Muno, M. P. (2001). Modeling the low-state spectrum of the X-ray Nova XTE J1118+480. *ApJ*, **555**, 483–488.

Fabian, A. C. (1999). The obscured growth of massive black holes. *MNRAS*, **308**, L39–L43.

Fabian, A. C., Guilbert, P. W., Motch, C., Ricketts, M., Ilovaisky, S. A., and Chevalier, C. (1982). GX 339-4 – Cyclotron radiation from an accretion flow. *A&A*, **111**, L9.

Fabian, A. C., Iwasawa, K., Reynolds, C. S., and Young, A. J. (2000). Broad iron lines in Active Galactic Nuclei. *PASP*, **112**, 1145–1161.

Falcke, H. (2001). The silent majority: Jets and radio cores from low-luminosity black holes. *Rev. Mod. Astronom.*, **14**, 31.

Falcke, H. and Markoff, S. (2000). The jet model for Sgr A*: Radio and X-ray spectrum. *A&A*, **362**, 113–118.

Falcke, H., Nagar, N. M., Wilson, A. S., and Ulvestad, J. S. (2000). Radio sources in Low-Luminosity Active Galactic Nuclei. II. Very Long Baseline Interferometry detections of compact radio cores and jets in a sample of LINERs. *ApJ*, **542**, 197–200.

Fanaroff, B. L. and Riley, J. M. (1974). The morphology of extragalactic radio sources of high and low luminosity. *MNRAS*, **167**, 31P–36P.

Fender, R., Corbel, S. ., Tzioumis, T., McIntyre, V., Campbell-Wilson, D., Nowak, M., Sood, R., Hunstead, R., Harmon, A., Durouchoux, P., and Heindl, W. (1999). Quenching of the radio jet during the X-ray high state of GX 339-4. *ApJ*, **519**, L165–L168.

Fender, R. P. (2001). Powerful jets from black hole X-ray binaries in low/hard X-ray states. *MNRAS*, **322**, 31–42.

Fender, R. P., Hjellming, R. M., Tilanus, R. P. J., Pooley, G. G., Deane, J. R., Ogley, R. N., and Spencer, R. E. (2001). Spectral evidence for a powerful compact jet from XTE J1118+480. *MNRAS*, **322**, L23–L27.

Fenimore, E. E. and Ramirez-Ruiz, E. (1999). The observational basis for central engines in Gamma-ray bursts. In *ASP Conf. Ser. 190: Gamma-Ray Bursts: The First Three Minutes*, page 67.

Ferland, G. J., Korista, K. T., Verner, D. A., Ferguson, J. W., Kingdon, J. B., and Verner, E. M. (1998). CLOUDY 90: Numerical simulation of plasmas and their spectra. *PASP*, **110**, 761–778.

Ferrarese, L. and Merritt, D. (2000). A fundamental relation between supermassive black holes and their host galaxies. *ApJ*, **539**, L9–L12.

Fiore, F., Pellegrini, S., Matt, G., Antonelli, L. A., Comastri, A., della Ceca, R., Giallongo, E., Mathur, S., Molendi, S., Siemiginowska, A., Trinchieri, G., and Wilkes, B. (2001). The BeppoSAX view of the X-ray active nucleus of NGC 4258. *ApJ*, **556**, 150–157.

Foster, A. J., Fabian, A. C., and Ross, R. R. (1986). Neutron star model atmospheres - A comparison with MXB 1728-34. *MNRAS*, **221**, 409–426.

Frail, D. A., Kulkarni, S. R., Nicastro, S. R., Feroci, M., and Taylor, G. B. (1997). The radio afterglow from the gamma-ray burst of 8 May 1997. *Nature*, **389**, 261–263.

Frank, J., King, A., and Raine, D. (1992). *Accretion power in astrophysics.* Cambridge University Press, 1992.

Frontera, F., Zdziarski, A. A., Amati, L., Mikolajewska, J., Belloni, T., Del Sordo, S., Haardt, F., Kuulkers, E., Masetti, N., Orlandini, M., Palazzi, E., Parmar, A. N., Remillard, R. A., Santangelo, A., and Stella, L. (2001a). A measurement of the broadband spectrum of XTE J1118+480 with BeppoSAX and its astrophysical implications. *ApJ, in press.* astro-ph/0107199.

Frontera, F., Palazzi, E., Zdziarski, A. A., Haardt, F., Perola, G. C., Chiappetti, L., Cusumano, G., Dal Fiume, D., Del Sordo, S., Orlandini, M., Parmar, A. N., Piro, L., Santangelo, A., Segreto, A., Treves, A., and Trifoglio, M. (2001b). Broadband spectrum of Cygnus X-1 in two spectral states with BeppoSAX. *ApJ*, **546**, 1027–1037.

Fujita, Y., Inoue, S., Nakamura, T., Manmoto, T., and Nakamura, K. E. (1998). Emission from isolated black holes and MACHOs accreting from the interstellar medium. *ApJ*, **495**, L85.

Göğüş , E., Woods, P. M., Kouveliotou, C., van Paradijs, J., Briggs, M. S., Duncan, R. C., and Thompson, C. (1999). Statistical properties of SGR 1900+14 bursts. *ApJ*, **526**, L93–L96.

Galeev, A. A., Rosner, R., and Vaiana, G. S. (1979). Structured coronae of accretion disks. *ApJ*, **229**, 318–326.

Garcia, M., Brown, W., Pahre, M., McClintock, J., Callanan, P., and Garnavich, P. (2000). XTE J1118+480. *IAU Circular*, **7392**, 2.

Gebhardt, K., Bender, R., Bower, G., Dressler, A., Faber, S. M., Filippenko, A. V., Green, R., Grillmair, C., Ho, L. C., Kormendy, J., Lauer, T. R., Magorrian, J., Pinkney, J., Richstone, D., and Tremaine, S. (2000). A relationship between nuclear black hole mass and galaxy velocity dispersion. *ApJ*, **539**, L13–L16.

Georgantopoulos, I. and Papadakis, I. E. (2001). RXTE observations of Seyfert 2 galaxies: evidence for spectral variability. *MNRAS*, **322**, 218–230.

George, I. M. and Fabian, A. C. (1991). X-ray reflection from cold matter in active galactic nuclei and X-ray binaries. *MNRAS*, **249**, 352–367.

Ghisellini, G. and Celotti, A. (2001). The dividing line between FR I and FR II radio–galaxies. *submitted to A&A. astro-ph/0106570.*

Ghisellini, G., Guilbert, P. W., and Svensson, R. (1988). The synchrotron boiler. *ApJ*, **334**, L5–L8.

Ghisellini, G., Haardt, F., and Matt, G. (1994). The contribution of the obscuring torus to the X-ray spectrum of Seyfert galaxies – A test for the unification model. *MNRAS*, **267**, 743.

Ghisellini, G., Lazzati, D., Celotti, A., and Rees, M. J. (2000). Compton dragged gamma-ray bursts: the spectrum. *MNRAS*, **316**, L45–L49.

Gierliński, M., Zdziarski, A. A., Poutanen, J., Coppi, P. S., Ebisawa, K., and Johnson, W. N. (1999). Radiation mechanisms and geometry of Cygnus X-1 in the soft state. *MNRAS*, **309**, 496–512.

Gierlinski, M., Zdziarski, A. A., Done, C., Johnson, W. N., Ebisawa, K., Ueda, Y., Haardt, F., and Phlips, B. F. (1997). Simultaneous X-ray and gamma-ray observations of CYG X-1 in the hard state by GINGA and OSSE. *MNRAS*, **288**, 958–964.

Gilfanov, M., Churazov, E., and Revnivtsev, M. (1999). Reflection and noise in Cygnus X-1. *A&A*, **352**, 182–188.

Gilfanov, M., Churazov, E., and Revnivtsev, M. (2000). Comptonization, reflection and noise in black hole binaries. In *Proc. of the 5th CAS/MPG Workshop on High Energy Astrophysics*. astro-ph/0002415.

Gilli, R., Salvati, M., and Hasinger, G. (2001). Testing current synthesis models of the X-ray background. *A&A*, **366**, 407–417.

Green, A. R., McHardy, I. M., and Lehto, H. J. (1993). On the nature of rapid X-ray variability in active galactic nuclei. *MNRAS*, **265**, 664.

Grove, J. E., Johnson, W. N., Kroeger, R. A., McNaron-Brown, K., Skibo, J. G., and Phlips, B. F. (1998). Gamma-ray spectral states of galactic black hole candidates. *ApJ*, **500**, 899.

Guainazzi, M., Matt, G., Molendi, S., Orr, A., Fiore, F., Grandi, P., Matteuzzi, A., Mineo, T., Perola, G. C., Parmar, A. N., and Piro, L. (1999). BeppoSAX confirms extreme relativistic effects in the X-ray spectrum of MCG-6-30-15. *A&A*, **341**, L27–L30.

Haardt, F. (1994). Ph.D. thesis, SISSA, Trieste.

Haardt, F. and Maraschi, L. (1991). A two-phase model for the X-ray emission from Seyfert galaxies. *ApJ*, **380**, L51–L54.

Haardt, F. and Maraschi, L. (1993). X-ray spectra from two-phase accretion disks. *ApJ*, **413**, 507–517.

Haardt, F., Done, C., Matt, G., and Fabian, A. C. (1993). The high-energy spectrum of Cygnus X-1 revisited. *ApJ*, **411**, L95–L98.

Haardt, F., Maraschi, L., and Ghisellini, G. (1994). A model for the X-ray and ultraviolet emission from Seyfert galaxies and galactic black holes. *ApJ*, **432**, L95–L99.

Haardt, F., Maraschi, L., and Ghisellini, G. (1997). X-ray variability and correlations in the two-phase disk-corona model for Seyfert galaxies. *ApJ*, **476**, 620.

Hasinger, G., Altieri, B., Arnaud, M., Barcons, X., Bergeron, J., Brunner, H., Dadina, M., Dennerl, K., Ferrando, P., Finoguenov, A., Griffiths, R. E., Hashimoto, Y., Jansen, F. A., Lumb, D. H., Mason, K. O., Mateos, S., McMahon, R. G., Miyaji, T., Paerels, F., Page, M. J., Ptak, A. F., Sasseen, T. P., Schartel, N., Szokoly, G. P., Trümper, J., Turner, M., Warwick, R. S., and Watson, M. G. (2001). XMM-Newton observation of the Lockman Hole. I. The X-ray data. *A&A*, **365**, L45–L50.

Haswell, C. A., Hynes, R. I., King, A. R., Stull, J., Ioannou, Z., and Webb, N. A. (2000a). XTE J1118+480. *IAU Circular*, **7407**, 1.

Haswell, C. A., Skillman, D., Patterson, J., Hynes, R. I., and Cui, W. (2000b). XTE J1118+480. *IAU Circular*, **7427**, 1.

Herrnstein, J. R., Moran, J. M., Greenhill, L. J., Diamond, P. J., Inoue, M., Nakai, N., Miyoshi, M., Henkel, C., and Riess, A. (1999). A geometric distance to the galaxy NGC 4258 from orbital motions in a nuclear gas disk. *Nature*, **400**, 539–541.

Heyvaerts, J. F. and Priest, E. R. (1989). A model for a non-Keplerian magnetic accretion disk with a magnetically heated corona. *A&A*, **216**, 230–244.

Ho, L. C. (1999). The Spectral Energy Distributions of Low-Luminosity Active Galactic Nuclei. *ApJ*, **516**, 672–682.

Ho, L. C. and Peng, C. Y. (2001). Nuclear luminosities and radio loudness of Seyfert nuclei. *ApJ*, **555**, 650–662.

Ho, L. C., Feigelson, E. D., Townsley, L. K., Sambruna, R. M., Garmire, G. P., Brandt, W. N., Filippenko, A. V., Griffiths, R. E., Ptak, A. F., and Sargent, W. L. W. (2001). Detection of nuclear X-ray sources in nearby galaxies with Chandra. *ApJ*, **549**, L51–L54.

Homan, J., Wijnands, R., van der Klis, M., Belloni, T., van Paradijs, J., Klein-Wolt, M., Fender, R., and Méndez, M. (2001). Correlated X-ray spectral and timing behavior of the black hole candidate XTE J1550-564: A new interpretation of black hole states. *ApJS*, **132**, 377–402.

Honma, F. (1996). Global structure of bimodal accretion disks around a black hole. *PASJ*, **48**, 77–87.

Hua, X. and Lingenfelter, R. E. (1992). Angle-dependent Green's functions for relativistic Compton reflection. *ApJ*, **397**, 591–599.

Hynes, R. I., Mauche, C. W., Haswell, C. A., Shrader, C. R., Cui, W., and Chaty, S. (2000). The X-ray transient XTE J1118+480: Multiwavelength observations of a low-state minioutburst. *ApJ*, **539**, L37–L40.

Ichimaru, S. (1977). Bimodal behavior of accretion disks - Theory and application to Cygnus X-1 transitions. *ApJ*, **214**, 840–855.

Igumenshchev, I. V. and Abramowicz, M. A. (2000). Two-dimensional models of hydrodynamical accretion flows into black holes. *ApJS*, **130**, 463–484.

Igumenshchev, I. V., Abramowicz, M. A., and Narayan, R. (2000). Numerical simulations of convective accretion flows in three dimensions. *ApJ*, **537**, L27–L30.

Illarionov, A. F. and Syunyaev, R. A. (1972). Compton scattering by thermal electrons in X-ray sources. *Astron. Zh.*, **49**, 58.

Ipser, J. R. and Price, R. H. (1982). Synchrotron radiation from spherically accreting black holes. *ApJ*, **255**, 654–673.

Ipser, J. R. and Price, R. H. (1983). Comptonization effects in spherical accretion onto black holes. *ApJ*, **267**, 371–383.

Janiuk, A. and Czerny, B. (2000). Properties of the two-temperature corona model for active galactic nuclei and galactic black hole X-ray binaries. *New Astronomy*, **5**, 7–24.

Kanbach, G., Straubmeier, C., Spruit, H. C., and Belloni, T. (2001). Correlated msec X-ray and optical emission from XTE J1118+480. *Nature, in press. astro-ph/0108199.*

Katz, J. I. (1977). X-rays from spherical accretion onto degenerate dwarfs. *ApJ*, **215**, 265–275.

Kerr, R. P. (1963). Gravitational field of a spinning mass as an example of algebraically special metrics. *Phys. Rev. Lett.*, **11**, 237.

Klimchuk, J. A., Antiochos, S. K., and Norton, D. (2000). Twisted coronal magnetic loops. *ApJ*, **542**, 504–512.

Kluźniak, W. and Ruderman, M. (1998). The central engine of Gamma-ray bursters. *ApJ*, **508**, L113–L113.

Kormendy, J. and Richstone, D. (1995). Inward bound—The search for supermassive black holes in galactic nuclei. *ARA&A*, **33**, 581.

Koshut, T. M., Kouveliotou, C., Paciesas, W. S., van Paradijs, J., Pendleton, G. N., Briggs, M. S., Fishman, G. J., and Meegan, C. A. (1995). Gamma-ray burst precursor activity as observed with BATSE. *ApJ*, **452**, 145.

Kouveliotou, C., Meegan, C. A., Fishman, G. J., Bhat, N. P., Briggs, M. S., Koshut, T. M., Paciesas, W. S., and Pendleton, G. N. (1993). Identification of two classes of gamma-ray bursts. *ApJ*, **413**, L101–L104.

Kouveliotou, C., Dieters, S., Strohmayer, T., van Paradijs, J., Fishman, G. J., Meegan, C. A., Hurley, K., Kommers, J., Smith, I., Frail, D., and Murakami, T. (1998). An X-ray pulsar with a superstrong magnetic field in the soft gamma-ray repeater SGR 1806-20. *Nature*, **393**, 235–237.

Krolik, J. H. (1999). Instabilities in α-disks. In *ASP Conf. Ser. 161: High Energy Processes in Accreting Black Holes*, page 315.

Kusunose, M. and Mineshige, S. (1995). Hot accretion disks with nonthermal pairs. *ApJ*, **440**, 100–107.

Kusunose, M. and Zdziarski, A. A. (1994). Hot accretion disks with pairs: Effects of magnetic field and thermal cyclo–synchrotron radiation. *ApJ*, **422**, 737–745.

La Franca, F., Gregorini, L., Cristiani, S., de Ruiter, H., and Owen, F. (1994). Deep VLA observations of an optically selected sample of intermediate redshift QSOs and the optical luminosity function of the radio loud QSOs. *AJ*, **108**, 1548–1556.

Laor, A., Fiore, F., Elvis, M., Wilkes, B. J., and McDowell, J. C. (1997). The soft X-ray properties of a complete sample of optically selected quasars. II. Final results. *ApJ*, **477**, 93.

Lawrence, A. (1987). Classification of active galaxies and the prospect of a unified phenomenology. *PASP*, **99**, 309–334.

Lawrence, A. and Papadakis, I. (1993). X-ray variability of active galactic nuclei - A universal power spectrum with luminosity-dependent amplitude. *ApJ*, **414**, L85–L88.

Lawrence, A., Watson, M. G., Pounds, K. A., and Elvis, M. (1985). Continuous rapid X-ray variability and spectral changes in NGC 4051. *MNRAS*, **217**, 685–699.

Lee, J. C., Fabian, A. C., Brandt, W. N., Reynolds, C. S., and Iwasawa, K. (1999). First constraints on iron abundance versus reflection fraction from the Seyfert 1 galaxy MCG-6-30-15. *MNRAS*, **310**, 973–981.

Lee, J. C., Fabian, A. C., Reynolds, C. S., Brandt, W. N., and Iwasawa, K. (2000). The X-ray variability of the Seyfert 1 galaxy MCG-6-30-15 from long ASCA and RXTE observations. *MNRAS*, **318**, 857–874.

Lewin, W. H. G., Doty, J., Clark, G. W., Rappaport, S. A., Bradt, H. V. D., Doxsey, R., Hearn, D. R., Hoffman, J. A., Jernigan, J. G., Li, F. K., Mayer, W., McClintock, J., Primini, F., and Richardson, J. (1976). The discovery of rapidly repetitive X-ray bursts from a new source in Scorpius. *ApJ*, **207**, L95–L99.

Li, T. P., Feng, Y. X., and Chen, L. (1999). Temporal and spectral correlations of Cygnus X-1. *ApJ*, **521**, 789–797.

Liang, E. P. T. (1979). Electron-positron pair production in hot unsaturated Compton accretion models around black holes. *ApJ*, **234**, 1105–1112.

Lightman, A. P. and Eardley, D. M. (1974). Black holes in binary systems: Instability of disk accretion. *ApJ*, **187**, L1.

Lightman, A. P. and White, T. R. (1988). Effects of cold matter in active galactic nuclei - A broad hump in the X-ray spectra. *ApJ*, **335**, 57–66.

Lin, D. J., Misra, R., and Taam, R. E. (2001). Hydrodynamical winds from two-temperature plasma in X-ray binaries. *MNRAS*, **324**, 319–324.

Lipunova, G. V. (1999). Supercritical disk accretion with mass loss. *Astronomy Letters*, **25**, 508–517.

Livio, M., Ogilvie, G. I., and Pringle, J. E. (1999). Extracting energy from black holes: The relative importance of the Blandford-Znajek mechanism. *ApJ*, **512**, 100–104.

Lochner, J. C., Swank, J. H., and Szymkowiak, A. E. (1991). Shot model parameters for Cygnus X-1 through phase portrait fitting. *ApJ*, **376**, 295–311.

Longair, M. S., Ryle, M., and Scheuer, P. A. G. (1973). Models of extended radio sources. *MNRAS*, **164**, 243+.

Lu, E. T. and Hamilton, R. J. (1991). Avalanches and the distribution of solar flares. *ApJ*, **380**, L89–L92.

Lubiński, P. and Zdziarski, A. A. (2001). The strength and width of Fe Kα lines in Seyferts and their correlations with the X-ray slope. *MNRAS*, **323**, L37–L42.

Lynden-Bell, D. (1969). Galactic nuclei as collapsed old quasars. *Nature*, **223**, 690.

Maccarone, T. J., Coppi, P. S., and Poutanen, J. (2000). Time domain analysis of variability in Cygnus X-1: Constraints on the emission models. *ApJ*, **537**, L107–L110.

MacFadyen, A. I. and Woosley, S. E. (1999). Collapsars: Gamma-ray Bursts and explosions in "failed supernovae". *ApJ*, **524**, 262–289.

Machida, M., Hayashi, M. R., and Matsumoto, R. (2000). Global simulations of differentially rotating magnetized disks: formation of Low-β filaments and structured coronae. *ApJ*, **532**, L67–L70.

Madau, P., Ghisellini, G., and Fabian, A. C. (1994). The unified Seyfert scheme and the origin of the cosmic X-ray background. *MNRAS*, **270**, L17.

Madejski, G. M. (1998). Black holes in Active Galactic Nuclei: observations. In *Theory of Black Hole Accretion Disks*, page 21.

Magdziarz, P. and Zdziarski, A. A. (1995). Angle-dependent Compton reflection of X-rays and gamma-rays. *MNRAS*, **273**, 837–848.

Magorrian, J., Tremaine, S., Richstone, D., Bender, R., Bower, G., Dressler, A., Faber, S. M., Gebhardt, K., Green, R., Grillmair, C., Kormendy, J., and Lauer, T. (1998). The demography of massive dark objects in galaxy centers. *AJ*, **115**, 2285–2305.

Makishima, K., Kubota, A., Mizuno, T., Ohnishi, T., Tashiro, M., Aruga, Y., Asai, K., Dotani, T., Mitsuda, K., Ueda, Y., Uno, S., Yamaoka, K., Ebisawa, K., Kohmura, Y., and Okada, K. (2000). The Nature of Ultraluminous Compact X-Ray Sources in Nearby Spiral Galaxies. *ApJ*, **535**, 632–643.

Malzac, J., Beloborodov, A. M., and Poutanen, J. (2001). X-ray spectra of accretion discs with dynamic coronae. *MNRAS*, **326**, 417–427.

Markoff, S., Falcke, H., and Fender, R. (2001). A jet model for the broadband spectrum of XTE J1118+480. Synchrotron emission from radio to X-rays in the Low/Hard spectral state. *A&A*, **372**, L25–L28.

Matsuoka, M., Piro, L., Yamauchi, M., and Murakami, T. (1990). X-ray spectral variability and complex absorption in the Seyfert 1 galaxies NGC 4051 and MCG -6-30-15. *ApJ*, **361**, 440–458.

Matt, G. (2000). The broad band spectrum and variability of Seyfert 1. In *To appear in the proceedings of "X-Ray Astronomy '99", 1999, September 6-10, Bologna (Italy.* astro-ph/0007105.

Matt, G., Perola, G. C., and Piro, L. (1991). The iron line and high energy bump as X-ray signatures of cold matter in Seyfert 1 galaxies. *A&A*, **247**, 25–34.

Matt, G., Fabian, A. C., and Reynolds, C. S. (1997). Geometrical and chemical dependence of K-shell X-ray features. *MNRAS*, **289**, 175–184.

McBreen, B., Hurley, K. J., Long, R., and Metcalfe, L. (1994). Lognormal distributions in Gamma-ray bursts and cosmic lightning. *MNRAS*, **271**, 662.

McClintock, J. E., Garcia, M. R., Caldwell, N., Falco, E. E., Garnavich, P. M., and Zhao, P. (2001a). A black hole greater than 6 $M_\odot$ in the X-ray Nova XTE J1118+480. *ApJ*, **551**, L147–L150.

McClintock, J. E., Haswell, C. A., Garcia, M. R., Drake, J. J., Hynes, R. I., Marshall, H. L., Muno, M. P., Chaty, S., Garnavich, P. M., Groot, P. J., Lewin, W. H. G., Mauche, C. W., Miller, J. M., Pooley, G. G., Shrader, C. R., and Vrtilek, S. D. (2001b). Complete and simultaneous spectral observations of the black hole X-ray Nova XTE J1118+480. *ApJ*, **555**, 477–482.

McHardy, I. and Czerny, B. (1987). Fractal X-ray time variability and spectral invariance of the Seyfert galaxy NGC5506. *Nature*, **325**, 696–698.

McHardy, I. M. (1989). X ray variability of active galactic nuclei. In *Two Topics in X-Ray Astronomy, Volume 1: X Ray Binaries. Volume 2: AGN and the X Ray Background*, pages 1111–1124.

McHardy, I. M., Papadakis, I. E., and Uttley, P. (1998). Temporal and spectral variability of AGN with RXTE. In *The Active X-ray Sky: Results from BeppoSAX and RXTE*, page 509.

Meegan, C. A., Pendleton, G. N., Briggs, M. S., Kouveliotou, C., Koshut, T. M., Lestrade, J. P., Paciesas, W. S., McCollough, M. L., Brainerd, J. J., Horack, J. M., Hakkila, J., Henze, W., Preece, R. D., Mallozzi, R. S., and Fishman, G. J. (1996). The third BATSE Gamma-ray burst catalog. *ApJS*, **106**, 65.

Meier, D. L. (1982). The structure and appearance of winds from supercritical accretion disks. II - Dynamical theory of supercritical winds. *ApJ*, **256**, 681–692.

Meier, D. L. (1999). A magnetically switched, rotating black hole model for the production of extragalactic radio jets and the Fanaroff and Riley class division. *ApJ*, **522**, 753–766.

Melia, F. and Falcke, H. (2001). The supermassive black hole at the Galactic Center. *ARA&A*, **39**, 309–352.

Mendez, M. and van der Klis, M. (1997). The EXOSAT data on GX 339-4: further evidence for an "Intermediate" state. *ApJ*, **479**, 926.

Merloni, A., Vietri, M., Stella, L., and Bini, D. (1999). On gravitomagnetic precession around black holes. *MNRAS*, **304**, 155–159.

Meyer, F. and Meyer-Hofmeister, E. (1994). Accretion disk evaporation by a coronal siphon flow. *A&A*, **288**, 175–182.

Miller, K. A. and Stone, J. M. (2000). The formation and structure of a strongly magnetized corona above a weakly magnetized accretion disk. *ApJ*, **534**, 398–419.

Mineshige, S., Takeuchi, M., and Nishimori, H. (1994). Is a black hole accretion disk in a self-organized critical state? *ApJ*, **435**, L125–L128.

Mineshige, S., Kawaguchi, T., Takeuchi, M., and Hayashida, K. (2000). Slim-disk model for soft X-ray excess and variability of Narrow-Line Seyfert 1 Galaxies. *PASJ*, **52**, 499–508.

Mirabel, I. F. and Rodríguez, L. F. (1999). Sources of relativistic jets in the Galaxy. *ARA&A*, **37**, 409–443.

Mirabel, I. F. and Rodriguez, L. F. (1994). A superluminal source in the Galaxy. *Nature*, **371**, 46.

Mirabel, I. F., Dhawan, V., Mignani, R. P., Rodrigues, I., and Guglielmetti, F. (2001). A high-velocity black hole on a Galactic-halo orbit in the solar neighbourhood. *Nature*, **413**, 139–141.

Misra, R. and Taam, R. E. (2001). The influence of hydrodynamical winds on hot accretion disk solutions. *ApJ*, **553**, 978–986.

Mitsuda, K., Inoue, H., Koyama, K., Makishima, K., Matsuoka, M., Ogawara, Y., Suzuki, K., Tanaka, Y., Shibazaki, N., and Hirano, T. (1984). Energy spectra of low-mass binary X-ray sources observed from TENMA. *PASJ*, **36**, 741–759.

Miyamoto, S., Kimura, K., Kitamoto, S., Dotani, T., and Ebisawa, K. (1991). X-ray variability of GX 339-4 in its very high state. *ApJ*, **383**, 784–807.

Miyoshi, M., Moran, J., Herrnstein, J., Greenhill, L., Nakai, N., Diamond, P., and Inoue, M. (1995). Evidence for a black-hole from high rotation velocities in a sub-parsec region of NGC4258. *Nature*, **373**, 127.

Montroll, E. W. and Shlesinger, M. F. (1982). On $1/f$ noise and other distributions with long tails. *Proc. Natl. Acad. Sci. USA*, **79**, 3380.

Motch, C., Ilovaisky, S. A., and Chevalier, C. (1982). Discovery of fast optical activity in the X-ray source GX 339-4. *A&A*, **109**, L1–L4.

Motch, C., Ricketts, M. J., Page, C. G., Ilovaisky, S. A., and Chevalier, C. (1983). Simultaneous X-ray/optical observations of GX339-4 during the May 1981 optically bright state. *A&A*, **119**, 171–176.

Muno, M. P., Morgan, E. H., and Remillard, R. A. (1999). Quasi-periodic oscillations and spectral states in GRS 1915+105. *ApJ*, **527**, 321–340.

Mushotzky, R. F., Done, C., and Pounds, K. A. (1993). X-ray spectra and time variability of active galactic nuclei. *ARA&A*, **31**, 717–761.

Mushotzky, R. F., Cowie, L. L., Barger, A. J., and Arnaud, K. A. (2000). Resolving the extragalactic hard X-ray background. *Nature*, **404**, 459–464.

Nagar, N. M., Falcke, H., Wilson, A. S., and Ho, L. C. (2000). Radio sources in Low-Luminosity Active Galactic Nuclei. I. VLA detections of compact, flat-spectrum cores. *ApJ*, **542**, 186–196.

Nandra, K. (2001). X-ray variability of AGN and correlations with spectral properties. In *Invited review at the 33rd COSPAR Scientific Assembly, Warsaw, Poland*. To appear in Advances in Space Research. astro-ph/0012448.

Nandra, K. and Pounds, K. A. (1994). GINGA observations of the X-ray spectra of Seyfert galaxies. *MNRAS*, **268**, 405.

Nandra, K., George, I. M., Mushotzky, R. F., Turner, T. J., and Yaqoob, T. (1997a). ASCA Observations of Seyfert 1 Galaxies. II. Relativistic Iron K alpha Emission. *ApJ*, **477**, 602.

Nandra, K., George, I. M., Mushotzky, R. F., Turner, T. J., and Yaqoob, T. (1997b). On the dependence of the Iron K-line profiles with luminosity in active galactic nuclei. *ApJ*, **488**, L91.

Narayan, R. and Yi, I. (1994). Advection-dominated accretion: A self-similar solution. *ApJ*, **428**, L13–L16.

Narayan, R. and Yi, I. (1995a). Advection-dominated accretion: Self-similarity and bipolar outflows. *ApJ*, **444**, 231–243.

Narayan, R. and Yi, I. (1995b). Advection-dominated Accretion: Underfed Black Holes and Neutron Stars. *ApJ*, **452**, 710.

Narayan, R., Mahadevan, R., and Quataert, E. (1999). Advection-dominated accretion around black holes. In *Theory of Black Hole Accretion Disks*, page 148.

Narayan, R., Igumenshchev, I. V., and Abramowicz, M. A. (2000). Self-similar accretion flows with convection. *ApJ*, **539**, 798–808.

Narayan, R., Garcia, M. R., and McClintock, J. E. (2001). X-ray Novae and the evidence for black hole event horizons. In *Proceedings of the IX Marcel Grossmann Meeting*.

Nayakshin, S. and Kazanas, D. (2001). Narrow moving Fe Kα lines from magnetic flares in active galactic nuclei. *ApJ*, **553**, L141–L144.

Nayakshin, S., Kazanas, D., and Kallman, T. R. (2000a). Thermal instability and photoionized X-ray reflection in accretion disks. *ApJ*, **537**, 833–852.

Nayakshin, S., Rappaport, S., and Melia, F. (2000b). Time-dependent disk models for the microquasar GRS 1915+105. *ApJ*, **535**, 798–814.

Norman, C., Hasinger, G., Giacconi, R., Gilli, R., Gilmozzi, R., Kewley, L., Nonino, M., Rosati, P., Szokoly, G., Tozzi, P., Wang, J., Zheng, W., A., Z., Bergeron, J., Grogin, N., Koekemoer, A., and Schreier, E. (2001). A classic Type 2 Quasar. *ApJ, submitted. astro-ph/0103198.*

Novikov, I. D. and Thorne, K. S. (1973). In C. de Witt and B. S. de Witt, editors, *Black Holes–Les Astres Occlus*, page 343. Gordon & Breach, New York.

Nowak, M. A. (2000). Are there three peaks in the power spectra of GX 339-4 and Cyg X-1? *MNRAS*, **318**, 361–367.

Nowak, M. A. and Chiang, J. (2000). Implications of the X-ray variability for the mass of MCG -6-30-15. *ApJ*, **531**, L13–L16.

Oda, M. (1977). Cyg X-1 - A candidate of the black hole. *Space Science Reviews*, **20**, 757–813.

Osterbrock, D. E. (1974). *Astrophysics of gaseous nebulae.* San Francisco, W. H. Freeman and Co., 1974. 263 p.

Paczyński, B. (1971). Evolutionary processes in close binary systems. *ARA&A*, **9**, 183.

Paczynski, B. (1998). Are Gamma-ray bursts in star-forming regions? *ApJ*, **494**, L45.

Papaloizou, J. C. B. and Lin, D. N. C. (1995). Theory of accretion disks I: Angular momentum transport processes. *ARA&A*, **33**, 505–540.

Parker, E. N. (1979). *Cosmical magnetic fields: Their origin and their activity.* Oxford, Clarendon Press; New York, Oxford University Press, 1979, 858 p.

Patterson, J., Fried, R., Harvey, D., Cook, L., Masi, G., Kemp, J., Hannon, J., Buczynski, D., Vanmunster, T., Pidgley, L., Maxted, P., and Araujo-Betancor, S. (2000). XTE J1118+480. *IAU Circular*, **7412**, 2.

Petrucci, P. O., Haardt, F., Maraschi, L., Grandi, P., Matt, G., Nicastro, F., Piro, L., Perola, G. C., and De Rosa, A. (2000). Testing Comptonizing coronae on a long BeppoSAX observation of the Seyfert 1 galaxy NGC 5548. *ApJ*, **540**, 131–142.

Petrucci, P. O., Papadakis, I., Haardt, F., Maraschi, L., McHardy, I., and Uttley, P. (2001). Constraints on the high energy continuum of Seyfert galaxies from RXTE color-color and color-flux diagrams. In *To appear in Proc. of "X-ray astronomy 2000",(Palermo Sep. 2000), Eds. R. Giacconi, L. Stella, S. Serio, ASP Conf. Series, in press.* astro-ph/0101221.

Petschek, H. E. (1964). In *AAS-NASA Symp. on Physics of Solar flares*, NASA SP-50, page 425.

Piran, T. (1977). Secondary winds and evaporation from accretion discs. *MNRAS*, **180**, 45–56.

Piran, T. (1978). The role of viscosity and cooling mechanisms in the stability of accretion disks. *ApJ*, **221**, 652–660.

Politano, H. and Poquet, A. (1995). Model of intermittency in magnetohydrodynamic turbulence. *Phys. Rev. E.*, **52**, 636.

Pooley, G. G. and Waldram, E. M. (2000). XTE J1118+480. *IAU Circular*, **7390**, 2.

Popham, R., Woosley, S. E., and Fryer, C. (1999). Hyperaccreting black holes and Gamma-ray bursts. *ApJ*, **518**, 356–374.

Pounds, K. A., Nandra, K., Stewart, G. C., George, I. M., and Fabian, A. C. (1990). X-ray reflection from cold matter in the nuclei of active galaxies. *Nature*, **344**, 132.

Poutanen, J. and Coppi, P. S. (1998). Unification of spectral states of accreting black holes. In *Abstracts of the 19th Texas Symposium on Relativistic Astrophysics and Cosmology, held in Paris, France, Dec. 14-18, 1998. Eds.: J. Paul, T. Montmerle, and E. Aubourg (CEA Saclay).*, page E355.

Poutanen, J. and Fabian, A. C. (1999). Spectral evolution of magnetic flares and time lags in accreting black hole sources. *MNRAS*, **306**, L31–L37.

Pozdniakov, L. A., Sobol, I. M., and Siuniaev, R. A. (1976). Multiple Compton scattering by relativistic electrons - Monte Carlo calculations of the emission spectrum. *Soviet Astronomy Letters*, **2**, 55–57.

Prendergast, K. H. and Burbidge, G. R. (1968). On the nature of some galactic X-Ray sources. *ApJ*, **151**, L83.

Press, W. H. (1978). Flicker noises in astronomy and elsewhere. *Comments on Astrophysics*, **7**, 103–119.

Pringle, J. E. (1976). Thermal instabilities in accretion discs. *MNRAS*, **177**, 65–71.

Pringle, J. E. (1981). Accretion discs in astrophysics. *ARA&A*, **19**, 137–162.

Pringle, J. E. and Rees, M. J. (1972). Accretion disc models for compact X-ray sources. *A&A*, **21**, 1+.

Psaltis, D. (2001). Models of quasi-periodic variability in neutron stars and black holes. In *Invited review at the 33rd COSPAR Scientific Assembly, Warsaw, Poland.* To appear in Advances in Space Research. astro-ph/0012251.

Psaltis, D. and Norman, C. (2000). On the origin of quasi-periodic oscillations and broad-band noise in accreting neutron stars and black holes. *ApJ, submitted. astro-ph/0010316.*

Psaltis, D., Belloni, T., and van der Klis, M. (1999). Correlations in Quasi-periodic Oscillation and Noise Frequencies among Neutron Star and Black Hole X-Ray Binaries. *ApJ*, **520**, 262–270.

Quataert, E. and Gruzinov, A. (1999). Turbulence and particle heating in advection-dominated accretion flows. *ApJ*, **520**, 248–255.

Quataert, E. and Gruzinov, A. (2000). Convection-dominated accretion flows. *ApJ*, **539**, 809–814.

Quataert, E. and Narayan, R. (1999). Spectral models of advection-dominated accretion flows with winds. *ApJ*, **520**, 298–315.

Quataert, E., di Matteo, T., Narayan, R., and Ho, L. C. (1999). Possible evidence for truncated thin disks in the Low-Luminosity Active Galactic Nuclei M81 and NGC 4579. *ApJ*, **525**, L89–L92.

Różańska, A. and Czerny, B. (2000). Vertical structure of the accreting two-temperature corona and the transition to an ADAF. *A&A*, **360**, 1170–1186.

Ramirez-Ruiz, E., Merloni, A., and Rees, M. J. (2001). Quiescent times in gamma-ray bursts - II. Dormant periods in the central engine? *MNRAS*, **324**, 1147.

Rees, M. J. (1971). New interpretation of extragalactic radio sources. *Nature*, **229**, 312 and 510.

Rees, M. J. (1978). Accretion and the quasar phenomenon. *Phisica Scripta*, **17**, 193–200.

Rees, M. J. (1999). Some comments on triggers, energetics and beaming. *A&AS*, **138**, 491–497.

Rees, M. J. and Meszaros, P. (1994). Unsteady outflow models for cosmological gamma-ray bursts. *ApJ*, **430**, L93–L96.

Rees, M. J., Phinney, E. S., Begelman, M. C., and Blandford, R. D. (1982). Ion-supported tori and the origin of radio jets. *Nature*, **295**, 17–21.

Reeves, J. N. and Turner, M. J. L. (2000). X-ray spectra of a large sample of quasars with ASCA. *MNRAS*, **316**, 234–248.

Remillard, R., Morgan, E., Smith, D., and Smith, E. (2000). XTE J1118+480. *IAU Circular*, **7389**, 2.

Revnivtsev, M., Sunyaev, R., and Borozdin, K. (2000). Discovery of a 0.08 Hz QPO in the power spectrum of black hole candidate XTE J1118+480. *A&A*, **361**, L37–L39.

Reynolds, C. S. and Fabian, A. C. (1997). Special relativistic effects on the strength of the fluorescent Kalpha iron line from black hole accretion discs. *MNRAS*, **290**, L1–L5.

Reynolds, C. S., Nowak, M. A., and Maloney, P. R. (2000). A deep X-ray observation of NGC 4258 and its surrounding field. *ApJ*, **540**, 143–153. R00.

Reynolds, S. P. (1982). Theoretical studies of compact radio sources. I - Synchrotron radiation from relativistic flows. *ApJ*, **256**, 13–37.

Rhoades, C. E. and Ruffini, R. (1974). Maximum mass of a neutron star. *Phys. Rev. Lett.*, **32**, 324.

Romanova, M. M., Ustyugova, G. V., Koldoba, A. V., Chechetkin, V. M., and Lovelace, R. V. E. (1998). Dynamics of magnetic loops in the coronae of accretion disks. *ApJ*, **500**, 703.

Ross, R. R. and Fabian, A. C. (1993). The effects of photoionization on X-ray reflection spectra in active galactic nuclei. *MNRAS*, **261**, 74–82.

Ross, R. R. and Fabian, A. C. (1996). The spectra of accretion discs in low-mass X-ray binaries. *MNRAS*, **281**, 637.

Ross, R. R., Weaver, R., and McCray, R. (1978). The Comptonization of iron X-ray features in compact X-ray sources. *ApJ*, **219**, 292–299.

Rybicki, G. B. and Lightman, A. P. (1979). *Radiative processes in astrophysics*. New York, Wiley-Interscience, 1979.

Salpeter, E. E. (1964). Accretion of interstellar matter by massive objects. *ApJ*, **140**, 796–800.

Sanders, D. B., Phinney, E. S., Neugebauer, G., Soifer, B. T., and Matthews, K. (1989). Continuum energy distribution of quasars - Shapes and origins. *ApJ*, **347**, 29–51.

Sari, R. and Piran, T. (1999). GRB 990123: The optical flash and the fireball model. *ApJ*, **517**, L109–L112.

Shakura, N. I. and Suniaev, R. A. (1976). A theory of the instability of disk accretion on to black holes and the variability of binary X-ray sources, galactic nuclei and quasars. *MNRAS*, **175**, 613–632.

Shakura, N. I. and Sunyaev, R. A. (1973). Black holes in binary systems. Observational appearance. *A&A*, **24**, 337–355.

Shapiro, S. L., Lightman, A. P., and Eardley, D. M. (1976). A two-temperature accretion disk model for Cygnus X-1 - Structure and spectrum. *ApJ*, **204**, 187–199.

Shih et al. (2001). *In preparation*.

Shimura, T. and Takahara, F. (1995). On the spectral hardening factor of the X-ray emission from accretion disks in black hole candidates. *ApJ*, **445**, 780–788.

Sincell, M. W. and Krolik, J. H. (1997). The vertical structure and ultraviolet spectrum of X-ray–irradiated accretion disks in active galactic nuclei. *ApJ*, **476**, 605.

Sobczak, G. J., McClintock, J. E., Remillard, R. A., Bailyn, C. D., and Orosz, J. A. (1999). RXTE spectral observations of the 1996-1997 outburst of the microquasar GRO J1655-40. *ApJ*, **520**, 776–787.

Spitzer, L. (1962). *Physics of fully ionized gas*. New York, Wiley Interscience, 1962.

Spruit, H. (2000). Radiatively inefficient accretion disks. In C. K. et al., editor, *The neutron star black hole connection*. astro-ph/0003143.

Spruit, H. C. and Deufel, B. (2001). The transition from a cool disk to an ion supported flow. *A&A, submitted. astro-ph/0108497.*

Stella, L. and Rosner, R. (1984). Magnetic field instabilities in accretion disks. *ApJ*, **277**, 312–321.

Stella, L. and Vietri, M. (1998). Lense-Thirring precession and quasi-periodic oscillations in low-mass X-ray binaries. *ApJ*, **492**, L59.

Stella, L., Vietri, M., and Morsinkn, S. M. (1999). Correlations in the quasi-periodic oscillation frequencies of low-mass X-ray binaries and the relativistic precession model. *ApJ*, **524**, L63–L66.

Stepney, S. and Guilbert, P. W. (1983). Numerical FITS to important rates in high temperature astrophysical plasmas. *MNRAS*, **204**, 1269–1277.

Stern, B. (1999). Relativistic outflows in Gamma-ray bursts. In *ASP Conf. Ser. 161: High Energy Processes in Accreting Black Holes*, page 277.

Stern, B. E. and Svensson, R. (1996). Evidence for chain reaction in the time profiles of Gamma-ray bursts. *ApJ*, **469**, L109.

Stern, B. E., Poutanen, J., Svensson, R., Sikora, M., and Begelman, M. C. (1995). On the geometry of the X-ray–emitting region in Seyfert galaxies. *ApJ*, **449**, L13.

Stirling, A. M., Spencer, R. E., de la Force, C. J., Garrett, M. A., Fender, R. P., and Ogley, M. A. (2001). A relativistic jet from Cygnus X-1 in the low/hard X-ray state. *MNRAS, in press. astro-ph/0107192.*

Stone, J. M., Hawley, J. F., Gammie, C. F., and Balbus, S. A. (1996). Three-dimensional magnetohydrodynamical simulations of vertically stratified accretion disks. *ApJ*, **463**, 656.

Stone, J. M., Pringle, J. E., and Begelman, M. C. (1999). Hydrodynamical non-radiative accretion flows in two dimensions. *MNRAS*, **310**, 1002–1016.

Sunyaev, R. A. and Titarchuk, L. G. (1980). Comptonization of X-rays in plasma clouds - Typical radiation spectra. *A&A*, **86**, 121–138.

Svensson, R. (1996). Models of X-ray and γ-ray emission from Seyfert galaxies. *A&AS*, **120**, C475.

Svensson, R. and Zdziarski, A. A. (1994). Black hole accretion disks with coronae. *ApJ*, **436**, 599–606.

Sweet, P. A. (1958). The neutral point theory of solar flares. In *IAU Symp. 6: Electromagnetic Phenomena in Cosmical Physics*, volume 6, page 123.

Szuszkiewicz, E., Malkan, M. A., and Abramowicz, M. A. (1996). The observational appearance of slim accretion disks. *ApJ*, **458**, 474.

Tanaka, Y. and Lewin, W. H. G. (1995). *X-ray binaries*. Cambridge University Press, edited by Lewin, Walter H.G.; Van Paradijs, Jan; Van den Heuvel, Edward P.J.

Tananbaum, H., Gursky, H., Kellogg, E., Giacconi, R., and Jones, C. (1972). Observation of a correlated X-Ray transition in Cygnus X-1. *ApJ*, **177**, L5.

Thorne, K. S. (1994). *Black Holes and time warps: Einstein's outrageous legacy*. Picador.

Timmer, J. and Koenig, M. (1995). On generating power law noise. *A&A*, **300**, 707.

Tout, C. A. and Pringle, J. E. (1992). Accretion disc viscosity: a simple model for a magnetic dynamo. *MNRAS*, **259**, 604.

Tout, C. A. and Pringle, J. E. (1996). Can a disc dynamo generate large-scale magnetic fields? *MNRAS*, **281**, 219–225.

Turner, N. J. and Stone, J. M. (2001). A module for radiation hydrodynamic calculations with ZEUS-2D using flux-limited diffusion. *ApJS*, **135**, 95–107.

Uemura, M., Kato, T., Yamaoka, H., Buczynski, D., Takamizawa, K., and Trondal, O. (2000). XTE J1118+480. *IAU Circular*, **7390**, 1.

Urry, C. M. and Padovani, P. (1995). Unified schemes for radio-loud active galactic nuclei. *PASP*, **107**, 803.

Uttley, P. and McHardy, I. M. (2001). The flux-dependent amplitude of broadband noise variability in X-ray binaries and active galaxies. *MNRAS*, **323**, L26–L30.

van der Klis, M. (2000). Millisecond oscillations in X-ray binaries. *ARA&A*, **38**, 717–760.

van Paradijs, J., Groot, P. J., Galama, T., Kouveliotou, C., Strom, R. G., Telting, J., Rutten, R. G. M., Fishman, G. J., Meegan, C. A., Pettini, M., Tanvir, N., Bloom, J., Pedersen, H., Nordgaard-Nielsen, H. U., Linden-Vornle, M., Melnick, J., van der Steene, G., Bremer, M., Naber, R., Heise, J., in 't Zand, J., Costa, E., Feroci, M., Piro, L., Frontera, F., Zavattini, G., Nicastro, L., Palazzi, E., Bennet, K., Hanlon, L., and Parmar, A. (1997). Transient optical emission from the error box of the gamma-ray burst of 28 February 1997. *Nature*, **386**, 686–689.

Vaughan, S. and Edelson, R. (2001). Evidence for rapid Iron Kα line flux aariability in MCG -6-30-15. *ApJ*, **548**, 694–702.

Vaughan, S., Reeves, J., Warwick, R., and Edelson, R. (1999). X-ray spectral complexity in narrow-line Seyfert 1 galaxies. *MNRAS*, **309**, 113–124.

Velikhov, E. P. (1959). *Sov. Phys. JETP*, **36**, 995.

Wagner, R. M., Foltz, C. B., Shahbaz, T., Casares, J., Charles, P. A., Starrfield, S. G., and Hewett, P. (2001). The halo black hole X-ray transient XTE J1118+480. *ApJ*, **556**, 42–46.

Wagoner, R. V., Silbergleit, A. S., and Ortega-Rodríguez, M. (2001). 'Stable' QPOs and black hole properties from diskeoseimology. *ApJ, in press. astro-ph/0107168v2.*

Wardziński, G. and Zdziarski, A. A. (2000). Thermal synchrotron radiation and its Comptonization in compact X-ray sources. *MNRAS*, **314**, 183–198.

Wardziński, G. and Zdziarski, A. A. (2001). Effects of non-thermal tails in Maxwellian electron distributions on synchrotron and Compton processes. *MNRAS*, **325**, 963–971.

Watarai, K., Fukue, J., Takeuchi, M., and Mineshige, S. (2000). Galactic black hole candidates shining at the Eddington luminosity. *PASJ*, **52**, 133.

Watson, W. D. and Wallin, B. K. (1994). Evidence from masers for a rapidly rotating disk at the nucleus of NGC 4258. *ApJ*, **432**, L35–L38.

White, T. R., Lightman, A. P., and Zdiziarski, A. A. (1988). Compton reflection of gamma rays by cold electrons. *ApJ*, **331**, 939–948.

Wijnands, R. and van der Klis, M. (1999). The Broadband Power Spectra of X-Ray Binaries. *ApJ*, **514**, 939–944.

Wilman, R. J. and Fabian, A. C. (1999). Fitting the spectrum of the X-ray background: the effects ofhigh-metallicity absorption. *MNRAS*, **309**, 862–870.

Wilson, C. A. and McCollough, M. L. (2000). XTE J1118+480. *IAU Circular*, **7390**, 3.

Wood, K. S., Ray, P. S., Bandyopadhyay, R. M., Wolff, M. T., Fritz, G., Hertz, P., Kowalski, M. P., Lovellette, M. N., Yentis, D., Bloom, E. D., Giebels, B., Godfrey, G., Reilly, K., Saz Parkinson, P., Shabad, G., and Scargle, J. (2000). USA experiment and RXTE observations of a variable low-frequency quasi-periodic oscillation in XTE J1118+480. *ApJ*, **544**, L45–L48.

Woosley, S. E. (1993). Gamma-ray bursts from stellar mass accretion disks around black holes. *ApJ*, **405**, 273–277.

Wren, J. and McKay, T. (2000). XTE J1118+480. *IAU Circular*, **7394**, 4.

Yamaoka, K., Ueda, Y., Dotani, T., Durouchoux, P., and Rodriguez, J. (2000). XTE J1118+480. *IAU Circular*, **7427**, 2.

Zdziarski, A. A. (1985). Power-law X-ray and gamma-ray emission from relativistic thermal plasmas. *ApJ*, **289**, 514–525.

Zdziarski, A. A. (1986). Monte Carlo spectra from pair-equilibrium, weakly magnetized thermal plasmas. *ApJ*, **303**, 94–100.

Zdziarski, A. A. (1998). Hot accretion discs with thermal Comptonization and advection in luminous black hole sources. *MNRAS*, **296**, L51.

Zdziarski, A. A. (1999). X-rays and soft Gamma-rays from Seyferts, radio galaxies, and black-hole binaries. In *ASP Conf. Ser. 161: High Energy Processes in Accreting Black Holes*, page 16.

Zdziarski, A. A. and Grandi, P. (2001). The broadband spectrum of 3C 120 observed by BeppoSAX. *ApJ*, **551**, 186–196.

Zdziarski, A. A., Fabian, A. C., Nandra, K., Celotti, A., Rees, M. J., Done, C., Coppi, P. S., and Madejski, G. M. (1994). Physical processes in the X-ray/Gamma-ray source of IC4329A. *MNRAS*, **269**, L55.

Zdziarski, A. A., Poutanen, J., Mikolajewska, J., Gierlinski, M., Ebisawa, K., and Johnson, W. N. (1998). Broad-band X-ray/gamma-ray spectra and binary parameters of GX 339-4 and their astrophysical implications. *MNRAS*, **301**, 435–450.

Zdziarski, A. A., Lubinski, P., and Smith, D. A. (1999). Correlation between Compton reflection and X-ray slope in Seyferts and X-ray binaries. *MNRAS*, **303**, L11–L15.

Zeldovich, Y. B. and Novikov, I. D. (1964). *Sov. Phys. Dokl.*, **158**, 811.